

THESIS

PETROGENETIC ANALYSIS OF THE WENATCHEE RIDGE ORTHOGNEISS IN THE
NORTH CASCADE MOUNTAINS, WASHINGTON STATE

Submitted by

Richard Haster Zaggle

Department of Geosciences

In partial fulfillment of the requirements

For the Degree of Master of Science

Colorado State University

Fort Collins, Colorado

Fall 2014

Master's Committee:

Advisor: Jerry Magloughlin

John Ridley
Steven Strauss

Copyright by Richard Zaggle 2014

All Rights Reserved

ABSTRACT

PETROGENETIC ANALYSIS OF THE WENATCHEE RIDGE ORTHOGNEISS IN THE NORTH CASCADE MOUNTAINS, WASHINGTON STATE

Petrogenetic analysis of the Wenatchee Ridge Orthogneiss (WRO) (Magloughlin & Evans, 1987) in the Nason Terrane of the North Cascade Mountains has been undertaken in order to gain insight into epidote-bearing TTG plutonism associated with mid-Cretaceous orogenesis in the North American Cordillera. Discriminant analysis indicates the WRO is very similar to Archean TTGs based upon characteristic geochemical values ($Yb < 1$, $Sr/Y > 150$, $La/Yb > 15$, $Y < 6$) and thus may provide insight into Archean crustal generation processes.

Samples were taken from within the pluton and from within the surrounding banded gneiss (Tabor et al., 1987). The pluton is chemically heterogeneous and samples all show some degree of foliation which is concordant with the foliation in country rocks. Samples range from leucotondhemite to granodiorite and contain oligoclase, quartz, potassium feldspar, muscovite, biotite, and epidote. SiO_2 is 56.3-76.8% and REE data show that the samples are highly depleted in HREEs, variably depleted in LREEs, and have an average Eu/Eu^* of 1.36 ± 0.5 . Though positive Eu anomalies are typically associated with plagioclase accumulation, the WRO appears to lack any correlation between plagioclase and Eu/Eu^* .

Geochemical results and the tectonic setting of the WRO indicate the initial magma may have formed as a partial melt of overthickened eclogitic crust. The subsequent LREE depletion and high positive Eu anomalies in the most evolved samples may be controlled by amphibole,

epidote, and/or titanite fractionation. LA-ICP-MS analyses will indicate whether these phases had significant control on the REE signature of the WRO.

Deformation-driven differentiation would have controlled any fractionation of amphibole, epidote, and/or titanite in the WRO magma which has viscosities $\geq 10^{6.8}$ Pa·s at 1000°C calculated using the method of Giordano et al. (2008). Differentiation likely occurred simultaneously with intrusion into a lower crustal zone of plastic strain, resulting in the WRO's heterogeneity, sheeted nature, and syn-tectonic fabric.

ACKNOWLEDGEMENTS

I want to thank my wife for her endless love and support throughout this project. I could not have done any of this without her. A special thanks to the Geologic Society of America and CSU for funding my project. Thank you to my field assistant, Justin Lowe, for tromping through the jungles of the North Cascades and helping me find tonalite outcrops. I also want to thank Dr. Ridley, Dr. Hannah, Dr. Sutton for helping me in my time at CSU. My time spent in each of your offices was sometimes more valuable than class time. My biggest thanks goes to Dr. Jerry Magloughlin who took me in as a graduate student and taught me much of what I know about geology.

TABLE OF CONTENTS

ABSTRACT.....	ii
ACKNOWLEDGEMENTS.....	iv
1. INTRODUCTION	1
1.1. Purpose.....	1
2. REGIONAL GEOLOGY	3
2.1. Regional Geology of the Cascades.....	3
2.2. Local Geology	6
2.2.1. North Cascade Mountains	6
2.2.2. The Nason Terrane	9
2.2.3. Deformation.....	10
2.2.4. Metamorphism.....	10
2.3. Geologic Units.....	12
3. TONALITE REVIEW AND THE ARCHEAN TTG PROBLEM.....	21
3.1. Tonalite Review and Importance	21
3.2. Definitions.....	21
3.3. Adakite-TTG connection.....	27
3.4. Archean vs. Post-Archean TTGs.....	30
3.5. TTG Evolution	34
3.5.1. Archean TTG Petrogenetic Processes	34
3.5.2. Archean TTG Melt Location.....	38
3.6. Archean Crust Generation Issues	41
3.7. Post-Archean TTG Petrogenetic Processes.....	42
4. SAMPLING, PETROGRAPHY, AND MAGMATIC EPIDOTE	45
4.1. Sample Collection.....	45
4.2. Petrography of the WRO	47
4.2.1. Mineralogy.....	47
4.2.2. Spatial Distribution of Accessory Minerals.....	47
4.2.2.1. Epidote.....	47

4.2.2.2. Amphibole.....	47
4.2.2.3. Garnet.....	50
4.2.2.4. Biotite.....	51
4.2.3. Mineral Textures.....	53
4.2.3.1. Biotite and Muscovite.....	53
4.2.3.2. Epidote and Clinozoisite.....	55
4.2.3.3. Antiperthite.....	55
4.2.3.4. Plagioclase alteration.....	55
4.2.3.5. Amphibole growth.....	57
4.3. Magmatic Epidote.....	58
4.3.1. Background.....	58
4.3.2. Magmatic Determination.....	59
4.3.3. Epidote in the WRO.....	59
4.3.4. Implications of Occurrence.....	62
5. METAMORPHIC OVERPRINT.....	66
5.1. Background.....	66
5.2. Sample Selection.....	67
5.3. Methods.....	69
5.3.1. Quantification of metamorphic overprint using petrography.....	69
5.3.2. Criteria for creating the ITMTC.....	69
5.4. Results.....	79
5.5. Discussion.....	85
5.6. Conclusions.....	90
6. ARCHEAN COMPARISON.....	92
6.1. Purpose – Why identify and Archean Analog?.....	92
6.2. Indicative Archean Geochemistry.....	92
6.3. Methods.....	93
6.3.1. Archean Comparison.....	93
6.3.2. Sources of Archean Data.....	95
6.3.3. Chemical parameters used for tests.....	95
6.4. Results.....	96

6.4.1. Archean Analysis	96
6.4.2. Immobile Element Analysis.....	99
6.5. Discussion.....	102
6.6. Conclusion	106
7. GEOCHEMISTRY AND PETROGENESIS	107
7.1. Background.....	107
7.1.1. Models for TTG Genesis	107
7.2. Sampling and Analytical Methods.....	108
7.2.1. Sample Selection.....	108
7.2.2. Sample Preparation.....	110
7.2.3. Analytical Methods.....	110
7.3. Results.....	110
7.3.1. Major Elements.....	110
7.3.2. Trace Elements.....	117
7.4. Interpretation of Geochemical Data.....	124
7.4.1. Major Elements.....	124
7.4.2. Trace Elements.....	128
7.4.3. Multi-Element Diagrams	130
7.4.4. Additional Geochemistry Questions and Pressure Estimate Issues.....	136
7.4.4.1. What is the oxygen fugacity?.....	136
7.4.4.2. Is the WRO water rich or water poor?.....	137
7.5. Modeling Approach	137
7.5.1. Petrogenetic Modeling.....	138
7.5.1.1. Question 1: What was the original source of the magma?.....	138
7.5.1.1.1. WRO and BG Formation Models.....	138
7.5.1.1.2. Partial Melting	138
7.5.1.1.3. Fractional Crystallization.....	139
7.5.1.2. Question 2: What caused the LREE depletion and scatter amongst the WRO samples?.....	140
7.5.1.2.1. Modeling Methods	140

7.5.1.2.2. Apatite.....	140
7.5.1.2.3. Hornblende.....	143
7.5.1.2.4. Zircon.....	145
7.5.1.2.5. Epidote and Allanite	147
7.5.1.2.6. Titanite	149
7.5.1.2.7. Conclusions from petrogenetic modeling.....	151
7.5.1.3. Question 3: What is the cause of the positive Eu anomaly in the WRO and BG?	151
7.6. Discussion	157
8. MAGMA EMPLACEMENT AND DIFFERENTIATION.....	158
8.1. Overview.....	158
8.2. WRO and BG Magma Viscosity.....	158
8.3. Intrusion of Magma.....	160
8.4. Magma Differentiation.....	160
8.5. Differentiation by deformation	161
8.6. Models for simultaneous magma ascent and differentiation	162
8.6.1. Along hydro-fractures.....	162
8.6.2. Pervasively through pore spaces.....	163
8.7. Microstructural Evidence.....	165
8.8. Petrogenetic Impacts - Examples.....	167
8.8.1. Deformation within the magma chamber	167
8.8.2. Differentiation during intrusion	169
8.8.3. Differentiation by multiple methods.....	171
8.8.4. Differentiation by shear zone emplacement	171
8.9. Emplacement Interpretations for the WRO and BG Magmas	173
9. DISCUSSION AND CONCLUSIONS	174
9.1. Model 1	174
9.2. Model 2	175
9.3. Discussion of models	176
9.3.1. Model 1	176
9.3.2. Model 2	176

9.4. Conclusions.....	179
9.4.1. Has metamorphism altered the original igneous geochemistry?	179
9.4.2. Is the WRO an analogue of Archean TTG?.....	179
9.4.3. What is the preferred petrogenetic model for the WRO and BG genesis?	179
REFERENCES CITED.....	181
APPENDICES	191
Appendix A – Sample Descriptions / GPS Coordinates / Photographs.....	191
Appendix B – Thin Section Descriptions	234
Appendix C – ITMTC Table.....	254
Appendix D – Archean Comparison Data	256
Appendix E – WRO and BG Geochemical Data	259

1. INTRODUCTION

1.1 Purpose

The ultimate goal of this study is to determine the petrogenetic origin of the Wenatchee Ridge Orthogneiss (WRO) in the North Cascades Mountains of Washington State. This orthogneiss pluton is particularly interesting for a few reasons. The WRO is formed of magma known as a tonalite-trondhjemite-granodiorite (TTG) suite. TTG suites make up approximately 90% of Archean continental crust, however the petrogenetic mechanisms which created large volumes of TTG magma during the Archean are not well understood (Martin et al., 2005 and Condie, 2005). Archean TTG suites have been found to be chemically distinct from most modern TTGs, yet the WRO shows the chemical signature of Archean TTGs despite being Cretaceous in age. The WRO therefore presents a unique opportunity to study the evolution of TTG magma similar to Archean continental crust.

In addition to its potential use as an analogue of Archean TTG, the WRO contains significant amounts of magmatic epidote. Magmatic epidote is a rare accessory mineral in granitic rocks most commonly found in post-Archean TTG suites (Zen & Hammarstrom, 1984). The presence of magmatic epidote has unique implications for the pressure and temperature conditions at which the WRO magma crystallized.

Because the WRO is an orthogneiss, questions arise as to how much any metamorphism may have altered the chemistry from that of the original igneous rock. A petrographic method for determining the degree of metamorphic recrystallization is proposed within this study and the degree of recrystallization is compared with the strength of the foliation. Metasomatic changes that would be expected for rocks that have been progressively metamorphosed are determined by

observing mineralogy, textures, and fabric strength between WRO samples. The results of this analysis determine the degree of metasomatic alteration within the WRO samples.

The petrogenetic history of the WRO is investigated using major, minor, and trace element data. Geochemical plots determine the likely source of the WRO magma as well as petrogenetic mechanisms that could explain the variability between samples. Fractional crystallization is modeled for many trace phases to determine the likely phases which controlled chemistry during fractional crystallization or partial melting. Finally, multiple evolutionary models are proposed for the WRO pluton which take the source material, intrusion, and petrogenetic/evolutionary history into account.

This study aims to answer three key questions:

1. Has metamorphism altered the original igneous geochemistry?
2. Is the WRO and analogue of Archean TTG?
3. What is the preferred petrogenetic model for the WRO and banded gneiss (BG) genesis?

2. REGIONAL GEOLOGY

2.1. Regional Geology of the Cascades

The Cascades Crystalline Core (Cascades core) lies within the Coast Plutonic Complex (Figure 2.1) which comprises a >1500 km long, mid-Cretaceous to Paleogene orogenic belt and magmatic arc lying along the northwestern rim of the North American continent extending from Washington to the Yukon (Brown et al., 2000; Stowell et al., 2007). The Coast Plutonic Complex lies between the Insular superterrane to the west and the Intermontane superterrane to the east (Monger et al., 1982). The Coast Plutonic Complex has been constructed by the metamorphism of large areas of sedimentary and volcanic rocks, the emplacement of large volumes of magma, and the accretion of sea floor and oceanic arc terranes (Brown et al., 2000).

The southernmost exposure of the Coast Plutonic Complex lies within the Northern Cascades crystalline core (Cascades Core) (Stowell et al., 2007). The Cascades Core underwent a period of major contractional orogenesis in the mid-Cretaceous which resulted in a strong northwest-southeast trending fabric present in both the fabric and lithologic distribution throughout the area (Paterson & Miller, 1998; Miller et al., 2006; Stowell et al., 2007). Northeast-southwest directed shortening resulted in the Ingalls Ophiolite Complex thrusting over the Chiwaukum Schist on the Windy Pass thrust which dips to the southwest (Miller, 1985; Paterson et al., 1994). This overthrusting resulted in southwest-vergent folding, southwest-directed thrusting, and shearing (Paterson et al., 1998; Miller & Paterson, 2001; Miller et al., 2006; Stowell et al., 2007). This shortening and later extension resulted in several shear zones developing in the area including the White River Shear Zone (named by Magloughlin, 1988) which is a reverse shear zone that separates the Napeequa Complex from the Nason terrane (Figure 2.2) (Stowell et al., 2007).

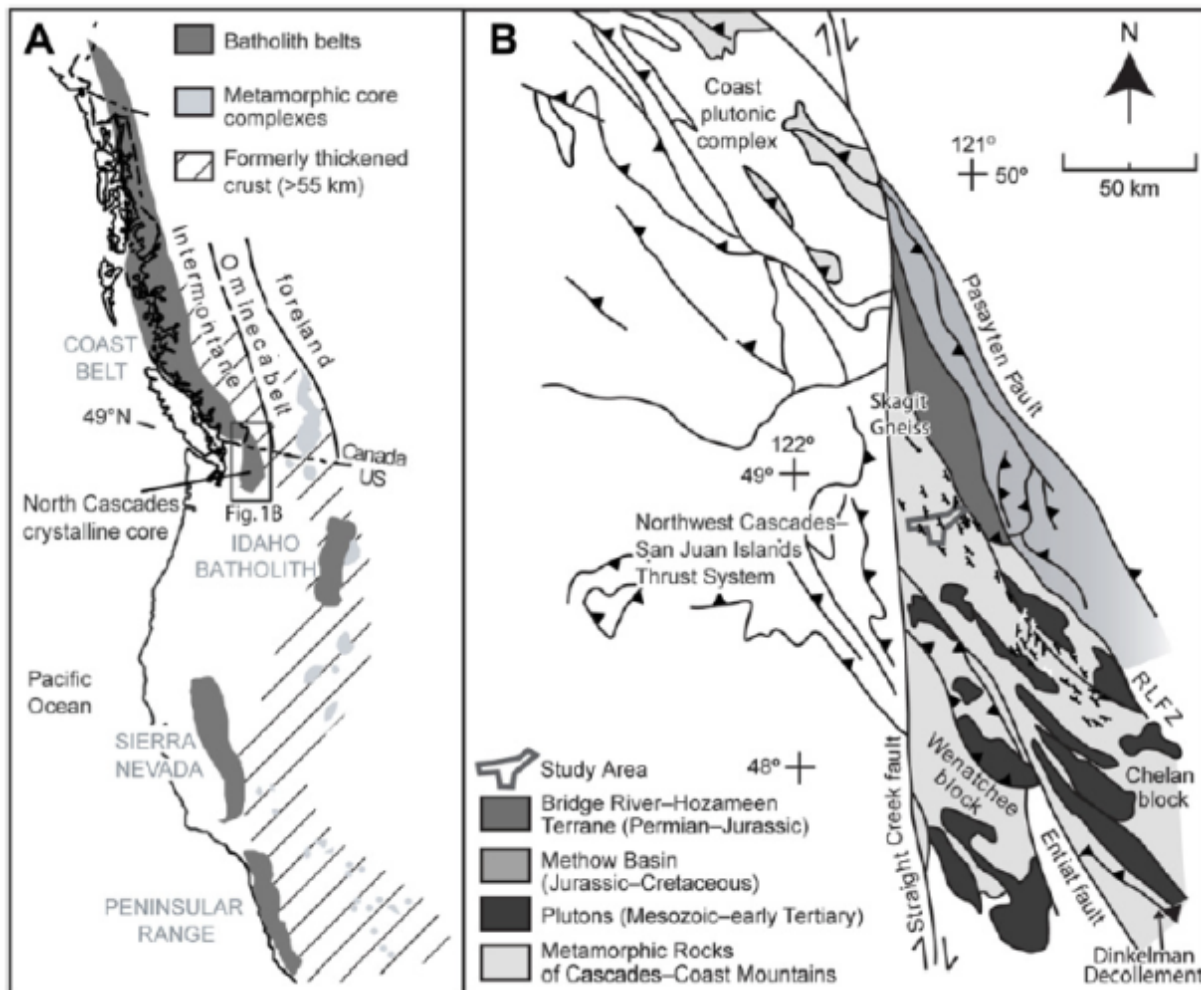


Figure 2.1. Figure from Wintzer (2012) showing the Intermontane superterrane, the extent of the Coast Plutonic Complex (A), and the North Cascades Crystalline Core (B).

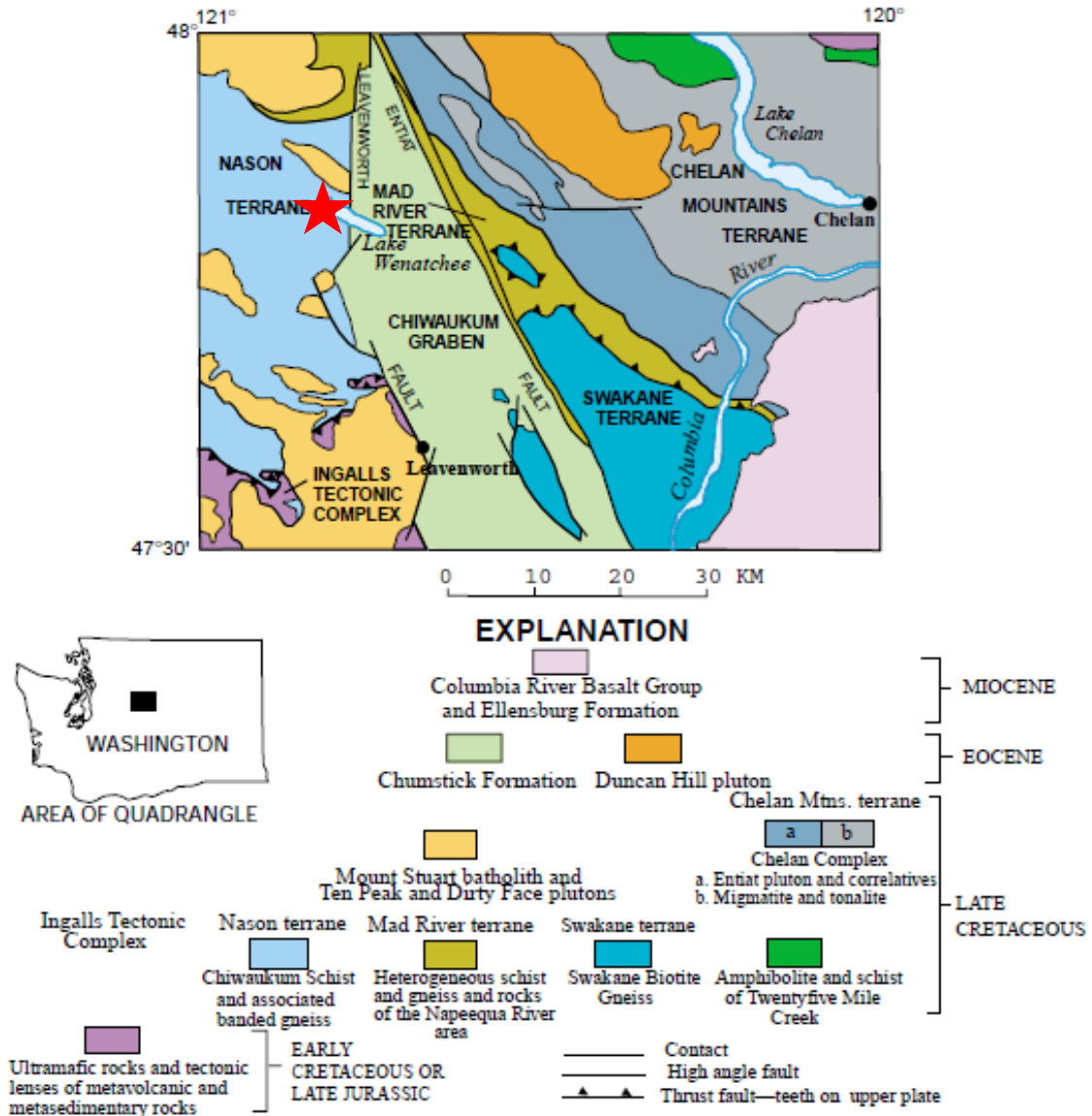


Figure 2.2. Generalized geologic map showing the five terranes of the North Cascades Mountains defined by (Tabor, et al., 1987). The red star indicates the general location of the study area (the Wenatchee Ridge Orthogneiss).

Two tectonic models have been proposed to explain the evolution of the Cascades Core (Miller & Paterson, 1992; Zuluaga & Stowell, 2008). The first model involves orogeny perpendicular contraction where the Insular superterrane collided with North America resulting in the burial and metamorphism of the Cascades Core (Miller & Paterson, 1992; Whitney & McGroder, 1989; Zuluaga & Stowell, 2008). The second model involves NE-SW dextral transpression occurring on a series of thrust and strike slip faults resulting in stretching within the Cascades Core (Brown & Talbot, 1989; Walker & Brown, 1991; Miller & Paterson, 1992). Evidence for Late Cretaceous thrusting and thermal relaxation and a rapid pressure increase presented by Stowell et al. (2007) supports the orogen normal contraction model to explain the formation of the Cascades Core (Zuluaga & Stowell, 2008).

2.2. Local Geology

2.2.1 North Cascade Mountains

Interpretations of the Northern Cascades before 1970 considered the area to be an in-place eugeo-synclinal metasedimentary and metavolcanic rock accumulation (Tabor, 1987). The idea that exotic components make up the Northern Cascades was first proposed by Danner (1970) who suggested the idea using fossil evidence from non-metamorphosed rocks west of the Straight Creek Fault (Tabor, 1987). Beck & Noson (1971) used paleomagnetic evidence to show that the western Cordillera was oriented differently than the North American continent. Using this evidence, Beck & Noson (1971) proposed that the western Cordillera, including the Stevens Pass area, was a separate plate that became welded to North America during the Tertiary. Using this and other evidence, Coney et al. (1980) proposed the existence of multiple suspect terranes along the entire western Cordillera. These terranes are considered by Coney et al. (1980) to be allochthonous to the North American continent and are thought to have been swept from the far

reaches of the Pacific ocean and accreted to the Cordilleran margin during the Mesozoic to Cenozoic. The Northern Cascades was included as one of the suspect terranes within the state of Washington (Coney et al., 1980; Tabor, 1987). The North Cascades crystalline core is comprised, at least in part, of the tectonostratigraphic terranes defined by Tabor et al. (1987). These five terranes, while considered tentative, include the Nason terrane, the Ingalls Tectonic Complex, the Swakane terrane, the Mad River terrane, and the Chelan Mountains terrane (Tabor et al., 1987). Structural levels within the Cascades core from lowest to highest are (1) the Swakane Gneiss and Napeequa Complex (Chelan Mountains terrane), (2) the Chiwaukum Schist and Nason Ridge Migmatite Gneiss (Nason Terrane), and (3) the Ingalls Ophiolite Complex (Stowell et al., 2007). The five tectonostratigraphic terranes are defined as fault-bounded geologic entities with distinctive stratigraphic sequences and structural histories different from those of neighboring terranes. It should be noted that features which define the terranes, such as the bounding faults can be difficult to distinguish in the highly metamorphosed areas of the North Cascades (Tabor, 1987). A summary of major characteristics of each terrane are shown on Table 2.1.

Table 2.1. Summary of major characteristics of each terrane as summarized by Tabor (1987).

Characteristics	Nason terrane	Ingalls Tectonic Complex	Swakane terrane	Mad River Terrane	Chelan Mountains terrane
Protolith Rock Type	Al-rich shale overlying shale and mafic volcanic rocks and minor limestone; rare ultramafite; fairly homogenous	Ultramafite, diabase, gabbro, basalt, gray-wacke, shale, and chert; heterogeneous	Sandstone of shale; possibly dacitic pyroclastic and rare mafic volcanic rocks and marble; no ultramafite; highly homogenous	Chert, mafic volcanic rocks, limestone, and minor shale; gabbroic intrusions; common ultramafite; heterogeneous	Cherty graywacke, arkose, shale, mafic volcanic rocks, and marble; minor ultramafite; gabbroic to tonalitic igneous plutons; heterogeneous
Contact Relations	Thrust contact with the Ingalls Tectonic Complex; probably imbricated with the Mad River terrane in a wide tectonic zone	Thrust over the Nason terrane; contact with other terranes covered by Tertiary rocks	In thrust contact with the Mad River terrane	Probably imbricated with the Nason terrane; probably thrust over the Swakane terrane; probably faulted against the Chelan Mountains terrane	Probably faulted against the Mad River terrane
Protolith Age	Probably Late Jurassic to Late Cretaceous	Late Jurassic	Precambrian	Pre-late Cretaceous	Permian(?) or Triassic or younger metasedimentary and metavolcanic rocks; Triassic plutons

2.2.2 The Nason Terrane

This study focuses on the Wenatchee Ridge Orthogneiss which is found within the Nason Terrane. The Nason Terrane is bounded to the east by the Leavenworth fault and by other faults including the Evergreen fault in the Straight Creek fault zone to the west (Figure 2.2) (Tabor, 1987). The terrane is overthrust by the Ingalls Tectonic Complex to the south and appears to be faulted against the Mad River terrane to the northeast (Tabor, 1987). The Nason Terrane is composed predominantly of the Chiwaukum Schist, Nason Ridge Migmatite Gneiss, and the Wenatchee Ridge Orthogneiss. The Nason Terrane is additionally intruded by several c. 96-91 Ma plutons including the Mt. Stuart Batholith, the Ten Peak pluton, and the Dirty Face pluton (Tabor et al., 1987; Stowell et al., 2011).

There is a north-south geologic variation across the Nason terrane which is distinguished by lithologic, chemical, and cooling history variations (Magloughlin, 1993). Cooling histories and time-temperature paths indicate rapid cooling in the south part of the terrane and slower cooling in the north (Magloughlin, 1993). Especially important to this study is the variation in plutonic rocks between the north and south parts of the terrane. The north contains metaluminous to peraluminous tonalite-gneisses and pegmatites; some of which contain magmatic epidote (Magloughlin, 1993). The south largely contains the Mount Stuart Batholith which is calc-alkaline and does not contain magmatic epidote (Magloughlin, 1993). Additionally, the southern Mount Stuart Batholith shows a large contact aureole while the northern intrusions, such as the Dirty Face Pluton, show no evidence for an aureole (Magloughlin, 1993). Magloughlin (1993) proposed three hypotheses which can account for the variations from north to south in the terrane. North-side-up tilt, large scale folding, or north-side-up major faults or shear zones are all possible mechanisms to explain the north-south variation (Magloughlin, 1993).

2.2.3 Deformation

Deformation within the Nason Terrane is best recorded by the Chiwaukum Schist and meta-tonalite gneisses found in the north and central parts of the terrane (Magloughlin, 1993). Deformation throughout the Nason Terrane is variable and may be largely erased to the south by the contact aureole associated with the Mount Stuart Batholith (Magloughlin, 1993). Primary layering is preserved in the Chiwaukum Schist in many places and records the deformational history along with quartz veins which were likely formed early in the structural evolution (Magloughlin, 1993). Magloughlin (1993) recognized four deformation events within the Nason terrane which are distinguished by a variety of microstructures predominately within the Chiwaukum schist. The dominant foliation seen in the Chiwaukum schist and WRO was created by the third deformational event (D_3).

2.2.4 Metamorphism

Within the Chiwaukum Schist and Nason Ridge Migmatite Gneiss in the Southern Part of the cascades core, three metamorphic events have been identified as M1, M2, and M3 (See Table 2.2 for a summary of metamorphic events (Evans & Davidson, 1999; Stowell & Tinkham 2003; Stowell et al., 2007). The oldest metamorphic minerals (M1) predate intrusion ages of the Late Cretaceous plutons, including the Mount Stuart Batholith, found within the Cascades core (Evans & Davidson, 1999; Stowell et al., 2007). M1 minerals include relatively high pressure phases such as garnet, staurolite, and kyanite in some areas (Plummer, 1980). The M1 crystallization may have occurred at 118 ± 15 Ma (Magloughlin & Edwards, 2003). This date is based on garnet Sm-Nd whole rock isochrons on a sample from Icicle Canyon, SW of Leavenworth.

Table 2.2. Modified table from Stowell et al. (2007) summarizing metamorphic events in the study area. M1 regional extent, pressures, and temperatures are poorly known. M1 amphibole was noted by Paterson et al. (1994). M1 age range is based on Sm-Nd chronology by Magloughlin (1993) (118 Ma) and data from (Stowell & Tinkham, 2003).

Metamorphic events affecting the <u>Nason Terrane, North Cascades, Washington</u>			
Metamorphic Events	Metamorphic Facies	Pressure (kbar)	Time (Ma)
M1 regional metamorphism	amphibolite?	3-6?	118-120
M2 contact metamorphism	amphibole-andalusite	<2-4	93-96
M3 regional metamorphism	amphibolite	6--9	86-88

M2 minerals such as andalusite, sillimanite, and cordierite are found near the late Cretaceous plutons and are inferred to have a contact metamorphic origin (Evans and Berti, 1986; Evans and Davidson, 1999). According to Plummer (1980), the M2 event was a dynamothermal contact metamorphism event which derived its heat from the intruding Mount Stuart batholith. Evidence for this includes the restriction of lower pressure M2 minerals (andalusite, sillimanite, and cordierite) to areas generally near the Mount Stuart batholith (Plummer, 1980). Evans & Davidson (1999) infer a maximum pressure of 3.0-3.5 kbar for the M2 event based on the range of the andalusite zone and the 3.75 ± 0.25 kbar triple point for Al_2SiO_5 polymorphs which corresponds to hydrated pelitic assemblages of minerals.

The M3 metamorphic event is a Barrovian-type event which occurs regionally on the North and East sides of the Mount Stuart batholith and overprints the M2 event (Evans and Davidson, 1999). The M3 event was recognized by the pseudomorphs of Staurolite + Kyanite + Biotite + Muscovite \pm Plagioclase after M2 andalusite as well as the Staurolite + Chlorite

assemblage after M2 cordierite in metamorphosed rocks north of the Mount Stuart batholith (Evans & Berti, 1986; Evans & Davidson, 1999; Stowell et al., 2007). Using thermobarometric, petrographic, and geochronologic data, the M3 mineral assemblages have been shown to indicate that the M3 event was a medium to high pressure metamorphic event which postdates the intrusion of the Mount Stuart batholith (Evans & Berti, 1986; Evans & Davidson, 1999; Stowell et al., 2007). Further thermobarometric studies indicate that there is a pressure gradient of the M3 metamorphism such that the pressures increase from southwest to the northeast across the Nason terrane (Stowell et al., 2007). The presence of this pressure gradient is debated across the Mount Stuart batholith area due to evidence of higher pressure M3 metamorphism in veinlets proposed by Evans & Davidson (1999).

2.3. Geologic Units

The Chiwaukum Schist

The majority of the Nason Terrane is composed of Chiwaukum Schist which is a predominantly pelitic to semi-pelitic mica schist (Tabor, 1987; Magloughlin, 1994). The Chiwaukum Schist commonly contains one or more of the aluminosilicate minerals kyanite, sillimanite, and/or andalusite as well as common amphibolite layers and minor amounts of quartz-mica schist, calc-silicates, cotecule, and marble (Magloughlin, 1986; Tabor, 1987). The Chiwaukum Schist also contains ultramafic tremolite, talc-anthophyllite, and serpentized metaperidotite which are concentrated near the terrane's bounding faults (Tabor, 1987). The metasediments of the Chiwaukum Schist are thought to be oceanic arc derived with minimal continental contamination (Magloughlin, 1993). Mixed schist and gneiss areas are common throughout the Chiwaukum Schist consisting of thin felsic sills, some of which are likely correlated with the Wenatchee Ridge Orthogneiss (Magloughlin, 1986).

There are three major metamorphic events recognized within the Chiwaukum Schist which are referred to as M1, M2, and M3 (Evans and Davidson, 1999). These events are detailed in section 2.2.4. The protolith age of the Chiwaukum Schist is unknown, but interpretations invoking the unit's relationship with the Ingalls Tectonic Complex, if correct, would make the protolith age Late Jurassic to Late Cretaceous (Tabor, 1987). However, Magloughlin (1993) used Sm-Nd and Rb-Sr dating to put a maximum age of Late Paleozoic to a possible minimum age of late Triassic on amphibolites from the Chiwaukum Schist.

Wenatchee Ridge Gneiss – Terminology

The other major lithology comprising the Nason terrane is the Wenatchee Ridge Gneiss which intrudes the Chiwaukum schist (Magloughlin, 1986). Recent researchers (e.g., Miller & Paterson, 2001; Stowell et al., 2011; Zuluaga & Stowell, 2008) have introduced the term “Nason Ridge Migmatite Gneiss” (from descriptions of the light colored migmatites on Nason Ridge by Tabor et al. (1993)) to refer to the banded gneiss outside of the orthogneiss pluton which has also been referred to as the “Wenatchee Ridge Gneiss” or “Wenatchee Ridge Orthogneiss.” The unit term “Wenatchee Ridge Gneiss,” when cited by older researchers (ex. Van Diver, 1964) typically refers to both the Nason Ridge Migmatite Gneiss (NRMG) and the Wenatchee Ridge Orthogneiss (WRO), the latter being a term introduced by Magloughlin (1986). This study will refer to the NRMG (or banded gneiss within the Chiwaukum Schist) separately from the concentration of felsic gneiss on Wenatchee Ridge, which will be referred to as the Wenatchee Ridge Orthogneiss.

Nason Ridge Migmatite Gneiss

As summarized by Zuluaga & Stowell (2008), four possible methods exist to explain the formation of migmatites such as the NRMG. These four methods include metasomatism, partial

melting, injection of foreign magma, and metamorphic differentiation (Brown, 1994; Winter, 2010). Van Diver (1964, 1967) interpreted the WRG to have formed by extensive metasomatism of the Chiwaukum Schist. Work by Magloughlin (1986) showed the WRG to be an orthogneiss composed mostly of two distinct phases; a fine grained biotite tonalite gneiss and a later, coarse-grained muscovite tonalite gneiss. Tabor (1987) interpreted the WRG to be derived from the Chiwaukum Schist by both metamorphic and igneous processes, inferring that both partial melting and magmatic injection were involved. Alternatively, Miller & Paterson (2001) have suggested that the majority of the Nason Ridge Migmatite Gneiss originated by magmatic injection alone. More recently, Zuluaga & Stowell (2008) have re-visited the idea that the NRMG evolved by two processes: partial-melting of country rock and intrusion of externally derived tonalitic melts. Evidence for the involvement of partial melting is based on the estimated temperature for the Nason Ridge Migmatite Gneiss (625°C-806°C) exceeding the estimated wet solidus (655°C at 10 kbar - 703°C at 3 kbar) proposed by Zuluaga & Stowell (2008). The partial melting theory explains the origin of discontinuous quartz-plagioclase lenses present throughout the Nason Ridge Migmatite Gneiss, however, many of these discontinuous quartz-plagioclase lenses could also be interpreted as entirely boudinaged dikes or sills (Magloughlin pers. comm., 2012). Indeed, very large boudins of the post-WRO tonalite pegmatite are also boudinaged.

Wenatchee Ridge Orthogneiss

The Wenatchee Ridge Orthogneiss is the lowest structural level within the Nason terrane and is the focus of this study (Stowell et al., 2007). The WRO is an approximately 93 Ma muscovite rich tonalite-trondhjemite to rarely granodiorite pluton which cores a northwest trending antiform overlain by the Nason Ridge Migmatite Gneiss and the Chiwaukum Schist to the Northeast and Southwest (Magloughlin, 1986; Stowell et al., 2007). The WRO is foliated and

deformed and the intrusive contacts and foliation within the WRO are concordant to the foliation in the Chiwaukum Schist (Magloughlin, 1986, 1994). This relationship provides evidence that the WRO intruded synchronously with regional deformation which deformed the Chiwaukum Schist. Meta-igneous, meta-sedimentary, and ultramafic blocks and bodies as large as tens of meters in diameter are present in the WRO with common metasomatic (blackwall) reaction zones separating the ultramafic rocks from the gneiss (Magloughlin, 1986). Many of these ultramafic bodies are interpreted by Tabor (1987) to be pieces of the overthrust Ingalls Tectonic Complex, but they may have a different origin. Because the WRO has been deformed as well as at least weakly metamorphosed, early interpretations of the unit considered it to be the metasomatic equivalent of the Chiwaukum Schist (Tabor, 1987; VanDiver, 1967). Indeed, many of the smaller gneissic intrusions appear to have adjusted mineralogically to amphibolite facies conditions (Magloughlin, 1994). However, geologic evidence indicates that the majority of the tonalitic gneiss in the Wenatchee Ridge area has an igneous origin. This evidence includes: igneous oscillatory zoning in plagioclase, the presence of large ultramafic bodies within the gneiss which are most easily interpreted as xenoliths (or stoped blocks), cross-cutting relationships with the Chiwaukum Schist, and discordant amphibolite and meta-sedimentary xenoliths within the gneiss (Magloughlin, 1986; Tabor, 1987). Some exposures of the WRO show cross-cutting relationships which indicate that there are ten or more tonalite phases, with differing mineralogies, that all intrude the Chiwaukum Schist (Magloughlin, 1994).

Extent of the Wenatchee Ridge Orthogneiss

There have been multiple interpretations of the WRO outline. These interpretations are generally based on field observations of areas which contain a certain percentage of tonalite in outcrop such that it is the dominant rock type within the pluton boundary. Figure 2.4 shows the

Wenatchee Ridge Gneiss as defined by Stowell et al. (2011) within the Nason ridge migmatite gneiss. Figures 2.5, 2.6, and 2.7 show the interpreted WRO boundaries by Tabor et al. (1987), Zuluaga & Stowell (2008), and Magloughlin (1993), respectively. Figures 2.8 and 2.9 show the WRO and banded gneiss outlines as defined by Tabor et al. (1987) and these boundaries will be used to distinguish two groups of samples taken for this project. Samples which fall within this WRO boundary will be referred to as WRO samples, and those falling within the banded gneiss will be referred to as BG samples.

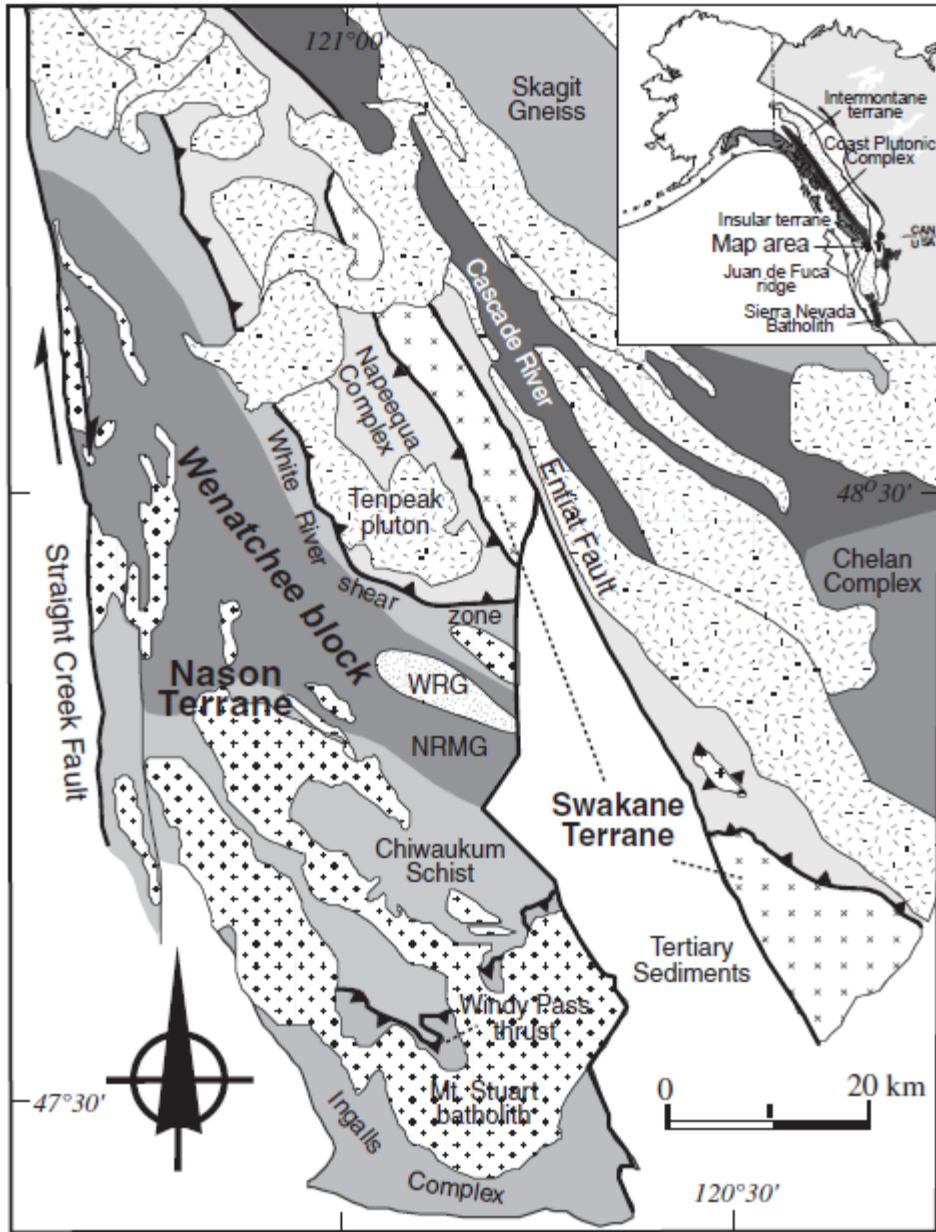


Figure 2.4. Figure from Stowell et al. (2011) showing the Wenatchee Ridge Orthogneiss (Wenatchee Ridge Gneiss in this figure) and the Nason Ridge Migmatite Gneiss.



Figure 2.5. Figure showing the Wenatchee Ridge Orthogneiss outline as defined by Tabor et al. (1987).



Figure 2.6. Figure showing the Wenatchee Ridge Orthogneiss outline as defined by Zuluaga & Stowell (2008).



Figure 2.7. Figure showing the Wenatchee Ridge Orthogneiss outline as defined by Magloughlin (1993).

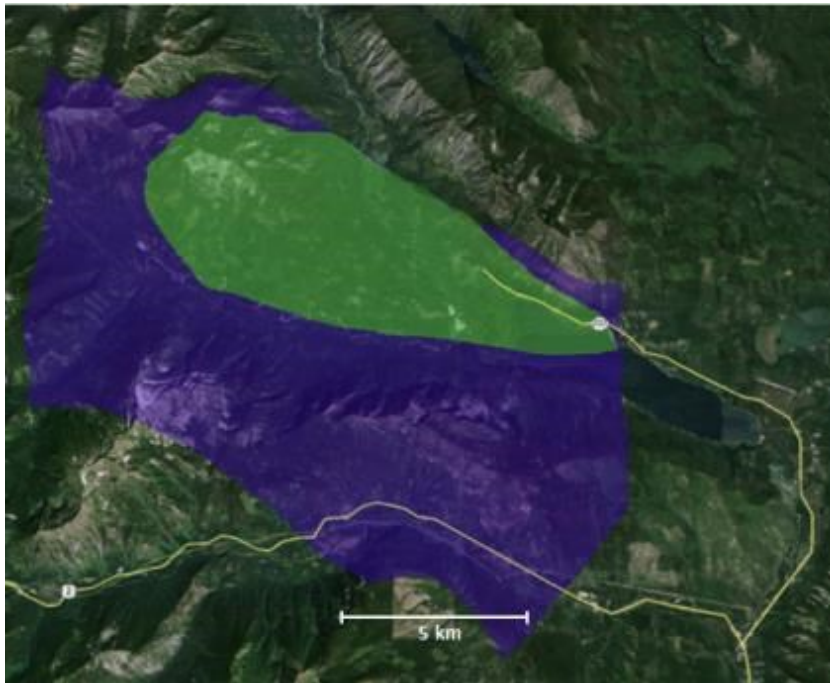


Figure 2.8. Figure showing the WRO (green) and banded gneiss (blue) boundaries defined by Tabor et al. (1987) which are used to separate the samples into WRO and BG samples.

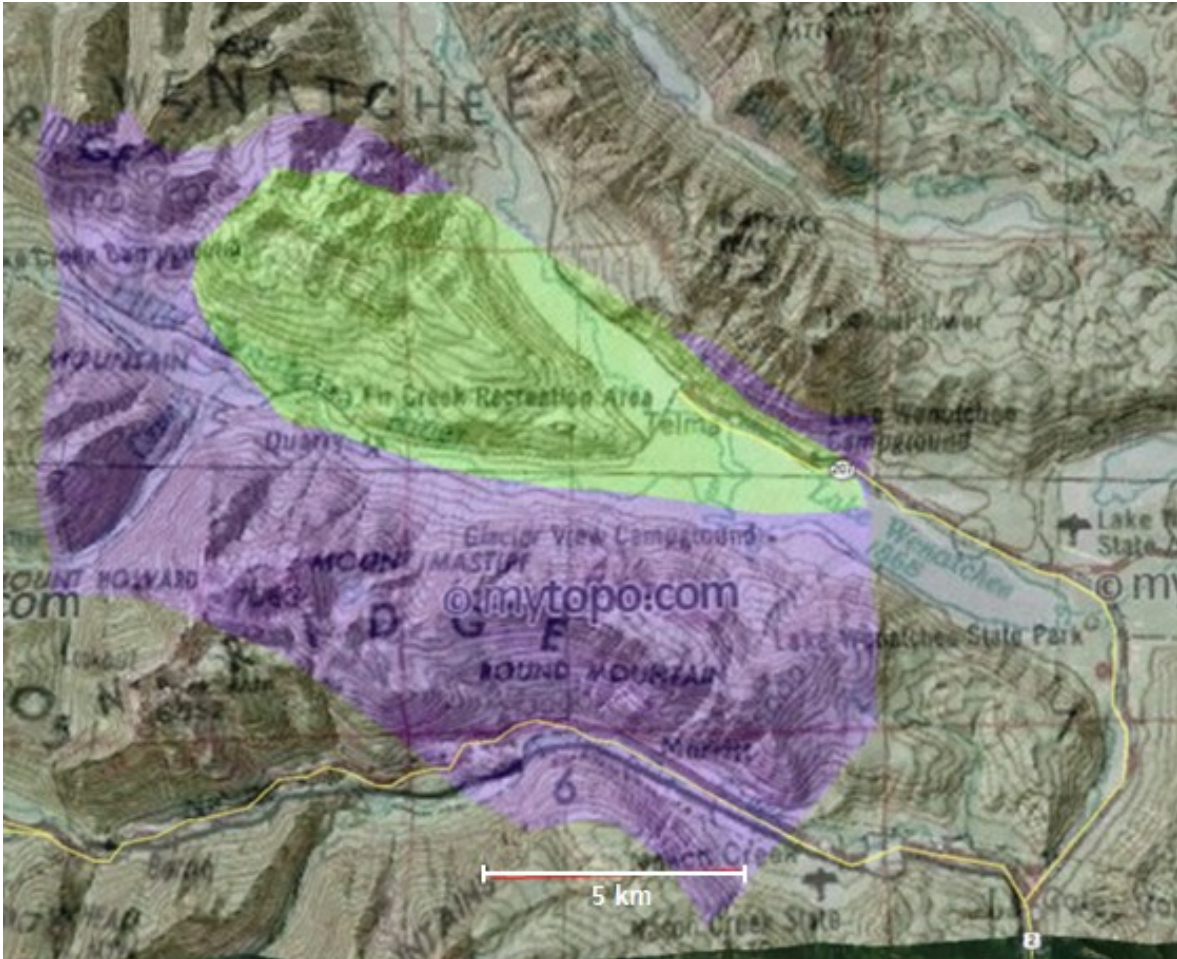


Figure 2.9. Figure with topo map (mytopo.com) showing the WRO (green) and banded gneiss (blue) boundaries defined by Tabor et al. (1987) which are used to separate the samples into WRO and BG samples.

3. TONALITE REVIEW AND THE ARCHEAN TTG PROBLEM

3.1. Tonalite Review and Importance

This chapter provides a summary of the definition, evolution, geochemistry, and relationships between TTG and associated rock types. Because a comparison between Archean TTGs and the WRO is an important part of this study, one goal of this chapter is to offer an overview of the petrogenesis of both Archean and post-Archean TTG suites and their connections to different tectonic settings.

Understanding tonalite-trondhjemite-granodiorite (TTG) suites is crucial to understanding the petrogenesis of the andesitic bulk composition characteristic of all continental crust (Rudnick, 1995). According to Martin et al. (2005) and Condie (2005), approximately 90% of 4.0-2.5 Ga continental crust is part of the TTG suite of rocks. Understanding the evolution of TTG suites will inherently lead to a greater understanding of early continental evolution and quantifying changes in TTG petrogenesis over time is crucial to understanding Earth's evolution (Condie, 2005).

The details of TTG petrogenesis over time have been the topic of many papers, questions, and debates within igneous petrology and Archean TTG literature (Rollinson and Martin, 2005). In order to fully understand TTG petrogenesis models, TTG suites and related rock types (adakites and sanukitoids) must first be well defined.

3.2. Definitions

TTG

Tonalite, trondhjemite, granodiorite suites are igneous rocks that are low in K-feldspar and predominately made up of quartz, plagioclase, and biotite (Martin et al. 2005). Major

element compositions of TTGs are 65-73 wt% SiO₂, alumina saturation indices (ASI or A/CNK where A/CNK= molar Al₂O₃/(CaO+Na₂O+K₂O) of 1.0 ± 0.05, and Mg numbers (molar ratio of MgO/(MgO+FeO)) of 0.3-0.5 (see Table 3.1) (Rapp et al., 2003). TTG suites have also been referred to in earlier research by Drummond and Defant (1990) as TTD (tonalite-trondhjemite-dacite). Granodiorite and dacite are intrusive and extrusive equivalents and TTG or TTD will be used interchangeably herein. Drummond and Defant (1990) also separated TTD into two categories; high-Al TTD and low-Al TTD. Low-Al TTD is low in Sr (<200ppm), shows a negative Eu anomaly, slightly increased light rare earth elements (LREEs), and the heavy rare earth elements (HREEs) form a flat line when plotted on a normalized spider plot (Drummond et al., 1990). High-Al TTD has high Sr (>300ppm up to >2000ppm), no (or a very small) Eu anomaly, low to medium K/Rb concentrations (typically below 550), high LREE concentrations, low HREE concentrations, low (<15ppm) Y, and low (<11ppm) Nb (Drummond et al., 1990). Tonalite and granodiorite can be identified on the standard IUGS classification of igneous rocks (Figure 3.1). Trondhjemite is an older term for a rock which is essentially a leucotonalite.

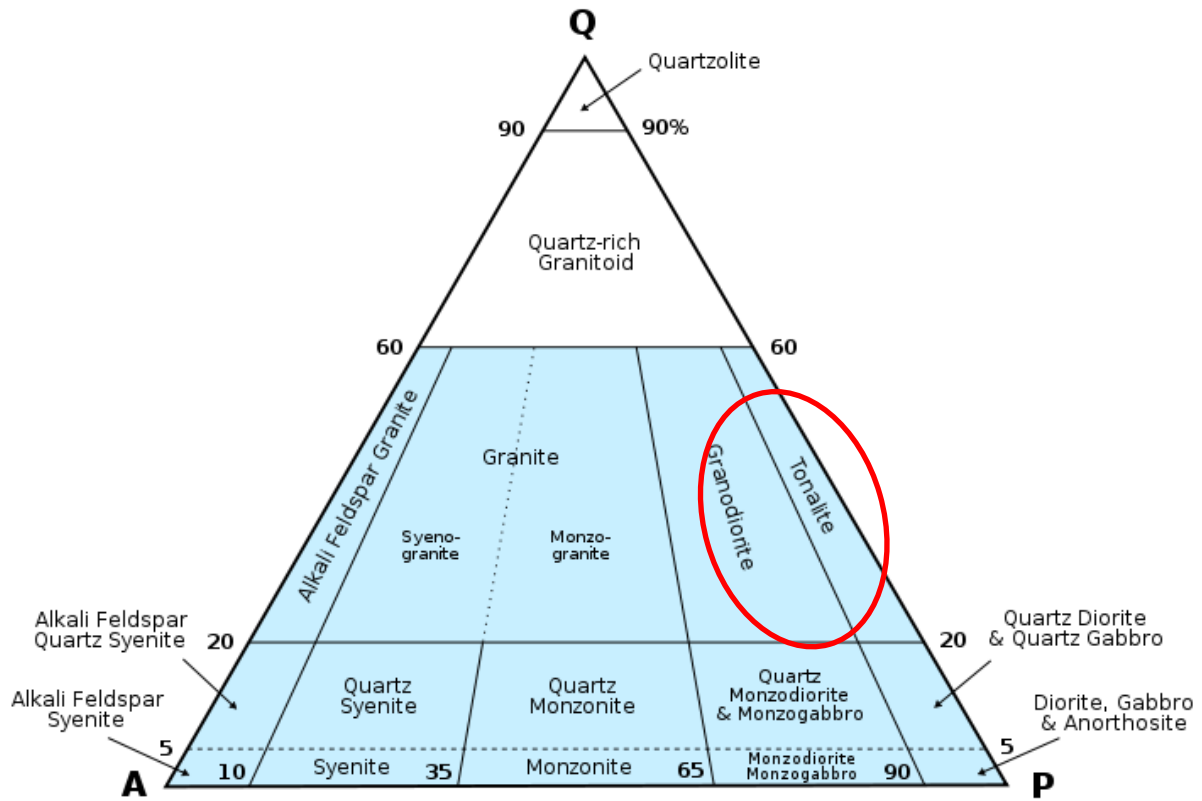


Figure 3.1. IUGS classification showing granodiorite and tonalite QAP compositions (after Streckeisen (1976)).

Table 3.1. Average compositions for high-Al TTGs (Drummond and Defant, 1990), typical TTGs (Condie, 2005), high and low silica adakites (Martin et al., 2005), and sanukitoids (Martin et al., 2005).

	High-Al TTGs					Low Silica Adakite	High Silica Adakite	Sanukitoid	TTGs			
	Cenozoic	Mesozoic	Paleozoic	Proterozoic	Archean				Early Archean	Late Archean	Proterozoic	Phanerozoic
wt. %												
SiO ₂	65.88	68.8	70.07	70.4	69.74	56.25	64.8	58.76	70.4	68.3	67.3	65.9
Al ₂ O ₃	17.49	17.7	16.54	16.05	15.08	15.69	16.64	15.8	15.2	15.5	15.8	16.5
TiO ₂	0.3	0.27	0.23	0.29	0.3	1.49	0.56	0.74	0.31	0.42	0.47	0.47
Fe ₂ O ₃	3.2	1.1	0.59	0.79	2.55	6.47	4.75	5.87	2.79	3.42	4.04	4.11
FeO		1.1	0.88	1.42								
MnO	0.08	0.06	0.06	0.06	0.03	0.09	0.08	0.09	0.06	0.07	0.08	0.09
CaO	4.79	4.3	3.14	2.27	3.04	7.69	4.63	5.57	2.74	3.26	3.42	4.36
MgO	1.26	0.69	0.8	0.66	1.23	5.15	2.18	3.9	0.96	1.39	1.48	1.67
K ₂ O	1.44	0.9	1.34	2.59	1.41	2.37	1.97	2.78	2.22	2.2	2.3	2.14
Na ₂ O	4.25	4.9	5.5	4.84	5.44	4.11	4.19	4.42	4.71	4.51	4.33	4
P ₂ O ₅	0.13	0.08	0.08	0.09	0.08	0.66	0.2	0.39	0.1	0.14	0.14	0.12
LOI	3.2	1.1	0.59	0.79	0.97							
Total	100.03	100.5	99.88	100.25	99.87	99.97	100	98.32	99.49	99.21	99.36	99.36
ppm												
Ni	7				15	103	20	72	17	22	23	12
Cr	6	6			19	157	41	128	45	35	55	32
Ba	670	512	328	855	301	1087	721	1543	500	769	717	716
Rb	23	17	28	76	43	19	52	65	76	67	63	63
Sr	760	546	613	547	559	2051	565	1170	362	515	473	493
Zr	65	117			77	188	108	184	152	154	152	122
Y	3				3	13	10	18	8.5	9.1	17.3	14.5
Nb	6				4	11	6	10	6.1	6.2	7.1	6.7
Th									4.1	8.1	6.1	7.6
Hf									3.8	4.7	4.3	3.4
U									1.2	1.5	2.1	1.9
La	9.3	13.3	8.2		16	41.1	19.2	59.9	22	36	26	17
Ce	17.1	25.3	16.2	38.5	23	89.8	37.7	126	40	65	45	34
Nd	9.3	12	8.3	15.4	6.4	47.1	18.2	54.8	16	25	18	16
Sm	1.3	1.7	1.7	2.99	1.8	7.8	3.4	9.8	2.9	4.2	3.5	3.1
Eu	0.6	0.67	0.52	0.859	0.6	2	0.9	2.3	0.82	1.07	0.95	0.84
Gd		1.3		2.44	1.02	4.8	2.8	6	2.2	2.9	3	2.8
Tb			0.22		0.2				0.31	0.38	0.49	0.4
Dy		0.85	0.635	1.87	0.68	2.8	1.9	3.2				
Ho					0.14							
Er				0.963	0.34	1.21	0.96	1.41				
Yb	0.55	0.4	0.29	0.896	0.45	0.93	0.88	1.32	0.82	0.71	1.33	1.16
Lu	0.05	0.05	0.05		0.12	0.08	0.17	0.26	0.14	0.11	0.23	0.18
K/Rb	519	436	487	299	283							
Rb/Sr	0.03	0.045	0.046	0.148	0.081							
K ₂ O/Na ₂ O	0.34	0.18	0.24	0.54	0.26	0.58	0.47	0.63	0.51	0.51	0.56	0.68
Mg#						0.61	0.48	0.57	40.8	46.2	43.2	45.4
Sr/Y						162.21	55.65	63.98	72	89	37	56
(La/Yb) _n	16.91	33.25	28.28		35.56	29.32	14.44	29.92	25	36	14.2	11.3
Nb/Ta									12	13	9.9	12.2
Ta									0.41	0.84	0.72	0.75

Adakite

Adakites and sanukitoids are commonly mentioned in research concerning TTGs. Adakites are intrusive or volcanic rocks typically in Cenozoic arcs that are commonly attributed to the subduction of young oceanic lithosphere (Drummond and Defant, 1990). They were first described by Kay (1978) and named for the place of their discovery, Adak Island, Alaska. Early research by Drummond and Defant (1990) defines adakite as a specific type of high-Al TTD with lower Y, Sc, Yb, and increased Sr/Y, La/Yb, Sr, and Zr/Sm compared to other TTD's. Although adakites are considered to be slab melt derived, research by Castillo (2006) suggests that some adakites may develop through fractional crystallization of amphibole bearing basaltic magmas. In general, adakites have trace element geochemistry very similar to TTG's but are more mafic (Drummond and Defant, 1990). Adakites can be separated by silica content into high silica adakites (with $\text{SiO}_2 > 60$ wt.%) and low silica adakites (with $\text{SiO}_2 < 60$ wt.%) (Martin, et al. 2005). High silica adakite (HSA) are suggested to have formed from melts derived from subducted basalt slabs that have interacted with peridotite, whereas low silica adakites (LSA) are formed by melting of a peridotitic mantle wedge whose composition has been modified by reaction with felsic slab-melts (Martin et al., 2005). LSA typically has higher REE concentrations and a positive Sr anomaly compared with HSA (Figure 3.2; Martin et al., 2005). Adakites are almost always associated with subduction and crustal melting and are therefore inherently related to both TTG suites and sanukitoids (Martin et al., 2005).

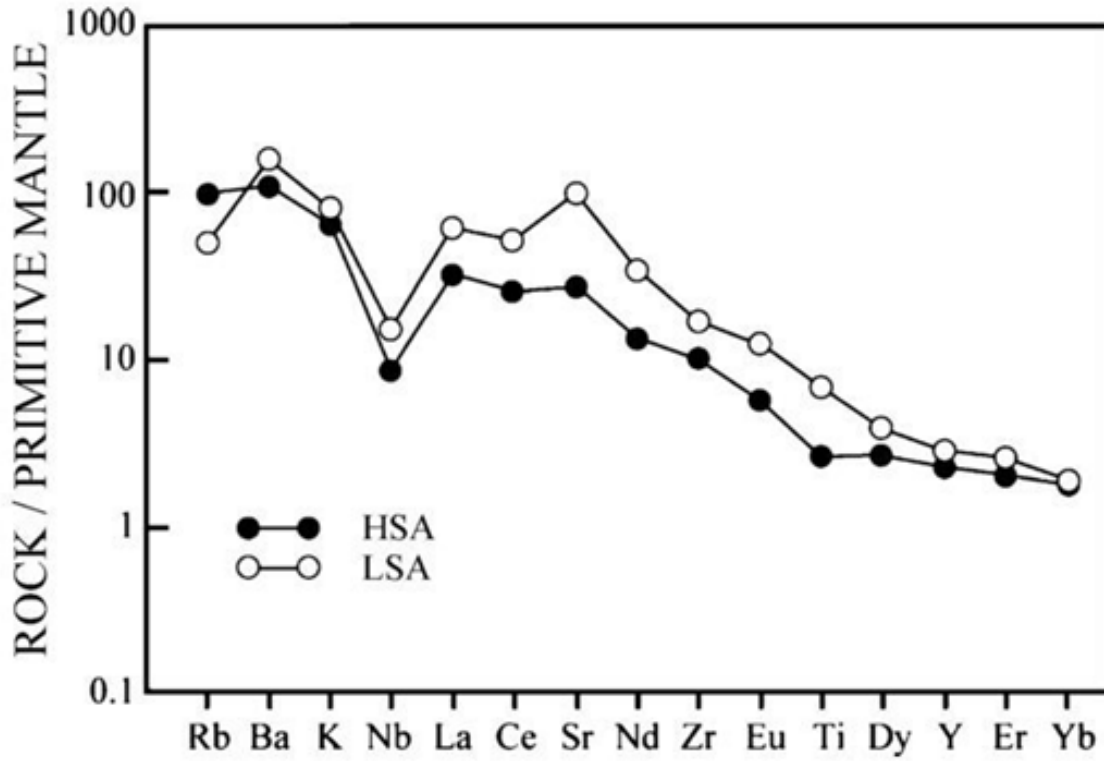


Figure 3.2. Trace element Spider diagram from Martin et al. (2005) showing how LSA differs from HSA. Values were normalized to primitive mantle from McDonough et al. (1992).

Sanukitoids

Sanukitoids are essentially high-Mg diorites that make up a small amount of Archean terrains and are proposed to have formed by the re-melting of mantle rocks that have been metasomatized by ~40% TTG type melts (Smithies and Champion, 2000). Sanukitoids are similar to TTG suites in that they are associated with the partial melting of basaltic crust (Martin et al., 2005). Chemically, sanukitoids are possibly analogous to low silica adakites and are distinguished by higher Mg-number, Ni, Cr, and LIL element concentrations than TTG's (Smithies and Champion, 2000). Characteristic sanukitoid compositions of ~ 200ppm Cr, ~100ppm Ni, ~60% SiO₂, and Mg-numbers of around 60 require a more mafic (mantle) source than Archean TTGs (Smithies and Champion, 2000).

3.3. Adakite-TTG connection

TTG suites have been shown to be the compositional analogue of HSA that form in subduction zones through significant mantle interaction, but little direct melting of the mantle wedge (Martin et al., 2005). Adakite and TTG are similar in REE characteristics (Figure 3.3). This chemical link leads to the assumption that the formation of TTGs, like adakites, does not involve much melting of the mantle wedge and occurs predominately in subduction zones by partial melting of the down-going oceanic crust (Martin et al., 2005; Drummond and Defant, 1990). The idea of this compositional similarity indicating similar petrogenesis was first proposed by Drummond and Defant (1990). Conversely, Condie (2005) provides geochemical evidence suggesting that TTG's and adakites are not the same chemically and therefore may have different origins. Kamber et al. (2002) also proposed that adakites and TTGs are not exactly the same but are instead related by fractional crystallization. A fractional crystallization relationship is rejected by Getsinger et al. (2009) who claim that intermediate products like

andesite would be present as part of this process and are not found with natural TTGs. Condie (2005) also rejects the idea of a fractional crystallization relationship between TTG and adakite due to the apparent absence of large volumes of mafic cumulate material and incorrect trace element trajectories from batch melting experiments, particularly the low La/Yb values.

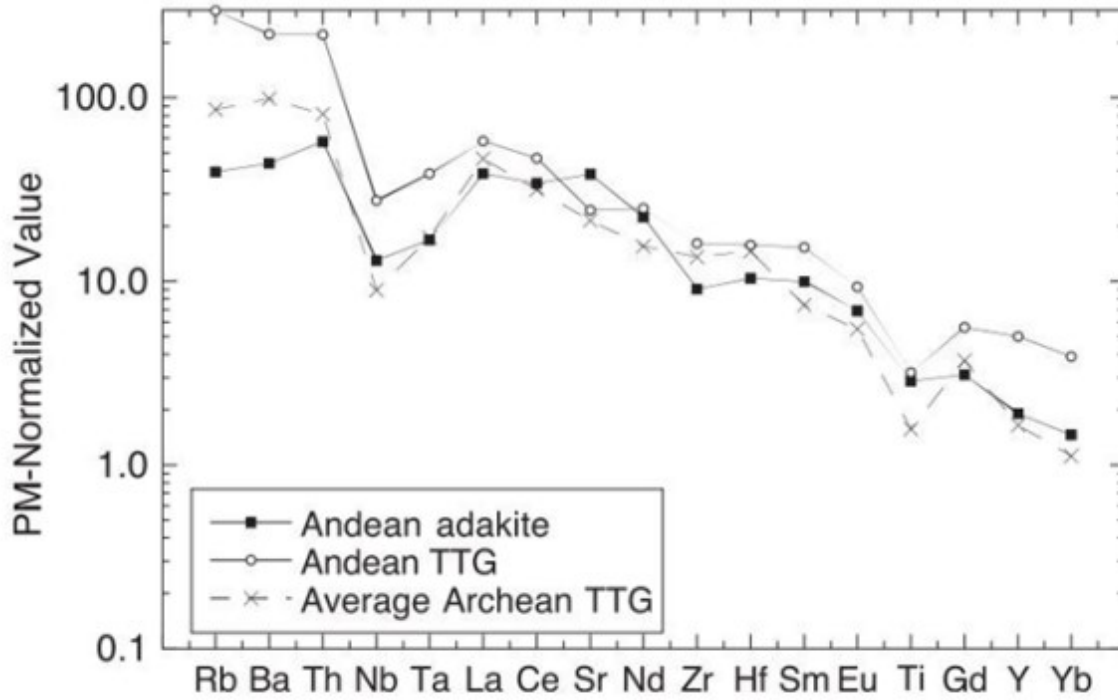


Figure 3.3. Normalized Spider plot from Condie (2005) showing the compositional relationship between “modern” adakite, TTG, and Archean TTGs. Data normalized to primitive mantle from Sun and McDonough (1989).

3.4. Archean vs. Post-Archean TTGs

Archean crust tends to belong to the TTG suite of rocks while modern crust predominately belongs to the calc-alkaline suite of rocks (Martin, 1993). TTGs are widespread within the Archean but continue to form throughout geologic time (Condie, 2005). Geochemically, Archean TTGs have high La/Yb ratios ($5 < \text{La/Yb} < 150$), and low Yb (< 8.5) whereas post-2.5 Ga granitoids produced in subduction zones have low La/Yb ratios (< 20) and relatively high Yb content ($4.5 < \text{Yb} < 20$) (Martin, 1993). These trace element constraints on Archean TTGs are often referred to as an “Archean signature.” Figure 3.4 shows the differences between Archean and post-Archean TTGs based on La/Yb ratios and Yb concentrations. The Low Yb and Y contents characteristic of Archean TTGs have been classically used as evidence for a slab melt derived rock, but this assumption has been cautioned by Castillo (2006).

Another difference between Archean and post-Archean TTGs is related to the amount of interaction between mantle material and the TTG magma (Martin and Moyen, 2002). This difference, based on trace element values, is such that Archean TTG magmas would presumably have little to no interaction with mantle material whereas modern magmas that may develop into TTGs would be forced to interact with mantle wedge material in modern subduction zones. The changing amount of mantle interaction in TTGs over time has been used by Martin and Moyen (2002) as evidence for a model of the progressive cooling of the earth. A high geothermal gradient in the Archean allowed widespread melting of subducting crust and because the increased buoyancy of the hot subducted lithosphere would have caused a low angle of subduction, there would not have been much mantle wedge material for the rising melts (TTGs) to interact with (Martin and Moyen, 2002). Additionally, subducting slabs were relatively hot in the Archean and the higher geothermal gradients allowed for partial melting of the subducting

slab to take place before the “modern” style dehydration reaction could take place in the mantle wedge leading to melt generation by hydration of the mantle material (Martin, 1993) (Figure 3.5).

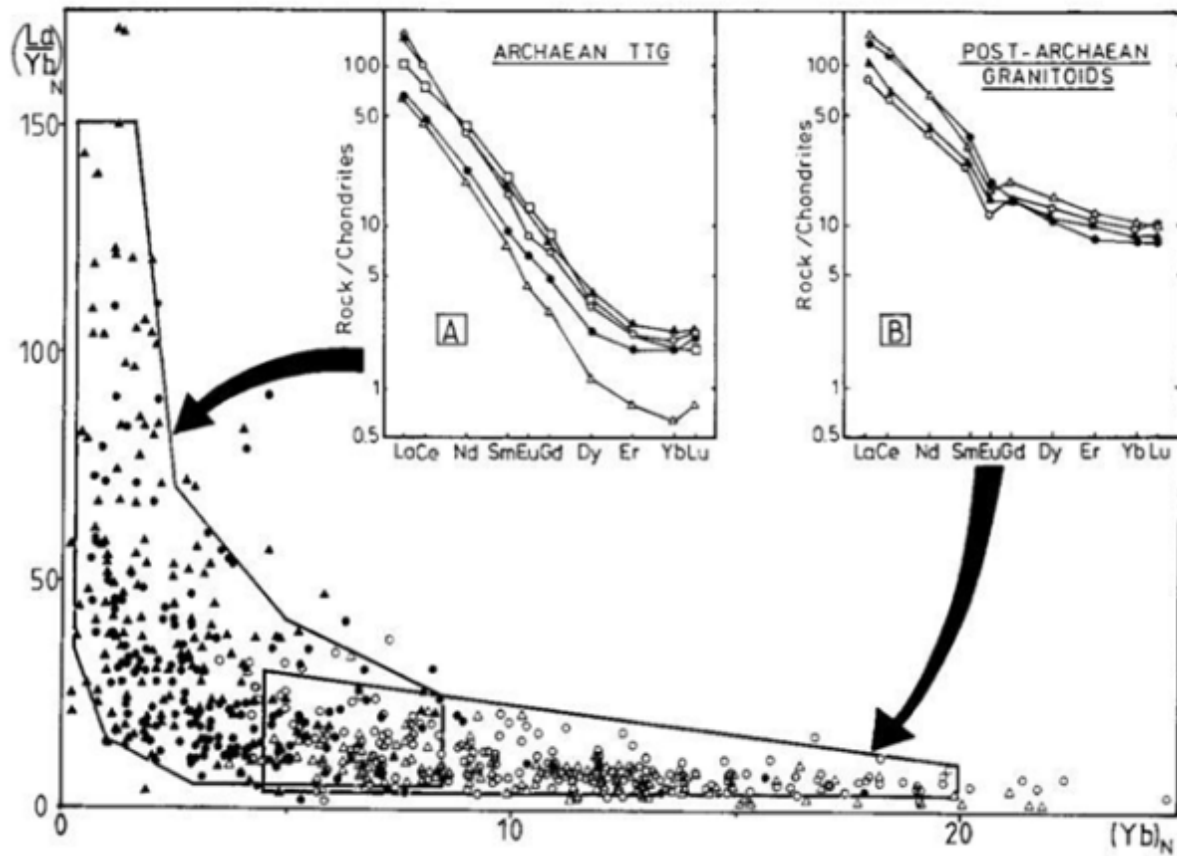


Figure 3.4. $(La/Yb)_N$ versus $(Yb)_N$ diagram showing REE changes in granitoids over time (Martin, 1993). The two REE plots and the diagram show that Archean granitoids are low in Yb and other REE concentrations while post-Archean granitoids have relatively high Yb and other REE concentrations (Martin, 1993).

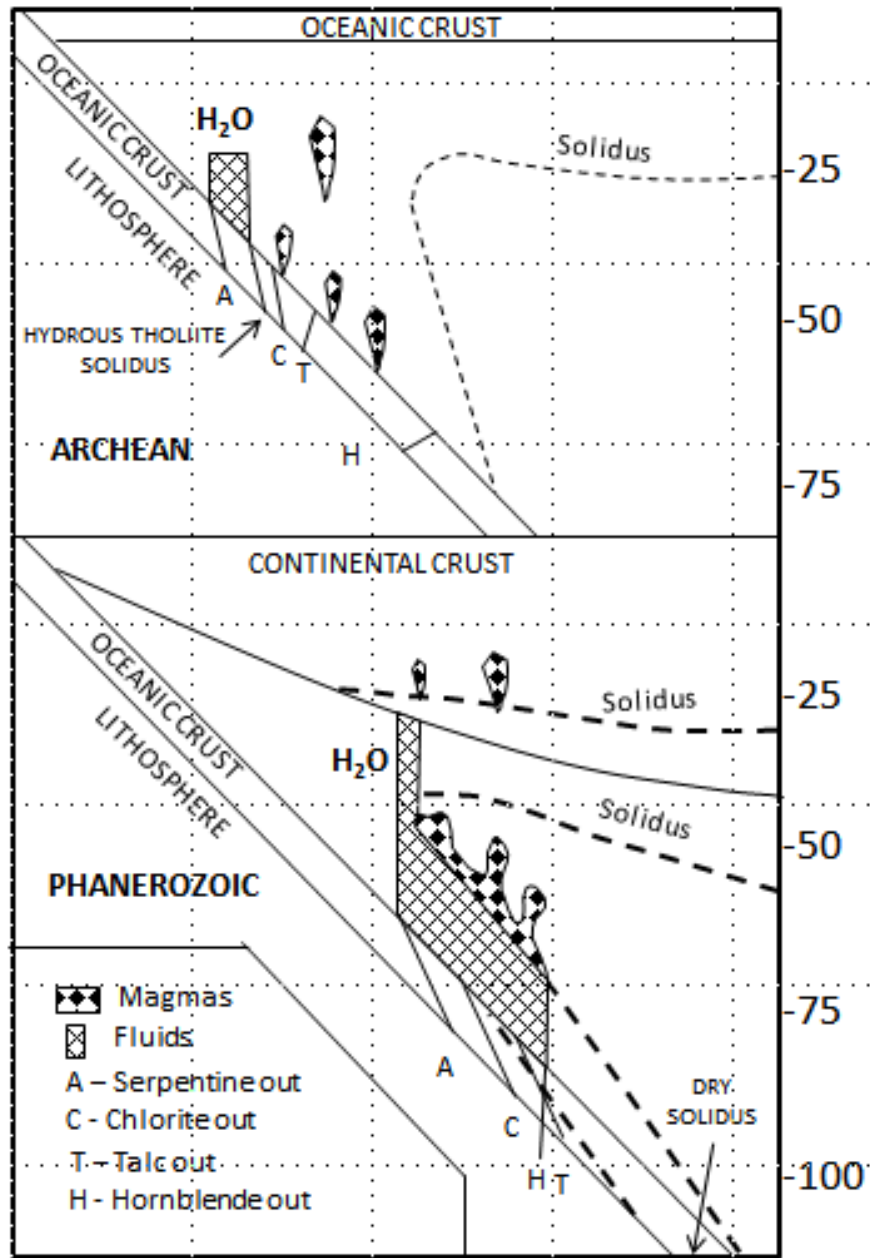


Figure 3.5. Cross sections through modern (bottom) and Archean (top) subduction zones modified from Martin (1986). Depths are in kilometers. In the Archean, the subducting crust melted before dehydration could occur; modern subduction allows for dehydration to occur before melting begins (Martin, 1986). The change in melt location will subsequently alter the magma's chemical signature.

Modern subducting slabs are relatively cold and much less likely to melt under current geothermal gradients which are low compared to those of the Archean (Martin, 1993). The lowered geothermal gradient allows for dehydration reactions to occur, introducing fluids into the mantle wedge and subsequently giving rise to “modern” mantle-derived magmas (Martin, 1993). Because modern subducting slabs have a higher angle of subduction, there is more opportunity for rising melts to interact with mantle wedge material (Martin and Moyen, 2002).

This temperature difference between “modern” and Archean slabs which may undergo subduction may be challenged by researchers such as de Wit (1998) who claim that Archean crust may not have been much hotter than the crust today. de Wit (1998) argues that Archean crust may have been dominated by mafic material which would have been more hydrous and therefore have dissipated heat more effectively. While this observation may not change methods of TTG formation in the later Archean, any difference in mantle dynamics in the early Archean would likely have an effect on the creation of the cratons.

3.5. TTG Evolution

A significant change in magma composition from the Archean into the Phanerozoic suggests that the details of TTG genesis have likely changed since the Archean (Martin, 1993). Petrogenetic processes in the Archean differ from modern processes in that they produced much larger volumes of TTG magma than modern processes (Martin, 1993). The extent to which modern tectonic processes may or may not have been active during the Archean is a matter of debate (Rapp et al., 2003).

3.5.1. Archean TTG Petrogenetic Processes

Much experimental petrology has been conducted in order to discover a protolith that, through petrogenetic processes, can produce the distinct chemical signature of Archean TTGs.

While a mafic protolith material has long been suspected for TTG petrogenesis, there have been two models of TTG genesis proposed. Broadly described, the TTG melt could be derived by partial melting or by fractional crystallization and researchers have provided evidence for and against each model (Rapp et al., 1991).

Partial Melting

Adakites and TTG's can both be produced experimentally by partially melting a mafic protolith and both melts leave behind a residue of garnet, amphibole, and clinopyroxene (Muir et al., 1995; Getsinger et al., 2009). Tonalite and trondhjemite have been successfully created through the experimental melting of mafic rocks as long as garnet and rutile remain as residual phases (Rapp et al., 1991; Rudnick, 1995). Jackson et al. (2005) found that hydrous basalt must be partially melted by 5-30% under 2-4 GPa of pressure to produce the trace and major element character of Archean TTGs. Other experiments have produced melts with chemical characteristics representative of Archean TTGs by partially melting amphibolite, eclogite, and garnet-amphibolite at pressures of 8 to 32 kbar but most successfully at 22 kbar (Rapp et al., 1991). Melting experiments by Rapp et al. (1991) also suggest that the large amounts of TTG present in the Archean can only be produced by the partial melting of either eclogite or garnet-amphibolite. Additional experimental melting evidence by Jackson et al. (2005) claims that large amounts of TTG magma can be segregated from an amphibolite to eclogite protolith.

Fractional Crystallization

Early interpretations on the evolution of TTG suggested that rather than partial melting of a basaltic source, the fractional crystallization of a basaltic parent magma (adakitic magma) could form TTG (Drummond, et al. 1996). A three step model for TTG formation proposed by Martin (1993) involved partial melting of the mantle to generate tholeiitic magma, partial

melting of the tholeiite to produce tonalitic magma, and finally fractional crystallization of the tonalitic magma to produce a differentiated TTG suite (Figure 3.6). Extensive fractional crystallization is also proposed by Kamber et al. (2002) as a method of TTG formation. Because Archean TTGs resemble typical mantle-derived magmas in terms of fluid-mobile trace element content, Kamber et al. (2002) conclude that TTGs are not derived from the melting of a subducting slab but are instead directly related to mantle-wedge derived magmas through fractional crystallization. This had previously been suspected to be a poor model for TTG formation because 80-90% fractional crystallization would have to take place in order to produce TTGs from a basaltic magma (Drummond et al., 1996). The fractional crystallization model also received criticism from Condie (2005) who similarly claims that over 50% fractional crystallization is needed to produce a TTG melt and the large amounts of mafic cumulate material that would result are not accounted for in the crust. Smithies (2000) also shows that the high volume of TTG in the crust is likely not produced from an adakitic melt because we only see a small amount of mafic restite in the crust. The problem involving the absence of large amounts of mafic cumulate material may be solved by the theory of lower crust delamination (Rudnick, 1995). It has been proposed that delamination could have removed the large amounts of restite present after massive fractional crystallization occurred to produce the TTG's from an adakitic melt (Getsinger et al., 2009). The delamination process has been used to explain the bulk intermediate composition of the entire continental crust and the delaminated material could be either restite from partial melting or ultramafic cumulates of crystals from fractionally crystallized basaltic magmas (Rudnick, 1995). Crustal delamination supports the generation of TTG's by fractional crystallization of a basaltic magma, but the process of delamination is difficult to document (Rudnick, 1995).

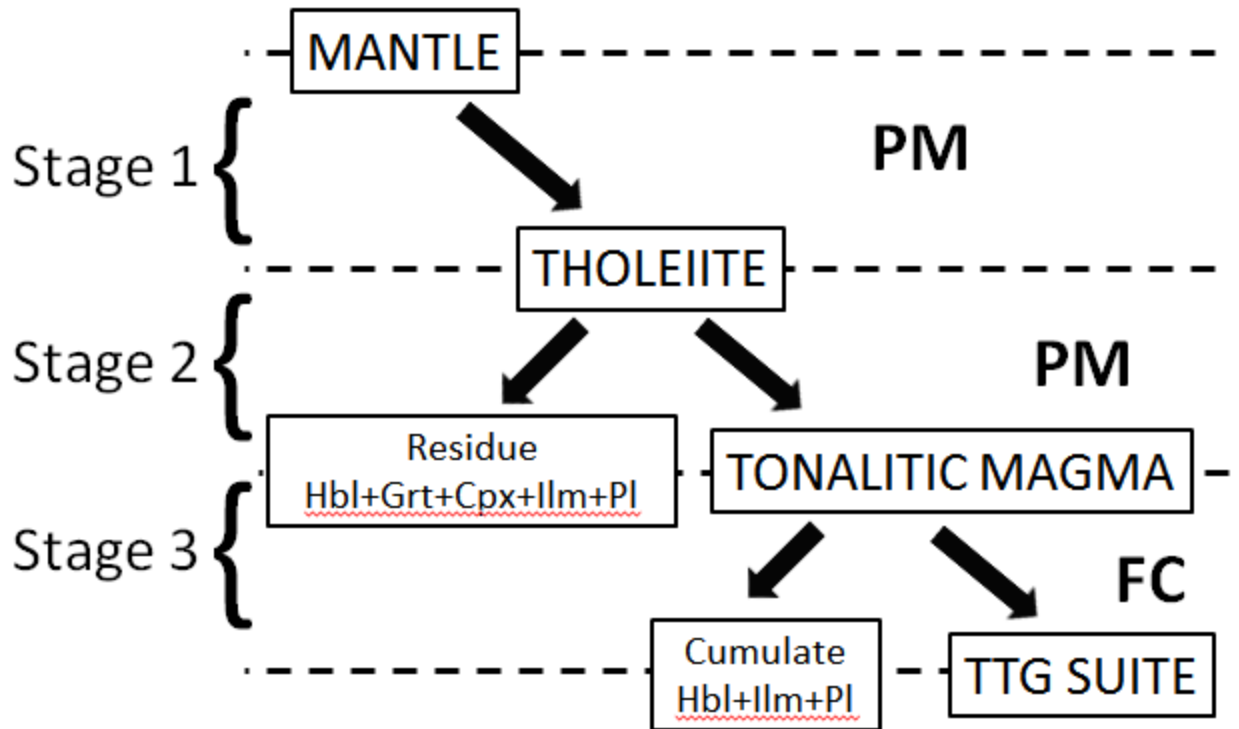


Figure 3.6. Three step model of TTG formation proposed by Martin (1993). Grt=Garnet; Hbl=Hornblende; Cpx=Clinopyroxene; Pl=Plagioclase; Ilm=ilmenite; PM=partial melting; FC=fractional crystallization.

3.5.2. Archean TTG Melt Location

While there are multiple models concerning the genesis of TTG suites and arguing the tectonic setting of their emplacement, no universal model has been accepted and many details are still being debated (Getsinger et al., 2009). Currently there is no agreement on where, tectonically, the melt is produced that forms TTG's. Mg numbers ($\text{Mg}^{2+}/(\text{Mg}^{2+} + \text{Fe}_{\text{Total}})$) x 100, where Fe_{Total} is Fe^{2+} as defined by Smithies and Champion (2000), are used throughout the TTG literature to try and explain the location of TTG genesis. As summarized by Martin and Moyen (2002), there have been two prominent melting models proposed: (1) melting of a subducting oceanic slab and (2) melting of underplated basaltic material under thickened oceanic crust. Geochemical evidence and detailed genetic models are used by different researchers to support or refute both models in explaining large amounts of TTG melt in the Archean.

Subduction Processes

Archean TTGs have been interpreted traditionally to be the partial melt of subducting hydrated basaltic slabs in the stability field of garnet \pm amphibole, or hornblende eclogite (Drummond et al., 1996; Smithies, 2000; Condie, 2005). Melts derived from a subducting slab are best achieved when the subduction angle is low, the subducting plate is hot, and the overriding lithosphere is thin (<45 km) (Drummond & Defant, 1990; Kincaid & Sacks, 1997). Experimental evidence from Kincaid and Sacks also suggests that slow subduction rates (<3cm/year) will result in higher slab surface temperatures. Gutscher et al., (2000) suggest that the initial temperature of a subducting slab does not matter and that as long as the angle of subduction allows the slab to be heated at around 80 km depth for a long enough time, the slab will melt. This genesis model is supported by the partial melting of basalt in experiments that led to majority melt compositions of high-Al TTD (>15% Al_2O_3) (Drummond et al., 1996). The

melting experiments performed by Drummond et al. (1996) produced, on average, 60% tonalite, 23% trondhjemite, 12% granodiorite, and 5% granite. Drummond et al. (1996) therefore concluded that the partial melting of a basaltic source with low K_2O will result in albite-rich TTGs.

Getsinger et al. (2009) claim that TTGs must be modified at some point in order to explain the variable Mg numbers observed within narrow ranges of SiO_2 values. This modification can be explained by Martin and Moyen (2002) who suggest that melts of the subducted slab must ascend through the mantle wedge and likely interact with mantle material. In order to find out how much a rock has interacted with the mantle wedge, geochemical indicators such as the Mg-number can be used (Getsinger et al., 2009). Martin (1986) proposed that the cooling of the earth would alter the location of magma genesis in subduction zones and therefore also alter the geochemical characteristics of the magmas. From 4.0-2.5 Ga, the increasing concentrations of $(CaO + Na_2O)$ and Sr in TTGs show that the amount of interaction with the mantle wedge was increasing over time (Martin and Moyen, 2002). This increased interaction is linked to the growing thickness of the mantle wedge as the angle of subduction increases due to a decrease in plate buoyancy caused by decreasing geothermal gradients over time (Martin and Moyen, 2002). Martin and Moyen (2002) present geochemical evidence supporting the melting of subducted crust as the major producer of TTGs from 4.0-2.5 Ga because of the proven interaction between TTGs and the mantle wedge material. It can be inferred that this “modification” of the TTGs would involve mantle wedge interaction. Martin and Moyen (2002) claim that the fusion of underplated metabasalt must be ruled out as a producer of TTG because of the lacking chemical evidence for mantle wedge interaction (Martin and Moyen, 2002). Melts of the underplated thickened crust would not interact with the mantle

as in the subduction process (Martin and Moyen, 2002). Alternatively, Drummond and Defant (1990) propose that high-Mg type adakites can be produced directly by melting the subducting slab without that melt reacting with mantle wedge material. It is possible, additionally, that dynamic melt segregation and equilibrium processes could alter the geochemical indicators which indicate that the mantle interaction is required, suggesting that the indicators are not directly representative regarding the extent of mantle interaction (Getsinger et al., 2009).

Underplated Crust Process

Although subduction zones have been typically associated with TTG's, Condie (2005) concluded that TTGs could form in any tectonic setting in which hornblende eclogite is stable and temperatures are 700°-800° C. Rapp et al. (1990) similarly concluded that while partial melting of eclogite does produce tonalite-trondhjemite melts, the melt environment should not necessarily be limited to subduction settings. Atherton and Petford (1993) first proposed that the formation of high-Al TTD suites described by Drummond and Defant (1990) could be created by the partial melting of newly underplated basaltic crust, which formed by magmatic accretion, as opposed to melting of a subducted plate. The example that they used was of TTD suite rocks that formed above a subduction zone involving a 60 Ma slab (Atherton and Petford, 1993). Drummond and Defant (1990), however, had proposed that only <25 Ma, hot subducted crust would have been able to melt even with the increased temperatures of the Archean. Smithies (2000) also concluded that the majority of TTG formation during the Archean (>3.0 Ga) was not due to subduction but rather the melting of hydrated basalt at the bottom of thickened crust. Their conclusion is supported by geochemistry that suggests Archean TTG is not analogous to Cenozoic adakite and therefore not linked to subduction processes alone (Smithies, 2000). Xu et al. (2002) offered clear evidence for non-arc adakite formation due to partial melting of the lower

crust associated with amphibole bearing eclogite delamination in the Ningzhen region of east China. Experimental melting done by Rapp et al. (2003) suggested that the source of partial melt to produce TTGs in the Archean may have been oceanic crust formed in a few different ways. The accretion of terranes associated with tectonic imbrication or intraoceanic subduction would lead to partial melting resulting in TTG magmatism at the base of juvenile, overthickened arc crust (Rapp et al., 2003). Because a subduction environment would likely entail the interaction of a melt with the mantle wedge material, and many Archean TTGs do not show evidence for mantle wedge interaction, Smithies and Champion (2000) concluded that partial melting of basaltic lower crust is a better model for TTG formation. Condie (2005) proposed that while adakites are truly slab melt derived, TTGs (especially high-Al TTGs) may be derived by partially melting the lowermost arc crust or oceanic plateau root zones. Muir et al. (1995) performed a study on a Cretaceous batholith that has the geochemical characteristics of a slab melt but was subsequently demonstrated, by Muir et al. (1995), to be the melt of underplated and overthickened continental crust. Greater heat during the Archean may favor slab melting, but modern extensive melt generation from the downgoing slab is very unlikely unless the slab is very young and hot or the subduction angle is very low (Peacock et al., 1994).

3.6. Archean Crust Generation Issues

Despite strong evidence from many researchers, the argument about how large amounts of TTG magma formed during the Archean is still a matter of debate. A conclusive model for Archean TTG formation must distinguish among fractional crystallization, partial melting (of overthickened crust or a subducting slab), and the amount of interaction between the TTG melt and mantle material.

There is a reasonable amount of agreement within the literature that TTGs do originate from the partial melting of a hydrous basaltic protolith, although fractional crystallization remains an alternative (Rapp et al., 1991; Rudnick, 1995; Muir et al., 1995; Jackson et al., 2005; Getsinger et al., 2009). Martin and Moyen (2002) provide evidence for TTG-mantle interaction which supports a subduction genesis model whereas Smithies and Champion (2000) provide evidence for no TTG-mantle interaction which supports an underplated crust genesis model. This continued discrepancy between ideas of TTG-mantle interaction requires further investigation. TTGs found in Archean crust seem less likely to be produced in large volumes from the melting of subducting slabs (Peacock et al., 1994). Considering the large volume of TTG rocks in Archean crust, the partial melting of underplated thickened crust may be a more practical model (Smithies and Champion, 2000; Peacock et al., 1994; Condie, 2005).

3.7. Post-Archean TTG Petrogenetic Processes

Post-Archean TTG genesis in relatively small amounts could be a result of any of the Archean TTG petrogenetic mechanisms, or entirely modern petrogenetic mechanisms. There are essentially two different petrogenetic processes which may form felsic magmas such as TTGs in an arc-type setting. These processes, generally described, are the partial melting of lower crustal mafic rocks such as amphibolite or eclogite, or the fractional crystallization of a basaltic magma (Brophy, 2008; Borg and Clyne, 1998). The mechanisms of partial melting and fractional crystallization are very simplified here and involve extensive complications which will be covered in more detail in chapter 7.

Partial Melting

The majority of models regarding modern TTG genesis involve the partial melting of hydrous lower mafic crust (Frost et al., 2006). Excepting this common starting point, models for

specific TTG localities tend to vary such that there is not a single accepted model for all TTG genesis. A popular model developed by Martin (1987) and used by Frost et al. (2006) involves the partial melting of tholeiitic garnet-bearing amphibolite which leaves a hornblende and garnet restite. This model produces trondhjemitic magma heavily depleted in HREEs (Frost et al., 2006). As stated for Archean TTGs, experimental research by Rapp et al. (2003) supports this model of TTG genesis by showing that partial melting of hydrous basalt by 10-40% at pressures greater than the garnet-in boundary (~10-14 kb) will produce the major and key trace element characteristics of TTGs (Frost et al., 2006).

Fractional Crystallization

Felsic magmas may also develop from a parental basaltic magma through the process of fractional crystallization or assimilation fractional crystallization (AFC) (Borg and Clyne, 1998). Assimilation fractional crystallization (AFC) has been recognized as a particularly difficult complication when trying to use geochemical data to interpret the petrogenetic history of a rock. In traditional geochemical modeling, assimilation and fractional crystallization were handled as completely separate processes. However, as pointed out by Depaolo (1981), the heat necessary for assimilation can be provided by fractional crystallization through the latent heat of crystallization. As stated earlier, fractional crystallization models for TTG magmas have received a lot of criticism due to the estimated 50-90% fractional crystallization that would have to occur and the lack of evidence for the large amount of mafic cumulate material that would result (Drummond & Defant, 1996; Smithies, 2000; Condie, 2005).

Post-Archean TTG Melt Location

Slab melting may have decreased extensively due to the progressive cooling of the Earth over geologic time, but some processes similar to those of the Archean may still persist. In

small areas of southern Chile, the subduction occurring has been shown to be hot enough to produce Archean-style conditions of magma genesis and the andesites produced match the geochemical parameters representative of Archean TTGs (Martin, 1993). There is also some debate as to whether slab melting may be occurring in areas of the Cascades such as Mount St. Helens (Defant & Drummond, 1993; Peacock et al., 1994).

Despite this, the majority of post-Archean magma formation at subduction zones is not associated with slab melting. Low geothermal gradients prevent slab melting and instead dehydrate the slab introducing aqueous fluids into a hot mantle material which melts and produces “typical” calc-alkaline magmas (Martin & Moyen, 2002). The fluids released in the dehydration reaction not only initiate melting in the mantle by lowering the solidus, they also enrich the melt composition with LILE (large ion lithophile elements) and LREEs (light rare earth elements) (Martin, 1993). As summarized by Rudnick (1995), this partial melting of mantle material has been assumed to be the main producer of modern continental crust, although mantle melting experiments fail to produce the more evolved material that makes up the majority of continental crust.

Because there is still no accepted model of Archean TTG formation, analysis of a young TTG which has the “Archean signature” provides a unique opportunity to gain insight into petrogenetic processes which may have been widespread during the Archean.

4. SAMPLING, PETROGRAPHY, AND MAGMATIC EPIDOTE

4.1. Sample collection

Samples of the WRO were collected from the field in the summer of 2012 (Figure 4.1). Fifty samples were collected, thirty were studied in thin section, and eighteen were used to obtain geochemical data. Samples were obtained both from within the pluton boundary (WRO) (green area in Figure 4.1) and from within the banded gneiss marginal zone (BG) (blue area of Figure 4.1). These samples came from areas along Highway 2, Nason Ridge, Wenatchee Ridge, and from roadsides around and between Wenatchee and Nason Ridge. Some samples were taken from a quarry of the WRO located to the East of Wenatchee Ridge. Forty five samples (both WRO and BG) were also used in this study which were collected by Dr. Jerry Magloughlin at various times.

What are broadly tonalitic samples were collected throughout the entire pluton body in order to capture any chemical and/or mineralogical variation which may exist. Samples were taken preferentially from areas which appeared to be unaltered, unweathered, and not in close proximity to ultramafic xenoliths, quartz veins, or pegmatites. Where possible, samples of the ultramafic bodies were taken in addition to a few samples of tonalitic pegmatite and marble. The UTM was recorded by GPS and a photo was taken at each sample site (see Appendix A).

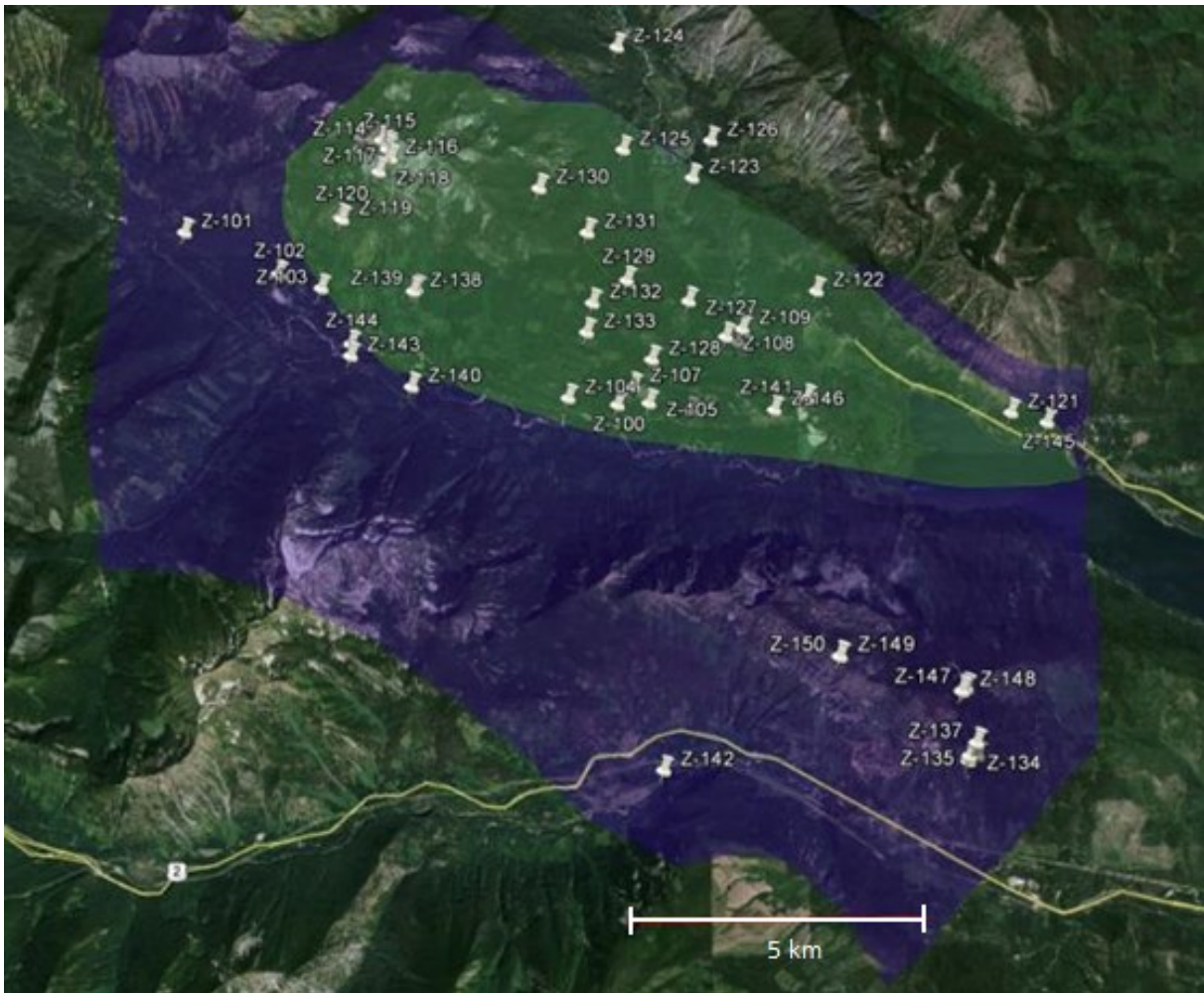


Figure 4.1. Map showing locations of all samples taken during the summer of 2012. The green pluton and blue banded gneiss boundaries (WRO and BG) were defined by Tabor et al. (1987).

4.2. Petrography of the WRO

Petrographic analysis of the WRO used 17 new, standard thickness, thin sections in addition to 45 thin sections of samples previously collected from the area by Dr. Jerry Magloughlin. The new thin sections were prepared by Quality Thin Sections, Arizona. Thin sections which were not heavily altered were polished at CSU using alumina grit. Thin section descriptions can be found in Appendix B.

4.2.1. Mineralogy

The most common mineral assemblage in the WRO is oligoclase + quartz + biotite + muscovite with varying amounts of accessory minerals, including hornblende, microcline, garnet, epidote, clinozoisite, zoisite, apatite, titanite, zircon, ilmenite, and rutile.

4.2.2. Spatial Distribution of Accessory Minerals

The spatial distribution of accessory minerals within the WRO and surrounding Chiwaukum Schist/NRMG is shown in Figures 4.2-4.5. The spatial distribution of accessory minerals was analyzed to determine if there is any mineralogic variation between the WRO and BG samples. All of the WRO and BG samples contained muscovite in variable concentrations.

4.2.2.1. *Epidote*

The spatial distribution of magmatic epidote is shown on Figure 4.2. Samples which have epidote meeting the criteria of magmatic epidote (discussed further in section 4.3) are more common in the core of the pluton whereas the BG samples more commonly contain either no epidote at all, or non-magmatic epidote.

4.2.2.2. *Amphibole*

Figure 4.3 shows the spatial distribution of samples containing amphibole. Amphibole tends to occur as uncommon sprays of a pale amphibole, likely tremolite, which is probably secondary

and resembles fibrolite. Amphibole in the BG samples is typically much darker in color (green to brown) and appears to be mostly primary. Amphibole is scattered throughout the region and occurs in both BG and WRO samples.

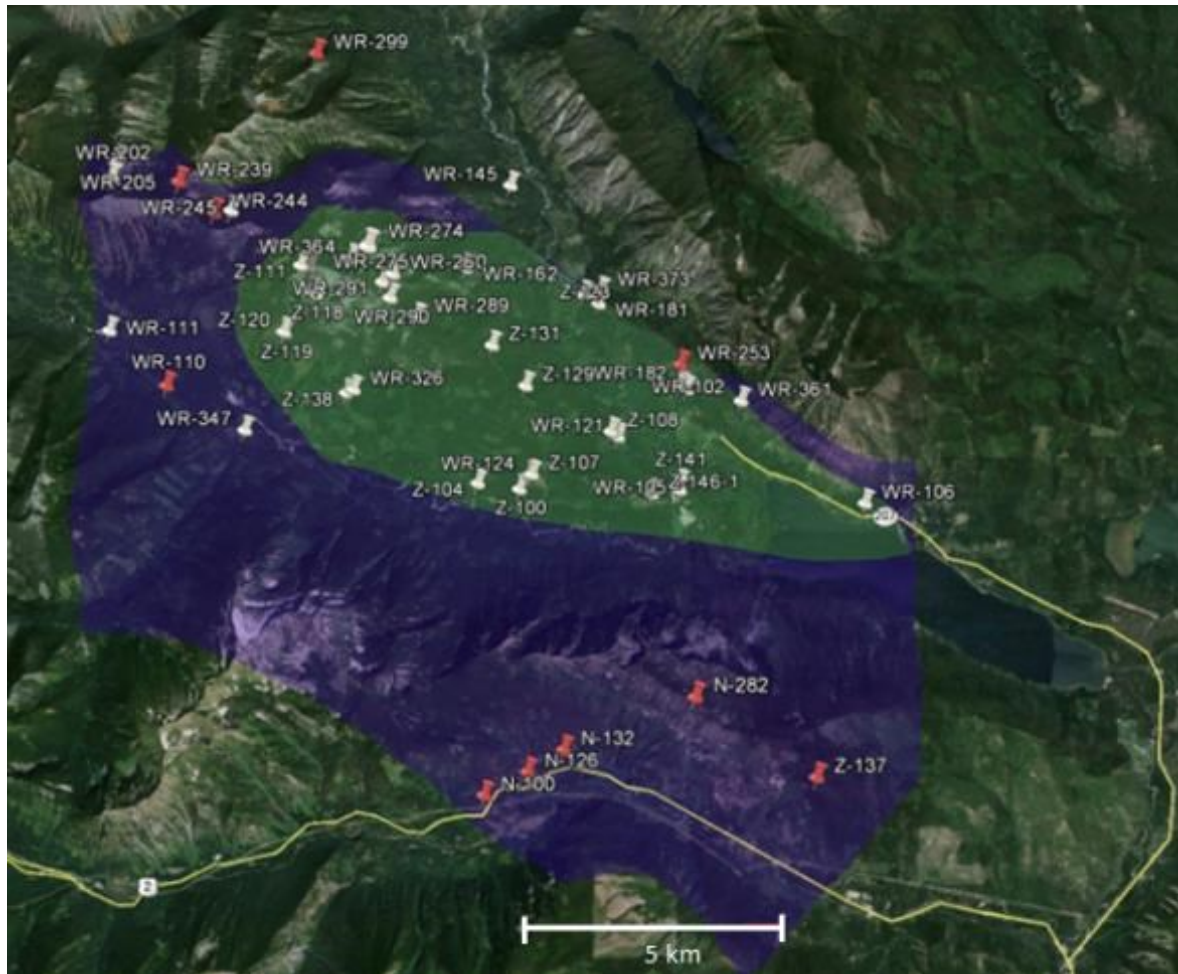


Figure 4.2. Map of occurrences of magmatic epidote within and around the WRO pluton. Red samples have no epidote whereas white samples have magmatic epidote.

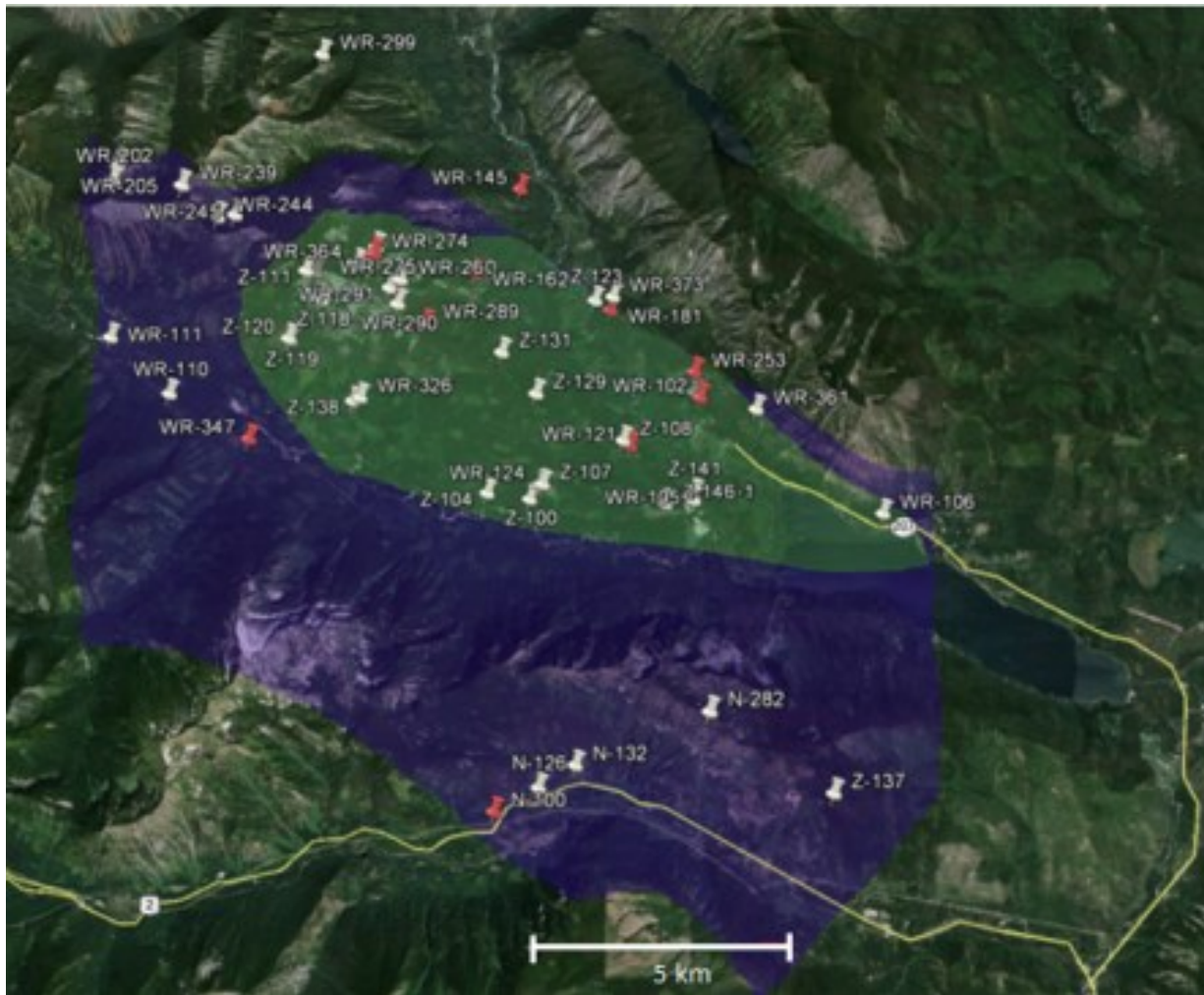


Figure 4.3. Map of occurrences of amphibole within and around the WRO pluton. Red samples contain amphibole whereas white samples do not.

4.2.2.3. Garnet

Figure 4.4 shows the spatial distribution of garnet; it occurs in both BG and WRO samples but appears to be more common within the WRO core (6 samples) rather than within the banded gneiss (1 sample). Samples off of highway 2 not sent out for geochemistry within the banded gneiss also contain garnet.

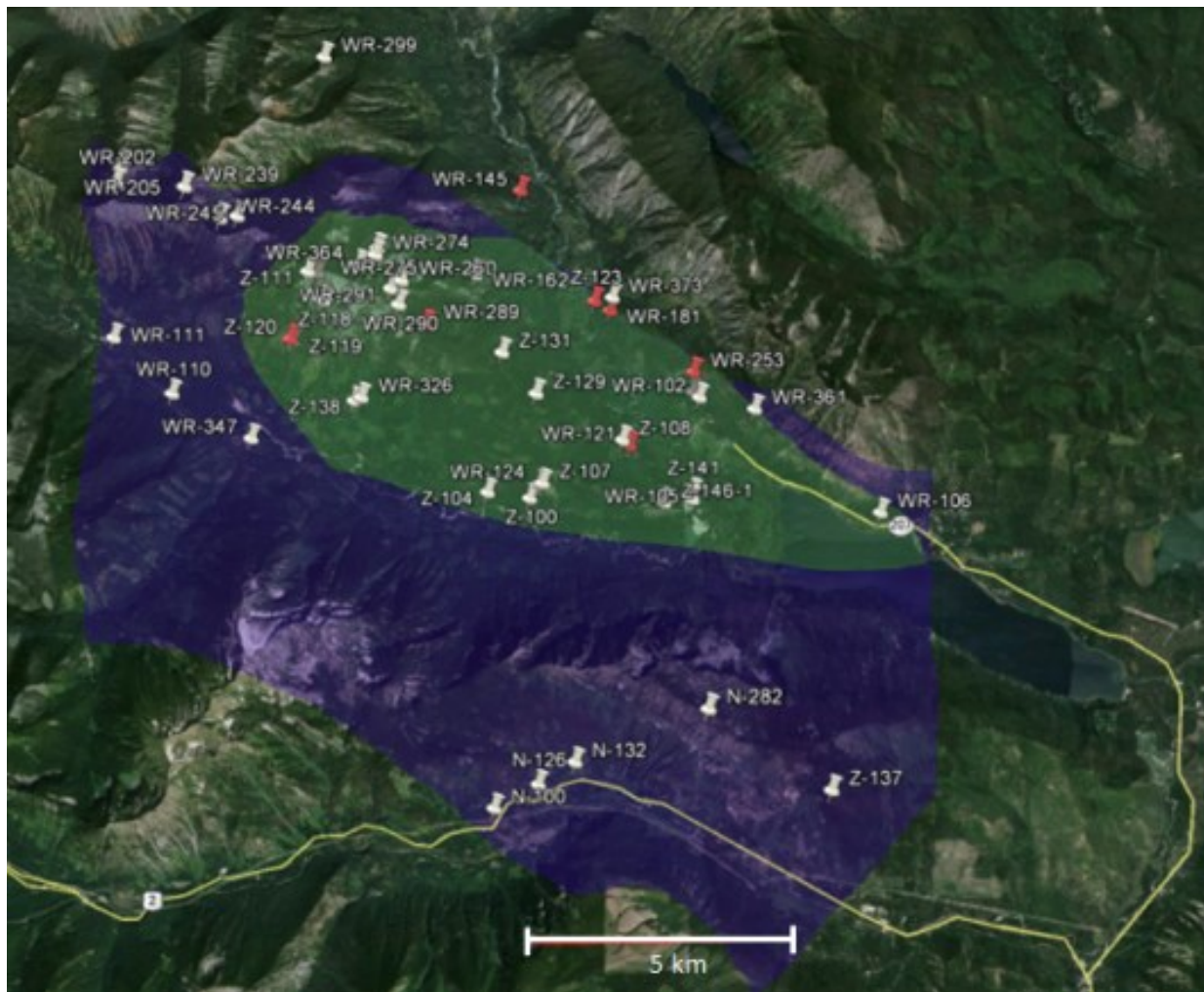


Figure 4.4. Map of occurrences of garnet within and around the WRO pluton. Red samples contain garnet; white samples do not.

4.2.2.4. *Biotite*

Figure 4.5 shows the spatial distribution of biotite throughout the WRO and BG samples. Most of the WRO and BG samples do contain biotite, yet many WRO samples (16%) contain only muscovite. This figure shows that most of the ultrafelsic (≥ 76 wt % SiO_2 and a lack of mafic minerals) samples are within the WRO pluton boundary (white samples in figure 4.5).

There appears to be no discrete mineral assemblage which is shared by either all of the WRO or BG samples. The WRO samples do, however, tend to have more magmatic epidote and a lower concentration of mafic minerals compared with the BG samples.

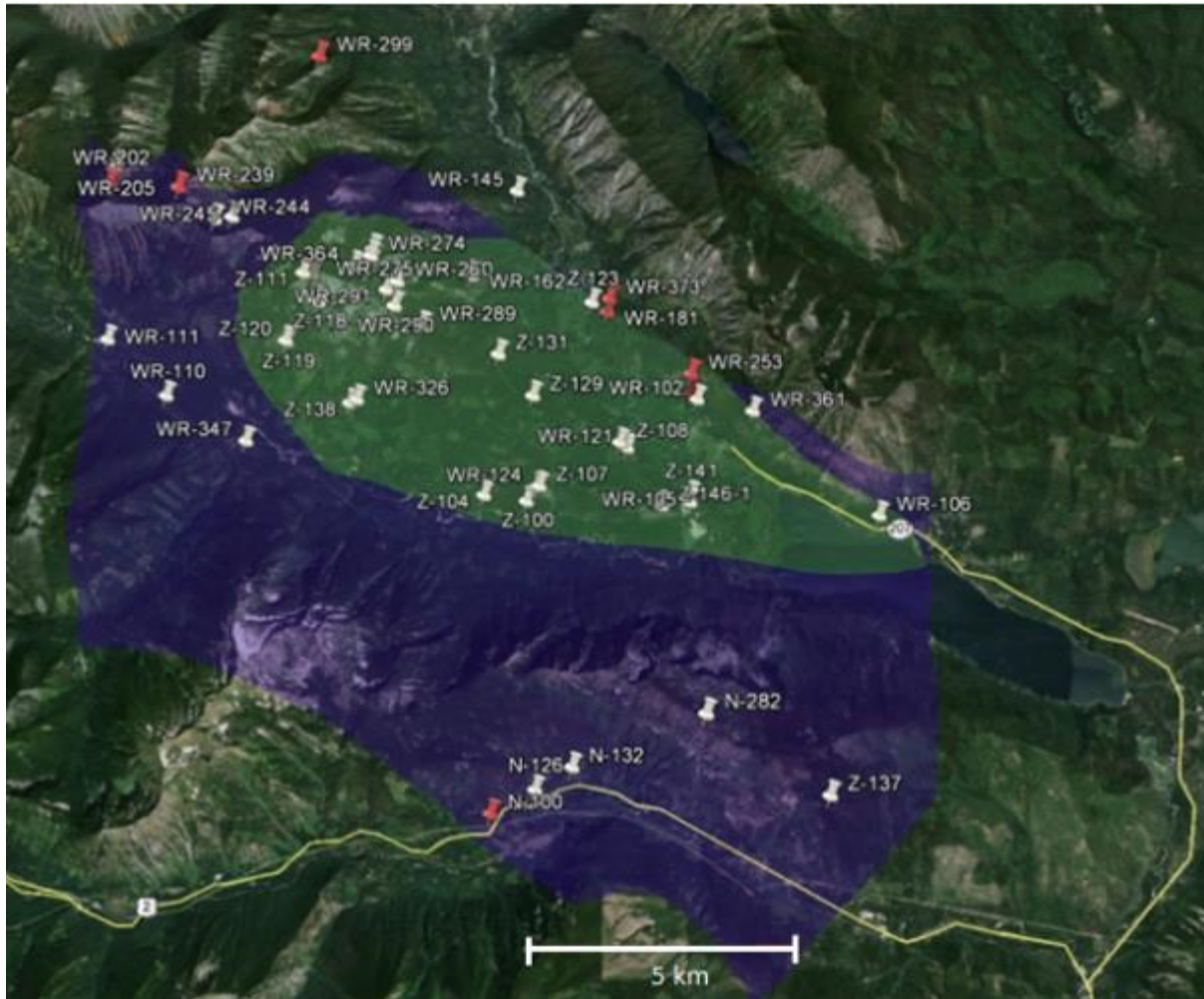


Figure 4.5. Map of occurrences of biotite within and around the WRO pluton. Red samples do not contain biotite; white samples do.

4.2.3. Mineral Textures

Mineral textures and assemblages are variable throughout both WRO and BG samples. There are, however, distinct mineral textures which appear in the majority of samples.

4.2.3.1. *Biotite and Muscovite*

Biotite and muscovite are commonly intergrown in the WRO and BG samples such that the crystals appear to have nucleated on one or another, potentially suggesting simultaneous growth. This relationship is present in sample Z-138 in Figure 4.6A. Because biotite tends to crystallize first in magmas, muscovite likely nucleated off of the existing biotite crystal. Biotite and muscovite growth could also be related to metamorphism. Biotite is locally altered to chlorite but this reaction has rarely gone to completion in any of the sections.

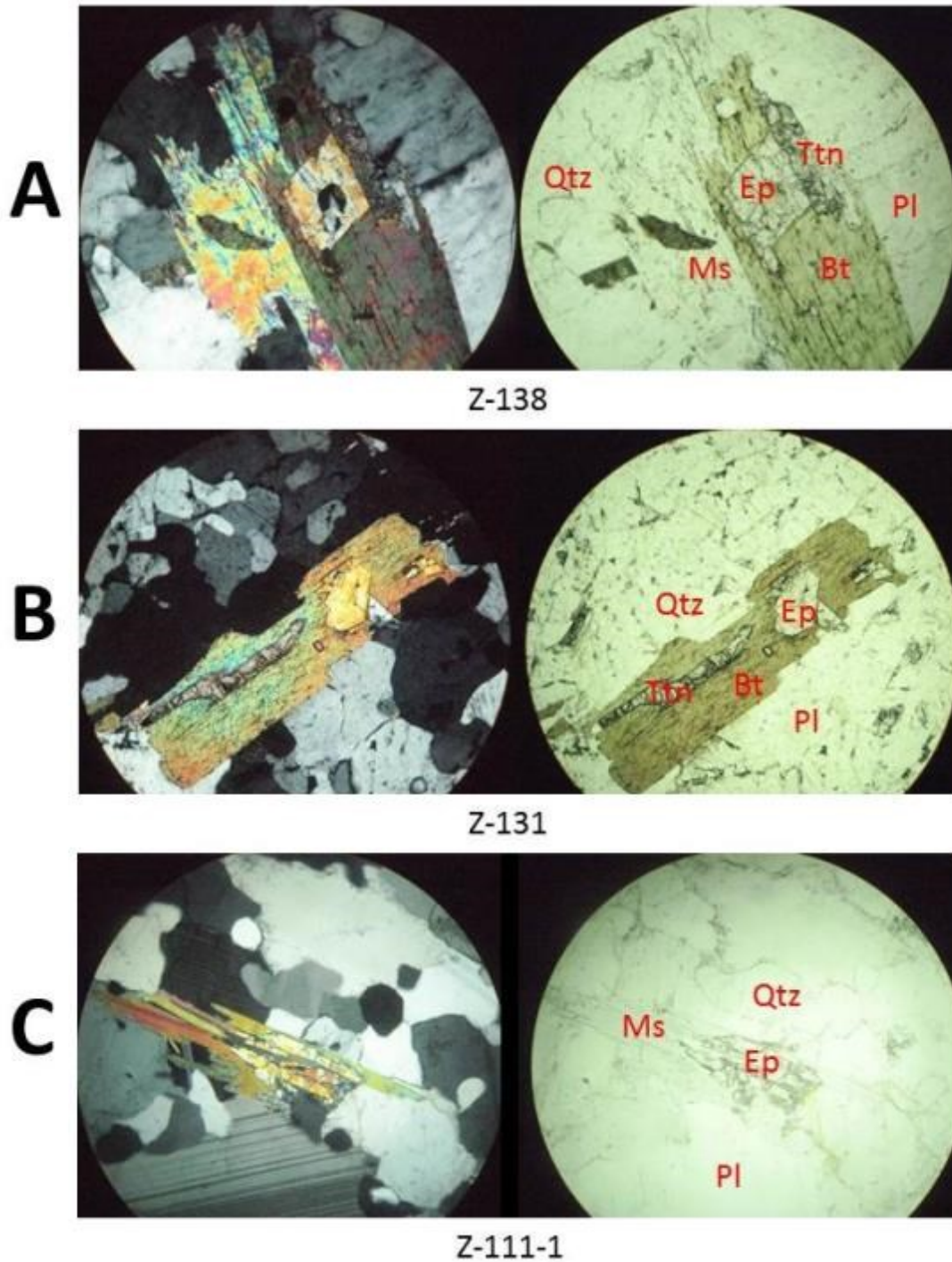


Figure 4.6. Photomicrographs (XPL left, PPL right) for 3 samples of the WRO showing magmatic epidote (Ep), titanite (Ttn), biotite (Bt), muscovite (Ms), plagioclase (Pl), quartz (Qtz), and the textural relationships between them. The field of view for Z-138 is 1mm and the other fields of view are all 2 mm.

4.2.3.2. *Epidote and Clinozoisite*

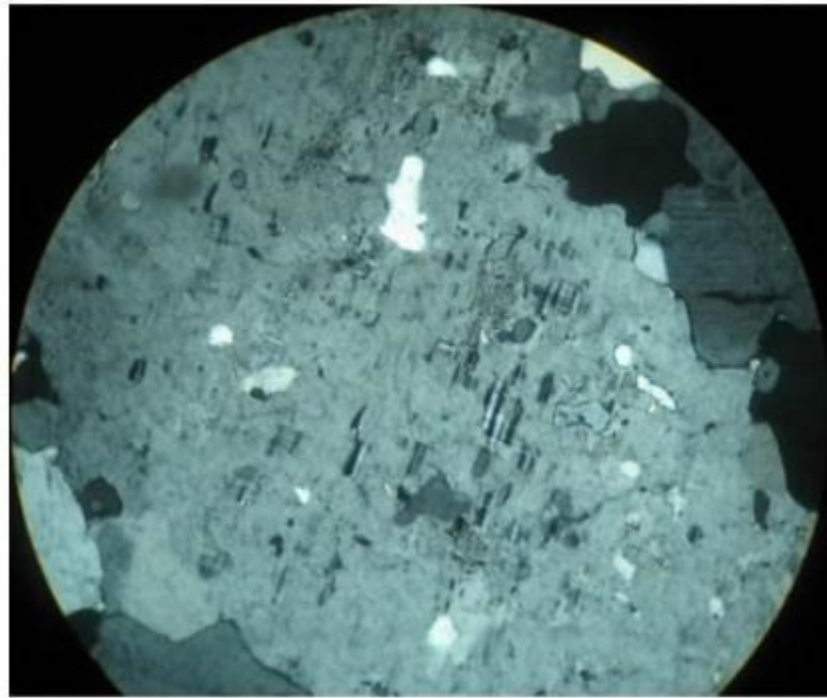
Another common texture is a relationship among epidote, muscovite, and/or biotite. A few examples of this texture are shown in Figures 4.6A and 4.6B. Epidote is almost nearly always found with biotite and/or muscovite and when not found with either, appears to be heavily resorbed or secondary. In the normal cases, epidote appears to have been protected from any retrograde reactions by being encased by the phyllosilicates. Clinozoisite commonly appears interstitially with plagioclase or included within plagioclase. In a few cases, clinozoisite forms the core or rim of epidote grains. Common epidote inclusions within biotite and muscovite indicate it crystallized before them.

4.2.3.3. *Antiperthite*

A somewhat rare occurrence is the presence of patchy antiperthite (microcline) which exists within plagioclase grains (Figure 4.7). Anti-perthite may be the result of exsolution of potassic feldspar upon cooling or anti-perthitic replacement (Deer et al., 2001). The erratic distribution of the anti-perthite in the WRO suggests that anti-perthitic replacement may be more likely (Deer et al., 2001).

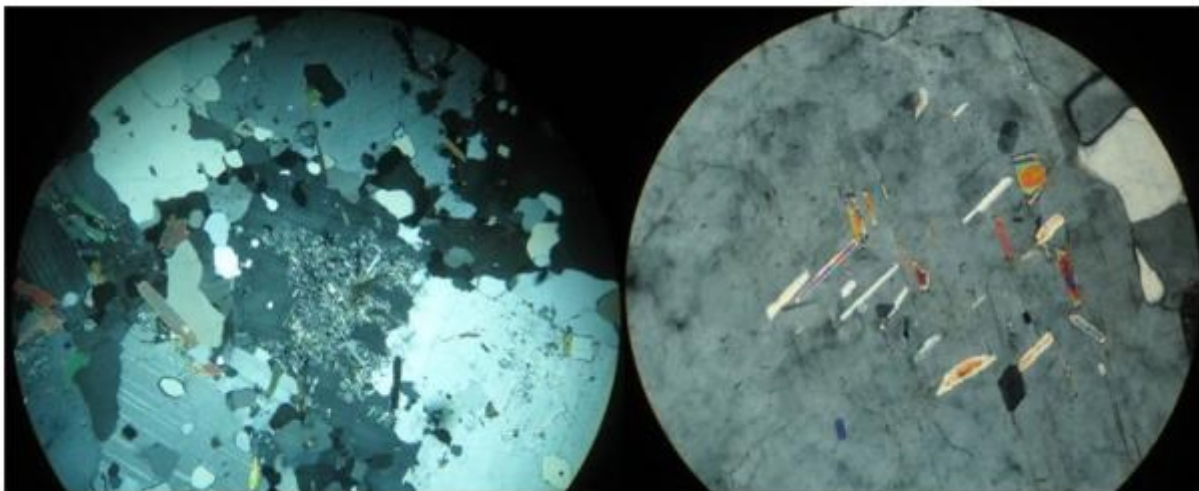
4.2.3.4. *Plagioclase alteration*

Plagioclase in the WRO and BG samples is uncommonly altered to sericite or saussurite. Plagioclase cores are much more commonly altered than rims (Figure 4.8). In some cases, sericitic alteration of plagioclase has taken place in the form of white mica which grows along cleavage planes within plagioclase grains (Figure 4.8). This is a hydration reaction which likely occurred upon retrograde metamorphism as the rocks cooled through lower amphibolite and greenschist facies conditions (Magloughlin, 1986).



WR-102-1

Figure 4.7. Photo of patchy anti-perthite from WR-102-1 in cross polarized light. Field of view is 2mm.



WR-105-12

WR-205-4

Figure 4.8. Photomicrograph of plagioclase alteration concentrated in the core of a plagioclase grain (WR-105-12, left image), and oriented plagioclase alteration (WR-205-4, right image). Field of view is 5 mm in the left image and 1 mm in the right image.

4.2.3.5. *Amphibole growth*

Several WRO and BG samples have pale amphibole crystals which appear as small, radiating masses typically associated with muscovite or biotite (Figure 4.9). These crystals, likely tremolite, look similar to fibrolite and likely represent secondary growth of metamorphic amphibole during retrograde metamorphism (Magloughlin, 1986). They may also be associated with ultramafic contamination to some degree (Magloughlin, 1986).

Because of the deformed and metamorphosed nature of the orthogneiss which is the focus of this study, textures of primary concern are those which indicate whether minerals are magmatic or metamorphic. These textures, their formation, and the results of metamorphism on igneous minerals will be covered in further detail in chapter 5.

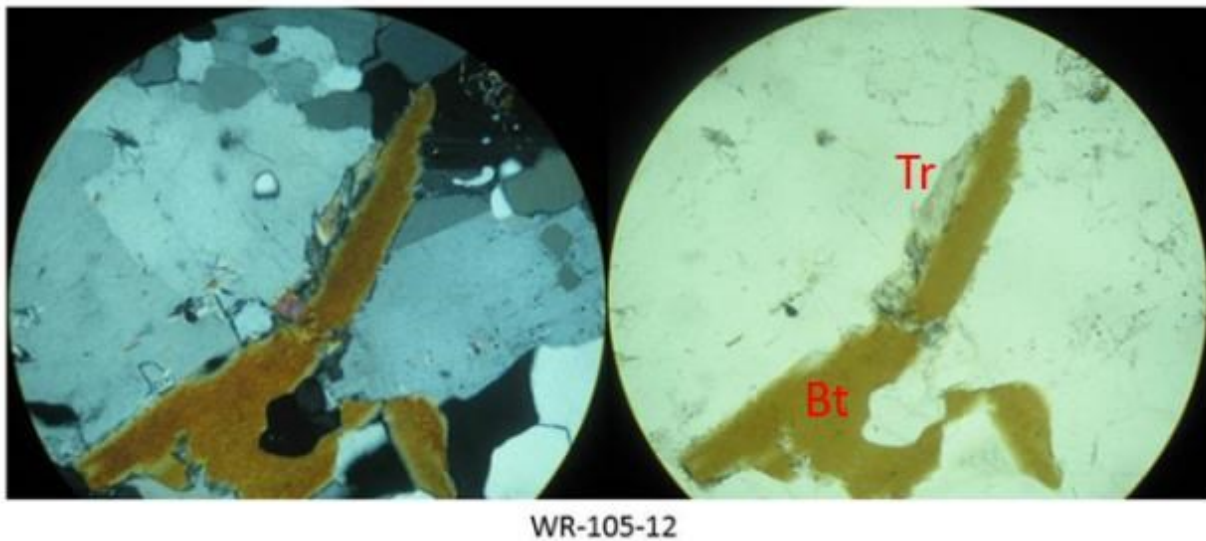


Figure 4.9. Photo of tremolite growth (Tr) off of biotite (Bt) from WR-105-12. The image on the left is in cross polarized light and the image on the right is in plane polarized light. The field of view is 5 mm in both images.

4.3. Magmatic Epidote

Many of the samples analyzed in this study contained epidote as a primary and/or secondary phase. The magmatic epidote in these rocks could have implications for the pressure conditions at which the initial magma intruded.

4.3.1. Background

Epidote is commonly thought of as a strictly metamorphic mineral, but has been observed for many years in granitoid type rocks (Zen & Hammarstrom, 1984). The first recorded observation of magmatic epidote was made by Cornelius (1915) who noted that epidote in a tonalite was a primary mineral and appeared to have crystallized early from the magma, before or contemporarily with biotite (Schmidt & Poli, 2004). More than 95% of magmatic epidote occurrences are within the TTG (tonalite-trondhjemite-granodiorite) suite of rocks (Schmidt and Poli, 2004).

Magmatic epidote was first utilized by Zen and Hammarstrom (1984) as an indicator of pressure conditions during crystallization. Early interpretations by Zen & Hammarstrom (1984) utilized experimental data from Naney (1983) and evidence from multiple epidote bearing plutons along the North American Cordillera. Ultimately, their interpretations suggested the presence of magmatic epidote would require plutons to have intruded at pressures exceeding 8 kb. Later evidence of magmatic epidote from other intrusions around the world led to the determination that epidote could be stable from 5-8 kb depending on magma composition, water content, and oxygen fugacity (Moench, 1986; Tulloch, 1986; Zen & Hammarstrom, 1986; Schmidt & Thompson, 1996; Schmidt & Poli, 2004).

In a reply to comments made on the earliest papers on magmatic epidote, Zen & Hammarstrom (1986) stressed that the emplacement pressure inferences made for magmatic

epidote must be made cautiously. They specifically state that there must be evidence for a reaction between hornblende and epidote and the mineral assemblage must be the same as in the original rocks that the study was based upon. Additionally, epidote must be recognized as a primary mineral before any conclusions can be made concerning petrogenesis.

4.3.2. Magmatic Determination

The following is a list of magmatic epidote criteria as summarized by Schmidt & Thompson (1996) and Schmidt et al. (2004) although the initial observations were made by Zen & Hammarstrom (1984), Moench (1986), Tulloch (1986), and Zen & Hammarstrom (1986).

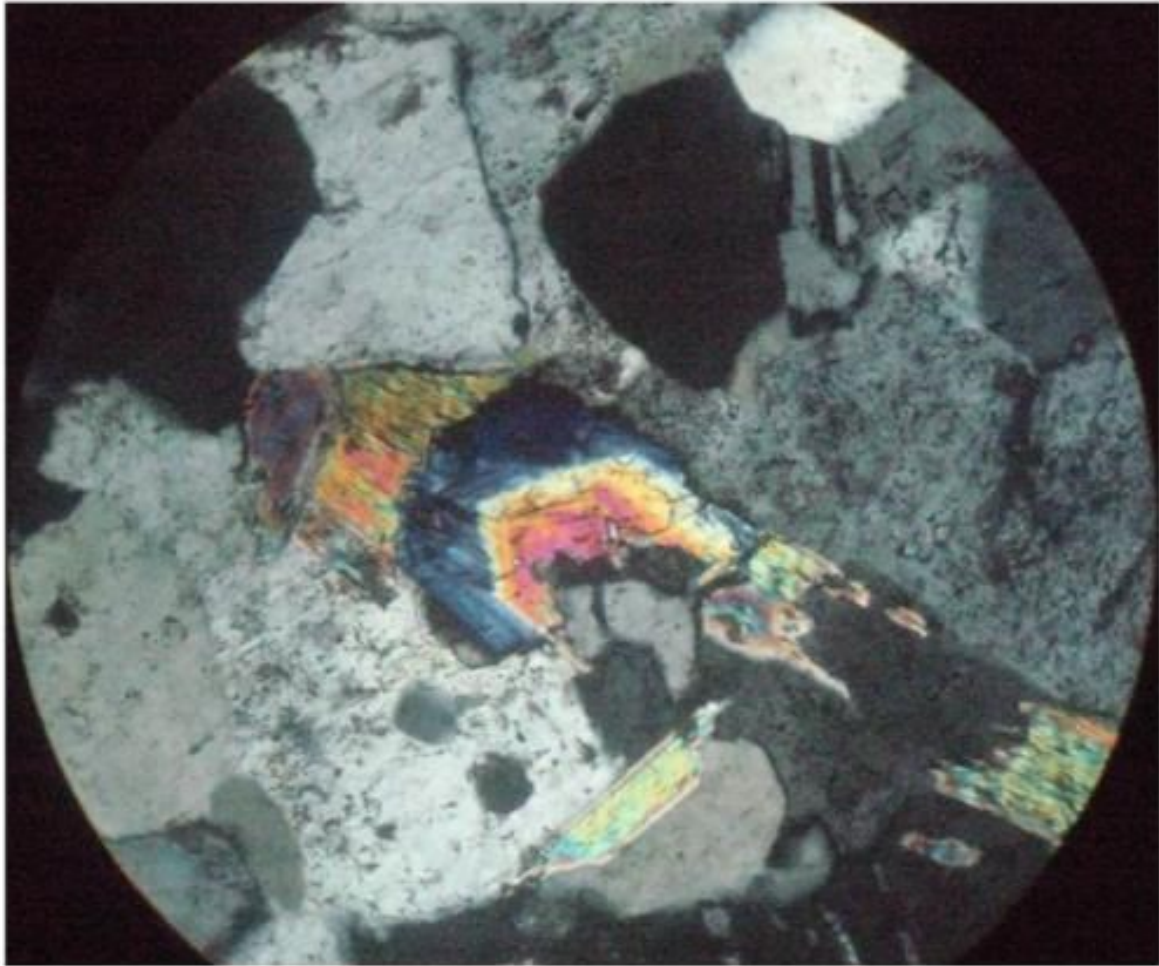
- Zonation with allanite-rich cores are strong evidence for a magmatic origin but zonation is not necessary.
- Ophitic textures suggesting epidote crystallization after hornblende or concurrent with biotite suggest a magmatic origin.
- Embayments where epidote comes in contact with quartz or feldspars in the matrix show that epidote was unstable during the final crystallization of the magma.
- Single, euhedral crystals embedded within a quartz or feldspar matrix with graphic intergrowth supports a magmatic origin.
- Finally, a lack of chloritization of biotite and unaltered plagioclase eliminate retrograde hydrothermal or greenschist facies overprinting.

4.3.3. Epidote in the WRO

Many rocks from the Wenatchee Ridge Orthogneiss do not show the correct mineral assemblage to be used as pressure indicators as Zen and Hammarstrom (1984) first indicated. Nearby pegmatite dikes cutting the Wenatchee Ridge Orthogneiss and containing identical

mineralogy were studied by Magloughlin et al. (2005) and Merkel (2007) and found to contain magmatic epidote which suggested that some epidote in the Wenatchee Ridge Orthogneiss may be magmatic. A Rb-Sr date on one pegmatite (epidote-plagioclase-muscovite isochron) yielded a date of 89 ± 6 Ma (Magloughlin, 1995). Because it was not initially obvious if the epidote in the Wenatchee Ridge Orthogneiss is magmatic or not, careful determination was done using petrography and the above criteria.

The majority of the epidote in the WRO is not associated with hornblende nor do they contain allanite-rich cores. Additionally, the plagioclase is commonly slightly altered to sericite or sausserite and at least slight chloritization of biotite is relatively common. However, 34 of the 64 sections studied of the WRO show clear evidence for magmatic epidote. As shown in Figure 4.6, euhedral epidote crystals are commonly contained within biotite and/or muscovite. Additionally, some epidote crystals are euhedral with oscillatory zoning, strongly suggesting a magmatic origin (Figure 4.10). Magmatic epidote is extremely common in the WRO samples and relatively rare in the BG samples.



WR-105-16

Figure 4.10. Photomicrograph from WR-105-16 (sample from Magloughlin, 1986) showing a crystal of oscillatory zoned epidote with a clinozoisite rim that was either encased by muscovite or has partially altered to muscovite. This is a clear example of magmatic epidote in the WRO. Field of view is 1 mm, XPL.

Magmatic and non-magmatic epidote seem to occur together in a few samples of the WRO. However, the epidote that appears to be subsolidus may be older and more resorbed magmatic epidote. The epidote-hornblende relationship is almost completely lacking in these samples, partly because hornblende is rare in these rocks. Instead, the epidote is most commonly associated with biotite, muscovite, and even chlorite, although the chlorite is almost certainly after biotite. As an included mineral, epidote crystallized before biotite and muscovite and this relationship has been noted by Schmidt & Poli (2004) to occur between 1.0 to 1.5 GPa in H₂O-saturated tonalite, generally consistent with conclusions reached by Merkel (2007). Epidote inclusions within biotite have alternatively been interpreted to be xenocrysts carried from depth within the biotite which crystallized when the magma was still 50-80% melt (Evans & Vance, 1987; Schmidt & Poli, 2004). Unfortunately the issue remains that crystallization sequences are still unknown at H₂O-undersaturated conditions (Schmidt & Poli, 2004).

4.3.4. Implications of Occurrence

The occurrence of magmatic epidote in a TTG suite indicates general pressure conditions at which the TTG was emplaced. There have been issues regarding whether these pressure estimates, backed up by Al-in-hornblende barometry, are measuring the emplacement pressure or the pressure at which epidote crystallized (Zen & Hammarstrom, 1986; Moench, 1986; Schmidt & Poli, 2004). Regardless, some pressure estimates based on the presence of magmatic epidote are generally considered to be reliable and are commonly used in magmatic epidote research. One method for estimating pressure conditions using magmatic epidote is based on crystallization sequence within a fluid saturated tonalite (Figure 4.11) (Schmidt & Poli, 2004). Crystallization of epidote is later with decreasing pressure. If this diagram is used for the WRO, which contains no hornblende (possibly because it crystallized early and was removed from the

melt), the evidence that epidote crystallized before biotite yields pressure estimates of 0.8 to >1.0 GPa (Figure 4.11). There is no evidence of epidote crystallizing before plagioclase, although possible zoisite inclusions within plagioclase in sample Z-119 may additionally indicate crystallization pressures greater than 1 GPa. Pressure estimates may also be performed using one of many stability field diagrams created by experimental TTG/magmatic epidote researchers.

above 1.0 GPa hornblende → **epidote** → plagioclase → biotite → quartz → K-feldspar;
1.0 to 0.8 GPa hornblende → plagioclase → **epidote** → biotite → quartz → K-feldspar;
0.8 to 0.6 GPa hornblende → plagioclase → biotite → **epidote** → quartz → K-feldspar;
0.6 to 0.5 GPa hornblende → plagioclase → biotite → quartz → **epidote** → K-feldspar.

Figure 4.11. Pressure estimates based on crystallization sequence from Schmidt and Poli (2004). The place of epidote in the sequence moves to the right with decreasing pressure. Crystallization sequences within an H₂O-undersaturated magma are unknown (Schmidt and Poli, 2004).

Pressure estimates may also be performed using one of many stability field diagrams (Figure 4.12), created by experimental TTG/magmatic epidote research. Figure 4.12 shows the stability field of magmatic epidote for tonalite at 1.9 GPa in a water saturated magma. The occurrence of garnet in a few of the WRO and BG samples will additionally help to constrain crystallization and possible emplacement pressures near 1.5 GPa (15 kb). The epidote-bearing

pegmatites which cut the WRO and BG contain rare garnet as well and at least one case in which garnet cross cuts epidote, indicating increasing pressure (Magloughlin et al., 2005).

It should again be emphasized that pressure estimates based on the presence of magmatic epidote are based on when epidote crystallized, which may have been when the magma was still in a crystal mush state. In the case where epidote is encased by biotite, some researchers have suggested that the biotite and epidote may represent xenocrysts which have been carried up from depth (Evans & Vance, 1987; Schmidt & Poli, 2004). If this is the case for the WRO, the epidote may have crystallized at depth and been carried upward where the entire TTG magma crystallized at lower pressures. This may be because epidote which crystallized at depth became unstable as the magma moved upward and epidote which was contained within biotite was armored by the biotite crystal. However, there is ample thermobarometric evidence in the area to indicate the WRO was emplaced at 8-10 kb (Magloughlin, 1986). In addition, the Si-rich nature of these magmas indicates high viscosities and thus possibly minimal upward transport once crystallization was well progressed. Details of the WRO magma viscosity and emplacement will be addressed in chapter 8.

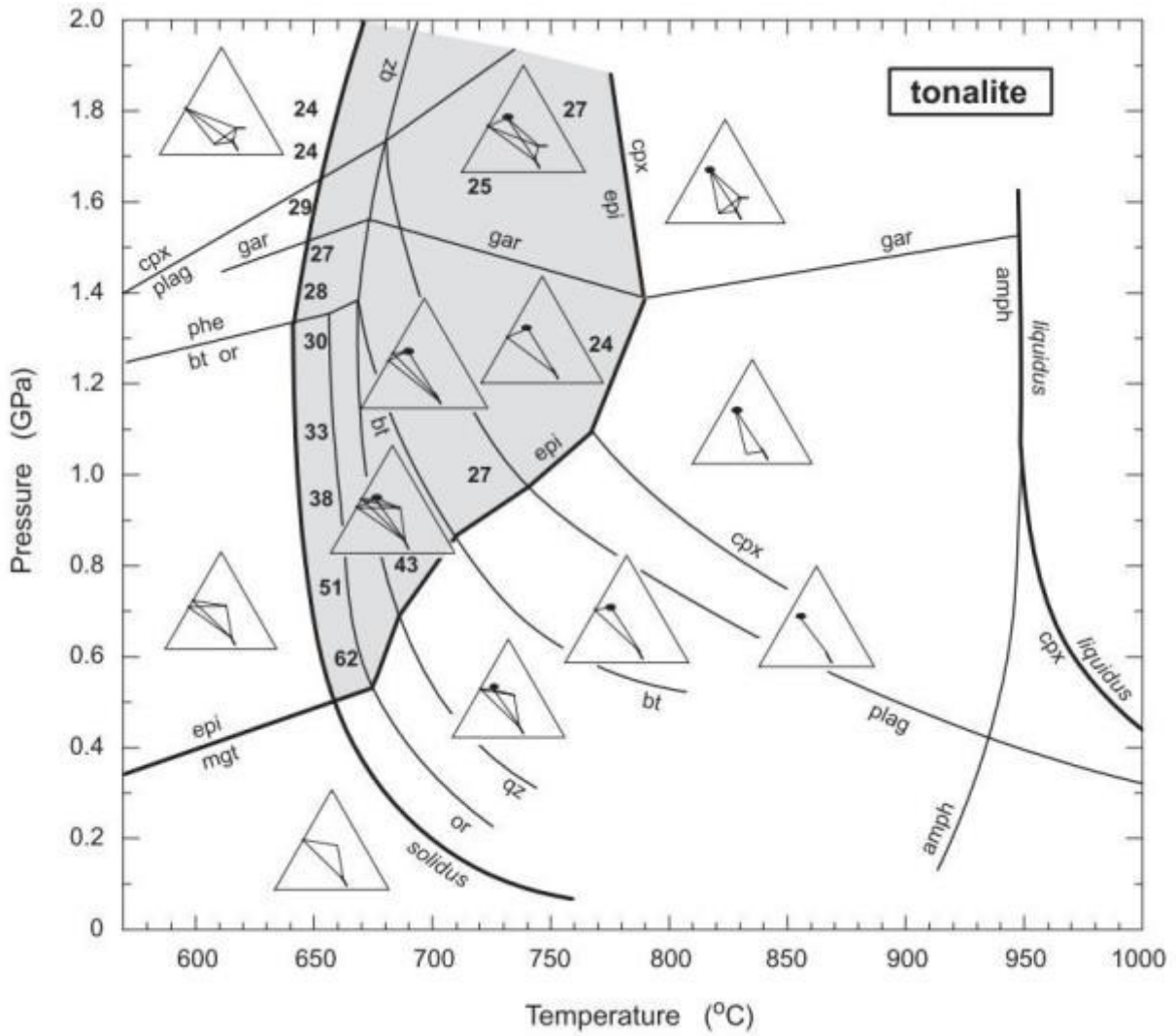


Figure 4.12. Pressure-temperature diagram showing the magmatic epidote stability field for tonalite (gray area) at 1.9 GPa in a H₂O-saturated magma. Triangles are ACF diagrams and the numbers represent experimental epidote compositions in Fe pfu. Figure from Schmidt & Poli (2004) after Schmidt & Thompson (1996).

5. METAMORPHIC OVERPRINT

5.1. Background

Many orthogneiss research papers fail to provide evidence of isochemical metamorphism. Most commonly, authors consider the presence of oscillatory zoning in plagioclase to be the primary indication that the rock is an orthogneiss. In addition to the presence of zoning, if sericitic, sausseritic, or chloritization alteration is not pervasive in the rock, it is commonly assumed that the igneous geochemistry is unaltered.

A metamorphic overprint checklist was developed as a more reliable petrographic indicator of metasomatic alteration. For this study, it is intended to be a simple and inexpensive way to demonstrate that an igneous rock which is deformed and/or metamorphosed has or has not been altered from the original igneous geochemistry. Ideally, this checklist could eventually be used to indicate where a sample lies in the gradual transition from an igneous to metamorphic rock. This thin section checklist will hereafter be referred to as the igneous to metamorphic transition checklist (ITMTC).

A petrologic analysis of the WRO requires evidence that the composition of the orthogneiss has not been changed from the original igneous composition. The deformational event that created a widespread foliation in the WRO may have coincided with metasomatism that could have altered the original igneous composition. Some of the WRO samples appear more altered than others, but it is unknown how much of this alteration is due to metamorphism and how much is due to weathering. The WRO magma was likely emplaced at amphibolite facies pressure and temperature conditions (Magloughlin, personal communication, 2012) which may have resulted in some retrograde style metamorphism upon cooling.

5.2. Sample Selection

Samples for the ITMTC were selected based on their location within the pluton and their general composition. Tonalitic samples from within (WRO) and outside (BG) of the pluton boundary were selected for this analysis (Figure 5.1). Some samples which were collected prior to this study by Dr. Jerry Magloughlin were also included in this analysis (WR and N samples in Figure 5.1). The WRO and BG pluton boundaries were defined by Magloughlin (1993) and Zuluaga & Stowell (2008), respectively.

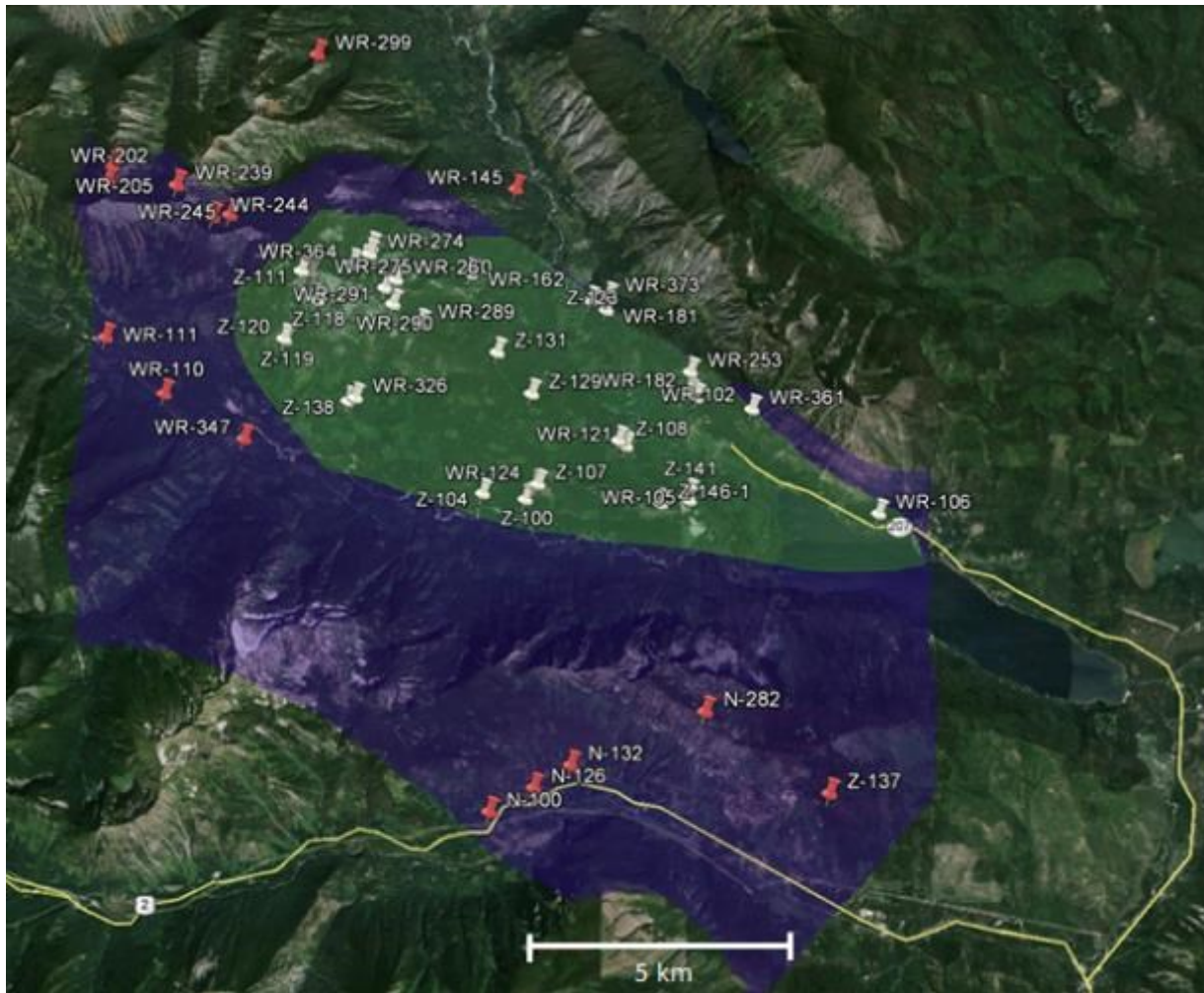


Figure 5.1. Map of locations for all samples which were used in the metamorphic overprint analysis. Red samples are located within the banded gneiss on the pluton periphery (BG samples). White samples are considered within the actual pluton boundary. The green pluton and blue banded gneiss boundaries are defined by Magloughlin (1993) and Zuluaga & Stowell (2008), respectively.

5.3. Methods

5.3.1. Quantification of metamorphic overprint using petrography

The ITMTC was created in order to categorize the amount of metamorphic overprint in each sample as well as to simultaneously categorize other properties of the samples such as epidote content and degree of alteration. Upon completing this checklist, correlations between the mineralogy and textural observations of the WRO can be established which will indicate whether the igneous geochemistry of the WRO was altered by metamorphism or not.

The concept behind this checklist is that it is possible to quantify the mineralogical and textural changes which occur as deformation and metamorphism intensify. The WRO samples are variably deformed and if deformation has driven significant metamorphism, there should be a progressive increase of those metamorphic effects throughout the samples. A lack of associated changes in mineralogy and texture in the samples which would indicate progressive metamorphism may provide evidence that the samples have not been significantly altered by metamorphism.

5.3.2. Criteria for creating the ITMTC

Biotite Ti Content

The concentration of Ti in biotite has been noted by many researchers, but the increasing biotite Ti content is a behavior noted in prograde metamorphism (Cesare, et al., 2008). Titanium concentration in biotite increases with increasing metamorphic conditions as long as Ti saturated phases such as rutile, ilmenite, or titanite are present (Guidotti, 1984). Therefore, in order to know if the Ti-biotite relationship is effective at gauging the grade of metamorphism, we need to know if titanite, ilmenite, or rutile is present in each case.

Because the WRO likely started out at high temperature and pressure by intruding into rocks at amphibolite facies, metamorphism from that event would be retrograde and the Ti content in biotite would presumably decrease as pressure and temperature decreased. Indeed, according to Cesare et al. (2008), biotite Ti content does decrease upon cooling as it is replaced by Mg. The decreasing Ti content can be balanced by growing a new Ti-bearing phase, presumably adjacent to the biotite grain. This balance can also be accomplished by growing the biotite grain larger, but would require K exchange with a K-bearing source (Cesare et al., 2008).

Sample Evaluation

The Ti content of biotite was gauged petrographically by estimating the pleochroic color of biotite grains and placing them into one of five categories. With increasing biotite Ti content, the colors will be blue-green (1), brown-green (2), dark brown (3), red-brown (4), and red (5). These colors correspond roughly to contents of <5, 4-7, 7-10, 10-13, and >13 wt. percent Ti in biotite (Figure 5.2) (Troger, 1979). Figure 5.3 shows representative biotite samples from the WRO that are considered to have high Ti-content (category 5) and low Ti-content (category 1). Samples which did not contain any biotite have no data in this category. If the Ti-content of biotite is linked in any way to the degree of metamorphism, it may be evident through correlation between the pleochroic color estimate and the foliation strength.

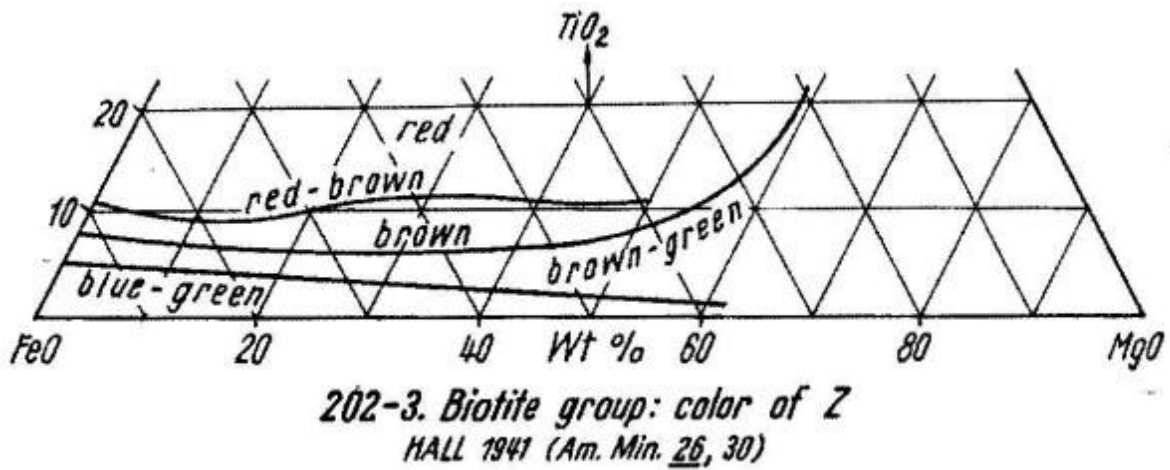


Figure 5.2. Graph from Troger (1979) which shows how the pleochroic color of biotite relates to Ti content.

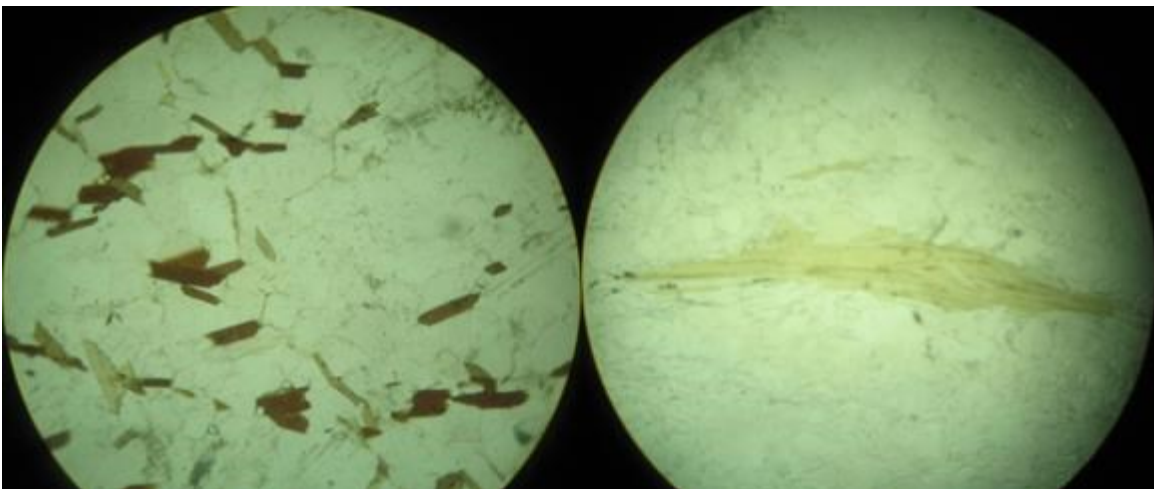


Figure 5.3. Photos showing what were considered to be high Ti-biotites (left from WR 110-1) and low Ti-biotites (right from WR 102-2). Field of view in both images is 2mm.

Twinning and zoning in plagioclase

Plagioclase twins and zonation indicative of an igneous origin would presumably be erased by subsequent metamorphism and/or deformation of the igneous rock. Slightly obscured twins, deformation twins, or relict zonation (preferentially altered Ca-rich cores, for example) may indicate that metamorphism has altered the grains and possibly the entire composition of the rock.

As metamorphic grade increases, the anorthite content of plagioclase grains also increases for metamorphic plagioclase (Deer et al., 2001). Because the WRO tonalites are thought to have intruded under amphibolite facies conditions, the anorthite content would presumably decrease as the pressure and temperature conditions decreased.

Currently the classification scheme for plagioclase in the thin section checklist is based on the presence of normal or reverse zoning in the plagioclase grain. The zonation is rated on a scale of one to four. The categories are as follows:

1. No zoning in plagioclase
2. Normal zoning (Ca-rich core, Na rim)
3. Reverse zoning (Na-rich core, Ca rim)
4. Both normal and reverse zoning (oscillatory, or in separate grains)

Sample Evaluation

Plagioclase grains in the tonalite were inspected for various types of twinning and/or zoning and the extent to which the twins or zones were obscured or destroyed by deformation/metamorphism. The method used to distinguish normal from reverse zoning involves measuring extinction angle differences between cores and rims as outlined by Nesse (2000). A more calcic portion of a plagioclase grain will typically have a higher extinction angle

than a more sodic portion (Nesse, 2000). The Michel Levy method outlined by Nesse (2000) was additionally used to determine the plagioclase composition by measuring multiple plagioclase grains in thin section and taking an average. Ideally, if metamorphism has altered the anorthite content of the plagioclase grains, there should be some correlation between the degree of deformation (quantified by strength of foliation) and the anorthite content. Likewise, if deformation and/or metamorphism has erased igneous plagioclase textures, we would expect to see no igneous zonation in samples with high foliation strength and intact igneous zonation in samples with low foliation strength.

Quartz grain size

As the amount of strain in a rock increases, quartz grain size commonly decreases via processes ranging from brittle fracturing to subgrain rotation recrystallization (SGR) and grain boundary migration (GBM) recrystallization (Passchier and Trouw, 2005). At amphibolite grade conditions, which were the likely conditions upon WRO intrusion, GBM and SGR are the most likely mechanisms for quartz grain size reduction. GBM is characterized by lobate grain boundaries, pinning microstructures, and recrystallized grains which may show no evidence of deformation (Passchier and Trouw, 2005). It may be possible that SGR mechanisms would have become active during retrograde conditions in the WRO if deformation continued at lower temperatures (Passchier and Trouw, 2005). If SGR has occurred within the WRO, subgrains which replace older, larger quartz grains may be seen (Passchier and Trouw, 2005). It should also be noted that while temperature does have a significant control on quartz deformation, other factors such as strain rate, the presence of water, and differential stress are also important to consider (Passchier and Trouw, 2005).

Sample Evaluation

Quartz grains were measured in each sample using the “in-ocular” ruler which was calibrated with a micrometer. An average of the quartz grain size measurements was taken from each thin section and subsequently used in the thin section checklist. If the metamorphism and deformation has affected the grain size of quartz, we would expect to see a correlation between the strength of foliation and quartz grain size.

Presence of perthite/anti-perthite

Potassium feldspar with exsolved albite is referred to as perthite while plagioclase with exsolved potassic feldspar is referred to as antiperthite (Winter, 2010). The presence of perthite or anti-perthite was recorded, first to identify how common the texture is throughout the WRO samples, and second because it may have important implications for the metamorphism of the WRO. According to Deer et al. (2001), anti-perthite is typically restricted to metamorphic rocks. Anti-perthite is most commonly hosted by plagioclase in the oligoclase to andesine range and is thought to be the result of exsolution where the potassium may have otherwise formed sericite (Deer et al., 2001). Conversely, K-feldspar blebs showing erratic distribution and irregular size may be a result of anti-perthitic replacement and not of exsolution origin.

Sample Evaluation

Figure 4.7 shows an example of anti-perthite which was seen in some of the WRO samples. The presence of perthite in the samples was recorded using one of the following categories: perthite present (1), no perthite or anti-perthite present (2), anti-perthite present (3). No samples contained both perthite and anti-perthite.

Degree of plagioclase alteration (sericite or saussurite)

Sericitization is a process in which minerals such as plagioclase are hydrated to produce sericite, which is a fine-grained white mica (Winter, 2010). Saussuritization is a similar process

which additionally involves epidote and/or zoisite (Winter, 2010). This category was predominately used to quantify the average amount of alteration present in the plagioclase grains in each sample. The amount of alteration seen in plagioclase grains may also relate to the strength of metamorphism. Conversely, the alteration may be due to other processes such as weathering or hydrothermal activity.

Sample Evaluation

The amount of alteration, either sericitic or saussuritic, in plagioclase grains was grouped into categories ranging from 0 to 100%. There were five separate categories with individual ranges of 0-10% (category 1), 10-30% (2), 30-50% (3), 50-80% (4), and 80-100% (5). Figure 5.4 shows examples of high and low alteration. Because metamorphism is commonly driven by deformation and involves fluid phases which would promote plagioclase alteration, we would expect to see a correlation between the amount of deformation (measured by foliation strength) and the amount of plagioclase alteration.

Strength of foliation

The degree of foliation development in the WRO samples is likely linked to the degree of deformation experienced. Because deformation commonly facilitates metamorphism, we would expect to see more evidence of metamorphic reactions in the most deformed samples. The formation of foliations in the WRO samples may have occurred by processes such as mechanical rotation of tabular grains, solution transfer, dynamic recrystallization, or oriented growth in a stress field (Passchier and Trouw, 2005). While the amount of strain certainly has an effect on the amount of permanent deformation (foliation), other factors such as rock composition, fluid pressure, fluid composition, temperature, pressure, and stress orientation are also important when considering foliation development (Passchier and Trouw, 2005).

Sample Evaluation

The scale of this category ranges from 0 to 9 with a 0 representing no visible foliation and a 9 representing a strong foliation continuous throughout the thin section. The degree of foliation development in each sample was estimated using the chart shown in Figure 5.5.

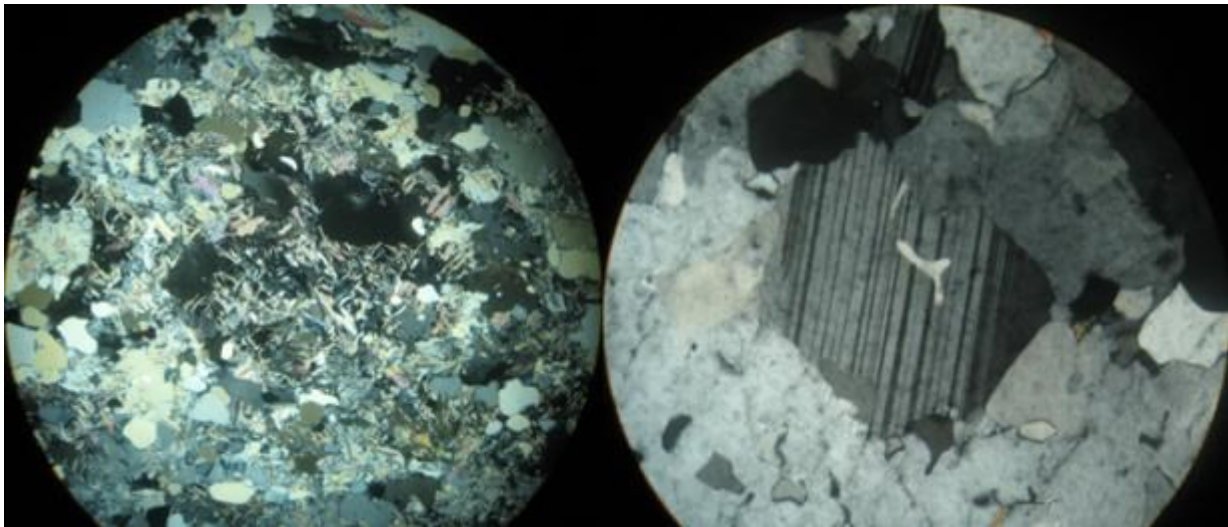


Figure 5.4. Photos showing high sericitic alteration (left from WR 102-2) and low sericitic alteration (right from WR 124-2). Field of view in both images is 5mm.

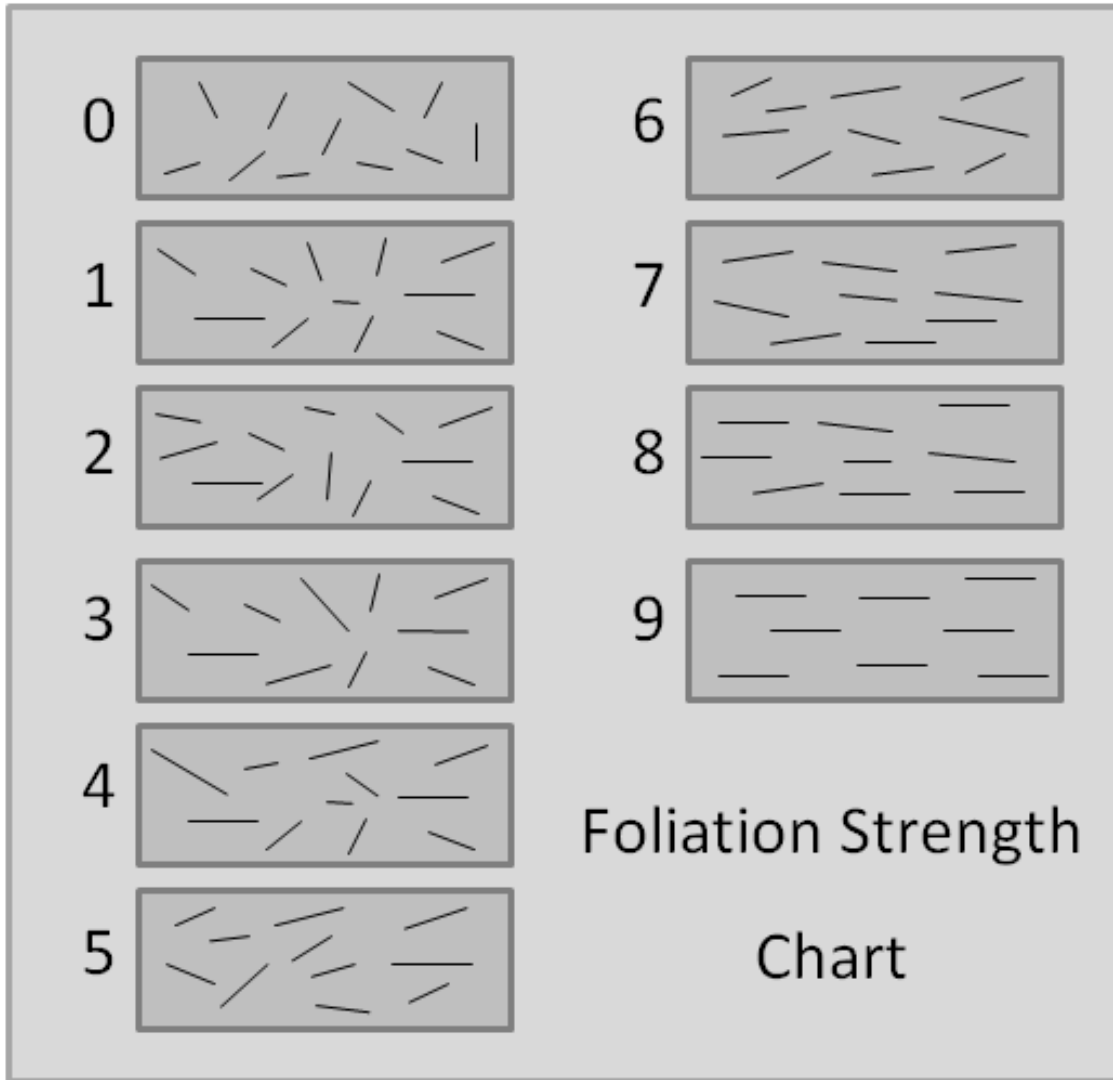


Figure 5.5. Chart showing foliation strength ratings from 0 to 9.

Chloritization of Biotite

Chloritization is a process in which chlorite replaces any mafic mineral typically at low temperature where water is available (Winter, 2010). The chloritization of biotite could be due to retrograde metamorphism, secondary low grade metamorphic overprint, or secondary alteration. If metamorphism is being driven by deformation, a correlation between the chloritization of biotite and foliation strength would be expected.

Sample Evaluation

Samples were evaluated by petrographic analysis of biotite grains in each sample to identify if any chloritization has taken place. Each sample was then placed into one of three categories: chloritization is present (1), not present (2), there was no biotite in the section (3).

Presence of Metamorphic Minerals

The presence of a strictly metamorphic mineral would indicate that metamorphism has had a significant effect on the WRO samples. This is somewhat problematic, however, because metamorphic minerals such as epidote and muscovite are common as magmatic phases in the WRO samples. For this checklist, the identification of magmatic versus metamorphic epidote and muscovite was recorded throughout the analysis. Samples which have distinctly metamorphic minerals may be expected to show a correlation with the foliation strength such that more strongly foliated samples are more likely to grow metamorphic minerals. That being said, the textures indicative of metamorphic or igneous origin for muscovite and epidote were a key part of this analysis.

Sample Evaluation

Sample evaluation in this category involved the determination of magmatic and/or metamorphic epidote and muscovite based on textural and spatial relationships. The

determination of magmatic epidote was based on the criteria outlined in detail in Chapter 3. The determination of magmatic muscovite was based on the relative size and shape of the muscovite grains such that large, subhedral grains were considered to be magmatic while smaller, anhedral grains or aggregates were considered to be of metamorphic origin.

5.4. Results

The overall results are shown by Tables 11.1 and 11.2 in Appendix C. WRO and BG samples have been analyzed separately using the thin section checklist and their results will be presented separately outside of the overall summaries of petrographic observations.

Biotite Ti content

The results of the biotite Ti analyses can be seen plotted against foliation strength in Figures 5.6 and 5.7 for the WRO and BG samples, respectively. Biotite is commonly present with inclusions of titanite or with titanite in contact with biotite. Biotite is rarely in contact with ilmenite or rutile.

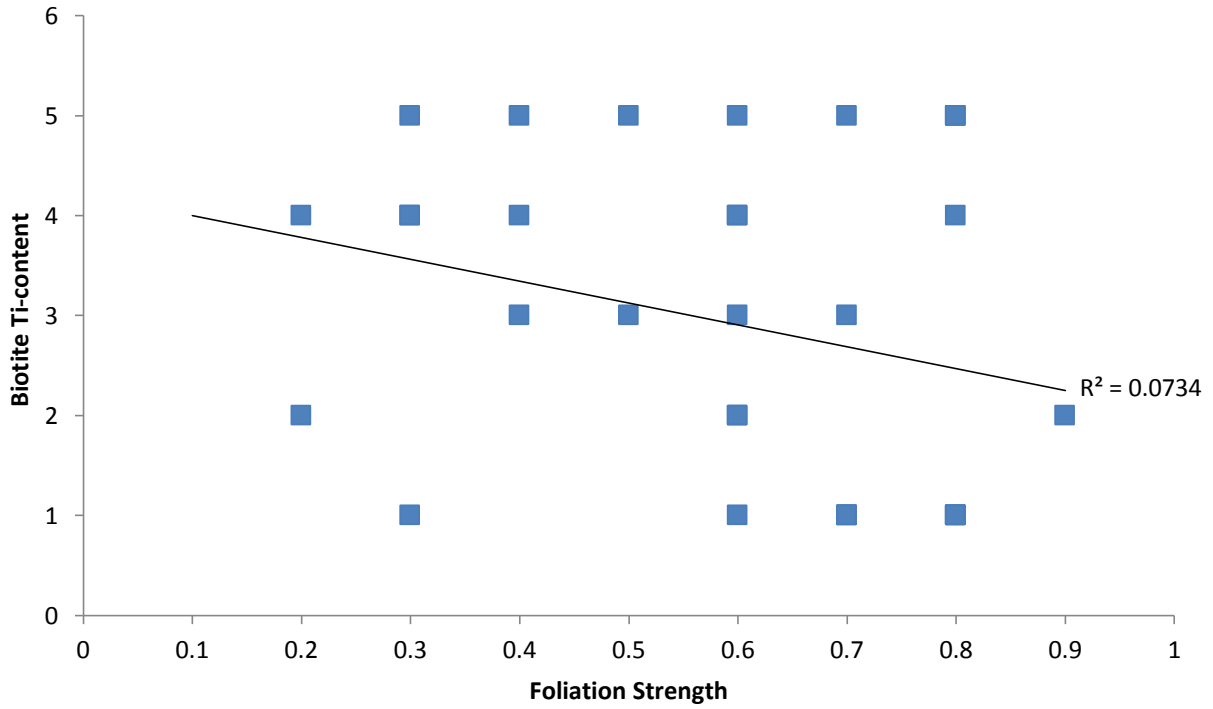


Figure 5.6. Graph of biotite Ti content versus foliation strength for the WRO samples.

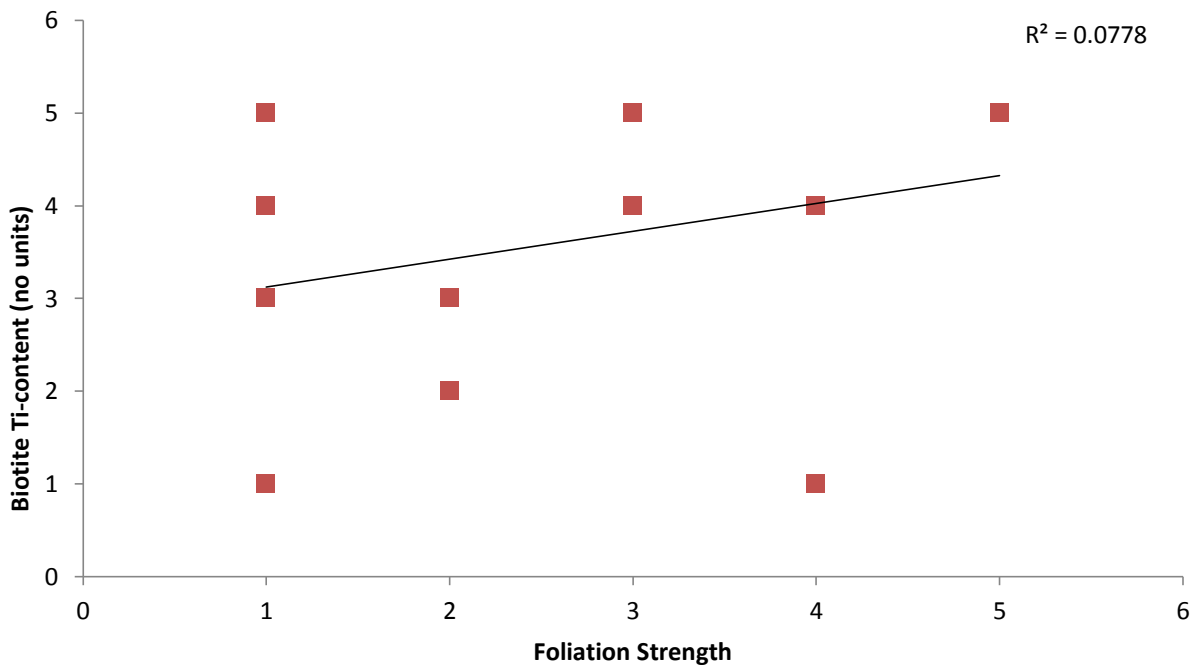


Figure 5.7. Graph of biotite Ti content versus foliation strength for the BG samples.

Twinning and zoning in plagioclase

Normal zonation in plagioclase identified by extinction angles and/or clear oscillatory zonation occurs in 10 of the 39 WRO samples (26%) and 13 of the 23 of the BG samples (56%). The average foliation strength is 5.8 (n=10) for WRO samples with normal zoning and 5.0 (n=29) for those without. The average foliation strength is 5.9 (n=13) for BG samples with normal zoning and 5.9 (n=10) for samples without.

Quartz grain size

Plots of quartz grain size versus foliation strength are shown in Figures 5.8 and 5.9 for the WRO and BG samples, respectively. Microstructures indicative of SGR or GBM recrystallization in quartz were not found in the WRO samples. The most common deformational microstructure was a slight to moderate undulatory extinction in quartz.

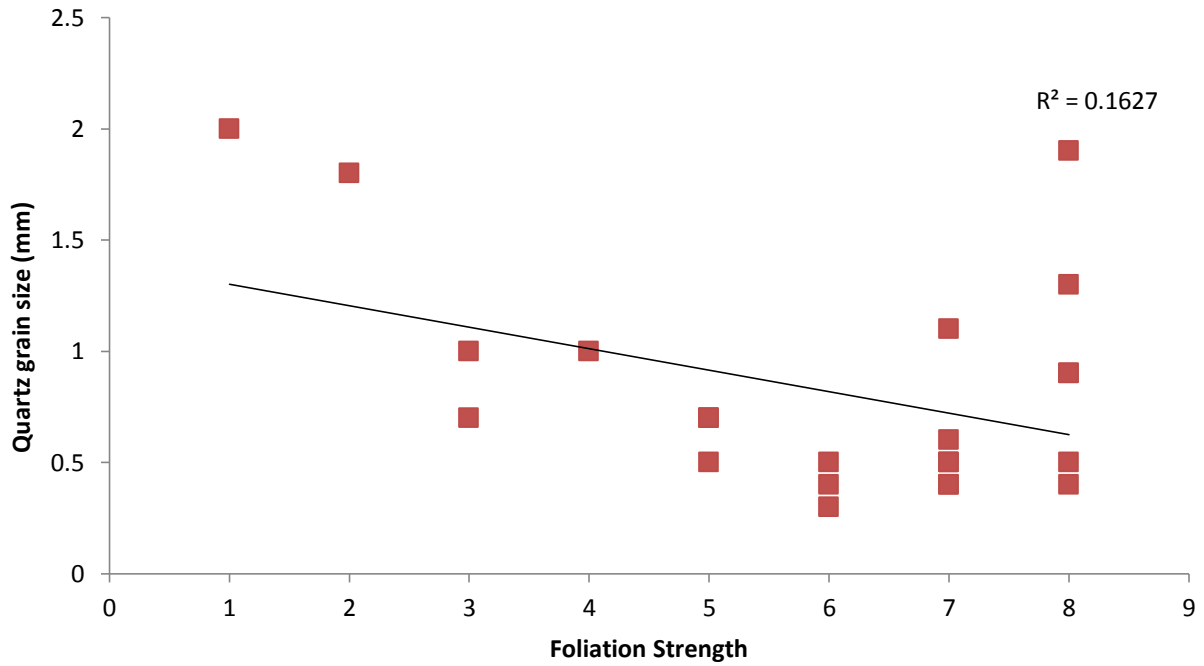


Figure 5.8. Graph of quartz grain size versus foliation strength for the WRO samples.

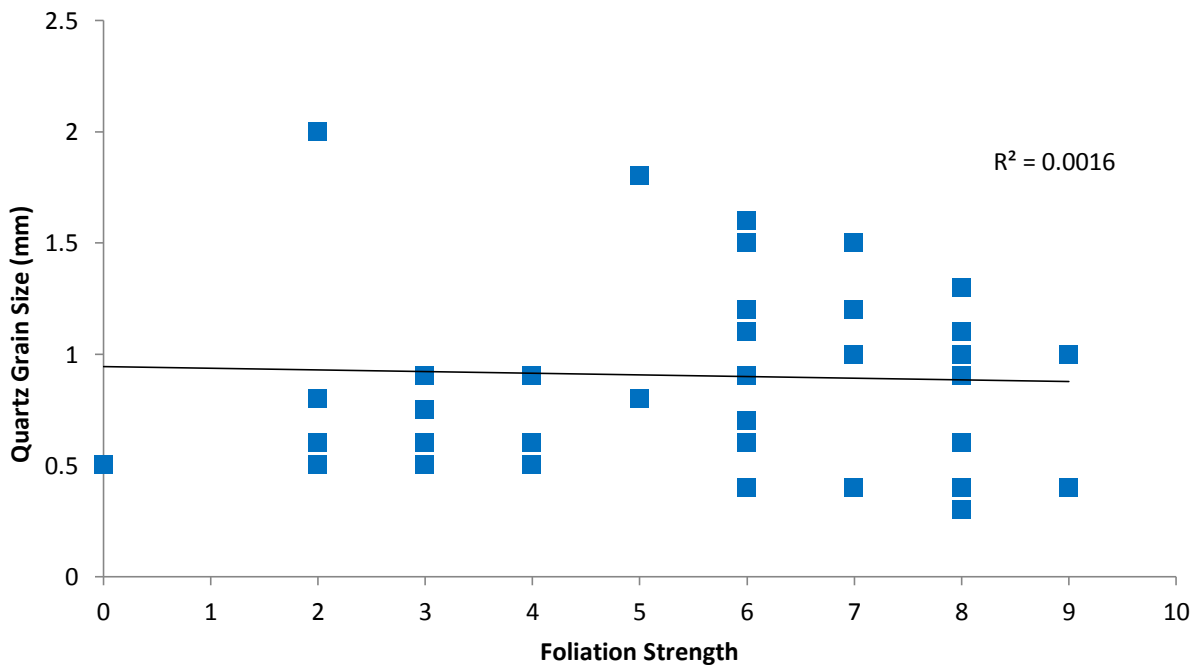


Figure 5.9. Graph of quartz grain size versus foliation strength for the BG samples.

Presence of perthite/anti-perthite

Antiperthite, where present, always occurs as irregular intergrowths within plagioclase of oligoclase composition (Figure 4.7). Five of the WRO samples and five of the BG samples have anti-perthite. Only two of the BG samples have perthite.

Degree of plagioclase alteration

Sericite was generally more common than sausserite in altered plagioclase grains. Additionally, the cores of plagioclase grains were preferentially altered in relation to the rims in the majority of both BG and WRO samples. Plots of plagioclase alteration versus foliation strength can be seen in Figures 5.10 and 5.11 for the WRO and BG samples, respectively.

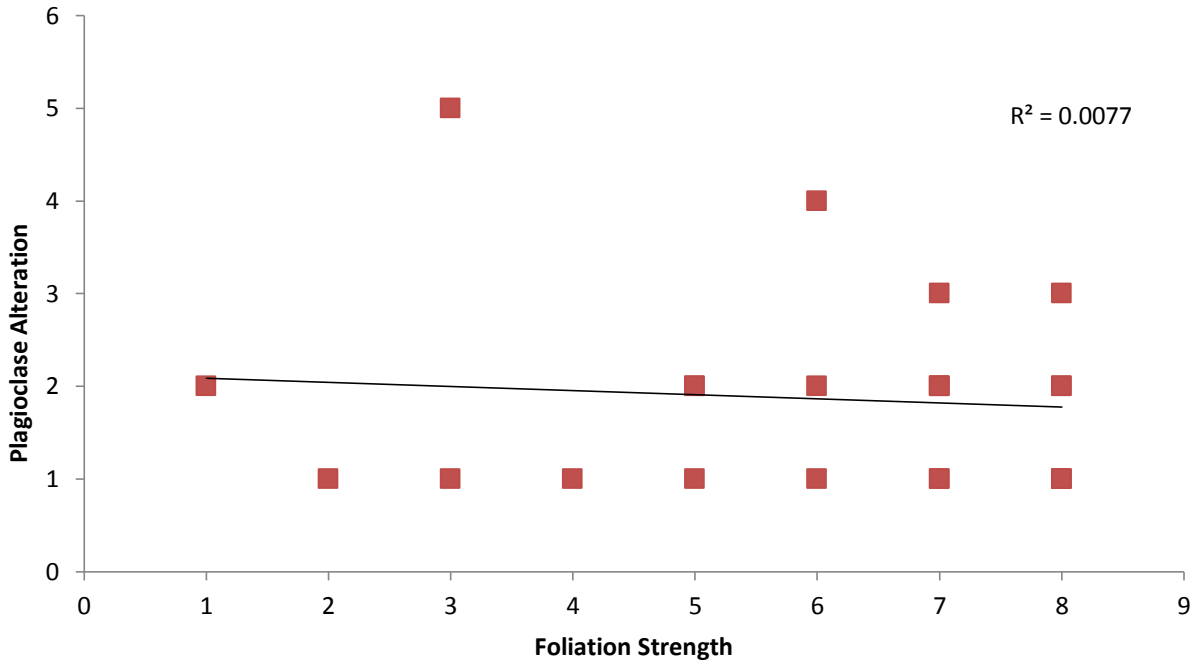


Figure 5.10. Graph of plagioclase alteration versus foliation strength for the BG samples.

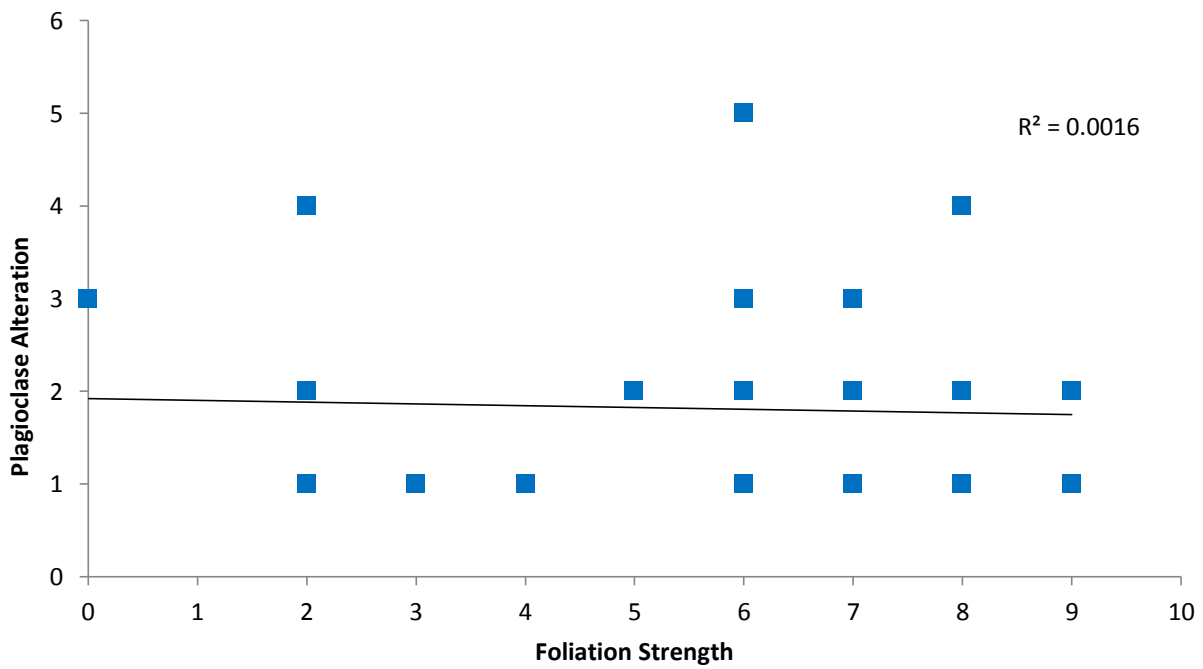


Figure 5.11. Graph of plagioclase alteration versus foliation strength for the BG samples.

Strength of foliation

Foliation in the WRO is most commonly defined by biotite and/or muscovite and ranges widely in strength among the samples. The average foliation strength rating for WRO and BG samples is very close at 5.3 and 5.9, respectively.

Chloritization of biotite

From the checklist, the average foliation strength where biotite has undergone chloritization is 5.6 for the WRO samples (n=22, SD=2.1) and 5.5 for the BG samples (n=12, SD=2.1). The average foliation strength for samples with unaltered biotite is 4.9 for the WRO samples (n=14, SD=2.6) and 6.9 for BG samples (n=10, SD=1.2). Given the standard deviations, there is no statistical difference between the WRO and BG samples regarding foliation strength and altered or un-altered biotite. Three of the WRO samples and one of the BG samples contain no biotite.

Presence of metamorphic minerals

While some traditionally metamorphic minerals are found as igneous phases in the WRO, there are a few WRO samples which contain sillimanite, secondary epidote, metamorphic muscovite, or secondary amphibole, which are all considered to be metamorphic phases. The average foliation strength for WRO samples with only magmatic, magmatic and metamorphic, only metamorphic, and no epidote is shown on Figure 5.12. Figure 5.13 shows the same graph for the BG samples.

5.5. Discussion

The common textural relationships between biotite and titanite may indicate that titanite is acting as a Ti buffering phase in the WRO upon cooling in some cases. Titanite would not be acting as a Ti-reducing phase in cases where titanite is included within biotite. The Principle of

Inclusion indicates that titanite must have grown before biotite and could therefore not have grown in order to reduce biotite Ti content. Because of the minimal amount of a Ti-rich phase required to work as a Ti-releasing mechanism, any Ti-reducing reaction between biotite and microscopic rutile or ilmenite crystals may not be visible in thin section. A correlation between the amount of Ti in biotite and the strength of the foliation would be expected, but is not the case for the BG or WRO samples (Figs.5.6, 5.7).

Normal zonation in plagioclase is more common in BG than WRO samples but does not show the anticipated anti-correlation with foliation strength. For the WRO samples, normal zonation, indicative of igneous growth, is more common in samples that have a stronger foliation than those with no normal zonation. Similarly, the BG samples show the same average foliation strength for samples with and without normal zonation. Instead of foliation formation having erased normal zonation, it appears to have had no effect, the opposite effect, or have no statistical significance in some cases, which is perplexing. The An content of plagioclase also had no correlation with foliation strength such that deformation appears to have had no control on plagioclase growth.

Quartz shows little to no evidence for SGR or GBM recrystallization which indicates that high grade deformation and metamorphism may not have significantly affected the entire WRO equally. However, quartz in 22 of the WRO samples (56%) and 18 of the BG samples (78%) did show variable degrees of undulose extinction formed by deformation. There was no evidence of brittle deformation in these thin sections, therefore the deformation mechanisms which resulted in the undulose extinction must have taken place at greater than 300° (Passchier and Trouw, 2005). The undulose extinction in quartz may be the result of dislocation creep and bulging recrystallization (BLG) at lower grade conditions (300-400°C) (Passchier and Trouw, 2005). At

low to moderate grade conditions, however, evidence for pressure solution would be expected, assuming fluids were available, and does not appear in any of the sections studied. It may be that the quartz was deformed synchronously with the foliation formation, or that the undulose extinction is an overprint of a former high-grade quartz deformation which removed evidence of strain (Passchier and Trouw, 2005). Undulose extinction in quartz does not show any simple relationship with foliation strength such that samples with deformed quartz do not always have high foliation strength ratings.

According to Deer et al. (2001), the antiperthite present in five WRO and five BG samples could be of metamorphic origin. However, because of the erratic distribution of microcline blebs in oligoclase, it may be that the anti-perthite is due to replacement and not exsolution. Regardless, the textures could indicate that a metamorphic reaction or exsolution took place in these 10 samples.

Preferentially altered cores in the plagioclase grains were Ca-rich as opposed to the unaltered Na rims and this relationship additionally supports the interpretation that the plagioclase grains are of igneous origin. If plagioclase grains have undergone some amount of albitization in which Na is substituted in for Ca, the additional Ca may account for the presence of saussurite and/or secondary epidote present in some samples (Fiebig and Hoefs, 2002).

Because the biotite and muscovite grains that define a foliation in the WRO samples somewhat commonly contain euhedral inclusions of titanite and epidote, the process of mechanical rotation of grains with a high aspect ratio is the most likely foliation development mechanism. Many other foliation formation processes such as dynamic re-crystallization would likely alter euhedral inclusions during the process. If the foliation had formed via processes such

as dissolution-precipitation, pressure solution seams would be expected, which are not present in any of the sections (Passchier and Trouw, 2005).

The foliation strength for the WRO samples appears to be slightly higher, on average, at 5.6 for the samples with chloritized biotite compared to 4.9 for samples with unaltered biotite. The average foliation strength is higher at 6.9 for the non-chloritized BG samples than the chloritized samples at 5.5. However, given the standard deviations for these results, none of the averages are significant. Chloritization of biotite is likely not a good indicator of metamorphic overprint or chemical change in this case. As biotite is replaced by chlorite, K^+ is exchanged for H^+ (Fiebig and Hoefs, 2002). In these cases, it would be good to know what is happening with the excess potassium. It may be leaving the system, or the excess potassium could contribute to the growth of muscovite (sericite), or overgrowths on existing muscovites.

Samples with metamorphic epidote would presumably show higher foliation ratings than those in which magmatic epidote textures are preserved. However, WRO samples with only metamorphic epidote have the lowest foliation ratings while samples with magmatic epidote textures have much higher foliation ratings (Figure 5.12). BG samples show the predicted results where samples with metamorphic epidote have higher foliation ratings than those which preserve magmatic textures (Figure 5.13). Again, the highest foliation strength rating is for the category which shows no epidote present. It may be that high levels of deformation, leading to the strong foliation rating, also led to the loss of epidote by destabilization. It should be noted that the dissimilar numbers of samples used to create the averages in Figures 5.12 and 5.13 may cause the findings to be unreliable.

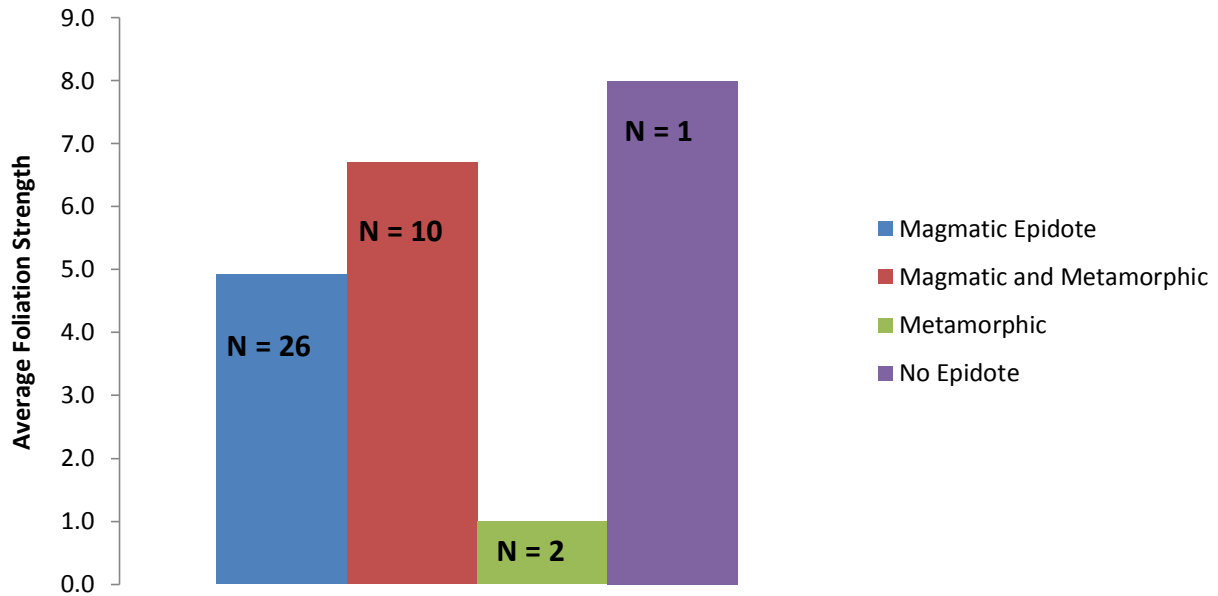


Figure 5.12. Graph of magmatic and metamorphic epidote occurrences compared with foliation strength for the WRO samples.

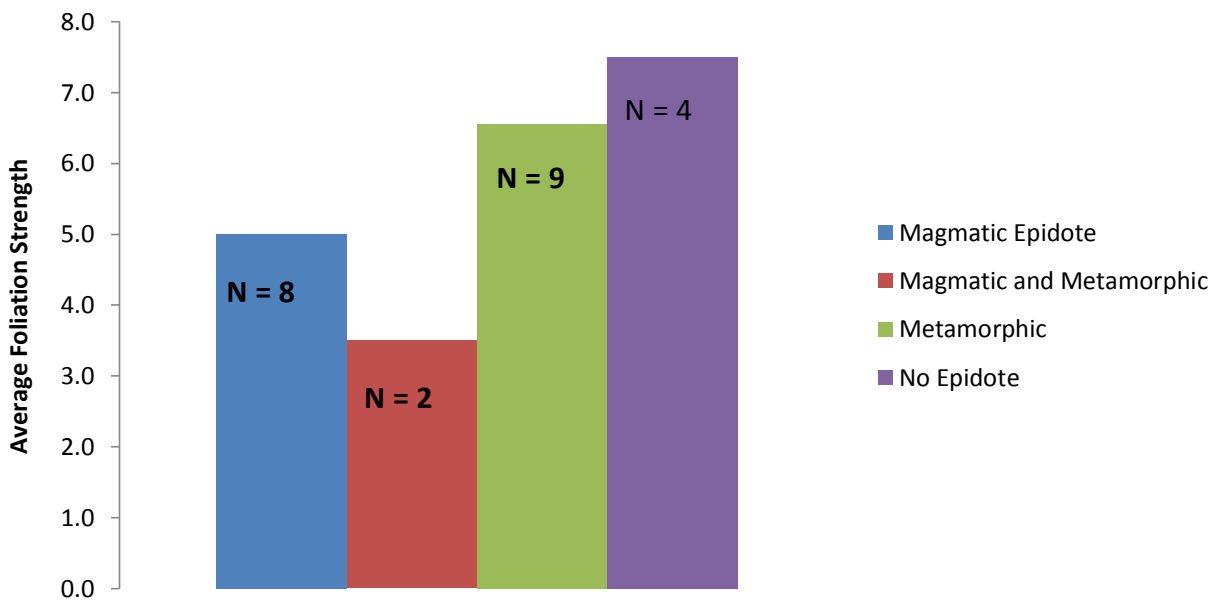


Figure 5.13. Graph of magmatic and metamorphic epidote occurrences compared with foliation strength for the BG samples.

Future work

This checklist would benefit from tests which involve more discrete data and less categorical data (e.g. modal percentages obtained using imaging software). The thin section checklist could also benefit from microprobe analyses of minerals. For example, if the biotite Ti content is to be ultimately utilized as an indication of the degree of metamorphism, electron microprobe analyses will be needed as done by Cesare et al. (2008).

This checklist works primarily off of the assumption that deformation drives metamorphism and therefore that the degree of metamorphic overprint can be gauged by the strength of the foliation. Because there are so many factors controlling the degree to which a foliation will form in a rock, this may not be a valid assumption to make. Other factors such as rheology, presence of minerals with high aspect ratios, presence of fluids, and the stress orientations are very important to know in order to understand how a rock behaves under stress. Considering that this is a system based on petrography alone, some of the assumptions mentioned are crucial to its effectiveness until more accurate methods can be used (EBSD to quantify fabric strength and/or spot compositional analyses).

Ideally, a system like the ITMTC could be used to provide igneous and metamorphic petrologists an inexpensive way to identify where their samples lie in the progressive transition from an igneous to metamorphic rock.

5.6. Conclusion

The ITMTC found a few indications of metamorphic effects such as the presence of secondary epidote, muscovite, and antiperthite. The thin section checklist data did not reveal correlations expected for metasomatized rocks. Based on a lack of many anticipated correlations with foliation strength, especially a lack of new growth of metamorphic minerals, the results of

the thin section checklist suggest metamorphism has not significantly altered the composition of the WRO samples. Samples not containing minerals interpreted to be metamorphic, and samples not pervasively altered should have a mostly-preserved original composition.

6. ARCHEAN COMPARISON

6.1. Purpose - Why identify an Archean Analog?

As discussed in Chapter 3, approximately 90% of 4.0-2.5 Ga continental crust by volume is part of the tonalite-trondhjemite-granodiorite (TTG) suite of igneous rocks. Despite the abundance and volumetric importance of Archean TTGs, the petrogenetic processes that formed them are poorly understood due to reworking, removal from their original tectonic setting, alteration, and limited exposure. The identification of a relatively young Archean TTG analog that is unaltered, well exposed, and proximal to its tectonic setting, will lead to a greater understanding of early continental evolution. The null hypothesis of this specific test is that the Wenatchee Ridge Orthogneiss (WRO) is a Mesozoic analog of Archean TTG.

6.2. Indicative Archean Geochemistry

Archean TTGs have high La/Yb ratios ($5 < \text{La/Yb} < 150$), and low Yb (< 8.5), compared to post-2.5 Ga granitoids produced in subduction zones that have low La/Yb ratios (< 20) and relatively high Yb content ($4.5 < \text{Yb} < 20$) (Martin, 1993). These trace element constraints on Archean TTGs are often referred to as the “Archean signature”. Drummond and Defant (1990) also separated TTD into two categories; high-Al TTD and low-Al TTD. Low-Al TTD is low in Sr ($< 200\text{ppm}$), shows a negative Eu anomaly, slightly increased light rare earth elements (LREEs), and the heavy rare earth elements (HREEs) form a flat line when plotted on a spider plot (Drummond et al., 1990). High-Al TTD has high Sr ($> 300\text{ppm}$ up to $> 2000\text{ppm}$), no Eu anomaly or a very small one, low to medium amounts of K/Rb, high LREE content, low HREE content, low Y ($< 15\text{ppm}$), and low Nb ($< 10-11\text{ppm}$) (Drummond et al., 1990). TTG geochemistry is further described in Chapter 3.

6.3. Methods

6.3.1. Archean comparison

The initial comparison of the WRO to Archean TTGs was done by plotting the WRO samples on a diagram created by Martin (1993) containing separate fields for Archean and Post-Archean TTGs based on Yb, La, and Y values (Figure 6.1). Based on this plot alone, the WRO appears to have the Archean geochemical signature. However, to test this comparison, the comparison of WRO samples to other well documented TTGs and granitoids was done by discriminant analysis using statistiXL. Discriminant analysis seeks to find linear combinations of variables that produce the maximum difference between defined groups (Davis, 2002). Ideally, the groups will be separated as much as possible while also having the least amount of ‘inflation’ within groups (Davis, 2002). The first discriminant analysis was conducted to compare the WRO and BG samples to Archean TTGs. S-I-A-M granitoid types are included in the analysis along with additional TTGs of differing origins. S-I-A-M is a classification scheme for granitoids in which granitoids are interpreted to have a sedimentary, igneous, anorogenic, and mantle origin (Winter, 2010). A second discriminant analysis was performed using only a selection of elements immobile during metamorphism in order to avoid any possible geochemical alteration of the WRO.

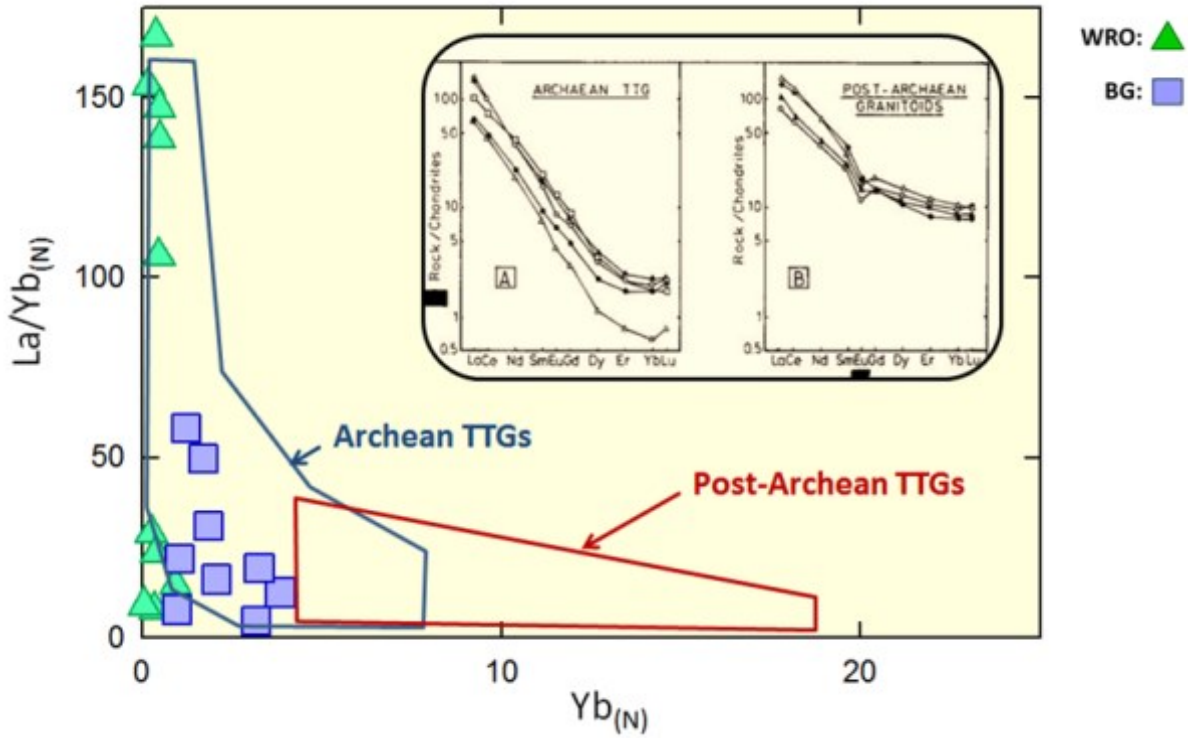


Figure 6.1. $(La/Yb)_N$ versus $(Yb)_N$ diagram showing the Archean geochemical signature of the WRO and BG samples (modified from Martin, 1993). The two REE plots and the diagram show that Archean granitoids are low in Yb and other REE concentrations while post-Archean granitoids have relatively high Yb and other REE concentrations (Martin, 1993).

6.3.2. Sources of Archean Data

Well-categorized TTG suite and granitoid rock samples were chosen from four research articles and a petrology textbook to serve as reference populations representing TTGs and granitoids derived from different tectonic settings and time periods. Samples were compared to tonalite data from Martin et al. (2004), Drummond & Defant (1990), Condie (2005), Nehring et al.(2009), and granitoid data from Winter (2010). Within the data from the four articles, there are 15 different populations of TTGs ranging in age from early Archean to Cenozoic. The 15 different populations also represent different types of petrogenetic mechanisms associated with different tectonic settings. The different populations represent partial melting of subducting slabs, partial melting of overthickened underplated crust, and fractional crystallization from a basaltic parent magma. Data from Winter (2010) includes four representative samples of S-I-A-M type granitoids and one sample of a typical Archean TTG. Raw data used for the comparison is given in tables 11.3 and 11.4 in Appendix D.

Following are the number of samples used for each category in the analysis: WRO: 15, BG: 15, Archean_DD: 7 (average), Archean_Winter: 355 (average), A-type: 148 (average), I-type: 1074 (average), S-type: 704 (average), M-type:17 (average), TTG gneiss 3.2 Ga: 6, TTG<3 Ga: 666 (average), 3<TTG<3.5 Ga: 320 (average), Cenozoic: 7 (average), Proterozoic: 752 (average), Phanerozoic: 698 (average), Early Archean: 212 (average), Late Archean: 831 (average).

6.3.3. Chemical parameters used for tests

The elements La, Yb, and Y were used to analyze the relationship with Archean TTGs because they are characteristic of Archean TTGs and have been used for similar analyses by Drummond and Defant (1990) and Martin (1993). For the immobile element analysis, trace

elements Ti, Cr, Zr, and Y were chosen as they are generally immobile during metamorphism (Winter, 2010).

6.4. Results

6.4.1. Archean Analysis

Test results for discriminant analysis using statistiXL are displayed in many different tables and figures which will be explained for each case. Only the relevant discriminant plots that were created for each discriminant function were included for each case. Plots were only chosen which had functions that represented the most variation amongst the samples, best separated the samples, and kept the data into the least inflated clusters.

The first discriminant analysis compared the WRO and BG samples to the reference populations based on elements characteristic of Archean granitoids. The percent of variability (Table 6.1) shows what percent of the total variance between groups belongs to each eigenvalue. Here, function 1 makes up 71 percent of the variability. The canonical correlation shows how well a function separates the groups. The high r value of the canonical correlation (on a scale from 0-1) of function 1 shows that it separates the groups well. Functions 2 and 3 also are good separators of the groups but make up less percent of the variability. The Wilks' Lambda value (Table 6.2) shows how significant each eigenvalue and therefore discriminant function is. The Chi Squared value and P-value of function 1 is most significant. Function 2 is somewhat significant and function 3 is rather insignificant. Standardized discriminant functions (Table 6.3) are calculated from a pooled covariance matrix for each discriminant function. The magnitude of the variable value indicates how much each element contributes to each discriminant function. Function 1 is strongly defined by Yb. Function 2 is defined by Y and Yb. Function 3 involves La, Yb, and Y. Raw discriminant scores are shown on Table 6.4.

Explained Variance (Eigenvalues)			
	Function 1	Function 2	Function 3
Eigenvalu	10.164	3.285	0.786
% of Var.	71.402	23.078	5.520
Cum. %	71.402	94.480	100.000
Can.Corr.	0.954	0.876	0.663

Table 6.1. Explained variance for the Archean discriminant analysis.

Wilks' Lambda			
	Function 1- 3	Function 2- 3	Function 3- 3
Wilks' Lam	0.012	0.131	0.560
Chi Sq	177.912	81.403	23.195
DF	48	30	14
P	0.000	0.000	0.057

Table 6.2. Wilks' Lambda and significance values for the Archean discriminant analysis.

Standardised Discriminant Function Coefficients			
Variable	Function 1	Function 2	Function 3
Y	-0.225	-3.564	-0.714
La	0.418	-0.020	0.930
Yb	1.153	3.446	0.333

Table 6.3. Standardized discriminant function coefficients for the Archean discriminant analysis.

Casewise Discriminant Scores				
Case	Group	Fn 1	Fn 2	Fn 3
39	Proterozoic 2	1.021	-2.596	0.214
33	3<TTG<3.5 Ga	-0.008	-4.583	0.827
36	Archean_DD	-0.620	1.994	0.638
51	Archean_Winter	1.037	1.837	1.943
50	A-type	15.508	4.012	-0.256
18	BG	-1.846	0.961	-0.882
19	BG	-1.133	-0.416	0.430
20	BG	-1.654	0.995	-0.506
21	BG	-0.869	-3.012	-0.962
22	BG	-0.826	-2.424	-0.420
23	BG	-0.799	0.455	0.891
24	BG	-1.271	0.825	-0.377
25	BG	-1.028	1.383	0.353
26	BG	-1.145	1.408	-0.841
27	BG	-1.330	0.545	0.221
28	BG	0.314	0.319	-0.817
29	BG	1.449	1.177	-0.189
30	BG	2.431	1.724	-0.623
31	BG	1.108	1.480	-0.649
35	Cenozoic	-0.731	2.619	-0.005
37	Early Archean	0.177	0.416	0.720
48	I-type	4.063	-1.944	-0.184
38	Late Archean	0.586	-0.703	2.038
47	M-type	2.895	-3.977	-2.907
40	Phanerozoic	0.372	-1.667	-0.439
49	S-type	3.831	-2.629	-0.742
41	TTG gneiss (3.2 Ga)	0.649	-0.554	4.131
42	TTG gneiss (3.2 Ga)	0.643	-0.489	1.054
43	TTG gneiss (3.2 Ga)	0.215	-0.716	-0.128
44	TTG gneiss (3.2 Ga)	4.057	-2.269	-0.476
45	TTG gneiss (3.2 Ga)	0.595	0.257	-0.302
46	TTG gneiss (3.2 Ga)	0.881	-0.546	-1.010
34	TTG<3Ga	0.095	-2.499	1.182
32	TTG>3.5 Ga	0.569	-2.289	1.602
1	WRO	-2.113	1.049	-0.864
2	WRO	-2.056	0.728	-0.863
3	WRO	-2.144	1.373	-0.892
4	WRO	-1.377	0.076	0.477
5	WRO	-1.572	0.050	0.023
6	WRO	-1.410	-0.069	0.424
7	WRO	-1.948	0.447	-1.077
8	WRO	-2.004	0.778	-0.828
9	WRO	-2.083	0.665	-0.998
10	WRO	-2.139	1.333	-0.886
11	WRO	-1.835	0.225	-0.874
12	WRO	-1.005	1.292	1.574
13	WRO	-1.852	0.987	-0.339
14	WRO	-1.216	0.456	0.927
15	WRO	-1.309	0.100	0.596
16	WRO	-1.279	0.260	0.986
17	WRO	-1.892	1.155	-0.910

Table 6.4. Raw discriminant scores for the Archean discriminant analysis.

6.4.2. Immobile Element Analysis

In the results of the discriminant analysis involving chemical parameters immobile during metamorphism, function 1 makes up the majority of the variability and function 2 makes up most of the remainder (Table 6.5). The high r values of the canonical correlation for functions 1 and 2 shows that they separate the groups well. Functions 3 and 4 are reasonably good separators of the groups but make up a very low percent of the variability. The Chi Squared value and P-value of function 1 (Table 6.6) show that it is the most significant. Function 2 is somewhat less significant and functions 3 and 4 are rather insignificant. Function 1 is contributed to mostly by the elements Y, Zr and TiO_2 (Table 6.7). Function 2 involves mostly TiO_2 , Cr, and Zr. Function 3 involves predominately Cr and Function 4 involves TiO_2 . Raw discriminant scores can be seen in Table 6.8.

Explained Variance (Eigenvalues)				
	Function 1	Function 2	Function 3	Function 4
Eigenvalu	17.992	2.373	0.467	0.263
% of Var.	85.291	11.249	2.214	1.245
Cum. %	85.291	96.540	98.755	100.000
Can.Corr.	0.973	0.839	0.564	0.456

Table 6.5. Explained variance for the immobile metamorphic elements discriminant analysis.

Wilks' Lambda				
	Function 1- 4	Function 2- 4	Function 3- 4	Function 4- 4
Wilks' Lan	0.008	0.160	0.540	0.792
Chi Sq	169.561	65.049	21.889	8.281
DF	64	45	28	13
P	0.000	0.027	0.786	0.825

Table 6.6. Wilks' Lambda and significance values for the immobile metamorphic elements discriminant analysis.

Standardised Discriminant Function Coefficients				
Variable	Function 1	Function 2	Function 3	Function 4
TiO2	-0.539	-0.166	-0.568	0.992
Cr	0.382	0.627	0.864	0.168
Zr	0.543	1.061	-0.200	-0.506
Y	0.836	-0.676	0.101	0.217

Table 6.7. Standardized discriminant functions for the immobile metamorphic elements discriminant analysis.

Casewise Discriminant Scores					
Case	Group	Fn 1	Fn 2	Fn 3	Fn 4
35	Proterozoic 2	2.782	1.229	1.487	0.611
29	3<TTG<3.5 Ga	1.676	0.746	0.043	-0.261
32	Archean_DD	-1.297	0.745	0.127	-0.221
47	Archean_Winter	0.735	1.935	0.395	-0.665
46	A-type	17.595	-1.340	-0.808	-1.436
18	BG	-2.210	-0.497	-0.324	-0.093
19	BG	-1.287	1.066	-1.524	0.021
20	BG	-1.740	0.170	-0.260	-0.621
21	BG	-0.861	0.294	-1.739	3.592
22	BG	0.056	1.523	-0.862	1.589
23	BG	-1.235	0.357	-0.625	-0.787
24	BG	-1.105	0.877	-0.710	-0.637
25	BG	-1.018	1.135	-0.394	-1.277
26	BG	-1.074	0.184	-0.547	-0.801
27	BG	-1.676	-0.244	0.089	-0.607
31	Cenozoic	-1.696	0.046	-0.421	-0.211
33	Early Archean	1.140	2.384	1.123	-0.463
44	I-type	4.868	-2.124	0.347	0.784
34	Late Archean	0.877	1.938	0.459	-0.174
43	M-type	4.980	-3.454	-0.100	1.020
36	Phanerozoic	1.426	0.245	0.487	0.577
45	S-type	5.529	-1.739	0.993	0.516
37	TTG gneiss (3.2 Ga)	-0.279	2.078	-0.671	-0.714
38	TTG gneiss (3.2 Ga)	-0.307	0.254	-1.163	1.843
39	TTG gneiss (3.2 Ga)	0.777	0.071	-0.018	-0.103
40	TTG gneiss (3.2 Ga)	5.487	-1.566	-0.459	-0.120
41	TTG gneiss (3.2 Ga)	1.561	1.861	3.013	2.242
42	TTG gneiss (3.2 Ga)	3.002	4.336	-2.862	-0.017
30	TTG<3Ga	1.628	2.158	1.270	-0.077
28	TTG>3.5 Ga	1.617	1.724	0.490	-0.262
1	WRO	-2.542	-1.037	0.014	-0.577
2	WRO	-2.454	-1.109	-0.040	-0.417
3	WRO	-2.625	-0.938	0.042	-0.604
4	WRO	-2.420	-1.294	-0.192	0.078
5	WRO	-2.167	-1.074	0.206	-0.074
6	WRO	-2.658	-1.346	-0.410	0.678
7	WRO	-2.122	-1.294	0.051	-0.514
8	WRO	-2.421	-1.142	-0.022	-0.464
9	WRO	-2.326	-1.159	0.071	-0.587
10	WRO	-2.039	-0.053	1.280	-0.443
11	WRO	-2.146	-1.339	0.045	-0.201
12	WRO	-2.392	-0.699	0.238	-0.747
13	WRO	-1.326	0.943	2.641	-0.007
14	WRO	-2.719	-1.161	-0.289	0.478
15	WRO	-2.505	-1.250	-0.173	0.410
16	WRO	-2.778	-1.272	-0.405	0.337
17	WRO	-2.309	-1.170	0.108	-0.593

Table 6.8. Raw discriminant scores for the immobile metamorphic elements discriminant analysis.

6.5. Discussion

Because of the complexity of the raw results, the easiest way to analyze the results of the discriminant analyses is by looking at the discriminant plots for each case. In the analysis of the WRO and BG samples using elements characteristic of Archean TTGs, the WRO samples are generally clustered into the upper left quadrant of the graph (Figure 6.2). Table 6.4 shows that the WRO samples are much more uniform than the BG samples with $Fn1$ near -1 to -2 and $Fn2$ mostly 0-1. There is minimal inflation of the group and a couple of outlying samples. Other samples that fall into this same quadrant include many of the BG samples and both the average compositions of Archean and Cenozoic TTGs defined by Drummond and Defant (1990). It is worth noting that the Early Archean sample from Condie (2005) and the Archean sample from Winter (2010) plot very near the WRO samples and within a loose cluster of BG samples.

The discriminant analysis involving immobile elements created the tightest cluster of WRO samples in the lower left quadrant of the plots in Figure 6.3 with a few scattered WRO and BG samples falling on the left half of the plot. Other samples that fell into the left half of the plot include both the Archean and Cenozoic samples from Drummond and Defant (1990) and 2 of the 6 TTG gneiss samples from Nehring et al. (2009).

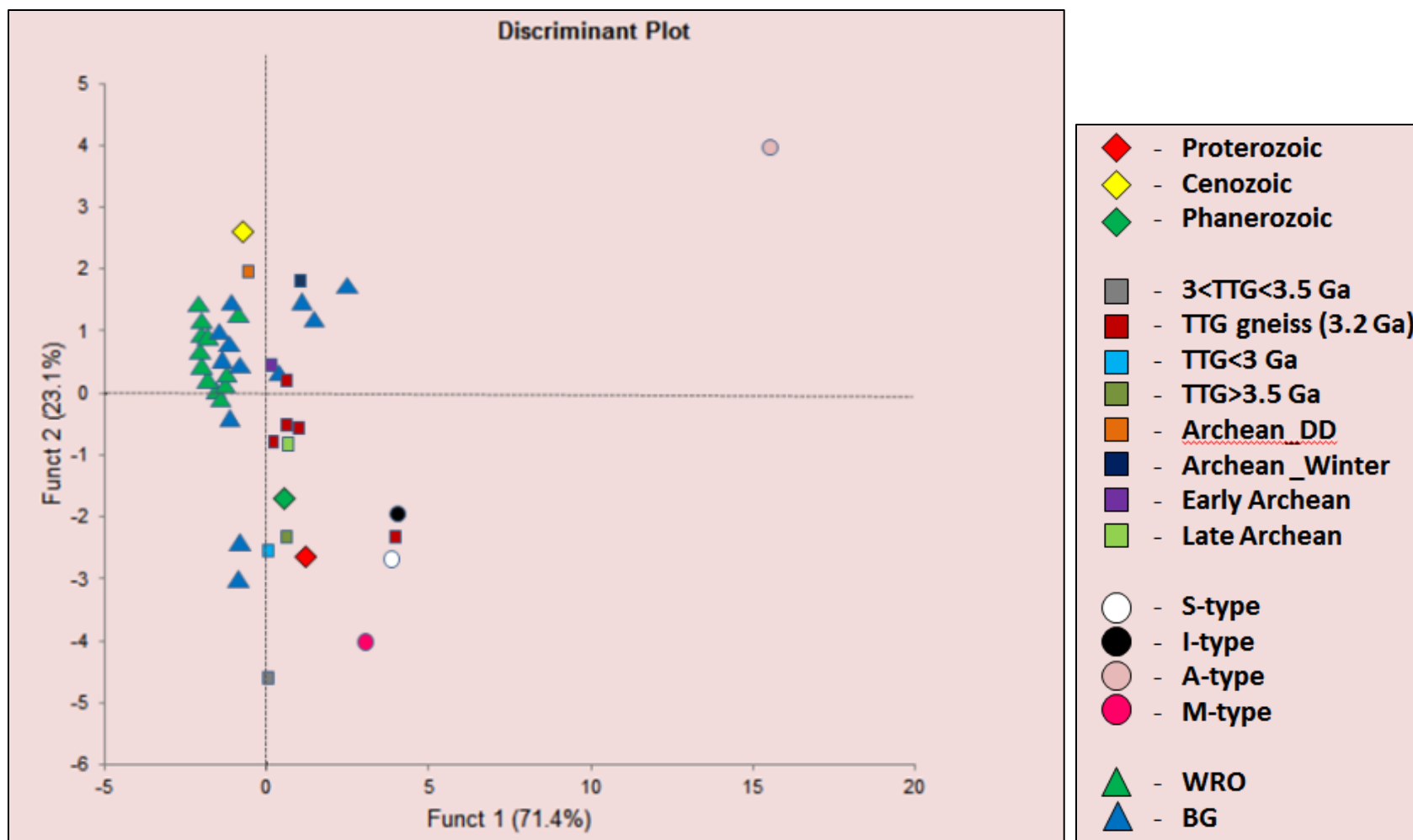


Figure 6.2. Discriminant plot showing the analysis between WRO and BG samples and other populations based on characteristic elements of Archean granitoids.

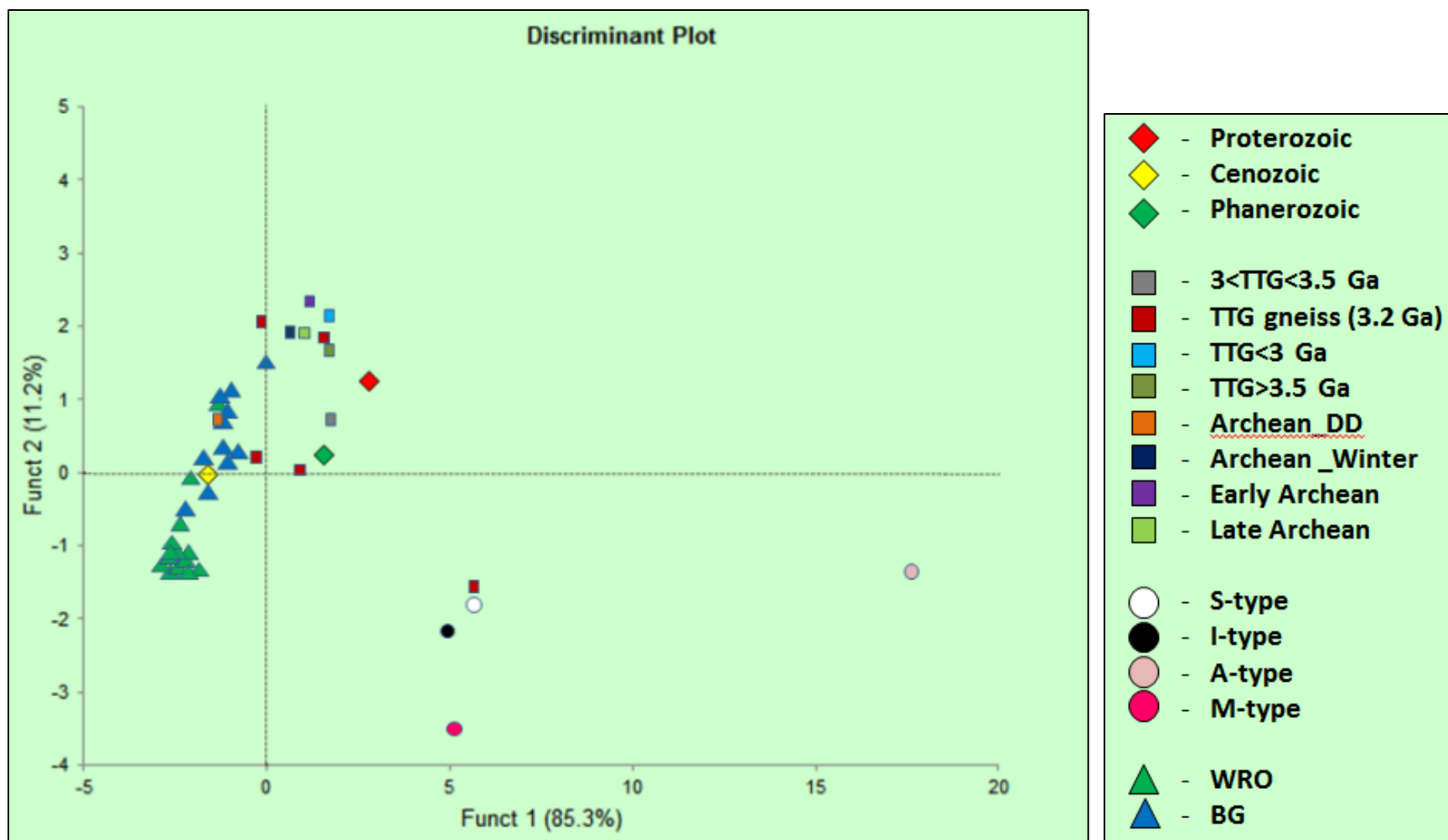


Figure 6.3. Discriminant plot showing results of analysis based on immobile elements.

From the two discriminant analyses, the WRO samples are most commonly grouped with the Archean and Cenozoic samples from Drummond and Defant (1990). The other similar groups in each case were almost exclusively with other Archean TTG samples. The Cenozoic samples from Drummond and Defant (1990) are originally from research done by Clark et al. (1988) on dacite samples from the El Valle Volcano in Panama. TTG suites were originally defined as TTDs (tonalite, trondhjemite, dacite) by Drummond and Defant (1990). As intrusive/extrusive equivalents, granodiorite and dacite are considered interchangeable in this paper. The Cenozoic samples from the El Valle Volcano were interpreted to be the melts from young subducting lithosphere (Defant et al., 1991). The geochemical characteristics of the slab melts, $Yb < 1$, $Sr/Y > 150$, La/Yb ratios > 15 , and $Y < 6$, can be explained by the partial melting of a source rock leaving a garnet and amphibole residue (Defant et al., 1991). The average values of these geochemical parameters for the WRO and BG samples are $Yb=0.36$, $Sr/Y=767.7$, $La/Yb=162.7$, and $Y=4.34$, which meet these geochemical criteria.

The Archean samples from Drummond and Defant (1990) are originally from research on Archean tonalities/trondhjemites in Barberton, South Africa done by Condie and Hunter (1976) and Glikson (1976). Glikson (1976) determined that the tonalities are derived by partial melting of eclogite within depths of 30-50 km. Glikson also noted a strong positive Eu anomaly in the “ancient” tonalities which is another characteristic shared with the WRO and BG samples. Condie and Hunter (1976) similarly concluded that the tonalities were best accounted for by 10% partial melting of eclogite. The geochemical similarities of Cenozoic and Archean TTGs with the WRO and BG samples suggest they may have similar petrogenetic histories.

The discriminant analysis could be improved by using individual data points for each category instead of using averages for some and individual analyses for others. If the

compositions that are averages of large numbers of samples were plotted individually, a more reliable assessment of the WRO and BG clusters may indicate if the clusters are distinguishable or not.

6.6. Conclusion

The null hypothesis that the Wenatchee Ridge samples represent a Mesozoic analog of Archean TTG may not be rejected based on this limited analysis. The discriminant analysis comparison between samples from the Wenatchee Ridge gneiss and other well classified TTG suites determined that the WRO and BG samples are most closely related to averages of Cenozoic and Archean TTGs which both represent partial melt of an eclogitic source rock (Condie and Hunter, 1976; Glikson, 1976; Drummond and Defant, 1990; Defant et al., 1991). Drummond and Defant (1990) used both the Cenozoic and Archean TTGs as examples of partial melts of hot subducting slabs. It is possible that the Wenatchee Ridge gneiss samples represent a partial melt of some source rock with a garnet and amphibole residue, but that may not exclusively involve the melting of a hot subducting slab. Melting experiments by Rapp et al. (1991) concluded that while partial melting of eclogite does produce tonalite-trondhjemite type melts, the melt environment should not necessarily be limited to subduction settings. TTG with the Archean geochemical signature can be formed by partial melting of subducting crust or overthickened underplated crust. Research has also shown that TTG type melts in small volumes, relative to those of the Archean, can be produced by fractional crystallization of a typical calc-alkaline magma, which means that fractional crystallization cannot be ruled out. The discriminant analysis has shown that the Wenatchee Ridge gneiss does have geochemical similarities to Archean TTGs. Details of the WRO's petrogenesis are explored in the next chapter.

7. GEOCHEMISTRY AND PETROGENESIS

7.1. Background

7.1.1 Models for TTG Genesis

There are essentially two different petrogenetic processes which may form felsic magmas in an arc-type setting. These processes, generally described, are the partial melting of lower crustal mafic rocks such as amphibolite or eclogite or the fractional crystallization of a basaltic magma derived by partial melting of mantle peridotite (Brophy, 2008; Borg and Clyne, 1998).

Extensive fractional crystallization of a basaltic magma as a method of TTG formation was proposed by researchers such as Martin (1993) and Kamber et al. (2002) and is discussed in greater detail in Chapter 3. The similar fluid-mobile trace element characteristics between TTGs and “typical” mantle derived magmas tend to indicate that TTGs are related to basaltic magma through fractional crystallization. Drummond, et al. (1996), Smithies (2000), and Condie (2005) argue that this method of TTG formation requires 50-90% fractional crystallization and there is no evidence for such high amounts of mafic cumulates in the crust. The fractional crystallization theory also receives criticism from Condie (2005) who similarly claims that over 50% fractional crystallization is needed to produce a TTG melt and the large amounts of mafic cumulate material that would result are not accounted for in the crust. Crystal fractionation has additionally been considered to be a poor model for the majority of TTG suites, in particular where there is a lack of contemporaneous basaltic and intermediate rocks (Atherton and Petford, 1993). Additionally, Atherton & Petford (1993) noted that the derivation of rocks with >70% SiO₂ from mantle material is unlikely.

The majority of theories regarding TTG genesis involve the partial melting of hydrous lower mafic crust (Frost et al., 2006). Excepting this common starting point, models for specific TTG localities tend to vary such that there is not a single accepted model for all TTG genesis. A popular model developed by Martin (1987) and used by Frost et al. (2006) involves the partial melting of tholeiitic garnet-bearing amphibolite which leaves a hornblende and garnet restite. This model produces trondhjemitic magma heavily depleted in HREEs (Frost et al., 2006). Experimental research by Rapp et al. (2003) supports this model of TTG genesis by showing that partial melting of hydrous basalt by 10-40% at pressures greater than the garnet-in boundary will produce the major and key trace element compositions characteristic of TTGs (Frost et al., 2006). While this idea has many supporters in current literature, it does suffer from an inability to explain how extremely large volumes of TTG were formed during the Archean.

Similarly, the WRO may have been formed by partial melting or fractional crystallization. Plots of the WRO and BG geochemistry and models of petrogenetic processes such as partial melting and fractional crystallization will be evaluated to determine the source and petrogenetic history of WRO and BG magmas.

7.2. Sampling and Analytical Methods

7.2.1 Sample Selection

Samples were selected for geochemical analysis based on the petrographic results discussed in chapters 4 and 5. Petrographic analysis was used to identify which samples were least altered by metamorphism. The degree of alteration was evaluated by assessing the degree of sericitic or sausseritic alteration of plagioclase as well as the chloritization of biotite.

Geographic location (Figure 7.1) was also considered in order to get the best coverage of the entire WRO pluton body as well as the widest possible distribution of BG samples. The least altered samples with the best geographic extent were selected for geochemical analysis.

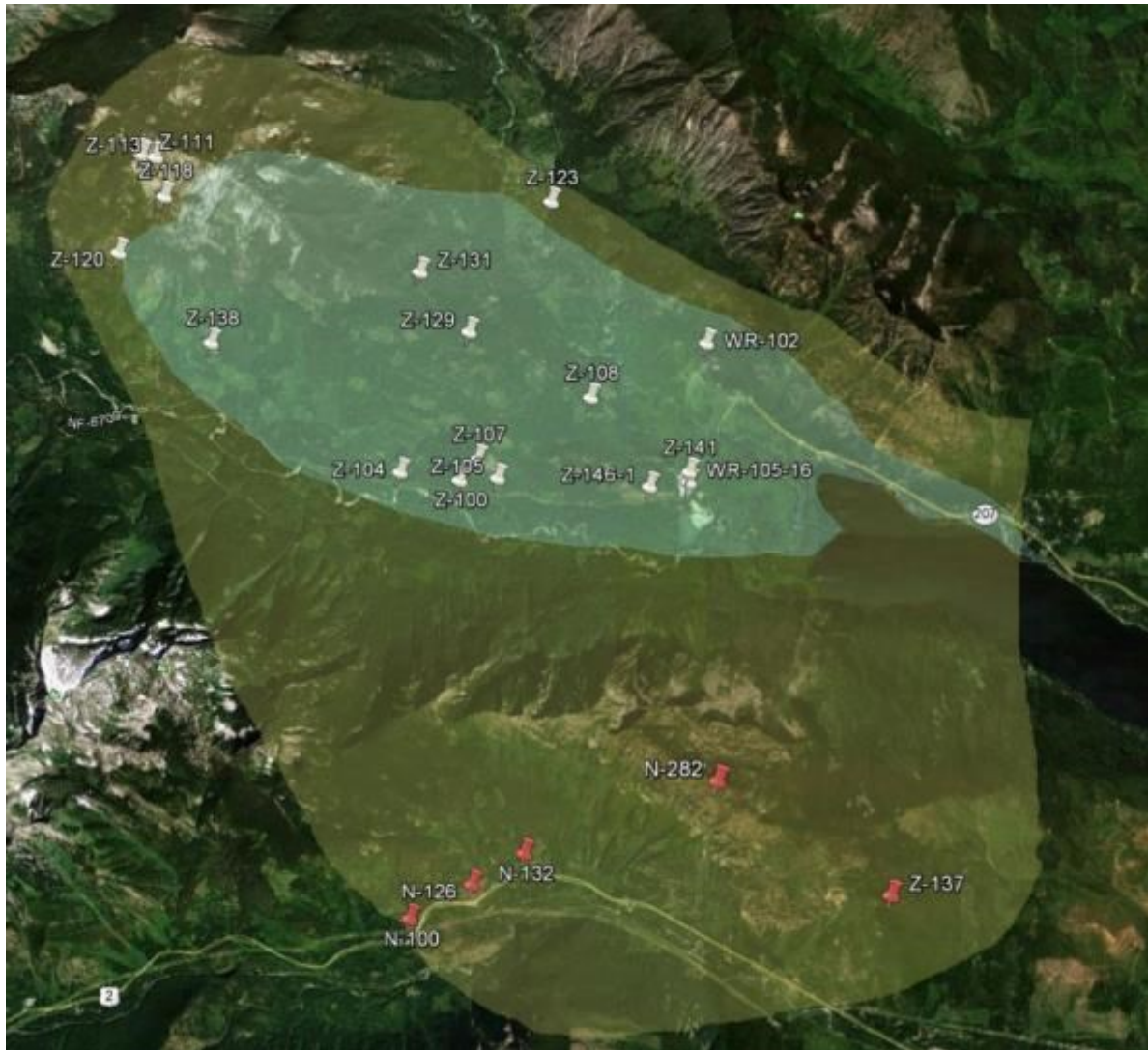


Figure 7.1. Map showing locations of all samples which were used to obtain geochemical data. The red samples are BG samples within the yellow pluton boundary as defined by Magloughlin (1993). The WRO samples are colored white and generally lie within the blue pluton boundary defined by Zuluaga & Stowell (2008).

7.2.2 Sample preparation

All samples had oxidation and weathering rinds removed with a rock saw and the subsequent saw blade marks were removed by grinding on an iron lapwheel with silicon carbide grit. After cleaning, samples were crushed to pea size using a hammer in a clean area. The pea size pieces were then powdered using a tungsten carbide disk mill.

7.2.3 Analytical Methods

Each powder was sent to the University of Minnesota analytical geochemistry lab for major, trace, and rare earth elements. Major elements were analyzed using a Thermo Scientific iCAP 6500 dual view ICP-OES. Samples were diluted before the analysis using Cesium as a matrix modifier and Yttrium as an internal standard. Trace and rare earth elements were analyzed using a Thermo Scientific XSERISE 2 ICP-MS with ESI PC3 Peltier cooled spray chamber, SC-FAST injection loop, and SC-4 autosampler. Samples were diluted appropriately and 20ppb of Indium internal standard was added. All elements except Li were analyzed using He/H₂ collision-reaction mode.

7.3. Results

The data for the WRO and BG samples are summarized in Table 11.5 in Appendix E. Plots for major, trace, and rare earth elements will be shown below and discussed later in the chapter. Note that plots and models in this chapter also show WRO and BG data from Magloughlin (1986) and Magloughlin (1993).

7.3.1 Major Elements

The WRO and BG samples have high concentrations of silica, with an average concentration for WRO of 73.3 ± 2.6 wt% and for BG of 69.2 ± 5.9 wt%. Samples are variably enriched in LILEs (Sr, K, Rb, Ba, Th) and depleted in HFSEs (notably Nb, P, Zr, Ti, Hf, Y, and

Yb) compared with mid-ocean ridge basalt (MORB). Figure 7.2 shows a molecular normative An-Ab-Or granitic classification based on plagioclase compositions calculated using a CIPW norm (fields from Barker (1979)). The CIPW norm was calculated from major element data with FeO and Fe₂O₃ adjusted, cation norm calculated, and normalized to 100 percent following Irvine and Baragar (1971). The granitoid classification shows that, of the 47 samples, thirty six are classified as trondhjemites. Eight samples are classified as tonalites, two as granite, and one as granodiorite.

Figure 7.3 shows an AFM diagram after Irving and Baragar (1971). This diagram shows that the majority of samples plot on a calc-alkaline trend with a few BG samples trending closer to tholeiitic. Figure 7.4 shows that 96% of WRO are peraluminous ($Al_2O_3 > (Na_2O + K_2O + CaO)$) with 4% being metaluminous ($Al_2O_3 < (CaO + Na_2O + K_2O)$ and $Al_2O_3 > (Na_2O + K_2O)$) (Winter, 2010). 55% of BG samples are peraluminous and 45% are metaluminous.

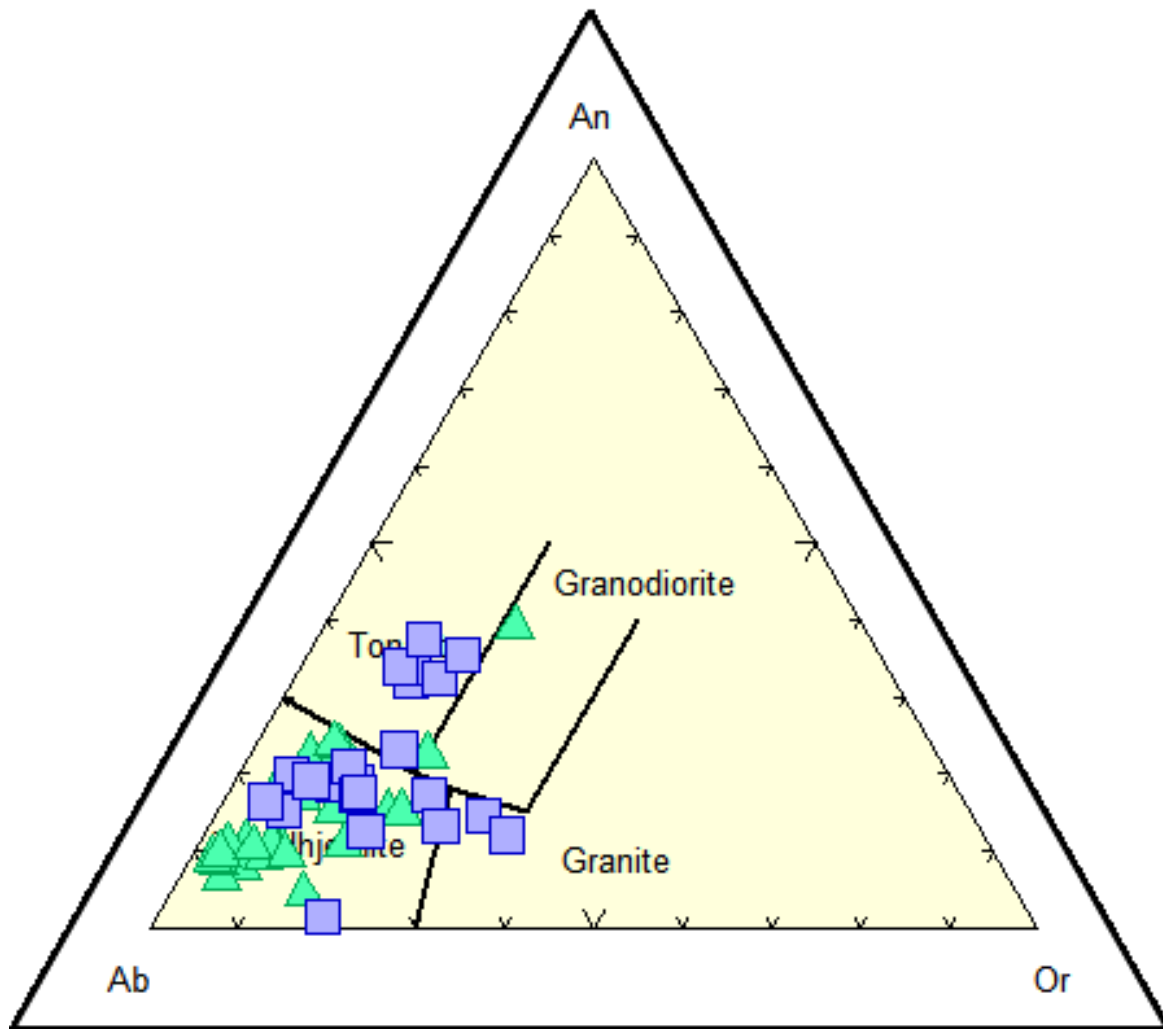


Figure 7.2. Molecular normative An-Ab-Or granitic classification with fields from Barker (1979). Green triangles are WRO samples and blue squares are BG samples.

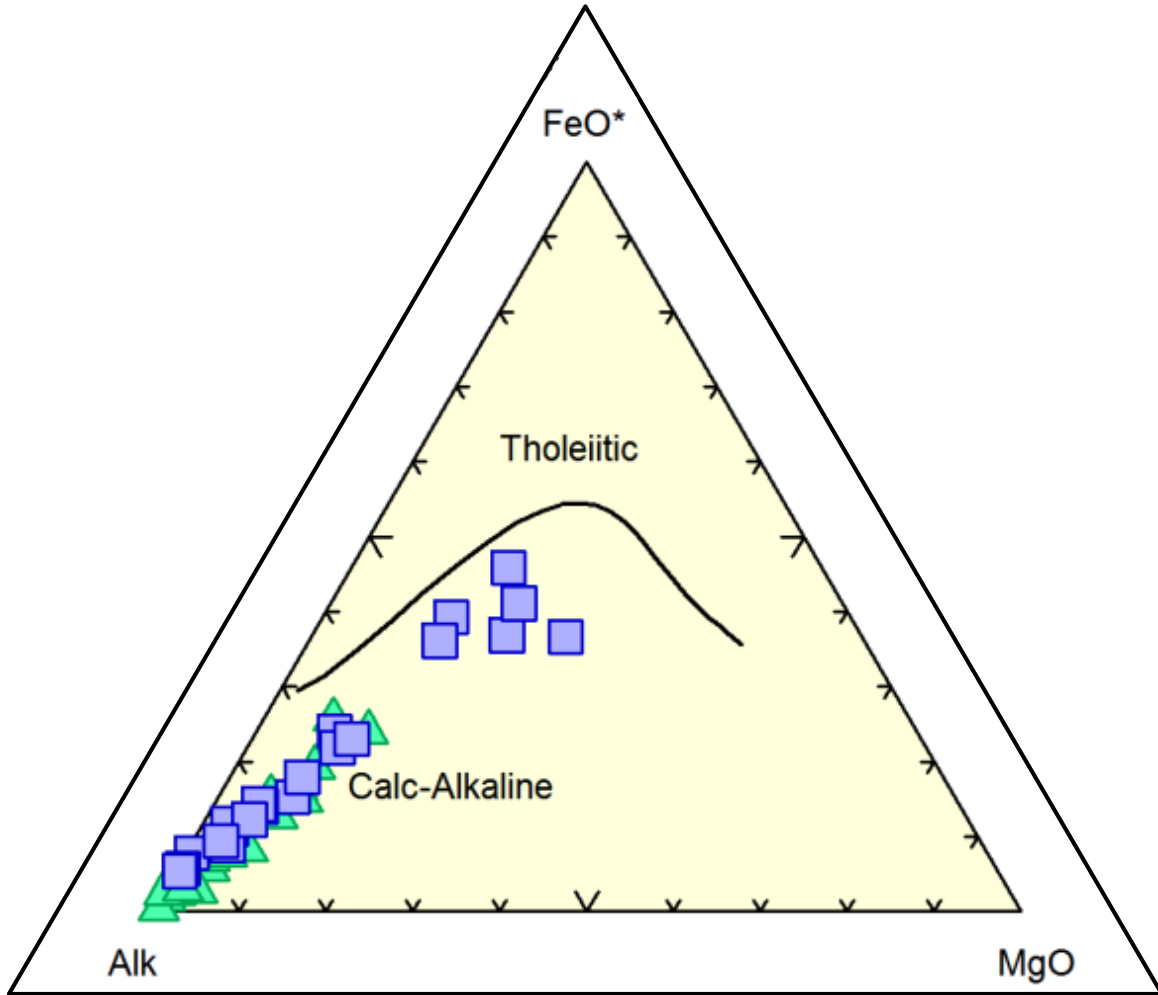


Figure 7.3. AFM diagram after Irvine & Baragar (1971). Green triangles are WRO samples and blue squares are BG samples.

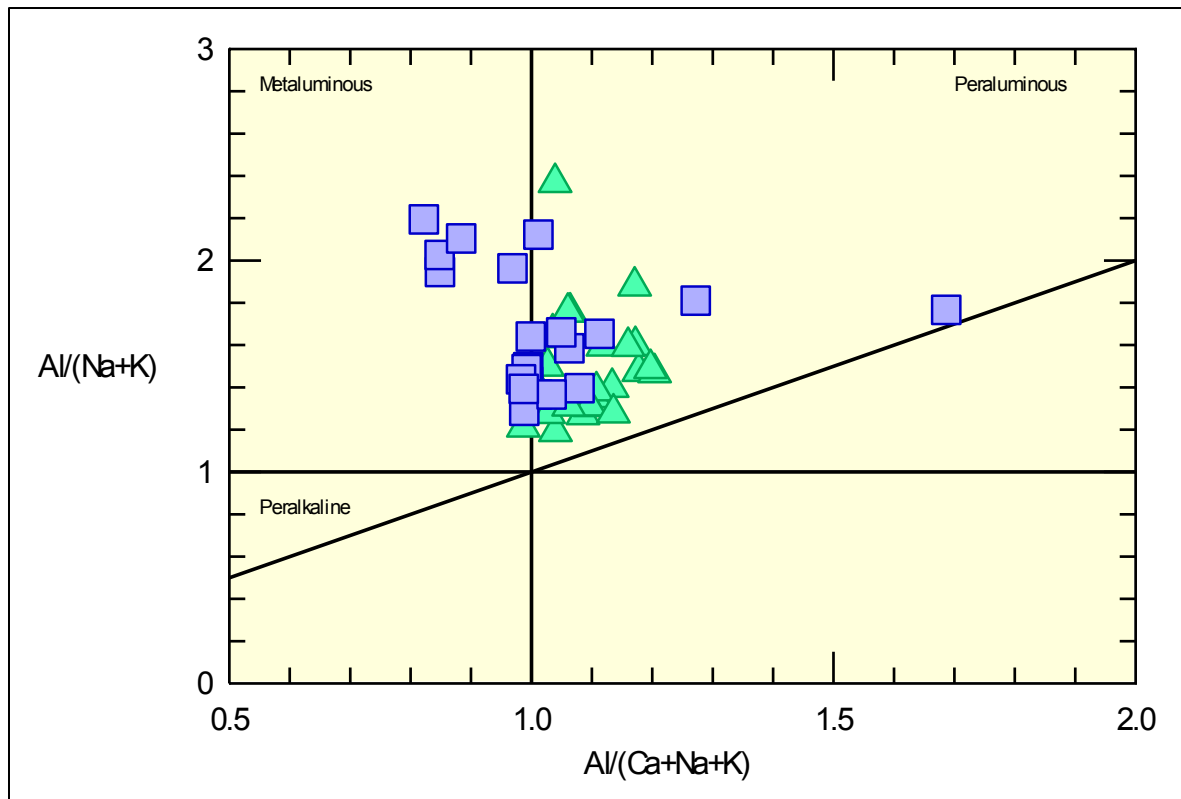


Figure 7.4. Alumina saturation diagram after Maniar & Piccoli (1989) using Shand's Indices.

Green triangles are WRO samples and blue squares are BG samples.

Figure 7.5 shows a series of Harker diagrams in which major element concentrations are plotted against silica content. Compatible elements such as Mg, Fe, Ti, and Mn decrease with increasing silica content whereas Na increases. Al decreases with increasing silica content and K shows a scattered trend. The trends/patterns of WRO and BG samples are similar for all major oxides except K_2O .

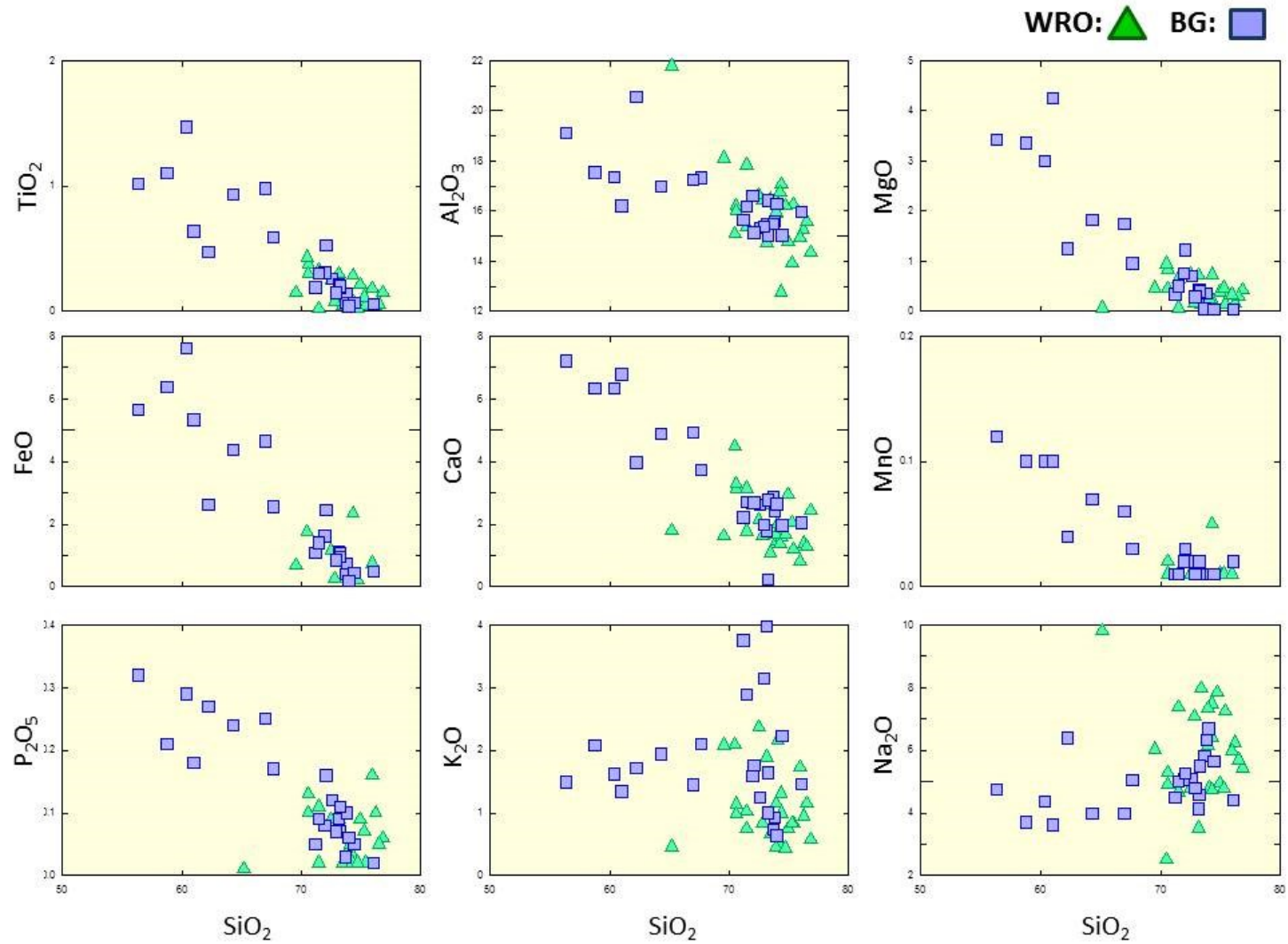


Figure 7.5. Major element Harker diagrams of eight percent TiO_2 , Al_2O_3 , MgO , FeO , CaO , MnO , P_2O_5 , K_2O , and Na_2O vs weight percent SiO_2 for WRO and BG samples.

7.3.2 Trace Elements

LREEs tend to be highly enriched whereas HREEs are at very low concentrations approaching MORB values. Chondrite-normalized REE plots for the WRO and BG samples are shown in Figures 7.6 and 7.7. Figures 7.8 and 7.9 show trace elements normalized to MORB with a combination of LILEs and HFSEs. Both BG and WRO samples are enriched in LILEs. LILE concentrations for the WRO and BG samples are very similar, but the WRO samples tend to be much more depleted in HFSEs. Additionally, it is worth noting that the WRO samples are much more scattered than the BG samples. The WRO samples are much more depleted in Zr, Hf, Nb, Ti, Y, and Yb when compared to the BG samples, and the individual depletions are also highly variable. The LILE concentrations for the WRO samples are generally consistent whereas the HFSEs are scattered. The WRO samples, again, show variably weak to strong depletions in REEs (LREE, MREE, and HREE) when compared to the BG samples, which are highly uniform. The LREE depletions for the WRO samples in particular are highly variable and unusual. For a few WRO samples, LREE and HREE are depleted while MREE (particularly Eu) remains high. The REE plots show a steep negative trend (note the scale which had to be extended down to 0.01). The geometric mean for La/Yb values (a measure of LREE enrichment) is 85 for the WRO samples and 18.5 for the BG samples. The REE plots commonly show a positive Eu anomaly for both WRO and BG samples. Average Eu/Eu^* is 1.43 ± 0.59 for the WRO samples and 1.39 ± 0.45 for the BG samples.

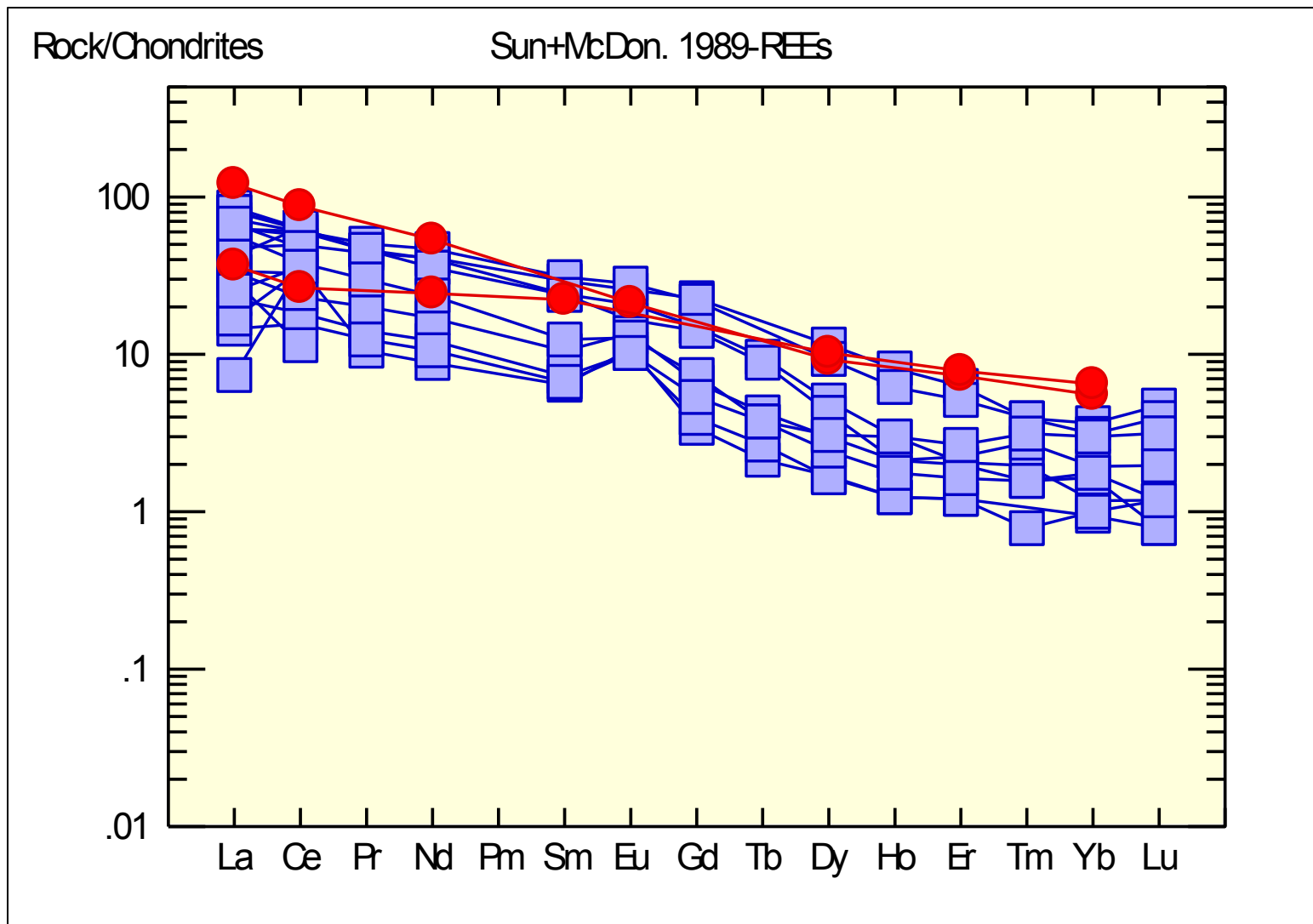


Figure 7.6. REE diagram of BG samples normalized to chondrite values of Sun & McDonough (1989). Red samples are experimental TTG melts from Rapp and Watson (1995) and Zamora (2000).

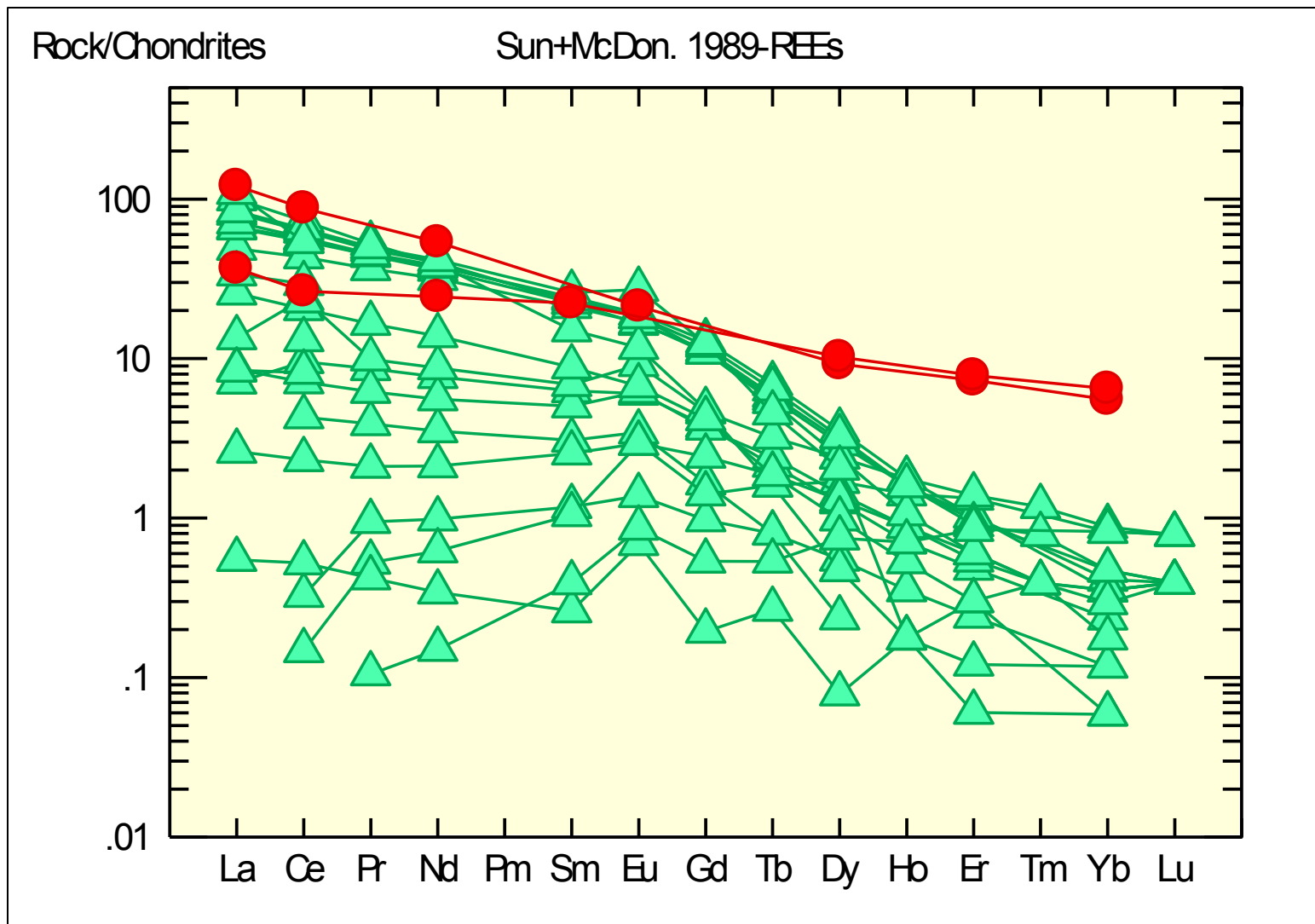


Figure 7.7. REE diagram of WRO samples normalized to chondrite values of Sun & McDonough (1989). Red samples are experimental TTG melts from Rapp and Watson (1995) and Zamora (2000).

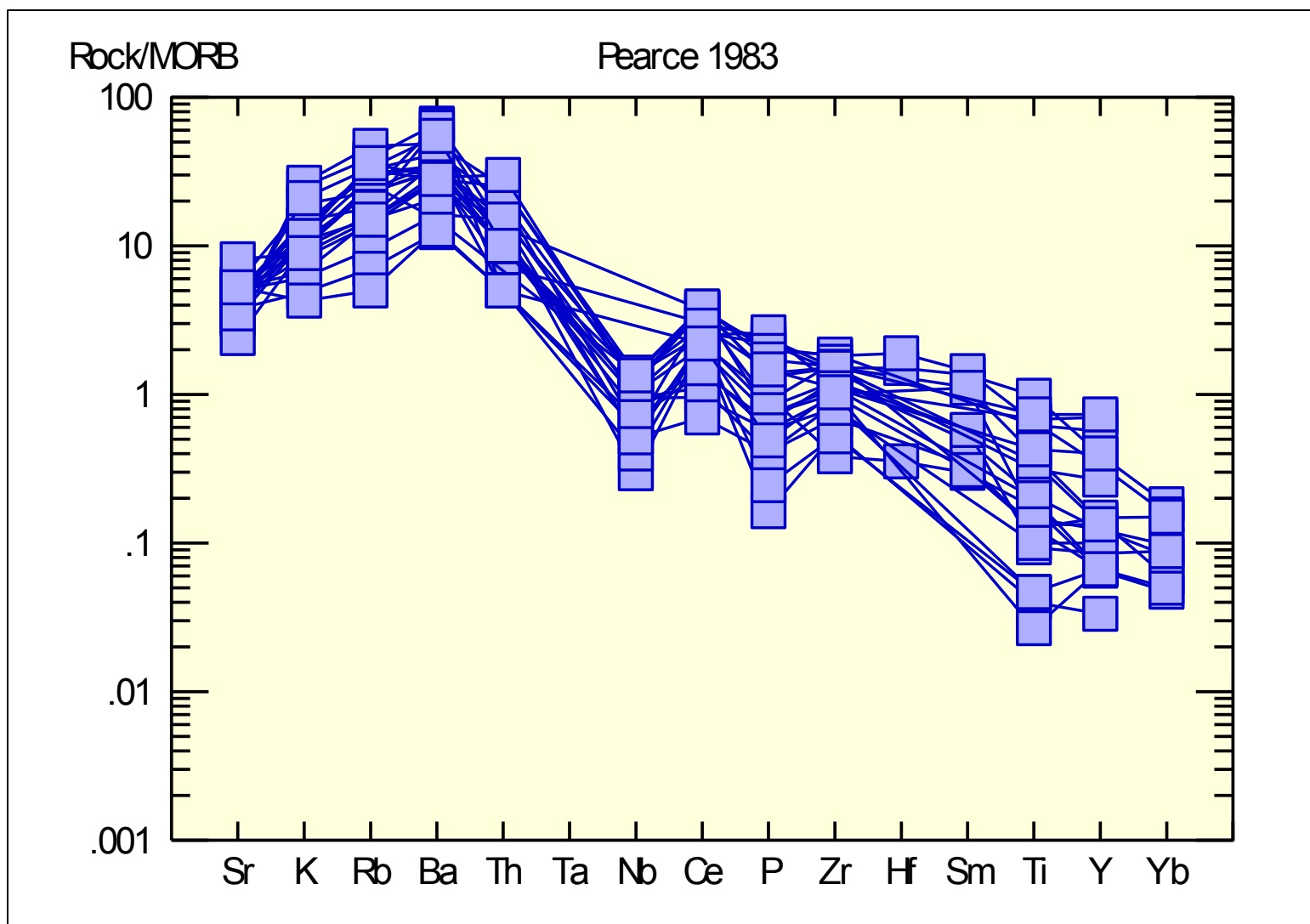


Figure 7.8. Multi-element diagram for BG samples normalized to MORB using values from Pearce (1983).

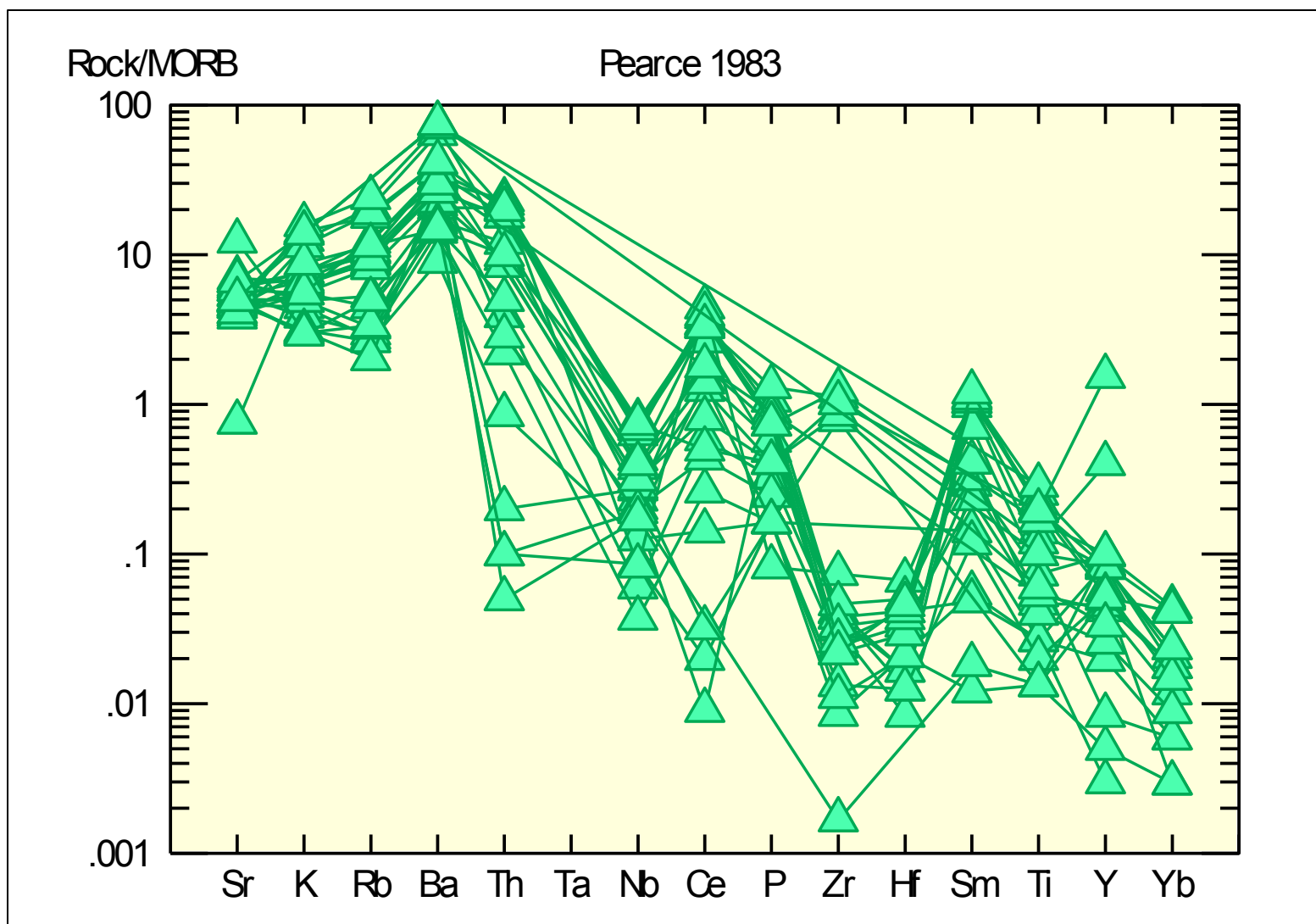


Figure 7.9. Multi-element diagram for WRO samples normalized to MORB using values from Pearce (1983).

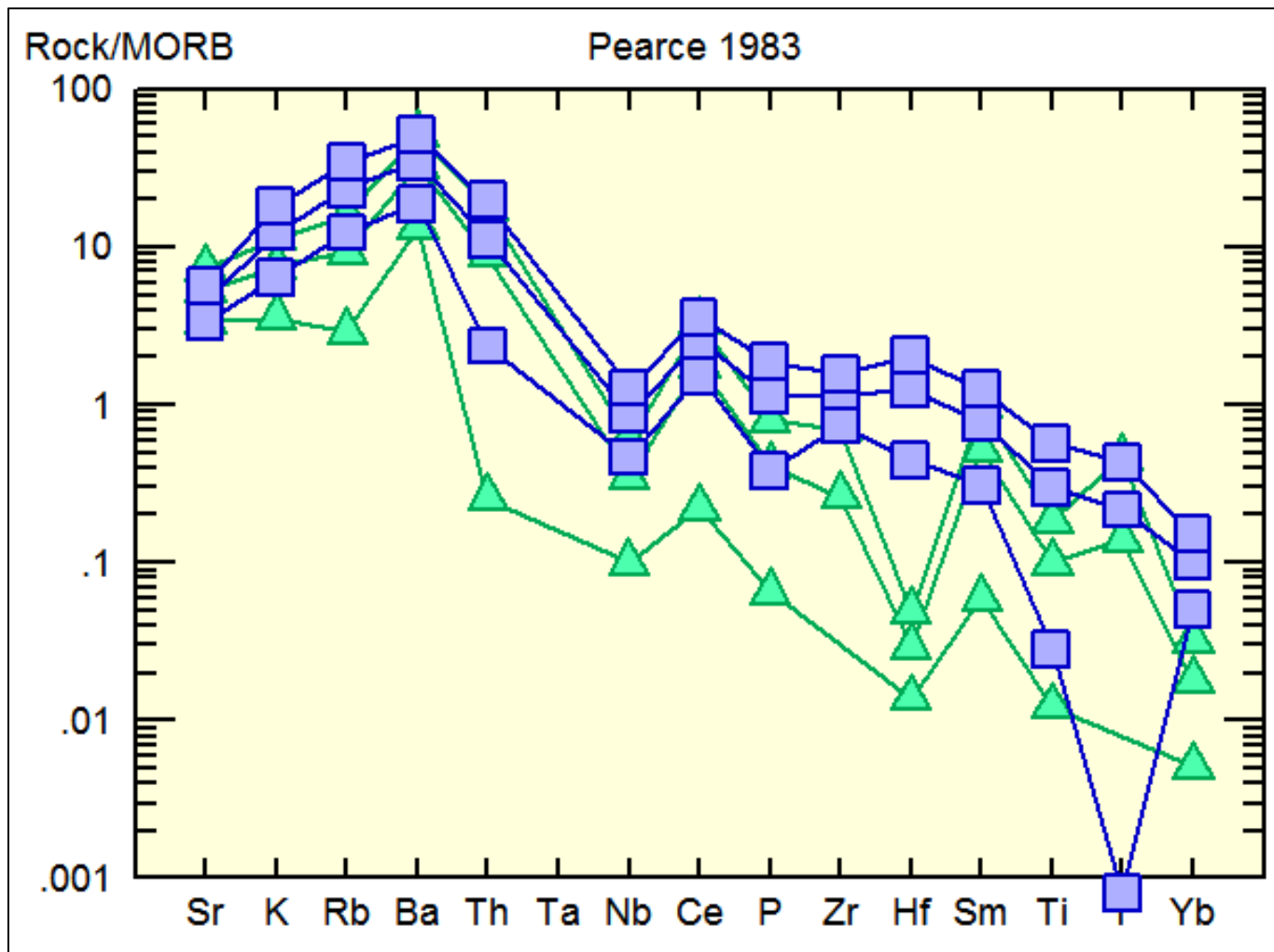


Figure 7.10. Average values for the WRO and BG samples normalized to MORB using values from Pearce (1983). Middle blue line is the average for BG samples, top blue line is +1 standard deviation, bottom line is -1 standard deviation. Green lines represent the WRO samples.

Figure 7.11 shows a tectonic discrimination plot for the WRO and BG samples based on Y and Nb values after Pearce et al. (1984). WRO and BG samples plot in the fields of Volcanic Arc Granitoids and Syn-Collisional Granitoids.

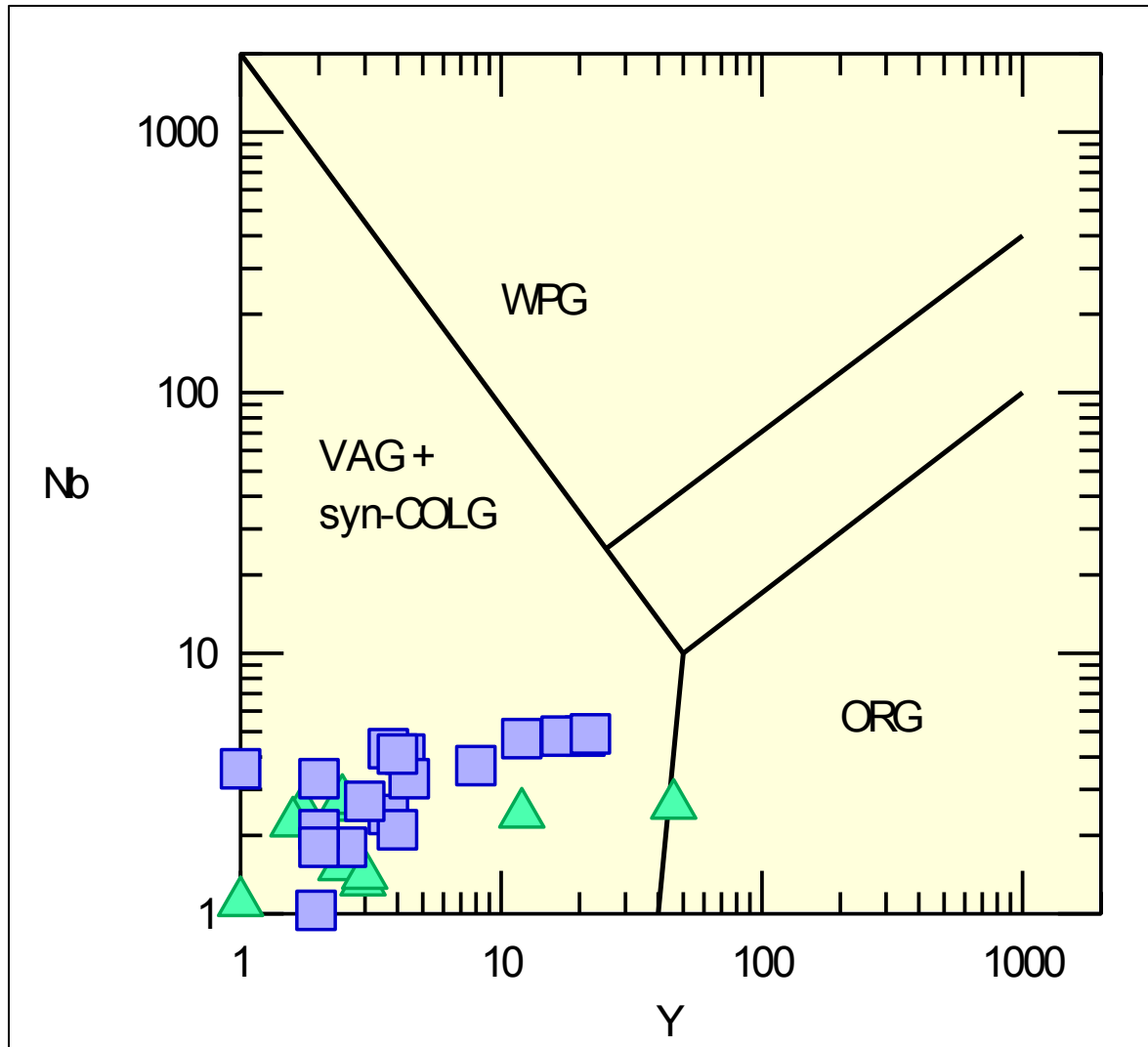


Figure 7.11. Tectonic discrimination diagram after Pearce et al. (1984). Green triangles are WRO samples and blue squares are BG samples.

7.4. Interpretation of Geochemical Data

7.4.1. Major Elements

The An-Ab-Or granitic classification diagram (figure 7.2) shows that the majority of the WRO and BG samples are classified as trondhjemites and the samples all belong to the TTG suite of igneous rocks, excepting the two granites which were both BG samples (N126-44 and N100-43, from research by Magloughlin (1993)). Because feldspar solid solution is taken into consideration, the normative An-Ab-Or calculation provides a more accurate representation of feldspar composition and rock type than a typical modal classification. Rollinson (1993) states that this type of diagram is useful to identify original magma types in cases where granitic rocks have been metamorphosed and/or deformed, as is the case for the WRO and BG samples. The spread seen in the normative An-Ab-Or diagram is very similar to that shown by Archean TTGs on the same diagram (Rapp et al., 1991).

Rocks that plot along a calc-alkaline trend on an AFM diagram (figure 7.3) can be identified as a rock series likely associated with subduction-related plate tectonic processes (Winter, 2010). Though the samples do form a strong calc-alkaline trend, the presence of some BG outliers which appear to plot roughly along the tholeiitic trend indicate that the genesis of trondhjemitic rocks outside of the primary pluton body may be more complex. The majority of samples are peraluminous (figure 7.4), a conclusion also reached by Magloughlin (1986), with some of the BG samples and two of the WRO samples plotting as metaluminous. The high alumina saturation is manifested by the abundance of muscovite as well as the presence of rare garnet. The source of the WRO and BG magmas was likely rich in aluminum.

Peraluminous to metaluminous granitoids with high silica contents are commonly categorized as S or I type granitoids respectively. They form in subduction zones with

supracrustal, or intermediate to mafic sources, respectively. Because of their dominantly peraluminous nature, the WRO and BG samples would best be classified as S type granitoids, a conclusion also reached by Magloughlin (1986) based on variable $^{87}\text{Sr}/^{86}\text{Sr}$ values. The partial melting of sedimentary rocks enriched in aluminum due to weathering processes is a possible explanation for the WRO pluton, but much of the geochemical data does not match with typical S-type granitoids. For example, average SiO_2 , Na_2O , and Al_2O_3 values are much higher at 73 wt%, 5.98 wt% and 16.13 wt%, respectfully, than would be expected for average ($n = 704$) S-type granitoids compiled by Winter (2010) at 70.9 wt%, 2.5 wt%, and 14 wt%. TiO_2 , FeO , MnO , MgO , and P_2O_5 values are also much lower at 0.14 wt%, 0.66 wt%, 0.01 wt%, 0.35 wt%, and 0.05 wt%, respectfully, for the WRO and BG samples than those of average S-type granitoids at 0.4 wt%, 3.0 wt%, 0.1 wt%, 1.2 wt%, and 0.2 wt%, respectfully. Additionally, the WRO and BG samples do not plot together with either S or I type granitoids in the discriminate analysis performed in chapter 6.

The Harker diagrams indicate that the magmatic histories of the BG and WRO were in many respects similar. The trends present in the Harker diagrams (figure 7.5) are typical for the evolution of a magma suite such that Mg, Fe, Ti, and Mn decrease with increasing silica content. K would be expected to increase with increasing silica content, but instead shows an essentially flat trend for the BG until it becomes highly variable above 72% SiO_2 . For the WRO, there is a weak, possible decrease in K_2O . This transition from K enrichment to K depletion for the WRO samples may represent a change in the dominant fractionating phase which controls K such that a K-rich phase (orthoclase?) began fractionating at 70-72% SiO_2 . A plot of microcline % from the ITMTC vs. K_2O (Figure 7.12) shows that K_2O decreases with decreasing microcline content ($R^2 = 0.55$). This is not surprising, but could indicate that microcline was fractionating K_2O out of the

melt. Microcline abundance could also simply be the effect of K availability which may have been controlled by other phases earlier in the melt's history. Na_2O appears to increase with increasing silica content rapidly above 72% SiO_2 . Alternatively, partial melts of a source rock could have been initially poor in K and rich in Na until a K-rich phase began late melting when the magma became SiO_2 -rich. This late melting could have temporarily added K to some magmas which subsequently became diluted as the melt volume increased, relatively lowering K and Na concentrations along with SiO_2 . Regardless of mechanism, something clearly changed in the evolution of these magmas at approximately 70-72% SiO_2 . This may be due to the loss of an important Si-rich mineral and the replacement of the major fractionating or partial melting phases with minor or trace phases.

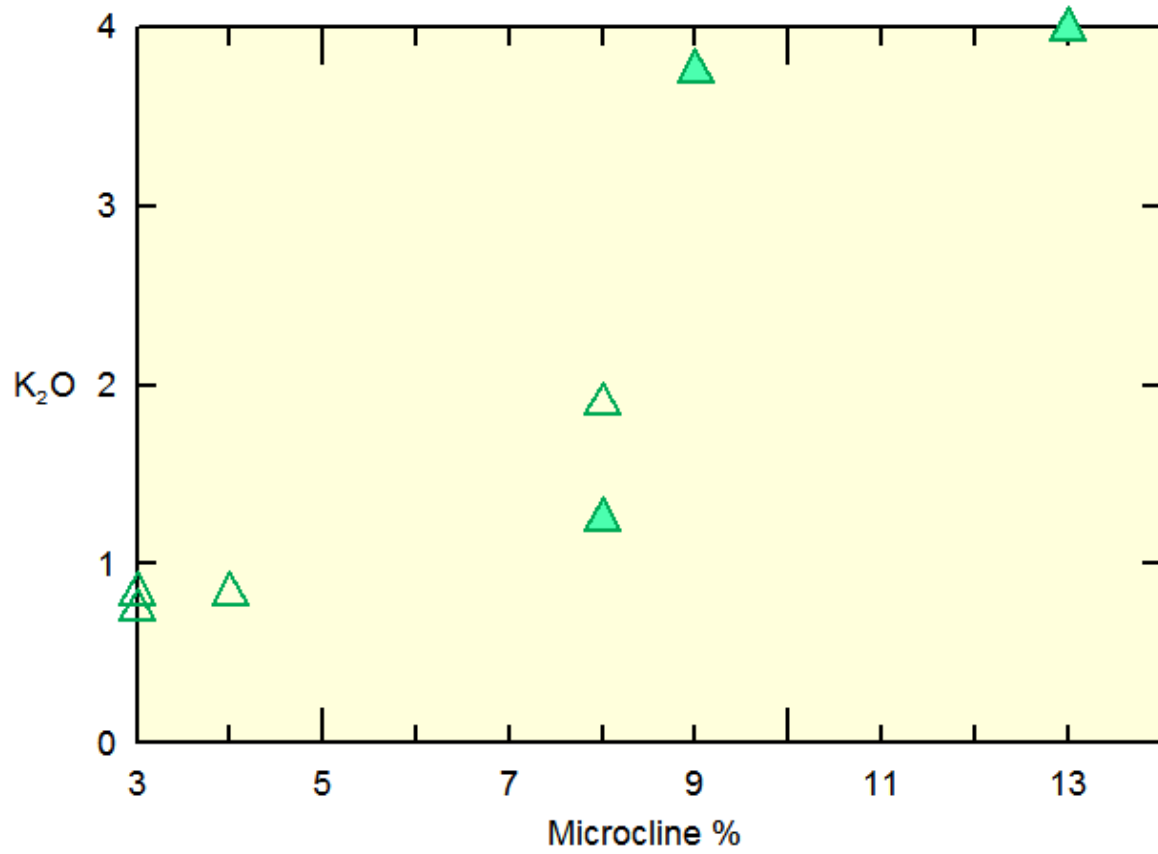


Figure 7.12. Plot of microcline % from the ITMTC and corresponding K₂O values for both WRO and BG samples ($R^2 = 0.55$).

7.4.2. Trace Elements

Trace elements, especially those which show extreme compatible or incompatible behavior, can be especially useful in determining the source and petrogenetic history of igneous rocks (Rollinson, 1993). Rare earth elements (REEs, La to Lu plus Y) are possibly the most useful of all the trace elements in igneous petrology (Rollinson, 1993). The usefulness of REEs comes from the fact that the different REEs, due to differences in ionic size and geochemical behavior, are uniquely fractionated by different geochemical processes (Rollinson, 1993). REEs are also useful because they are generally immobile in slightly altered rocks and can therefore be reliably used to represent to parent composition where other, more mobile, elements cannot (Rollinson, 1993).

The rare earth plots for all of the BG and some of the WRO samples are indicative of Archean TTGs and TTG suites formed by the partial melting of eclogite or amphibolite. Both the BG and WRO samples are depleted in HREE relative to LREE, indicating garnet and possibly amphibole were stable in the magma source region or fractionated in deeper magma chambers (Rapp et al., 1991; Rollinson, 1993). The HREE signature of the samples indicates that residual garnet is likely important which would suggest that melting took place below 35 km depth where garnet is stable (Girardi et al., 2012). Considering syn-tectonic emplacement of the WRO at approximately 31 km depth, this suggests melting could have originated not far below the currently exposed rocks. Magloughlin (1986, p.42) surmised a minimum depth of 42 km for the origin of the WRO magmas. Figure 7.6 compares the 20-25% partial melt experimental TTG from Rapp and Watson (1995) and Zamora (2000) which were produced from eclogitic source rocks. The experimental data matches the BG samples very well except for the positive Eu anomalies which will be discussed later in this chapter. The same experimental data are plotted

in Figure 7.7 for the WRO samples which are much lower in REEs. The initial formation of the BG and WRO magmas by the partial melting of eclogitic source rocks is a reasonable starting point because the rocks were intruded into amphibolite facies metamorphic rocks in a belt of overthickened crust (Magloughlin, 1993; Stowell et al., 2007). It stands to reason that there would be eclogitic conditions where partial melt could form beneath the amphibolite facies rocks if the geotherm could be reconstructed. A significant difficulty arises in the interpretation of the scatter in the WRO samples in both the REE and multi-element plots.

The scatter in REE data for the WRO samples is likely controlled by magmatic processes involving accessory phases such as zircon, monazite, allanite, titanite, and apatite. In felsic magmas, even a small amount of trace minerals may have a large effect on the REE pattern due to their high partition coefficients (Rollinson, 1993). The magmatic processes which caused the scatter in the WRO samples could be related to fractional crystallization, assimilation, or variable amounts of partial melting.

The WRO samples are unique in that some have depletions in LREEs relative to primitive mantle. Depletion of LREEs to form the WRO magmas may have been caused by the fractional crystallization of epidote, allanite, titanite, or monazite. Alternatively, the sample scatter could represent chemically variable source regions or degrees of partial melting. This dilemma will be visited further in the petrogenetic modeling section of this chapter. Enrichment or depletion of the MREEs may be controlled by hornblende or large amounts of titanite. MREEs do not tend to be depleted in the WRO samples and only appear relatively enriched in those few samples which have depletion of HREEs and LREEs. A hump in MREE is therefore a characteristic of some of the WRO samples. Because hornblende is not present in large amounts,

the MREEs are likely controlled by titanite and/or apatite. HREEs are likely to be controlled dominantly by zircon fractionation or variable amounts of garnet in the source region.

7.4.3. Multi-Element Diagrams

Multi-element diagrams commonly show a large number of peaks and troughs due to the differences in behavior between the large ion lithophile (LIL) elements and high field strength (HFS) elements (Rollinson, 1993). LIL elements (e.g., Cs, Rb, K, Ba, Eu^{2+}) tend to be more mobile which causes concentrations to be affected by aqueous fluids, whereas HFS elements (e.g., Y, Hf, Zr, Ti, Nb, Ta) tend to be immobile and controlled by the melt source and petrogenetic processes such as fractional crystallization (Rollinson, 1993).

The multi-element plots in Figures 7.8 and 7.9 show that WRO and BG samples have significant overlap, especially for the LIL elements. This overlap is better realized in a multi-element plot of the averages for WRO and BG samples (Figure 7.10). Many of the WRO samples are, however, distinct from the BG samples, particularly in HFS element values and Th. The multi-element diagrams are normalized to MORB for the WRO and BG samples.

The BG samples are more uniform and show LIL element enrichment and low values or depletion among the HFS elements. Sr, K, Rb, Th and Ba are enriched and are likely accounted for in the high amounts of plagioclase, muscovite, and biotite in the samples. Notable troughs in HFSEs include Nb, P, and Ti (average normalized values are 0.79 ± 0.46 , 1.14 ± 0.75 , and 0.3 ± 0.27 respectively). Ti and Nb are likely controlled by titanite, ilmenite, and/or rutile whereas P is likely controlled by apatite. Fractional crystallization of titanite, rutile, or ilmenite and apatite may have caused these depletions, or they could be the result of restite material left in the source after partial melting. The enrichments in Sr, K, Rb, and Ba could indicate that plagioclase and/or orthoclase accumulation occurred, since plagioclase and orthoclase tend to strongly partition

these elements. Plagioclase accumulation will, however, be shown to be an unlikely mechanism later in this chapter. K and Rb could also presumably be controlled by accumulation of micas. It is more likely that the initial melt was extremely rich in these LILs and they behaved as incompatible elements which remained preferentially partitioned in the melt.

The WRO samples are much more scattered in the multi-element plot and show lower enrichments in LILs and extremely variable depletions in HFSEs on average. Samples are similar to the BG samples in that they are enriched in Sr, K, Rb, Ba, Th and depleted in Nb, P, and Ti. However, the WRO samples are very different in that they are depleted (to variable degrees) in Th, Ce, Zr, Hf, Sm, Y, and Yb both relative to MORB and the BG samples. These depletions are further quantified in Figure 7.13. The extreme depletions in Zr and Hf indicate that zircon may have been a key fractionating phase from a melt which was potentially originally similar to BG. Zircon would also have had an effect on Y, Yb, and Th as the partitioning coefficients for these elements are high for zircon. Th, Ce, and Sm may have been controlled by fractionation of epidote or allanite which has extremely high partitioning coefficients for LREEs.

While there is much scatter in the WRO multi-element data, the LILEs generally have a consistent pattern. This is important because the LILEs are fluid mobile elements and would likely show a lot of scatter if the samples had been altered during metamorphism. The scatter for the WRO samples of HFSEs is likely controlled by the melt source and/or petrogenetic processes such as assimilation or fractional crystallization.

	WRO		BG	
	Values	SD	Values	SD
Th	7.89	8.86	11.1	8.75
Ce	1.55	1.56	2.55	1.02
Zr	0.23	0.42	1.16	0.42
Hf	0.02	0.02	0.17	0.5
Sm	0.35	0.45	0.78	0.47
Y	0.13	0.31	0.22	0.21
Yb	0.01	0.01	0.04	0.06

Figure 7.13. Average normalized concentrations for WRO and BG samples from the multi-element plots with standard deviations. Samples were all normalized to MORB (Pearce, 1983).

Figure 7.14 shows Harker plots of Zr, Ce, Zn, Ba, La, Pb, Th, and Ga versus SiO₂. The plots for Ba, Pb, and Zr show potential indications of two separate trends for the BG and WRO samples. While some of the Zr values for the WRO samples overlap those of the BG samples, the majority show an entirely different trend. This could indicate differing petrogenetic histories, but the WRO and BG samples do show significant overlap in the other plots. Very similar patterns are evident for Pb, Ba, and Th. There appears to be a general trend for all of the elements in that they decrease as SiO₂ content increases. If fractional crystallization played a major role in magma evolution, the correlation between these elements and SiO₂ indicate that from approximately 55 to 70% SiO₂, the fractionating phases that drove SiO₂ up did not partition Zr, Ce, Zn, Ba, La, Pb, Th, or Ga. However, at 70-72% SiO₂, the fractionating phases that drove up SiO₂ just before it became buffered did contain the elements Zr, Ce, Zn, Ba, La, Pb, Th, and Ga. Minerals which may have played an important role in this process include zircon, apatite, epidote and/or allanite, biotite, and potassium-feldspar. These trace minerals may have been the only phases in addition to quartz and feldspars fractionating from such a siliceous magma and as such had a strong effect on geochemistry despite their relatively low abundance.

Alternatively, the plots may indicate that extremely low fraction partial melts very rich in SiO₂ were poor in the elements of interest *until* the melt reached ~72% SiO₂ at which point minerals which contain reasonable amounts of the elements of interest began to melt. As the melt continued to evolve, with a higher % of melting, and became less siliceous, the amount of Ce, Ba, La, Pb, Th, and Ga decreased as the melt became diluted with other elements. Regardless of mechanism, these plots show similar trends to the Harker diagrams in Figure 7.5 such that something in the magma evolution changed drastically at around 70-72% SiO₂.

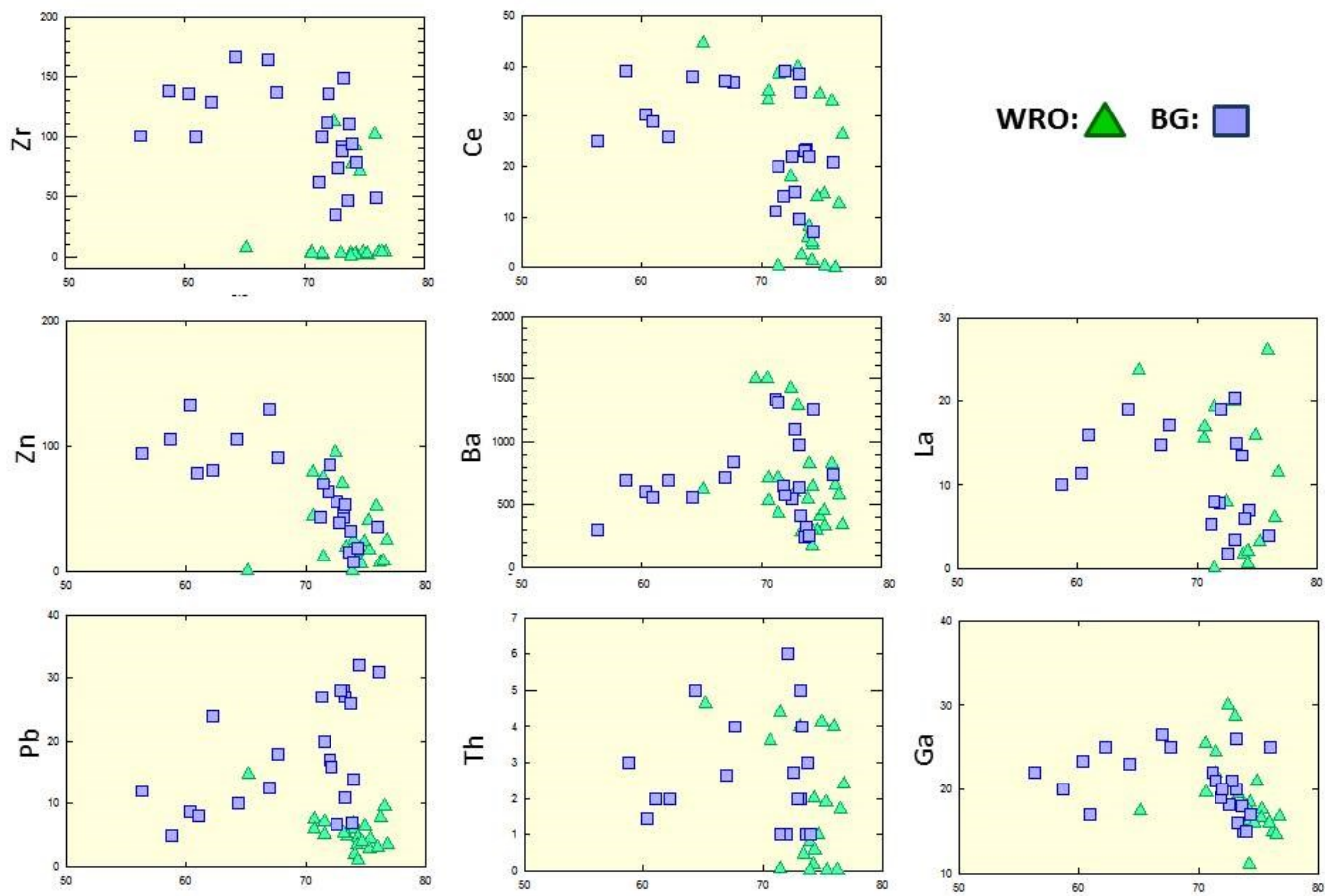


Figure 7.14. Harker plots of Zr, Ce, Zn, Ba, La, Pb, Th, and Ga versus SiO₂ for the WRO and BG samples.

The tectonic discrimination diagram (Figure 7.11) indicates that the WRO and BG magmas are similar to Volcanic Arc Granitoids and Syn-Collisional Granitoids. Shervais (2008) suggested in a paper on TTG genesis in ophiolites that the negative Nb, Hf, and Ti anomalies are indicative of subduction zone magmatism. Specifically, Rollinson (1993) suggests that negative Nb anomalies are indicative of continental crust involvement. Rollinson (1993) also cautions that while tectonic discrimination diagrams can be useful, they are empirically derived and must be used in conjunction with other information. The regional geology during the emplacement of the WRO and BG magmas would indicate that a syn-collisional (continental arc, active continental margin) type setting is reasonable.

The interpretation of much of the trace element data is ambiguous. Allegre & Minster (1978) claim that inconsistency in the concentration of compatible elements in a multi-element plot is likely to be caused by fractional crystallization. While there is some scatter in the HFSEs, Zn is the most compatible element plotted and shows a steady downward trend. This would indicate that fractional crystallization was not a dominant process. Conversely, there is higher variability in the incompatible elements which indicates that partial melting was the dominant variation process (Allegre and Minster, 1978). This variability is especially apparent in the LIL elements (Ba and Pb) and HFS elements having larger ionic radii (La and Th). Zr, Ce, and Ga have slightly smaller ionic radii and show reasonably consistent trends which are consistent with partial melting as the dominant variation process.

Rollinson (1993) pointed out that trace element analytical techniques can be problematic when studying granitic rocks because of the common occurrence of trace minerals that will take in normally incompatible elements. For this reason, Rollinson (1993) suggests that radiogenic isotope data may be more useful in determining the source of granitic rocks. Petrogenetic

modeling of the WRO and BG magmas will provide further insight into the interpretations which have just been discussed.

7.4.4. Additional Geochemistry Questions and Pressure Estimate Issues

7.4.4.1. What is the oxygen fugacity?

It has been shown by Schmidt & Poli (2004) that the P-T stability field of epidote in a magma increases with increasing oxygen fugacity. Conversely, extremely low oxygen fugacities would lead to reducing conditions in which magmatic epidote may not be stable. Although there is certainly magmatic epidote in these rocks, there is currently also evidence for somewhat reducing conditions in the magma. The argument for reducing conditions is based on the positive Eu anomalies in the REE plots for some of the WRO and BG samples. This anomaly is thought to result from Eu substituting into plagioclase as Eu^{2+} , which requires reducing conditions. This apparently contradictory evidence might be explained by divalent and trivalent Eu being sourced over a spectrum of oxidation states in the crust. Additionally, because Eu will be present to variable amounts in the divalent and trivalent state, there may be no problem with Eu availability in both valences. Schmidt and Poli (2004) recommend that the oxygen fugacity be determined using oxide mineral equilibria when possible before any conclusions on intrusion pressures are made using magmatic epidote. The most popular method for determining oxygen fugacity was developed by Buddington & Lindsley (1964) and involves analyzing coexisting magnetite and ilmenite. This method essentially calculates the temperature and oxygen fugacity at the last time the minerals equilibrated (Philpotts and Ague, 2009). Buddington & Lindsley (1964) found that for the same temperature, increasing oxygen fugacity leads to a decrease of TiO_2 in magnetite and an increase of Fe_2O_3 in ilmenite. In order to calculate the oxygen fugacity using this method, the compositions of both ilmenite and magnetite must be determined using advanced techniques

such as electron microprobe analysis (Philpotts and Ague, 2009). An even more crucial factor is that ilmenite and magnetite must both be present in the rock simultaneously, which is not the case in WRO or BG samples.

7.4.4.2. *Is the WRG water rich or water poor?*

Epidote phase stability diagrams are predominantly based on experiments performed on H₂O-saturated TTG magmas. Because the Wenatchee Ridge Gneiss TTGs are not especially volatile rich, given the low LOI results, the magma was potentially not H₂O saturated. Naney (1983) stated that hornblende requires a minimum of approximately 4 weight percent H₂O to exist in the granodiorite system at 200 MPa, and 2.5 weight percent to be stable at 800 MPa. Because of this, Naney (1983) also stated that the presence or absence of hornblende in a calc-alkaline rock may be a useful indicator of the minimum H₂O content within the parent magma system. Based on this, the absence of hornblende in the WRO may indicate that the magma was low in H₂O content.

However, it may also be that water-rich minerals were not stable for other reasons or that water escaped from the melt in some other way. Additionally, late stage pegmatites and quartz veins indicate that magma was likely water-rich at some point.

7.5. Modeling Approach

The ultimate goal of petrogenetic modeling is to use geochemistry to determine the source of the WRO magma and petrogenetic mechanisms that may have influenced the geochemical evolution resulting in the final WRO and BG rocks. The ideal model for the WRO and BG magma formation will need to successfully answer the following four questions:

1. What was the original source of the magma?
2. What caused the LREE depletion and scatter amongst the WRO samples?

3. What is the cause of the positive Eu anomaly?
4. How did crystals and/or batches of magma separate from the liquid or source region?

Question 4 will be addressed in chapter 8. The specific purpose of the fractionation modeling performed using IgPet computer software (Rockware, 2004) for this chapter is to determine the minerals which may have had an effect on the scatter present in the WRO data.

7.5.1. Petrogenetic Modeling

7.5.1.1. Question 1: What was the original source of the magma?

7.5.1.1.1. WRO and BG Formation Models

As discussed in Chapter 3, there are many possible methods of TTG formation. This study focuses on two different processes that are the most generally accepted producers of TTG magma. These processes, generally described, are partial melting and fractional crystallization.

7.5.1.1.2. Partial Melting

Felsic melts can be produced by the partial melting of intermediate to mafic rocks. Partial melting can occur in two different types of processes: batch melting (equilibrium melting) and fractional melting (Rayleigh melting). Batch melting involves a partial melt that is allowed to remain *in situ* such that the melt can equilibrate with the restite at the site of melting until magma leaves as a large body (Rollinson, 1993). Fractional melting occurs such that small amounts of melt are produced and instantly separated from the source. For the majority of TTG suites, batch partial melting is assumed to be the process of formation (Rollinson, 1993).

Without a reliable sample of the source material (or some possible parental rock at depth) in the region, modeling the process of batch melting for the WRO or BG samples would be uncertain. That being said, regional geologic evidence for overthickened crust, an abundance of oceanic rocks with basalt likely at depth, and a lack of co-eval mafic rocks in the area suggest

that the initial melt was generated via partial melting of basaltic material metamorphosed to amphibolite or eclogite facies. Additionally, as shown in Section 7.3.2., the WRO and BG magmas are very similar (chemically and mineralogically) to experimental TTG melts formed by the partial melting of eclogite or amphibolite.

7.5.1.1.3. Fractional Crystallization

In this process, felsic magmas develop from a parental (mafic or intermediate) magma through the process of fractional crystallization (FC) or assimilation fractional crystallization (AFC) (Borg & Clynne, 1998). The process of assimilation fractional crystallization (AFC) has been recognized as particularly difficult to model when using geochemical data to interpret the petrogenetic history of a rock. In traditional magma modeling, assimilation and fractional crystallization were handled as completely separate processes. However, as pointed out by Depaolo (1981), the heat necessary for assimilation can be provided by fractional crystallization through the latent heat of crystallization.

Fractional crystallization can also be separated into two general processes: equilibrium crystallization and Rayleigh crystallization. Similarly to partial melting, equilibrium FC involves crystals which are allowed to equilibrate with the melt as the crystal forms. Alternatively, Rayleigh FC occurs such that the newly formed crystals are quickly separated from the melt.

While fractional crystallization of a large basaltic magma chamber is not a likely model for the WRO and BG magmas, fractional crystallization within a magma chamber initially created via partial melting is a strong possibility. Given the data available, which forms a trend among samples with variable chemistry and mineralogy, it is most useful to model the range of observed compositions in terms of both Rayleigh and equilibrium fractional crystallization.

7.5.1.2. Question 2: What caused the LREE depletion and scatter amongst the WRO samples?

7.5.1.2.1. *Modeling Methods*

Partition coefficients were used from sources compiled by Rollinson (1993) for modeling of fractionating assemblages such as apatite, titanite, zircon, epidote, and hornblende. K_d values of dacitic magmas were used as K_d values from tonalitic to tondehmitic rocks are not well defined in the literature.

Trends were examined between pairs of elements. When a reasonable trend was found for element pairs, the model was entered using K_d values of the fractionating mineral of interest. If the K_d values were too similar and / or the trend in the data was linear, other pairs of elements were selected for modeling.

Minerals that may have had a significant effect on the sample scatter in the WRO samples were selected from the consideration of the multi-element spider diagrams discussed earlier in this chapter as well as what minerals were observed in the suite. Elements such as P, Nb, Ti, and Zr which were most different from MORB values and from the BG samples were inferred to be controlled by the trace minerals apatite, titanite, and zircon, respectively. The fractionation of these minerals from the most mafic and presumably earliest magma was modeled to determine if the removal of these minerals could have played a role in the formation of the various WRO magmas.

7.5.1.2.2. *Apatite*

Apatite fractionation was investigated with the elements Yb and Dy that have significantly different K_d values for a dacitic magma. The K_d value used for Yb was 13.8 and the K_d value used for Dy was 34.8. The model was run from 100 to 90% melt at 0.01 intervals using Z-141-1 as the parental magma as it is the most mafic.

In Figure 7.15a, the trend that represents the Rayleigh fractionation of apatite (the black line) matches reasonably well with the plotted data. Figure 7.15b shows the model for equilibrium FC and matches even more closely with the plotted WRO data.

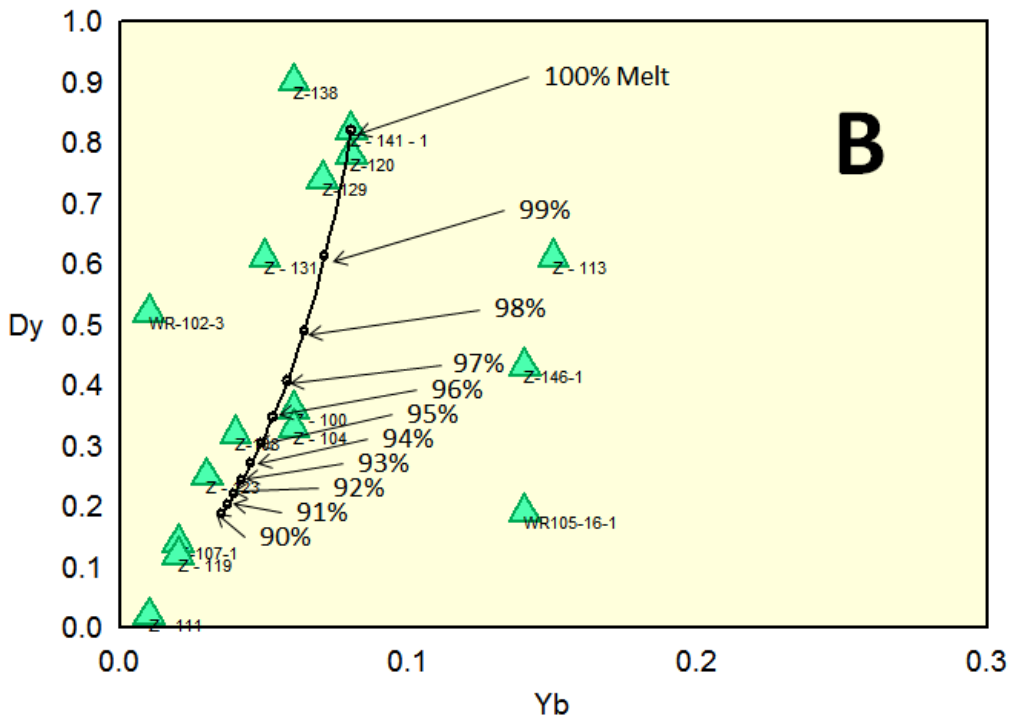
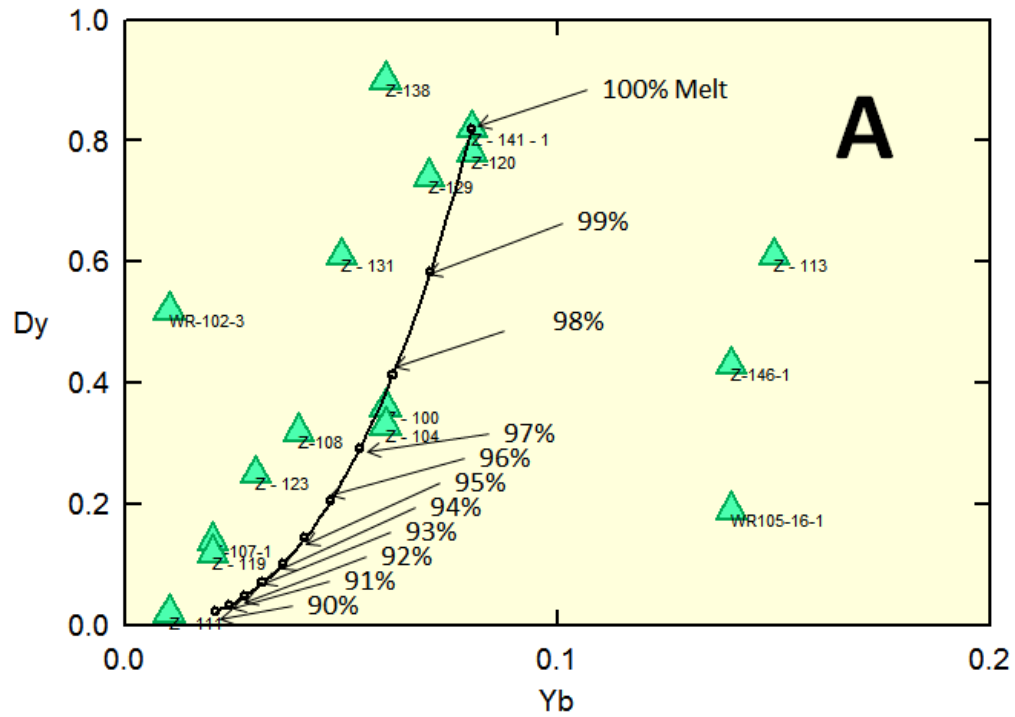


Figure 7.15. Apatite fractionation model via Rayleigh fractionation (A) and equilibrium fractional crystallization (B).

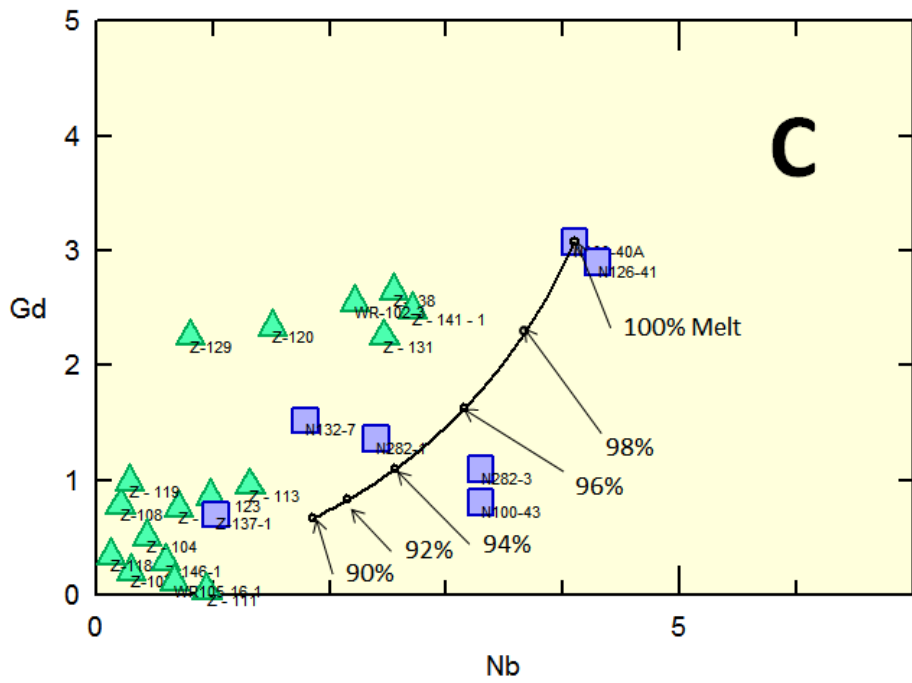
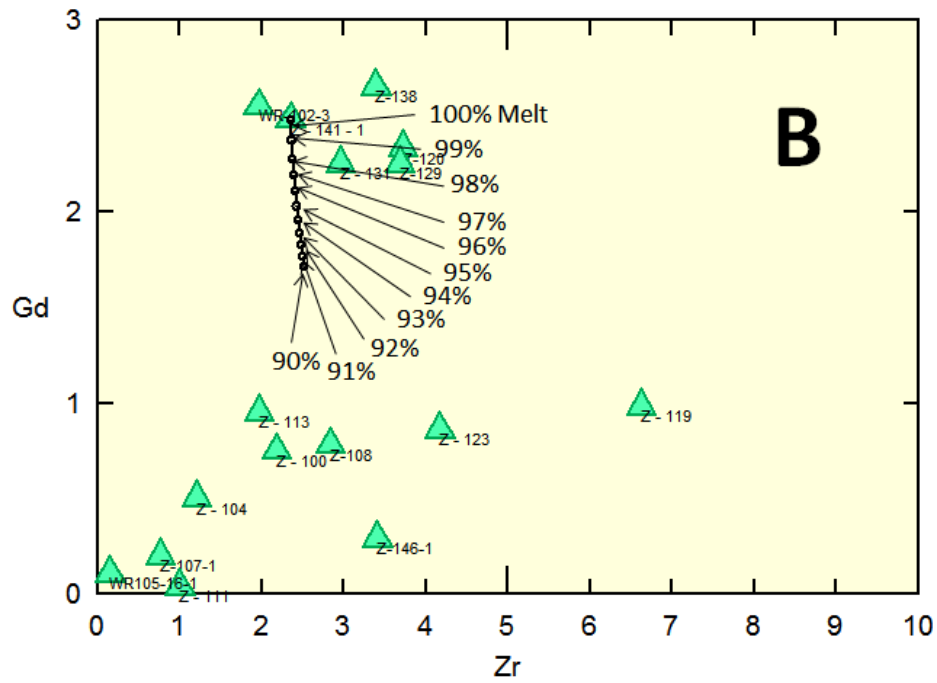


Figure 7.16. Hornblende fractionation model via Rayleigh fractionation (A – page 143), equilibrium fractional crystallization (B), and equilibrium fractional crystallization including the BG samples (C).

7.5.1.2.4. Zircon

The model for zircon fractionation uses Yb and Dy which have significantly different Kd values for a dacitic magma. The Kd value used for Yb was 191 and the Kd value used for Dy was 47.4. The model was run from 100 to 90% melt at 0.01 intervals using Z-141-1 as the parental magma.

The trend-line for Rayleigh fractionation of zircon does not match the trend of the plotted data (Figure 7.17a). However, the general trend of the data is displayed by the model. The trend is better displayed by the model of equilibrium fractionation of zircon (Figure 7.17b).

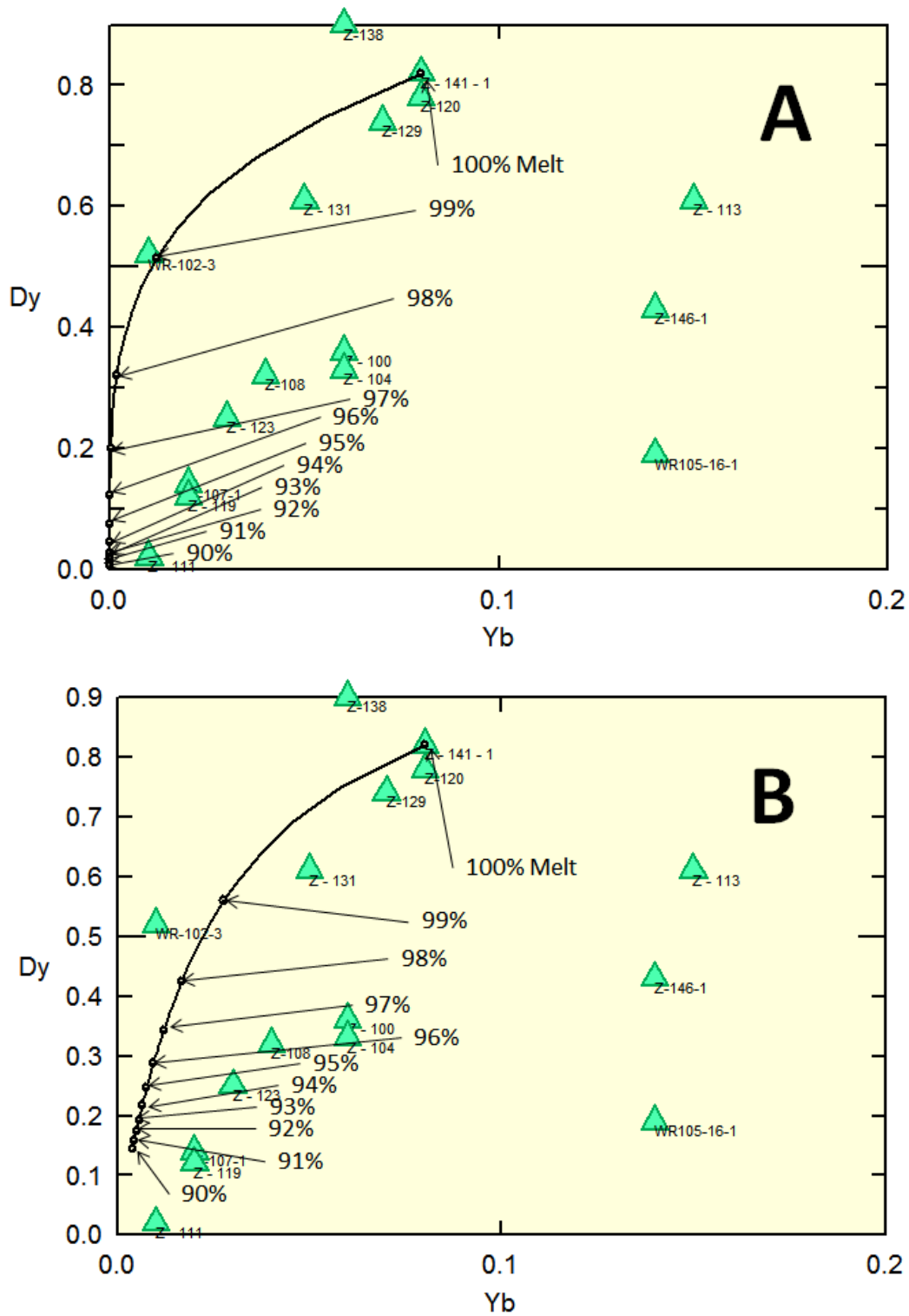


Figure 7.17. Zircon fractionation model via Rayleigh fractionation (A) and equilibrium fractional crystallization (B).

7.5.1.2.5. *Epidote and Allanite*

Figure 7.18 shows a model of epidote fractionation using K_d values of 820 for La and 205 for Sm. The model runs from 100-90% melt at 0.01 intervals using Z-141-1 as the parental magma. This plot matches the trend present in the data reasonably well for both Rayleigh fractionation (Figure 7.18a) and equilibrium fractionation (7.18b).

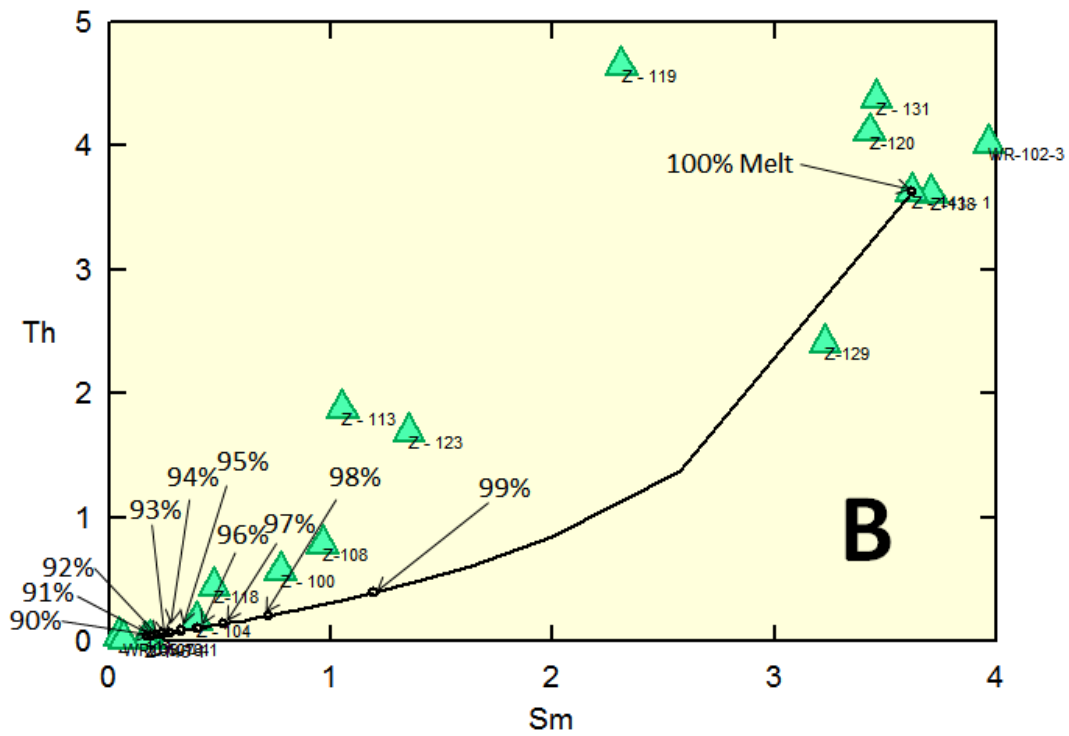
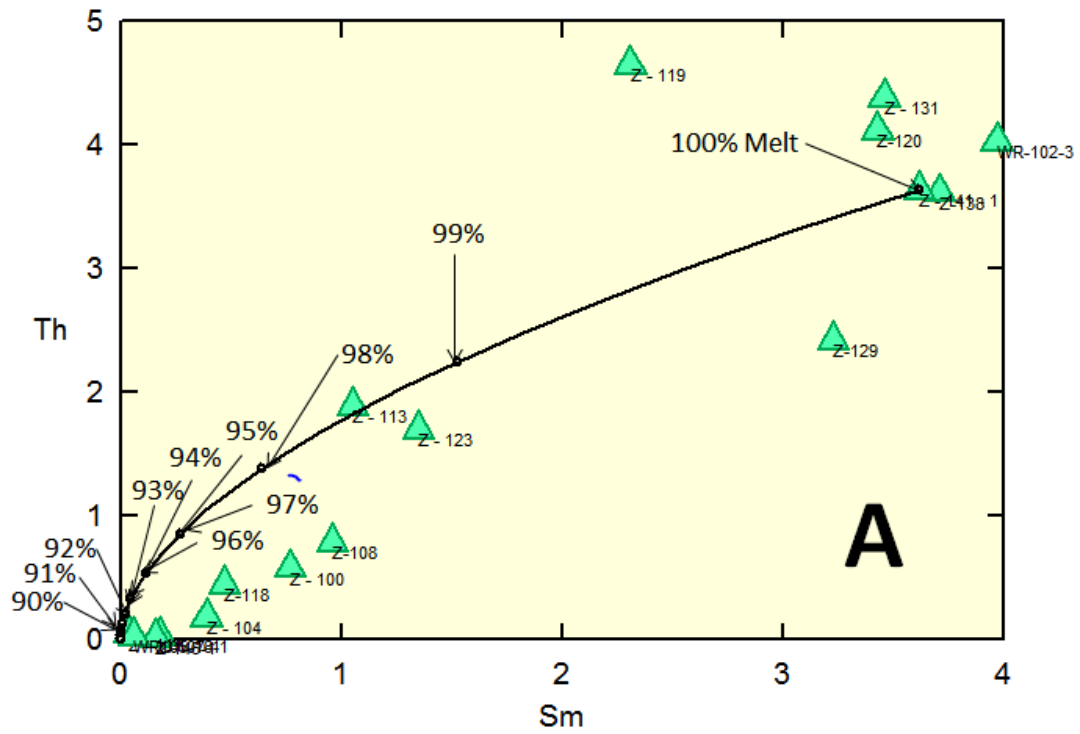


Figure 7.18. Epidote/allanite fractionation model via Rayleigh fractionation (A), equilibrium fractional crystallization (B).

7.5.1.2.6. Titanite

Titanite fractionation was modeled using La and Sm, two elements having reasonably different Kd values for titanite. The Kd value used for La was 4 and for Sm was 21. The model ran from 100-90% melt at a fractionation step of 0.01 using Z-141-1 as a starting material.

Figure 7.19a shows the model for Rayleigh fractionation and does not match the data well at an F range of 0.9 (90% of melt remaining). However, the model did begin to match when plotted at an F range of 0.75 (75% of melt remaining). Figure 7.19b shows the model of equilibrium crystallization and also does not match the plotted data well.

A better match with the plotted data for Sm and La can be seen when epidote fractionation is modeled again. The upper black line in Figure 7.16b is a model for epidote fractionation run from 100-90% melt. The Kd values for epidote (allanite) in this graph were 820 for La and 205 for Sm. The equilibrium fractionation model for epidote in this graph matches the data reasonably well. Looking at figure 7.19b, a model which included the fractionation of both epidote and titanite simultaneously would appear to match the model very well.

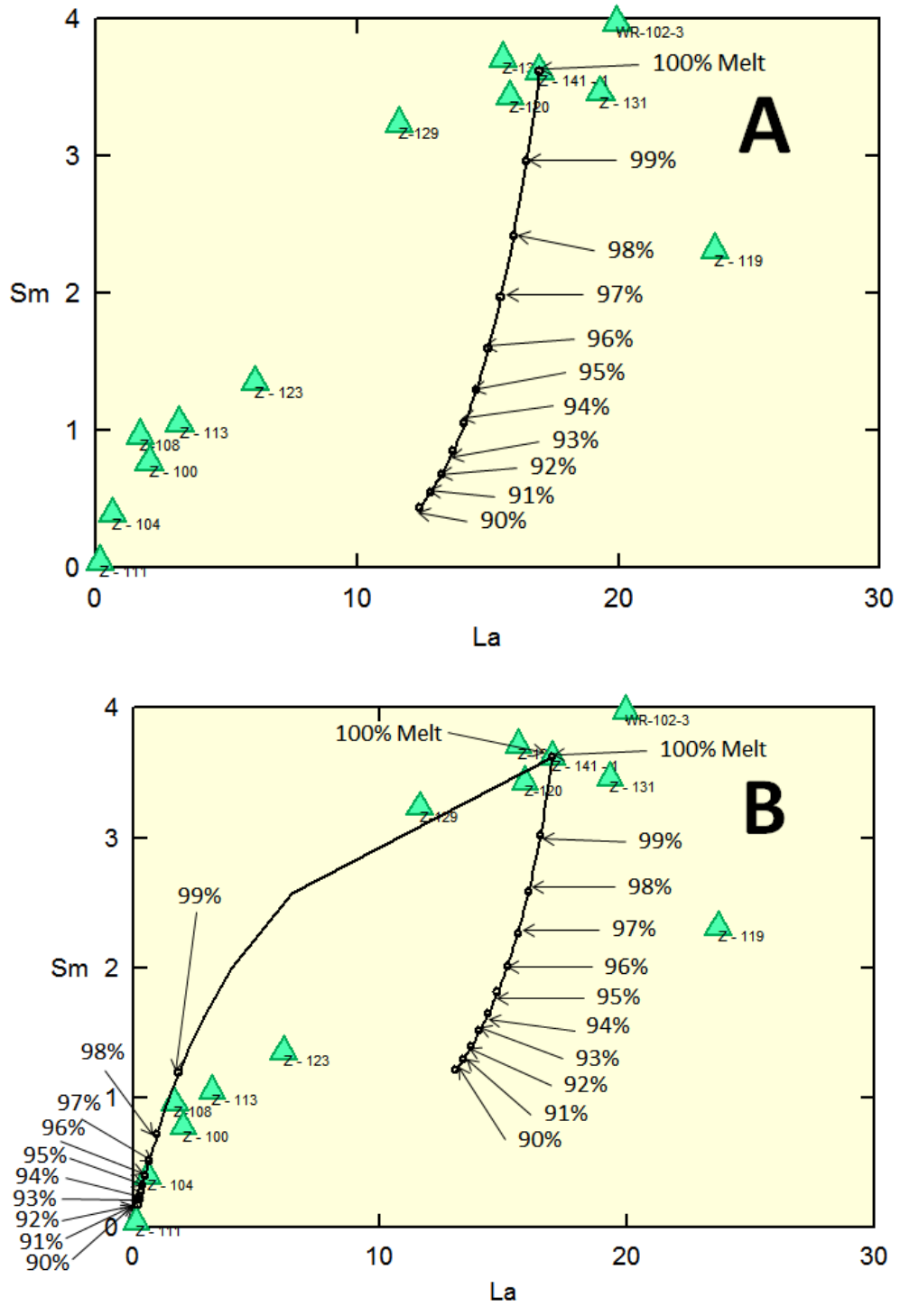


Figure 7.19. Titanite fractionation model via Rayleigh fractionation (A) and equilibrium fractional crystallization (B). Model B compares a line for epidote/allanite fractionation (top line).

7.5.1.2.7. *Conclusions from petrogenetic modeling*

Although they only occur as trace minerals, apatite, zircon, and epidote are shown by the models to have potentially played a significant role in magma evolution via equilibrium fractional crystallization or a process similar to it, such as *in-situ* crystallization. This makes sense due to the high viscosity of the WRO magma which may have created an environment where crystals were not easily separated from the melt. Epidote appears to have played a primary role in altering the chemistry via fractionation. This fact may be supported by research on epidote bearing pegmatites cutting the WRO by (Merkel 2007). Merkel (2007) identified six distinct populations of magmatic epidote with variable LREE chemistries. Fractional crystallization of these populations to variable degrees within the magma could lead to the observed REE and multi-element patterns displayed by the WRO samples. Merkel (2007) additionally noted that a variation in P content across epidote crystals marked the crystallization of apatite in the magma chamber which, as supported by the above modeling, likely separated from the magma at a later time. Hornblende and titanite fractionation did not contribute to magmatic evolution of the WRO. It is possible that hornblende and/or titanite fractionation may have played a larger role in the BG samples. That being said, there is petrographic evidence for titanite fractionation (via inclusion with epidote inside of biotite) such that titanite may have played a minor role in magma evolution. Additionally, hornblende may not have ever been present in the majority of magmas due to the likely low H₂O content.

7.5.1.3. ***Question 3: What is the cause of the positive Eu anomaly in the WRO and BG?***

Eu commonly does not lie along the expected trend with other REEs and instead shows either a positive or negative Eu anomaly (Rollinson, 1993). The WRO and BG samples show an average positive Eu anomaly (Eu/Eu*) of 1.36 ± 0.5 .

The Eu value was found using the normalized values of Sm and Gd. This anomaly occurs because while all other REE's are trivalent, Eu can occur partly as Eu^{2+} in relatively reducing environments (Terekhov and Shcherbakova, 2006). As Eu^{2+} , Eu can more easily substitute into feldspars (in the Ca site) and Ba-bearing minerals (Terekhov and Shcherbakova, 2006). As more plagioclase is added to the magma, Eu^{2+} would be added along with Na, Ca, and/or Sr. Eu fractionation between crystals and magma is chiefly controlled by plagioclase and potassium feldspar such that fractionation of feldspar or melting of a rock in which feldspar remains stable would create a negative Eu anomaly (Rollinson 1993, p. 138-139). Other minerals such as titanite, hornblende, clinopyroxene, orthopyroxene, and garnet may also contribute to an Eu anomaly but in the opposite way of feldspars such that a positive Eu anomaly may result (Rollinson, 1993). If the Eu anomaly is associated with the feldspar content of the rock, we would expect the Eu anomalies to correlate with the amount of plagioclase in the rock and/or the amount of Ca, Na, or Sr in the rock (Sr commonly substitutes into plagioclase as well) (Terekhov & Shcherbakova, 2006). Plots showing these relationships are shown on Figure 7.20. If the positive Eu anomaly is controlled by plagioclase, some changes in the magma composition must have occurred at comparatively low pressure within the field of plagioclase stability. If emplacement had occurred below that depth, plagioclase would have been unstable and not able to control the Eu anomaly. The limit of plagioclase stability for TTGs occurs at 35-40 km depth such that the partial melting, fractional crystallization, or assimilation which occurred to create the positive Eu anomalies took place above this depth if Eu was controlled by plagioclase (Girardi et al., 2012).

The data in Figure 7.20 indicate that elements common in plagioclase are not positively associated with Eu/Eu^* as would be expected if the Eu anomaly was controlled by plagioclase

accumulation. Instead, these elements show a slight negative or no correlation with Eu/Eu^* . These relationships indicate that plagioclase accumulation was not the cause of the Eu anomaly.

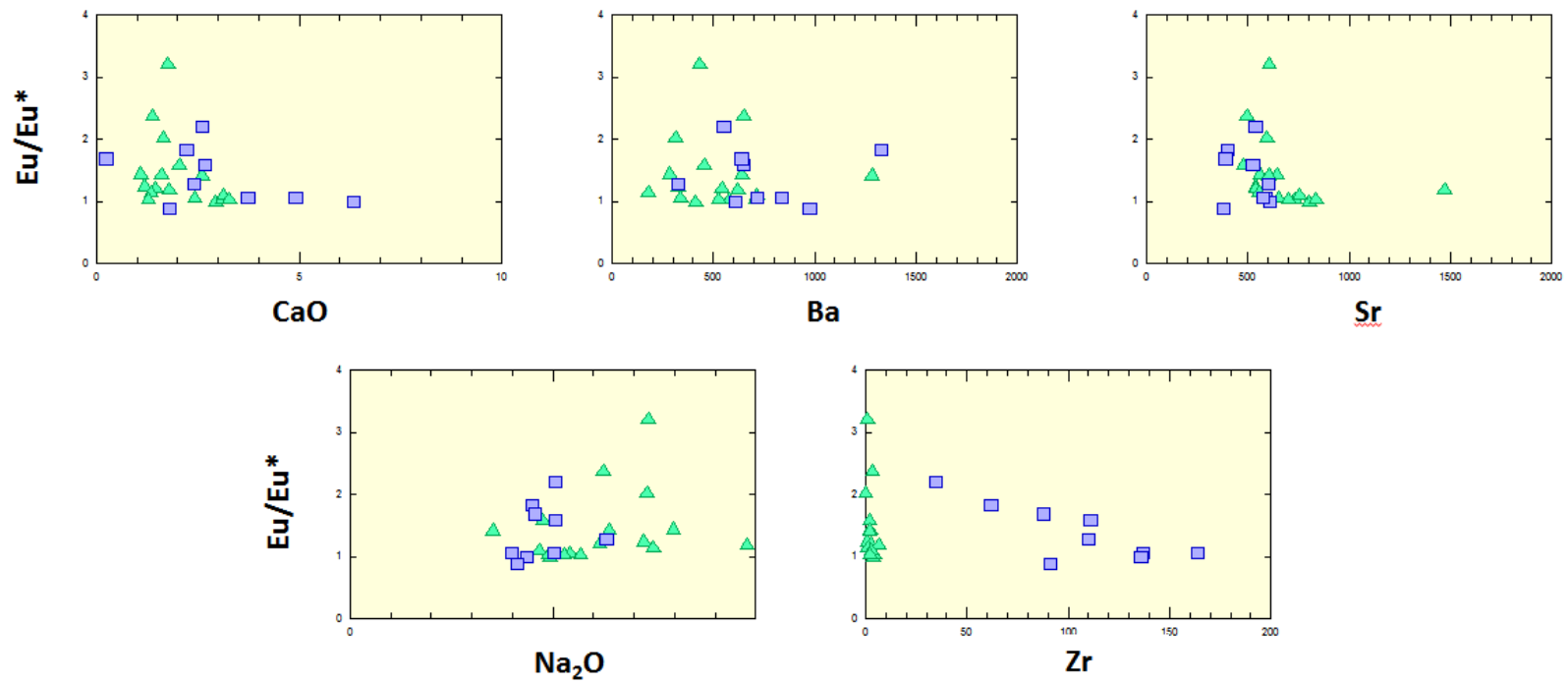


Figure 7.20. Plots of elements expected to be associated with plagioclase accumulation versus Eu/Eu^* . Green triangles are WRO samples and blue squares are BG samples.

Interestingly, Eu/Eu^* has the strongest correlation with Zr in the BG samples (Figure 7.20). A graph of $\text{La}/\text{Yb}(\text{N})$ (a measure of LREE enrichment) vs. Eu/Eu^* (Figure 7.21) shows that as LREE enrichment decreases, the positive Eu anomaly increases. This may indicate that whatever phase is fractionating LREE is additionally leaving Eu behind in the melt due to a low K_d value for Eu. Titanite, zircon, and/or amphibole may have controlled the Eu anomaly in this way, although zircon and amphibole are not likely to concentrate LREEs. The correlation with Zr could be related to zircon or titanite as Zr can substitute into titanite and allow additional substitution of trivalent REEs. Indeed, titanite is commonly in the WRO and BG samples and especially rich in certain early phases of the BG (Magloughlin, 1994). Conversely, this relationship could indicate that low percentage partial melts preferentially incorporate Eu over LREEs. The melt may have formed in a volume of reduced rock where Eu^{2+} behaved as an incompatible element and later moved into a less reducing environment allowing for epidote stability.

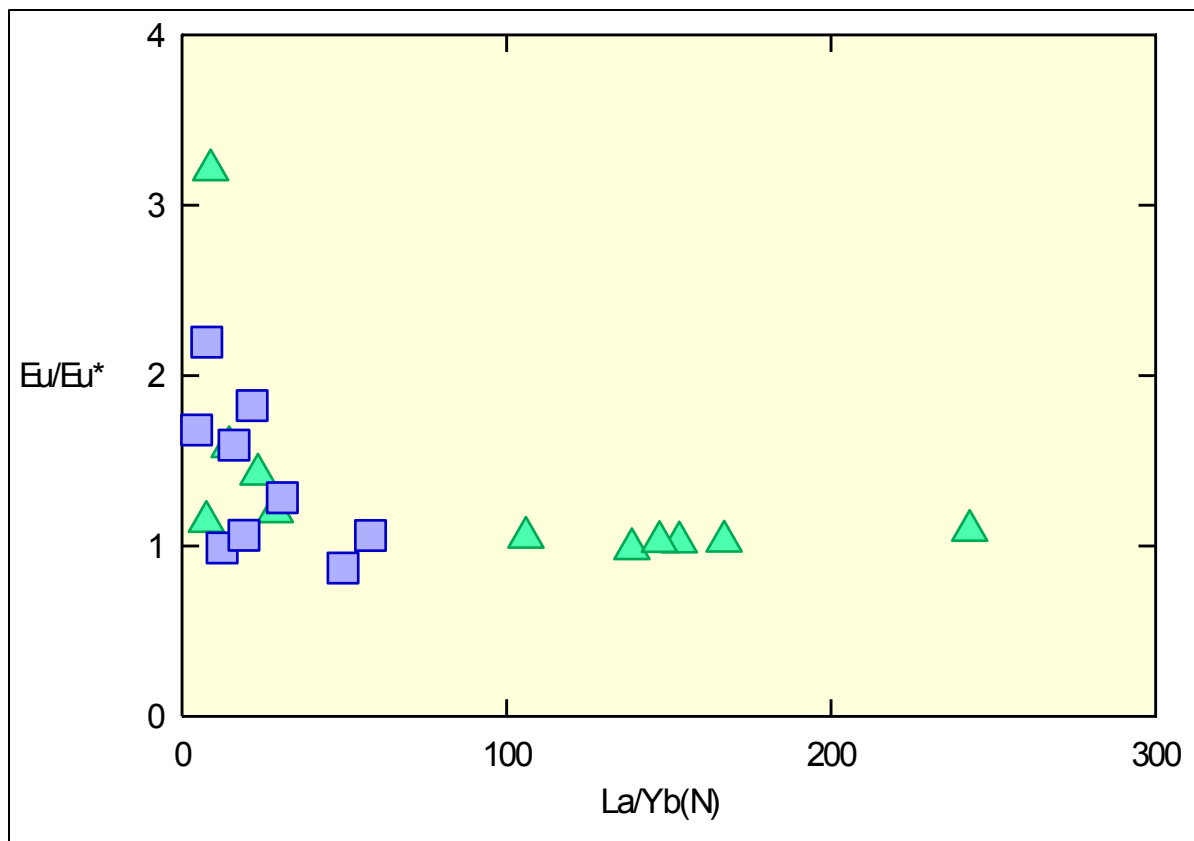


Figure 7.21. Graph of La/Yb(N) vs. Eu/Eu* showing that as LREE enrichment decreases, the positive Eu anomaly increases.

7.6. Discussion

Chemical and regional information indicate that the original source of melt for the WRO and BG magmas was likely provided by the partial melting of eclogite or amphibolite at depth. The variation within the WRO samples has been shown by modeling to be potentially related to the fractional crystallization of trace minerals from the original magma. Because most of the models run to 10% crystallization, any trace minerals that were shown to have a significant effect would have been in high abundance. Conversely, variable degrees of partial melting and variable residence times for separate batches of magma, potentially in transport, could create a similar trend in the geochemical data.

One problem with the modeling of fractional crystallization has to do with the actual degree of fractionation. As seen in the models, fractional crystallization runs from 100% to 90% melt. For the apatite fractional crystallization model (Figure 7.15b) to be viable to 90% melt, there would have to be an extremely high volume of apatite in the melt. A complete fractionation of 10% apatite would require approximately 5% P_2O_5 in the melt which is unreasonable (Ridley, pers. comm., 2014). The model does indicate that apatite fractionation did have an effect on the WRO and BG evolution; however the effect is not due entirely to apatite but instead to the fractional crystallization of many trace minerals simultaneously.

8. MAGMA EMPLACEMENT AND DIFFERENTIATION

8.1. Overview

This chapter will address question 4 from the previous chapter – How did crystals and/or batches of magma separate from the liquid or source region?

8.2. WRO and BG Magma Viscosity

The viscosity of the WRO and BG magma was calculated using ten major element oxide results, along with LOI, and the method of Giordano et al. (2008). This calculation yielded results of $\geq 10^6$ Pa·s at 1000°C. LOI was assumed to be dominantly representative of the water content of the magma. If half of the LOI is assumed to be due to F, the viscosity remains the same. This is an extremely high viscosity when compared to a viscosity of 10^{-10^2} Pa·s for a typical basaltic magma. Additionally, the viscosity of the WRO and BG magmas may have been even higher due to the fact that they likely had a low water content compared to typical TTGs and other granitoids and are dominantly peraluminous (both contributing factors which increase viscosity) (Dingwell et al., 1998). Because the viscosity is so high, petrogenetic processes such as partial melting or fractional crystallization would have to be aided by deformation in order to either remove melt from the source region or remove crystals from the melt (Vigneresse et al., 1996). This section will give a brief overview of differentiation processes and how deformation-driven differentiation may have played a role in the evolution of the WRO and BG magmas.

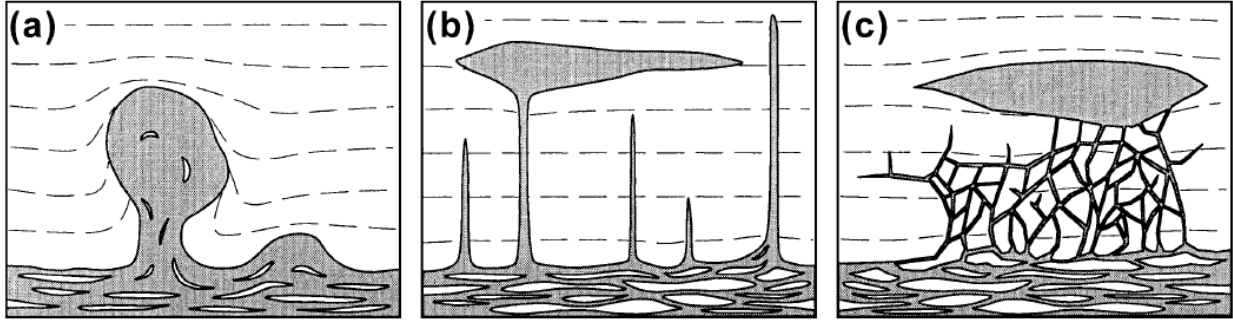


Figure 8.1. Figure from Bons et al. (2004) showing the 3 end member processes of magma emplacement. Magma may ascend through the crust by (a) diapirism, (b) diking, or (c) pervasive ascent through fracture or pore space networks.

8.3. Intrusion of Magma

There are 3 primary models proposed to explain the ascent of magma through the crust (Figure 8.1) (Bons et al., 2004; Philpotts and Ague, 2009). Magma may flow through the crust as a large diapir (Figure 8.1a), along a series of dikes (Figure 8.1b), or pervasively through fracture or pore space networks (Figure 8.1c) (Bons et al., 2004; Philpotts and Ague, 2009). Diapiric emplacement of buoyant magma that is at least partially molten is controlled by the ductile behavior of the host rock and is presumably a very slow process that cannot easily occur at shallow depths where brittle deformation dominates (Paterson and Vernon, 1995). The diking model allows for greater emplacement rates within the upper crust than the diapir model because viscous drag within the dike is the only real control on emplacement rates (Petford et al., 1993). The pervasive flow of magma through pore spaces is inherently dependent upon the permeability of the host rock, and is also likely a slow process, unless aided by deformation (Weinberg, 1999).

The mode by which magma ascends into the crust will determine the heterogeneity of the final igneous rock body by controlling the segregation of melts as well as the amount of mixing or mingling that may occur between different melt batches (Bons et al., 2004). Many plutons in the upper crust, including the WRO, are heterogeneous and that fact is best explained by the coalescence of melt batches with distinct geochemistry (Spiegelman and Kelemen, 2003). Magma bodies can develop distinct geochemical and mineralogical signatures through processes of magma differentiation.

8.4. Magma differentiation

Magmas and plutonic rocks on Earth are highly varied in composition and while the source material for a magma is important, the diversity of magmas is best explained by processes of magmatic differentiation (Philpotts and Ague, 2009). The possible mechanisms of magma differentiation, generally described, include immiscibility, magma mixing/mingling, wall-rock

assimilation, partial melting, and crystal fractionation (Philpotts and Ague, 2009; Tartèse and Boulvais, 2010). Crystal-liquid fractionation has been shown through chemical studies of phenocryst compositions as well as field evidence of igneous cumulate layering to be a dominant process of magma differentiation (Philpotts and Ague, 2009; Tartèse and Boulvais, 2010).

Crystal fractionation has been classically thought to be controlled by gravity and magmatic flow processes (Philpotts and Ague, 2009; Tartèse and Boulvais, 2010). However, if there is no density contrast between the phenocryst mineral and the remaining magma, even minerals whose high density would normally cause fractionation may not always be able to sink and separate from the liquid (Philpotts and Ague, 2009). This is especially true if the phenocryst is not able to overcome the yield strength of the remaining magma or if the viscosity of the magma is especially high, such as in the case of ultrafelsic magmas (Bea et al., 2005; Philpotts & Ague, 2009; Tartèse & Boulvais, 2010). Because the WRO and BG magmas were undoubtedly of a high viscosity, the yield strength of the melt would likely not be easily overcome by the phenocrysts even though many of the minerals investigated in the fractionation models are more dense than a typical felsic magma.

8.5. Differentiation by deformation

Because the sinking or floating of phenocrysts cannot always explain the separation of crystals from a magma, other mechanisms must be called upon (Philpotts and Ague, 2009). Flowage differentiation processes such as magma convection involve shear stresses that help move magma and transport crystals (Philpotts and Ague, 2009). Magma convection is possible in some circumstances, but researchers as early as Bowen (1920) recognized that differentiation of magmas via deformation is a viable mechanism for creating the common variation seen in igneous rocks. Consequently, the process of intrusion with simultaneous deformation is more

commonly called upon to explain the emplacement of magma, leading some researchers to suggest that all granitoid magmas are emplacement synchronously with deformation of some sort (Vigneresse, 1995).

Deformation can enhance liquid-crystal segregation and help facilitate the process of magma differentiation by separating liquid from early formed crystal mushes via a filter press-like mechanism (Moyen et al., 2003; Tartèse & Boulvais, 2010). Filter pressing, or filter differentiation, involves the separation of a melt and associated crystals by sieving (Propach, 1976). While this process is called upon in many cases to explain differentiation, Propach (1976) points out that the process is more theoretical than quantitative and the source of pressures which would initiate the mechanism are extremely variable.

Even with multiple models of how crystal fractionation may occur in high viscosity magma, Philpotts and Ague (2009) suggest that the way in which crystals are actually separated from the remaining magma is debatable in most cases.

8.6. Models for simultaneous magma ascent and differentiation

8.6.1. Along hydro-fractures

Bons et al. (2004) created a model which accounts for simultaneous transportation and differentiation of melt which assumes that melt predominately resides in hydro-fractures and moves by merging of these fractures (Tartèse and Boulvais, 2010). In this model, small batches of melt can either move on their own or coalesce with larger batches and then extrude from the source region (Bons et al., 2004).

Deformation plays an important role in this process such that higher deformation rates within the source region favor an early onset of melt extraction (Bons et al., 2004). This occurs because the accumulation of small batches of melt is stimulated and the result is that many

smaller batches of magma are likely to be emplaced with variable residence times in the source region (Bons et al., 2004). Variable residence times or heterogeneous sources of melt may explain the variability of igneous rocks commonly seen at the surface. However, channelized flow through hydrofractures can cause differentiation in itself, even with equilibrium transport, a homogeneous source, and constant partition coefficients (Spiegelman and Kelemen, 2003).

8.6.2. Pervasively through pore spaces

Vigneresse et al. (1996) observed how deformation can enable partial melts to more easily leave the source region via pore spaces during the early stages of melting. Once a minimum of 8% melt by volume has been achieved in the source material and the local percolation threshold (LPT) has been overcome (Figure 8.2), the melt can connect through pockets (Vigneresse et al., 1996). The liquid percolation threshold is the amount of melt necessary to form a continuous film of melt around grain boundaries (Vigneresse et al., 1996). Transport of the melt is aided by deformation which concentrates the local melt into dilatant sinks, which are essentially the pore spaces in the melting rock (Vigneresse et al., 1996). Once the amount of melt in the dilatant sinks has reached 20-25%, the melt escape threshold (MET) is reached and the magma can escape into the upper crust via conjugate fracture systems induced by the expansion of the melt (Vigneresse et al., 1996).

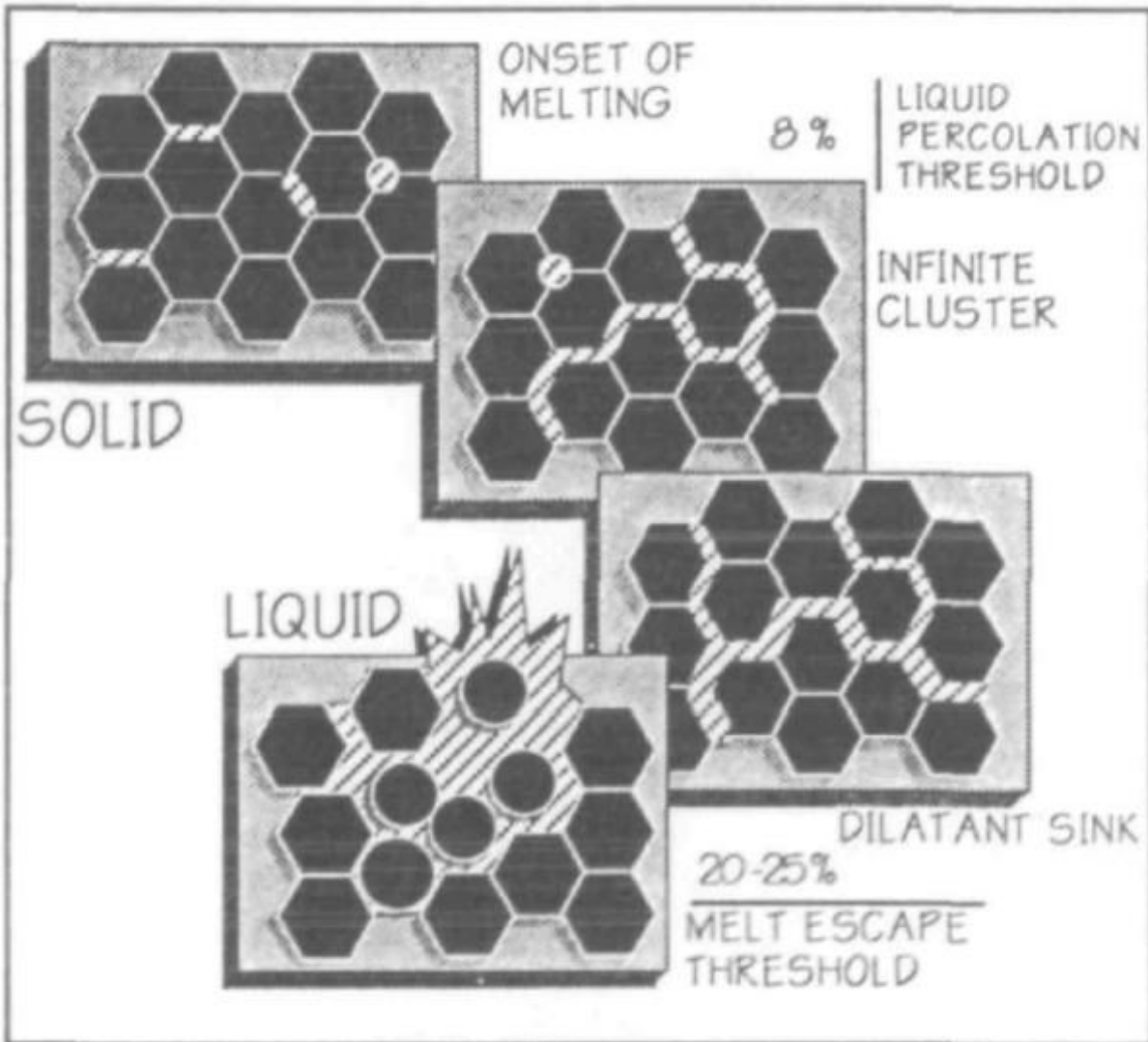


Figure 8.2. Drawing from Vigneresse et al. (1996) showing the transition from solid to melt as the liquid percolation threshold (LPT) is overcome at 8% melt and continuing melt (or coalescence via deformation) allows the melt escape threshold to be overcome at 20-25% melt.

Vigneresse et al. (1996) additionally recognized that the late segregation of magma caused by deformation can lead to changes in composition. As the crystal mush begins to solidify in the emplacement region and is subjected to regional deformation, the rigid framework of crystal fractionates is disrupted (Vigneresse et al., 1996). This is only possible when the rigid percolation threshold (RPT) is reached which is essentially the amount of solids that must exist in order to sustain a tridimensional framework (Bea et al., 2005). Through this process, any remaining melt can be removed from the inter-granular pore space into tensile fractures and will likely take any remaining incompatible elements with it (Vigneresse et al. 1996; Bea et al., 2005; Tartese & Boulvais, 2010).

A process such as early onset of the MET either by way of pore spaces or hydro-fractures may be able to explain the heterogeneity of the WRO samples. These methods are aided by the interpretation that the WRO and BG magmas intruded into an actively deforming terrane.

8.7. Microstructural Evidence

Hibbard (1987) provides an extensive overview of microstructural textures indicative of the deformation of crystal-melt mushes. He focuses on mineral textures indicating that fluid relocation has taken place, including the growth of potassium feldspar, quartz, myrmekite, and microaplite in low pressure “shadow” regions around earlier formed crystals. Fluid relocation, in this case, is synonymous with the filter pressing mechanism described earlier. Figure 8.3 shows the basic textural interpretations of “dynamic” crystallization in which the magma crystallized and melt relocated versus the “static” crystallization case in which melt remained static (Hibbard, 1987). Unfortunately, no pronounced examples of either end-member textures could be found in the thin sections of the WRO or BG samples.

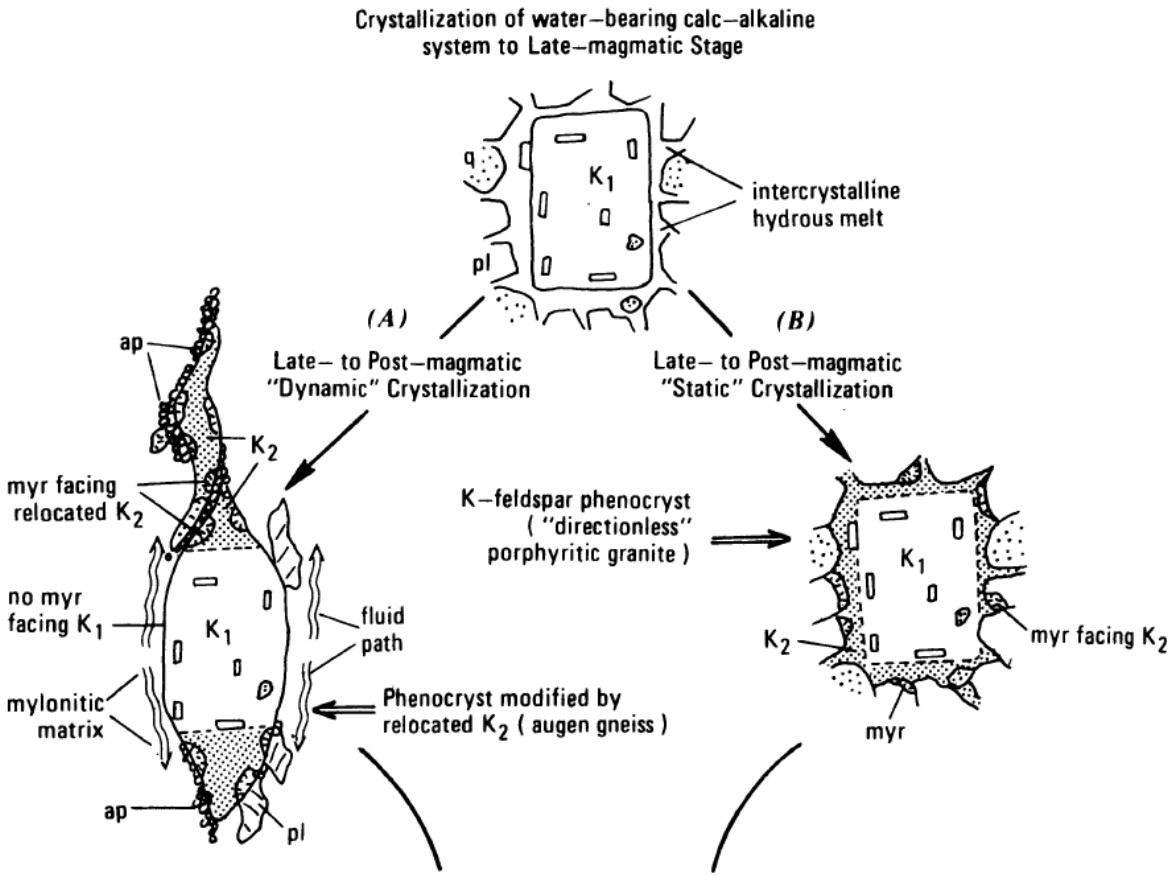


Figure 8.3. Drawing from Hibbard (1987) showing the textural evidence of minerals crystallized during deformation (dynamic crystallization) versus those which crystallized without deformation (static crystallization). Note that the intercrystalline melt has remained in the static case while the melt has been removed and minerals have grown in the “shadow” regions in the dynamic case.

8.8. Petrogenetic Impacts - Examples

Bowen (1920) was one of the first researchers to recognize that the separation of crystals from the parent magma will have the same geochemical impacts regardless of the mechanism. While fractional crystallization has been long recognized in igneous petrology, and differentiation via deformation received a lot of attention in the 1940s to 1970s, it has only recently been re-examined as a principle mechanism. The method by which deformation occurs in order to enable filter pressing is variable and many different models have been proposed.

8.8.1. Deformation within the magma chamber

As pointed out by Bea et al. (1994), the deformation driving differentiation does not always have to be driven by outside forces, but can also be initiated by movement within the magma chamber. Bea et al. (1994) used this idea to explain the vertical zonation of a large granite sill through filter pressing initiated by compaction of a crystalline mush (Figure 8.4). The resulting pluton had high P and extremely depleted U, Th, Y, and REE concentrations (Bea et al., 1994).

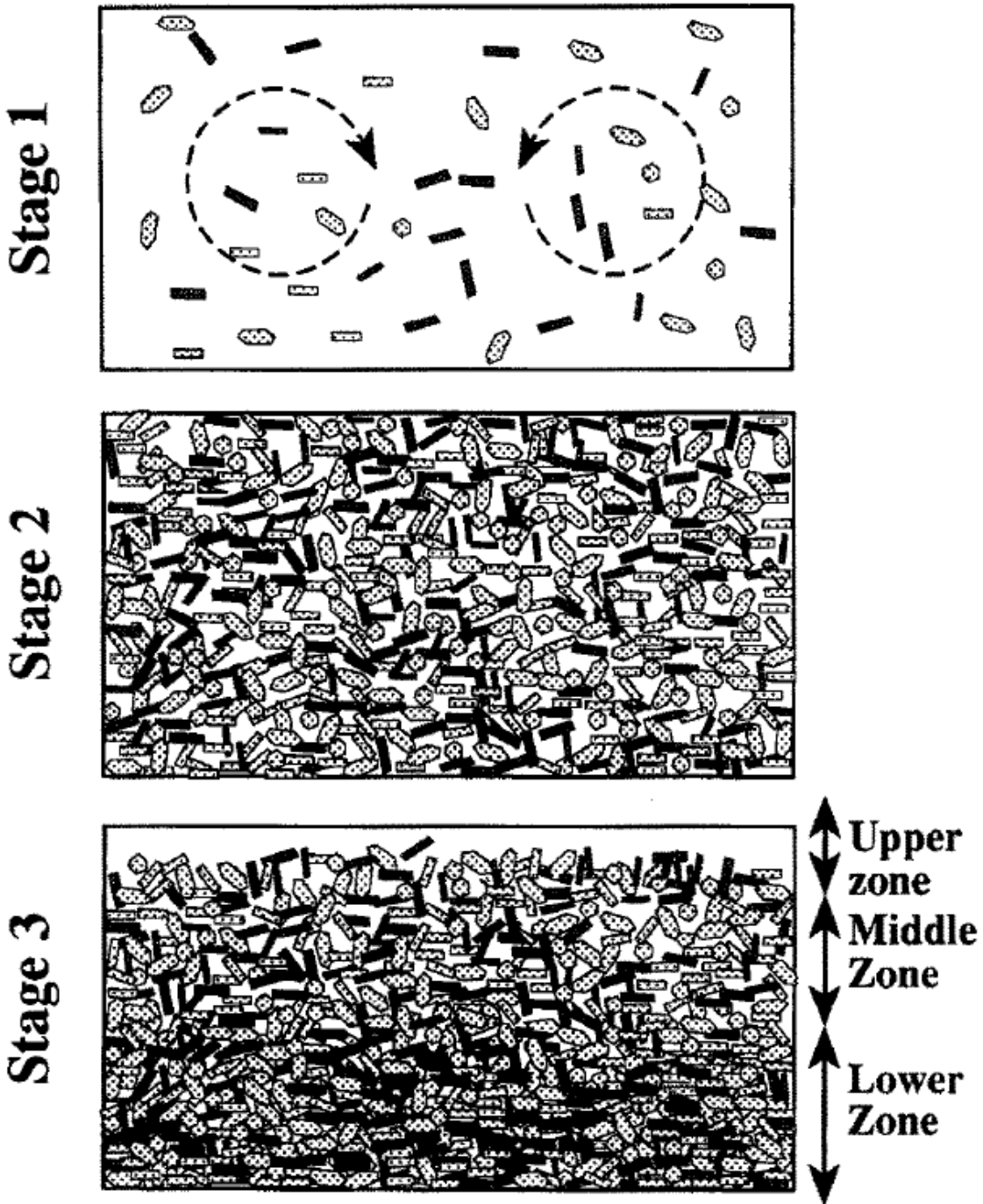


Figure 8.4. Schematic drawing from Bea et al. (1994) showing the development of vertical zonation via crystal accumulation and subsequent collapse of the 3 dimensional framework resulting in the intercrystalline fluid being expelled upwards.

8.8.2. Differentiation during intrusion

Tartèse & Boulvais (2010) explain mineralogical and geochemical variations between the Questembert and Lizio granites by claiming that their different emplacement depths correlate to different amounts of crystal fractionation, which was itself directly driven by differentiation as the magmas moved to their emplacement site. In their model (Figure 8.5), the Questembert granite became more evolved than its “twin,” the Lizio granite, simply because it covered greater distance during emplacement. The authors therefore claim that the further a magma travels through the crust, the more likely it is to leave crystals behind through processes similar to filter pressing (Tartèse and Boulvais, 2010).

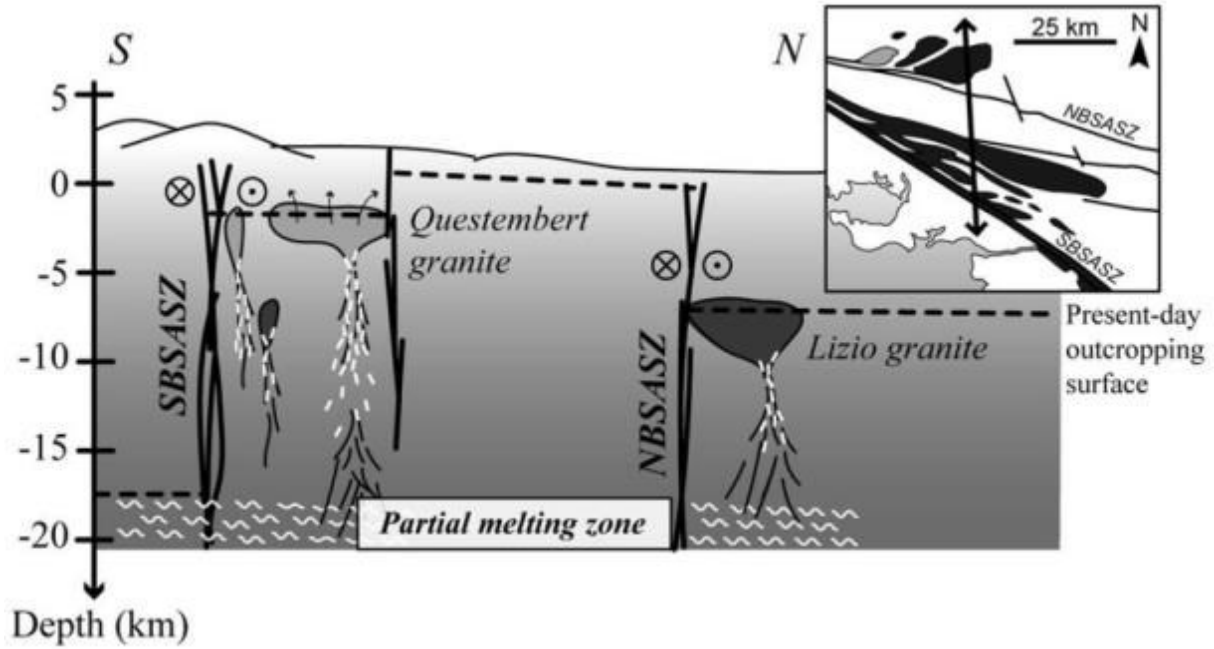


Figure 8.5. Cross section from Tartèse & Boulvais (2010) showing differentiation of the Questembert and Lizio granites as they make their way to the surface. The white dashed lines indicate crystals left behind during ascent.

8.8.3. Differentiation by multiple methods

In a study of the Stepninsk pluton in Russia, Bea et al. (2005) determined that variation within the pluton was the result of flow differentiation as well as the deformation driven separation of fluid from a crystal mush which had reached the rigid percolation threshold. They were able to show that the many igneous rocks of the area were related due to the similar compositions of amphibole and biotite in all of the samples. It was ultimately determined that monzodiorite and quartz-monzodiorites were the efficiently “squeezed” residua, granodiorites and monzogranites were essentially unfractionated magma batches, and leucogranites were the melt which had been segregated from the crystal mush. The results of this study led them to conclude that the dominant process of differentiation in granitic magmas intruded into compressive regimes is deformation-driven filter pressing.

8.8.4. Differentiation by shear zone emplacement

Moyen et al. (2003) interpreted the vertical zonation of the Closepet batholith complex to be the result of intrusion into an active shear zone which facilitated deformation driven differentiation upon emplacement. They found that the fabric intensity correlated to the emplacement depth and subsequent rate of crystallization of each magma “level.” Those magmas which had a longer residence time showed a strong syn-tectonic fabric, while the shallower intrusions, separated from the crystal mush below, showed a variably post-tectonic fabric (Figure 8.6) (Moyen et al., 2003).

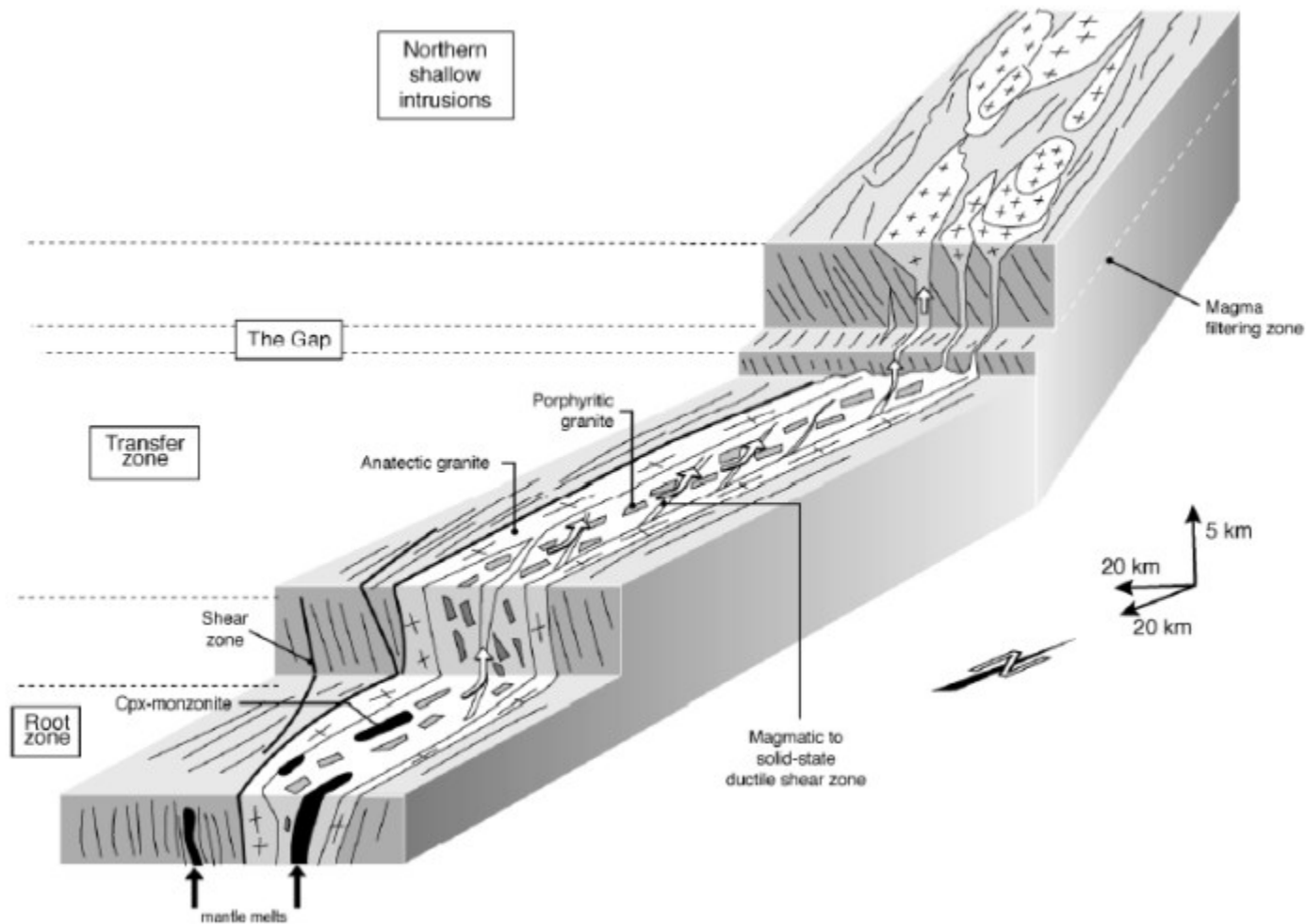


Figure 8.6. Schematic drawing from Moyen et al. (2003) showing a batholith intruded into a shear zone. Deeper intrusions show a strong syn-tectonic fabric while the uppermost intrusions, separated by deformation-driven differentiation within the shear zone, show an essentially post-tectonic fabric.

8.9. Emplacement Interpretations for the WRO and BG Magmas

There is no evidence that the WRO and BG magmas were part of a larger pluton, or emplaced in a well defined shear zone, although emplacement within a pervasive zone of lower crustal shear cannot be ruled out. However the examples discussed above show some similarities to the WRO such that differentiation could have occurred simultaneously with intrusion and likely also involved multiple mechanisms. Geochemical evidence discussed in chapter 7 indicates that very small degrees of partial melting, some degree of fractional crystallization, and the emplacement of multiple generations of magma with slightly variable petrogenetic histories may have all taken place during the development of the WRO pluton. The WRO and BG magmas could also represent the liquid “squeezed” from a crystal mush at depth, but no sample of any supposed “mush” has been identified. Because the viscosity of the magmas was likely very high, differentiation processes must have been aided by deformation in some fashion.

9. DISCUSSION AND CONCLUSIONS

Given the geochemical data, regional geologic setting, and generally accepted models for TTG formation/emplacement, two models for the formation of the WRO pluton will be evaluated.

9.1. Model 1

1. A magma chamber is formed at depth following partial melting of eclogite and/or amphibolite at depth.
2. Early fractional crystallization of amphibole explains the decreasing Fe-Mg trend seen in the BG, SiO₂ increase, further HREE and MREE depletion from that of the original melt, and the absence of amphibole in the majority of the WRO and BG. These moderately evolved melts of the eclogite or amphibolite with the hornblende removed are emplaced, from the main pluton body, as the BG magma. Fractional crystallization of hornblende may also explain the positive Eu anomaly since hornblende has a relatively low Kd value for Eu.
3. Fractional crystallization of titanite in the magma chamber further contributes to the Eu anomaly owing to titanite's low partition coefficient for Eu. Titanite also preferentially removes MREEs to HREEs, contributing to depleted MREE and HREEs in both the WRO and BG samples.
4. Fractional crystallization of epidote in the last of the melt within the pluton body, presumably mostly crystallized, leads to variable LREE depletion seen in the WRO samples.

5. The WRO pluton is emplaced during lower crustal deformation, resulting in a foliation shared with the Chiwaukum schist.

9.2. Model 2

1. No initial magma chamber is formed, but variable degrees of partial melting of the metabasaltic source rock at depth lead to slight chemical variability in melts that rise through the crust and coalesce at higher levels. Periods of high magmatic flux lead to the formation of larger, more chemically homogeneous magma bodies which rise through the crust.
2. Early, less evolved BG magmas are emplaced over a large area within the Chiwaukum schist.
3. Magma is emplaced synchronous with deformation which aids in the early onset of the Melt Escape Threshold at potentially 15-20% partial melt allowing very felsic melts to escape the source region. Early melts, which are potentially formed in a reducing environment, take incompatible elements including Sr, Ba, Th, and Eu^{2+} with them.
4. Fractional crystallization of trace minerals apatite, zircon, and epidote within individual magma bodies occurs simultaneously with transport or via deformation driven differentiation leading to the development of chemically variable magmas bodies. Apatite, zircon, and epidote fractionation cause the additional MREE, HREE, and LREE depletions, respectively, in the WRO magma.
5. The WRO pluton is emplaced along a preferential magma pathway creating a sheeted, heterogeneous pluton composed of different batches of partial melts and

surrounded by older BG intrusions. The final pluton is chemically heterogeneous but relatively mineralogically uniform with a syn-tectonic fabric.

9.3. Discussion of models

9.3.1. Model 1

Hornblende and titanite fractionation are not at all well represented by the petrogenetic modeling. It may be possible that hornblende and/or titanite fractionation occurred so early in the history of the magma that no “parental” amphibole or titanite-rich magma is represented in the sampling.

Epidote is known to preferentially partition LREEs, but at present, no measurement of REE concentrations in epidotes (or monazites) are available from the WRO samples. LA-ICP-MS analyses are needed on the WRO epidotes, which would enable calculation of true partition coefficients and re-modeling of fractionation. Merkel (2007) shows that variably LREE-rich epidotes do exist in the tonalitic pegmatites within the WRO pluton.

9.3.2. Model 2

The Harker diagrams in Figures 7.5 and 7.15 show that the BG samples do have some chemical variability, yet the REE and multi-element data for the BG samples show incredible uniformity even though they are found in different areas throughout the Chiwaukum schist. How can the chemical homogeneity of the BG magma be explained without the formation of a homogenous magma body at some time? This fact is certainly best explained by having a large, homogenous pluton body at depth.

While the fractional crystallization of apatite, zircon, and epidote are reasonably well modeled, it may be overcomplicated (Occam’s razor?) to call upon the fractional crystallization of ALL these trace minerals in order to explain the chemical variability. Additionally, any

chemical trend which can be explained by fractional crystallization could also have been formed via partial melting.

The biggest problem when trying to explain the evolution of the WRO and BG magmas from the initial source melt involves the differentiation from the initial partial melt. Many of the samples are much more evolved than an initial partial melt of eclogite. Figure 9.1 also shows how scatter in the WRO samples can be achieved by either variable degrees of partial melting (A) or variable degrees of fractional crystallization (B).

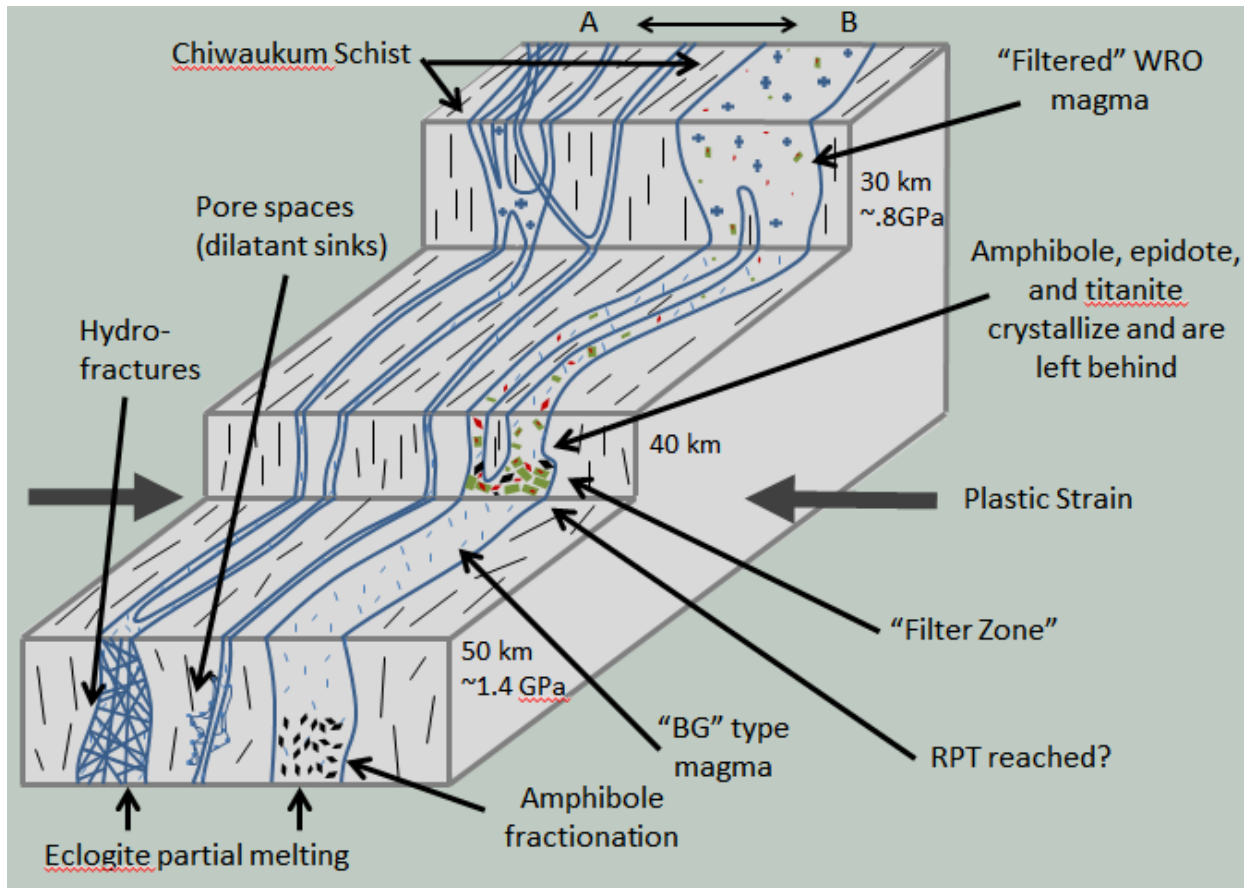


Figure 9.1. This figure essentially shows model 1 (B) and model 2 (A) in which a large magma body does (B) and does not (A) exist at depth. The early onset of melt extraction is reached in scenario A allowing partial melts of variable degrees to leave the source region and coalesce higher in the crust. Scenario B involves a large magma chamber at depth which undergoes FC of hornblende and later removal of trace minerals via deformation driven differentiation. Both scenarios can result in the formation of a high pressure, heterogeneous, syn-tectonic, TTG pluton which originally develops as a partial melt of eclogite or amphibolite at depth.

9.4. Conclusions

We return here to three questions posed in chapter 1.

9.4.1. Has metamorphism altered the original igneous geochemistry?

The mineralogical and textural analysis performed in chapter 4 along with the ITMTC fails to show the correlations that would be expected for rocks that have been variably metamorphosed. These data indicate that any metamorphism incurred has not significantly altered the geochemistry of the WRO samples. Additionally, the lack of scatter in LILEs (chapter 7) indicates that metamorphism did not alter the original igneous geochemistry.

9.4.2. Is the WRO an analogue of Archean TTG?

Discriminant analysis (chapter 6) shows that the WRO and BG do have geochemical similarities to Archean TTGs and are most closely related to Cenozoic and Archean TTG samples. Many of the WRO samples show REE patterns which are not consistent with those of Archean TTGs. Excepting these WRO samples, the null hypothesis that the Wenatchee Ridge samples represent a Mesozoic analog of Archean TTG is accepted.

9.4.3. What is the preferred petrogenetic model for the WRO and BG genesis?

The preferred scenario for the WRO formation involves elements of both scenarios discussed in section 9.3. Major, minor, and trace element data indicate that the WRO and BG magmas were most likely derived from the partial melting of basalt or oceanic sediments within overthickened crust at eclogite or amphibolite facies. A partial melting origin is supported by evidence for extremely over-thickened crust in the area during the time of magma emplacement (Magloughlin, 1993; Stowell et al., 2007). There are no coeval mafic rocks proximal to the WRO and BG magmas as would be expected for a pluton derived via fractional crystallization of a basaltic magma. Additionally, the depleted HREE, high Sr/Y, and high SiO₂ are unlikely to be

created by the fractionation of typical TTG minerals from a basaltic magma (Atherton & Petford, 1993; Drummond & Defant, 1996).

The extremely felsic nature and REE depletion of the WRO was either caused by the fractionation of minerals from the initial melt, or the coalescence of melts that experienced variable degrees of melting from slightly variable source regions or variable residence times. Although minerals can be identified that may contribute to the geochemical characteristics of the WRO, either by fractionation or partial melting, petrogenetic modeling cannot distinguish between the two proposals. Distinction between the proposals may be aided by identification of either crystal fractionate or restite material brought up in xenoliths or by the identification of coeval magmatic rocks which may improve the understanding of the WRO's formation.

REFERENCES CITED

- Allegre, C.J., and Minster, J.F., 1978. Quantitative models of trace element behavior in magmatic processes. *Earth and Planetary Science Letters*, v. 38, p. 1–25.
- Atherton, M.P., and Petford, N., 1993. Generation of sodium-rich magmas from newly underplated basaltic crust. *Nature*, v. 362, p. 144–146.
- Barker, F., 1979. “Trondhjemite; definition, environment and hypotheses of origin.” *Trondhjemites, dacites, and related rocks*. *Nature*, v. 1.
- Bea, F., Fershtater, G.B., Montero, P., Smirnov, V.N., and Molina, J.F., 2005. Deformation-driven differentiation of granitic magma: the Stepninsk pluton of the Uralides, Russia. *Lithos*, v. 81, p. 209–233.
- Bea, F., Pereira, M.D., and Corretgi, L.G., 1994. Differentiation of strongly peraluminous, perphosphorus The Pedrobernardo pluton, central Spain granites: The Pedrobernardo pluton, central Spain. *Geochimica et Cosmochimica Acta*, v. 58, p. 2609–2627.
- Beck, M.E., and Noson, L., 1971. Anomalous Palaeolatitudes in Cretaceous Granitic Rocks. *Nature*, v. 235, p. 11–12.
- Bons, P.D., Arnold, J., Elburg, M. a., Kalda, J., Soesoo, A., and van Milligen, B.P., 2004. Melt extraction and accumulation from partially molten rocks. *Lithos*, v. 78, p. 25–42.
- Borg, L.E., and Clyne, M. a., 1998. The Petrogenesis of Felsic Calc-alkaline Magmas from the Southernmost Cascades, California: Origin by Partial Melting of Basaltic Lower Crust. *Journal of Petrology*, v. 39, p. 1197–1222.
- Bowen, N.L., 1920. Differentiation by Deformation. *Proceeding of the National Academy of Sciences*, v. 6, p. 59–62.
- Brophy, J.G., 2008. A study of rare earth element (REE)–SiO₂ variations in felsic liquids generated by basalt fractionation and amphibolite melting: a potential test for discriminating between the two different processes. *Contributions to Mineralogy and Petrology*, v. 156, p. 337–357.
- Brown, M., 1994. The generation, segregation, ascent and emplacement of granite magma: the migmatite-to-crustally-derived granite connection in thickened orogens. *Earth-Science Reviews*, v. 36, p. 83–130.
- Brown, E., and Talbot, J., 1989. Orogen-parallel extension in the North Cascades crystalline core, Washington. *Tectonics*, v. 8, p. 1105–1114.

- Brown, E.H., Talbot, J.L., McClelland, W.C., Feltman, J. A., Lapen, T.J., Bennett, J.D., Hettinga, M. A., Troost, M.L., Alvarez, K.M., and Calvert, A. T., 2000. Interplay of plutonism and regional deformation in an obliquely convergent arc, southern Coast Belt, British Columbia. *Tectonics*, v. 19, p. 493.
- Buddington, A., and Lindsley, D.H., 1964. Iron-titanium oxide minerals and synthetic equivalents. *Journal of petrology*, v. 5, p. 310–357.
- Castillo, P.R., 2006. An overview of adakite petrogenesis. *Chinese Science Bulletin*, v. 51, p. 257–268.
- Cesare, B., Satish-Kumar, M., Cruciani, G., Pocker, S., and Nodari, L., 2008. Mineral chemistry of Ti-rich biotite from pegmatite and metapelitic granulites of the Kerala Khondalite Belt (southeast India): Petrology and further insight into titanium substitutions. *American Mineralogist*, v. 93, p. 327–338.
- Clark, L.F., Defant, M.J., Stewart, R.H., and Drummond, M.S., 1988. Geology and Petrogenesis of El Valle volcano, Panama. *Eos Trans. AGU*, v. 69, p. 1491.
- Condie, K.C., 2005. TTGs and adakites: are they both slab melts? *Lithos*, v. 80, p. 33–44.
- Condie, K.C., and Hunter, D., 1976. Trace element geochemistry of Archean granitic rocks from the Barberton region, South Africa. *Earth and Planetary Science Letters*, v. 29, p. 389–400.
- Coney, P., Jones, D., and Monger, J., 1980. Cordilleran suspect terranes. *Nature*, v. 288, p. 329–333.
- Cornelius, V.H.P., 1915. Geologische Beobachtungen im Gebiete des Fornogletschers (Engadin). *Centralblatt für Mineralogie Geologie und Palaontologie*, v. 8, p. 246–252.
- Deer, W.A., Howie, R.A., and Zussman, J., 2001. *Rock-Forming Minerals*. Oxford, UK, Geological Society.
- Defant, M.J., and Drummond, M.S., 1993. Mount St. Helens: potential example of the partial melting of the subducted lithosphere in a volcanic arc. *Geology*, v. 21, p. 547.
- Depaolo, D.J., 1981. Trace element and isotopic effect of combined wallrock assimilation and fractional crystallization. *Earth and Planetary Science Letters*, v. 53, p. 189–202.
- Dingwell, D., Hess, K., and Romano, C., 1998. Viscosity data for hydrous peraluminous granitic melts: comparison with a metaluminous model. *American Mineralogist*, v. 83, p. 236–239.
- Drummond, M.S., and Defant, M.J., 1990. A model for trondhjemite-tonalite-dacite genesis and crustal growth via slab melting: Archean to modern comparisons. *Journal of geophysical research*, v. 95, p. 21503–21.

- Drummond, M., and Defant, M., 1996. Petrogenesis of slab-derived trondhjemite-tonalite-dacite/adakite magmas. *Transactions of the Royal Society of Edinburgh: Earth Sciences*, v. 87, p. 205–215.
- Evans, B.W., and Berti, J.W., 1986. Revised metamorphic history for the Chiwaukum Schist, North Cascades, Washington. *Geology*, v. 14, p. 695–698.
- Evans, B.W., and Davidson, G.F., 1999. Kinetic control of metamorphic imprint during synplutonic loading of batholiths: An example from Mount Stuart, Washington. *Geology*, v. 27, p. 415.
- Evans, B.W., and Vance, J.A., 1987. Epidote phenocrysts in dacitic dikes, Boulder County, Colorado. *Contributions to Mineralogy and Petrology*, v. 96, p. 178–185.
- Fiebig, J., and Hoefs, J., 2002. Hydrothermal alteration of biotite and plagioclase as inferred from intragranular oxygen isotope- and cation-distribution patterns. *European journal of mineralogy*, p. 49–60.
- Frost, C.D., Frost, B.R., Kirkwood, R., and Chamberlain, K.R., 2006. The tonalite – trondhjemite – granodiorite (TTG) to granodiorite – granite (GG) transition in the late Archean plutonic rocks of the central Wyoming Province. *Earth*, v. 1444, p. 1419–1444.
- Getsinger, A., Rushmer, T., Jackson, M.D., and Baker, D., 2009. Generating High Mg-numbers and Chemical Diversity in Tonalite-Trondhjemite-Granodiorite (TTG) Magmas during Melting and Melt Segregation in the Continental Crust. *Journal of Petrology*, v. 50, p. 1935–1954.
- Giordano, D., Russell, J.K., and Dingwell, D.B., 2008. Viscosity of magmatic liquids: A model. *Earth and Planetary Science Letters*, v. 271, p. 123–134.
- Girardi, J.D., Patchett, P.J., Ducea, M.N., Gehrels, G.E., Cecil, M.R., Rusmore, M.E., Woodsworth, G.J., Pearson, D.M., Manthei, C., and Wetmore, P., 2012. Elemental and Isotopic Evidence for Granitoid Genesis From Deep-Seated Sources in the Coast Mountains Batholith, British Columbia. *Journal of Petrology*, v. 53, p. 1505–1536.
- Glikson, A., 1976. Trace element geochemistry and origin of early Precambrian acid igneous series, Barberton Mountain Land, Transvaal. *Geochimica et Cosmochimica Acta*, v. 40, p. 1261–1280.
- Guidotti, C., 1984. Micas in metamorphic rocks. *Reviews in Mineralogy and Geochemistry*,
- Gutscher, M.A., Maury, R., Eissen, J.P., and Bourdon, E., 2000. Can slab melting be caused by flat subduction? *Geology*, v. 28, p. 535.
- Hibbard, M.J., 1987. Deformation of Incompletely Crystallized Magma Systems : Granitic Gneisses and their Tectonic Implications. *The Journal of Geology*, v. 95, p. 543–561.

- Irvine, T.N., and Baragar, W.R. a., 1971. A Guide to the Chemical Classification of the Common Volcanic Rocks. *Canadian Journal of Earth Sciences*, v. 8, p. 523–548.
- Jackson, M.D., Gallagher, K., Petford, N., and Cheadle, M.J., 2005. Towards a coupled physical and chemical model for tonalite–trondhjemite–granodiorite magma formation. *Lithos*, v. 79, p. 43–60.
- Kamber, B.S., Ewart, A., Collerson, K.D., Bruce, M.C., and McDonald, G.D., 2002. Fluid-mobile trace element constraints on the role of slab melting and implications for Archaean crustal growth models. *Contributions to Mineralogy and Petrology*, v. 144, p. 38–56.
- Kay, R., 1978. Aleutian magnesian andesites: melts from subducted Pacific Ocean crust. *Journal of Volcanology and Geothermal Research*, v. 4, p. 117–132.
- Kincaid, C., and Sacks, S.I., 1997. Thermal and dynamical evolution of the upper mantle in subduction zones. *Journal of Geophysical Research*, v. 102, p. 12295–12315.
- Luchitskaya, M.V., Morozov, O.L., and Palandzhyan, S.A., 2005. Plagiogranite magmatism in the Mesozoic island-arc structure of the Pekulney Ridge, Chukotka Peninsula, NE Russia. *Lithos*, v. 79, p. 251–269.
- Magloughlin, J.F., 1986a. Metamorphic petrology, structural history, geochronology, tectonics and geothermometry/geobarometry in the Wenatchee Ridge area, North Cascades, Washington: University of Washington.
- Magloughlin, J.F., 1986b. Metamorphic petrology, structural history, geochronology, tectonics and geothermometry/geobarometry in the Wenatchee Ridge area, North Cascades, Washington.: University of Washington, Seattle.
- Magloughlin, J.F., 1988. The White River shear zone; a major north Cascades terrane boundary and compressional structure. *Abstracts with Programs - Geological Society of America* 20,, p. 395–396.
- Magloughlin, J.F., 1993a. A Nason Terrane trilogy; I, Nature and significance of pseudotachylite; II, Summary of the structural and tectonic history; III, Major and trace element geochemistry and strontium and neodymium isotope geochemistry of the Chiwaukum Schist, amphibolite, an: University of Minnesota.
- Magloughlin, J.F., 1993b. Nature and significance of pseudotachylite; II. Summary of the structural & tectonic history; III. Major and trace element geochemistry, and strontium and neodymium isotope geochemistry of the Chiwaukum Schist, amphibolite, and meta-tonalite gneiss of the: University of Minnesota.
- Magloughlin, J.F., 1994. Migmatite to fault gouge: Fault rocks and the structural and tectonic evolution of the Nason terrane, North Cascade Mountains, Washinton. *Geologic field trips in the Pacific Northwest: 1994 GSA Annual Meeting*, p. 2B1–2B17.

- Magloughlin, J.F., 1995. Rb-Sr Dating of Metasedimentary, Metavolcanic, and Metaplutonic Igneous Rocks from the Nason and Mad River Terranes, North Cascade Mountains, Washington. *ISOCHRON/WEST*, v. 62, p. 6–15.
- Magloughlin, J.F., and Edwards, L., 2003. SmNdMin: a program for modeling the Nd isotopic evolution of metamorphic porphyroblasts and their host rocks. *Computers & Geosciences*, v. 29, p. 447–455.
- Maniar, P.D., and Piccoli, P.M., 1989. Tectonic discrimination of granitoids. *Geological Society of America Bulletin*, v. 101, p. 635–643.
- Martin, H., 1986. Effect of steeper Archean geothermal gradient on geochemistry of subduction-zone magmas. *Geology*, v. 14, p. 753–756.
- Martin, H., 1987. Petrogenesis of Archean trondhjemites, tonalites, and granodiorites from eastern Finland: major and trace element geochemistry. *Journal of Petrology*, v. 28, p. 923–953.
- Martin, H., 1993. The mechanisms of petrogenesis of the Archean continental crust—Comparison with modern processes. *Lithos*, v. 30, p. 373–388.
- Martin, H., and Moyen, J.-F., 2002. Secular changes in tonalite-trondhjemite-granodiorite composition as markers of the progressive cooling of Earth. *Geology*, v. 30, p. 319.
- Martin, H., Smithies, R.H., Rapp, R., Moyen, J.-F., and Champion, D., 2005. An overview of adakite, tonalite–trondhjemite–granodiorite (TTG), and sanukitoid: relationships and some implications for crustal evolution. *Lithos*, v. 79, p. 1–24.
- Matzel, J.E.P., Bowring, S. a., and Miller, R.B., 2006. Time scales of pluton construction at differing crustal levels: Examples from the Mount Stuart and Tenpeak intrusions, North Cascades, Washington. *Geological Society of America Bulletin*, v. 118, p. 1412–1430.
- McDonough, W.F., Sun, I.S., Ringwood, A.E., Jagoutz, E., and Hofmann, A.W., 1992. Potassium, rubidium, and cesium in the Earth and Moon and the evolution of the mantle of the Earth. *Geochimica et Cosmochimica Acta*, p. 1001–1012.
- Merkel, I.S., 2007a. Pegmatitic trondhjemites from the north Cascade Mountains, Washington : multiple populations of magmatic epidote and their effect on trace element evolution: Colorado State University.
- Merkel, I.S., 2007b. Pegmatitic trondhjemites from the north Cascade Mountains, Washington : multiple populations of magmatic epidote and their effect on trace element evolution: Colorado State University.
- Miller, R.B., 1985. The ophiolitic Ingalls Complex, north-central Cascade Mountains, Washington. *Geological Society of America Bulletin*, v. 96, p. 27–42.

- Miller, R., and Paterson, S., 2001. Influence of lithological heterogeneity, mechanical anisotropy, and magmatism on the rheology of an arc, North Cascades, Washington. *Tectonophysics*, v. 342, p. 351–370.
- Miller, R.B., and Paterson, S.R., 1992. Tectonic implications of syn- and post-emplacement deformation of the Mount Stuart batholith for mid-Cretaceous orogenesis in the North Cascades. *Canadian Journal of Earth Science*, v. 29, p. 479–485.
- Miller, R., Paterson, S., Lebit, H., Alsleben, H., and Luneburg, C., 2006. Significance of composite lineations in the mid- to deep crust: a case study from the North Cascades, Washington. *Journal of Structural Geology*, v. 28, p. 302–322.
- Moench, R.H., 1986. Implications of magmatic epidote-bearing plutons on crustal evolution in the accreted terranes of Northwestern North-America and magmatic epidote and its petrologic significance - comment. *Geology*, v. 14, p. 187–188.
- Monger, J., Price, R., and Tempelman-Kluit, D., 1982. Tectonic accretion and the origin of the two major metamorphic and plutonic belts in the Canadian Cordillera. *Geology*, v. 10, p. 70–75.
- Moyen, J.-F., Nedelec, A., Martin, H., and Mudlappa, J., 2003. Syntectonic granite emplacement at different structural levels : the Closepet granite, South India. *Journal of Structural Geology*, v. 25, p. 611–631.
- Muir, R.J., Weaver, S.D., Bradshaw, J.D., Eby, G.N., and Evans, J. a., 1995. The Cretaceous Separation Point batholith, New Zealand: granitoid magmas formed by melting of mafic lithosphere. *Journal of the Geological Society*, v. 152, p. 689–701.
- Naney, M.T., 1983. Phase equilibria of rock forming ferromagnesian silicates in granitic systems. *American Journal of Science*, v. 283, p. 993–1033.
- Nehring, F., Foley, S.F., Holtta, P., and Van Den Kerkhof, a. M., 2009. Internal Differentiation of the Archean Continental Crust: Fluid-Controlled Partial Melting of Granulites and TTG-Amphibolite Associations in Central Finland. *Journal of Petrology*, v. 50, p. 3–35.
- Nesse, W.D., 2000. *Introduction to Mineralogy*. New York, Oxford University Press.
- Nishimura, K., 2009. A trace-element geochemical model for imperfect fractional crystallization associated with the development of crystal zoning. *Geochimica et Cosmochimica Acta*, v. 73, p. 2142–2149.
- Passchier, C.W., and Trouw, R.A.J., 2005. *Microtectonics*. Springer.
- Paterson, S.R., Miller, R.B., Anderson, J.L., Lund, S., Bendixen, J., Taylor, N., and Fink, T., 1994. Emplacement and evolution of the Mount Stuart Batholith, in *Geologic Field Trips in*

- the Pacific Northwest. Annual Meeting of the Geological Society of America, Department of Geological Sciences, Seattle, University of Washington, v. 2, p. 2F1–2F27.
- Paterson, S.R., Miller, R.B., Jose, S., and Stuart, M., 1998. Magma emplacement during arc-perpendicular shortening : An example from the Cascades uction • Asthenosphere Comer Flow. *Magma*, v. 17, p. 571–586.
- Paterson, S.R., and Vernon, R.H., 1995. Bursting the bubble of ballooning plutons : A return to nested diapirs emplaced by multiple processes. *GSA Bulletin*, v. 107, p. 1356–1380.
- Peacock, S.M., Rushmer, T., and Thompson, A.B., 1994. Partial melting of subducting oceanic crust. *Earth and Planetary Science Letters*, v. 121, p. 227–244.
- Pearce, J.A., 1983. Role of the sub-continental lithosphere in magma genesis at active continental margins., *in* In: Hawkesworth C.J. and Norry M.J., *Continental basalts and mantle xenoliths*, p. 230–249.
- Pearce, J.A., Harris, B.W., and Tindle, A.G., 1984. Trace element discrimination diagrams for the tectonic interpretation of granitic rocks. *Journal of Petrology*, v. 25, p. 956–983.
- Petford, N., Kerr, R.C., and Lister, J.R., 1993. Dike transport of granitoid magmas. *Geology*, v. 21, p. 845–848.
- Philpotts, A.R., and Ague, J.J., 2009. *Princliples of Igneous and Metamorphic Petrology*. Cambridge, Cambridge University Press.
- Plummer, C.C., 1980. Dynamothermal contact metamorphism superposed on regional-metamorphism in the pelitic rocks of the Chiwaukum Mountains area , Washington Cascades.
- Propach, G., 1976. Models of filter differentiation. *Lithos*, v. 9, p. 203–209.
- Rapp, R., Shimizu, N., and Norman, M., 2003. Growth of early continental crust by partial melting of eclogite. *Nature*, v. 425.
- Rapp, R.P., Watson, E.B., and Miller, C.F., 1991. Partial melting of amphibolite/eclogite and the origin of Archean trondhjemites and tonalites. *Precambrian Research*, v. 51, p. 1–25.
- Rollinson, H.R., 1993. *Using Geochemical Data: Evaluation, Presentation, Interpretation*. Longman Scientific & Technical and John Wiley & Sons, Inc.
- Rollinson, H., and Martin, H., 2005. Geodynamic controls on adakite, TTG and sanukitoid genesis: implications for models of crust formation. *Lithos*, v. 79, p. ix–xii.
- Rudnick, R., 1995. Making continental crust. *Nature*, v. 387, p. 571–578.

- Schmidt, M.W., and Poli, S., 2004. Magmatic Epidote. *Reviews in Mineralogy and Geochemistry*, v. 56, p. 399–430.
- Schmidt, M.A.X.W., and Thompson, A.B., 1996. Epidote in calc-alkaline magmas : An experimental study of stability , phase relationships , and the role of epidote in magmatic evolution. *American Mineralogist*, v. 81, p. 462–474.
- Shervais, J.W., 2008. California : Low-pressure slab melting and reaction with the mantle wedge. *The Geological Society of America*, v. 2438, p. 113–132.
- Smithies, R., 2000. The Archaean tonalite–trondhjemite–granodiorite (TTG) series is not an analogue of Cenozoic adakite. *Earth and Planetary Science Letters*, v. 182, p. 115–125.
- Smithies, R. H. & Champion, D.C., 2000. The Archaean High-Mg Diorite Suite: Links to Tonalite-Trondhjemite-Granodiorite Magmatism and Implications for Early Archaean Crustal Growth. *Journal of Petrology*, v. 41, p. 1653–1671.
- Spiegelman, M., and Kelemen, P.B., 2003. Extreme chemical variability as a consequence of channelized melt transport. *Geochemistry, Geophysics, Geosystems*, v. 4, p. n/a–n/a.
- Stowell, H., Bulman, G., Tinkham, D., and Zuluaga, C., 2011. Garnet growth during crustal thickening in the Cascades Crystalline Core, Washington, USA. *Journal of Metamorphic Geology*, v. 29, p. 627–647.
- Stowell, H.H., Bulman, G.R., Zuluaga, C.A., Tinkham, D.K., Miller, R.B., and Stein, E., 2007. Mid-crustal Late Cretaceous metamorphism in the Implications for tectonic models. v. 1200, p. 211–232.
- Stowell, H., and Tinkham, D., 2003. Integration of phase equilibria modelling and garnet Sm-Nd chronology for construction of P-T-t paths: examples from the Cordilleran Coast Plutonic Complex, USA. *Geological Society, London, Special Publications*, v. 220, p. 119–145.
- Streckeisen, A., 1976. To each plutonic rock its proper name. *Earth-Science Reviews*, v. 12, p. 1–33.
- Sun, S. -s., and McDonough, W.F., 1989. Chemical and isotopic systematics of oceanic basalts: implications for mantle composition and processes. *Geological Society, London, Special Publications*, v. 42, p. 313–345.
- Tabor, R.W., 1987. Possible Tectonostratigraphic Terranes in the North Cascades Crystalline Core, Washington. *Washington Division of Geology and Earth Resources Bulletin*, v. 77, p. 107–127.
- Tabor, R.W., Frizzell, V.A., Booth, D.B., Waitt, R.B., Whetten, J.T., and Zartman, R.E., 1993. *Geologic Map of the Skykomish River 30- by 60-Minute Quadrangle, Wahsington. U.S. Geological Survey*, v. Geologic I.

- Tabor, B.R.W., Frizzell, V.A., Whetten, J.T., Waitt, R.B., and Swanson, D.A., 1987. TO ACCOMPANY MAP I-1661 GEOLOGIC MAP OF THE CHELAN 30-MINUTE BY 60-MINUTE. Department of the Interior U.S. Geological Survey,.
- Tartèse, R., and Boulvais, P., 2010. Differentiation of peraluminous leucogranites “en route” to the surface. *Lithos*, v. 114, p. 353–368.
- Tate, M.C., and Johnson, S.E., 2000. Subvolcanic and Deep-Crustal Tonalite Genesis beneath the Mexican Peninsular Ranges. *The Journal of Geology*, v. 108, p. 721–728.
- Terekhov, E.N., and Shcherbakova, T.F., 2006. Genesis of positive Eu anomalies in acid rocks from the Eastern Baltic Shield. *Geochemistry International*, v. 44, p. 439–455.
- Troger, W.E., 1979. *Optical Determination of Rock-Forming Minerals*. Lubrecht & Cramer Ltd.
- Tulloch, A.J., 1986. Implications of magmatic epidote-bearing plutons on crustal evolution in the accreted terranes of Northwestern North-America and magmatic epidote and its petrologic significance - comment. *Geology*, v. 14, p. 186–187.
- Van Diver, B.B., 1964. *Petrology of the metamorphic rocks, Wenatchee Ridge area, central northern Cascades, Washington*: University of Washington.
- VanDiver, B.B., 1967. Contemporaneous faulting-metamorphism in Wenatchee Ridge area, Northern Cascades, Washington. *American Journal of Science*, v. 265, p. 132–150.
- Vigneresse, J.L., 1995. Control of granite emplacement by regional deformation. *Tectonophysics*, v. 249, p. 173–186.
- Vigneresse, J.L., Barbey, P., and Cuney, M., 1996. Rheological Transitions During Partial Melting and Crystallization with Application to Felsic Magma Segregation and Transfer. *Journal of Petrology*, v. 37, p. 1579–1600.
- Walker, N.W., and Brown, E.H., 1991. Is the southeast Plutonic Complex the consequence of accretion of the Insular superterrane? Evidence from U-Pb zircon geochronometry in the northern Washington Cascades. *Geology*, v. 19, p. 714–717.
- Weinberg, R.F., 1999. Mesoscale pervasive felsic magma migration: alternatives to dyking. *Lithos*, v. 46, p. 393–410.
- Whitney, D., and McGroder, M.F., 1989. Cretaceous crustal section through the proposed Insular-Intermontane suture, North Cascades, Washington. *Geology*, v. 17, p. 555–558.
- Winter, J.D., 2010. *Principles of Igneous and Metamorphic Petrology*. Prentice Hall.
- Wintzer, N.E., 2012. Deformational episodes recorded in the Skagit Gneiss Complex, North Cascades, Washington, USA. *Journal of Structural Geology*, v. 42, p. 127–139.

Wit, M.J. De, 1998. On Archean granites, greenstones, cratons and tectonics: does the evidence demand a verdict? *Precambrian Research*, v. 91, p. 181–226.

Xu, J.-F., Shinjo, R., Defant, M.J., Wang, Q., and Rapp, R.P., 2002. Origin of Mesozoic adakitic intrusive rocks in the Ningzhen area of east China: Partial melting of delaminated lower continental crust? *Geology*, v. 30, p. 1111.

Zen, E., and Hammarstrom, J.M., 1986. Implications of magmatic epidote-bearing plutons on crustal evolution of accreted terranes of Northwestern North-America and magmatic epidote and its petrologic significance - reply. *Geology*, v. 14, p. 188–189.

Zen, E., and Hammarstrom, J.M., 1984. Magmatic epidote and its petrologic significance. *Geology*, v. 12, p. 515.

Zuluaga C. A., and Stowell, H.H., 2008. Multidisciplinary approach to study migmatites : Origin and tectonic history of the Nason Ridge migmatitic gneiss, Wenatchee Block, Cascades. *Earth*, v. 12, p. 235–264.

APPENDICES

APPENDIX A. Sample Descriptions, GPS Coordinates, and Sample Photographs

ID: Z-100



GPS: 10T 0658097mE 5300539mN

Description: White mica biotite tonalite with a weak foliation

Area: Large outcrop on north side of the road. All tonalites here are well foliated/jointed.

ID: Z-101

GPS: 10T 0650597mE 5303290mN

Description: Good outcrop but mostly all Chiwaukum schist. No tonalite sample taken here.

Area: Mostly schist with minor banded gneiss and pegmatite.

ID: Z-102



GPS: 10T 0652234mE 5302608mN

Description: Coarse grained marble

Area: Old marble quarry on the south side of the road just outside of Soda Spring Campground.

ID: Z-103



GPS: 10T 0652976mE 5302390mN

Description: Another coarse grained marble with pyrite and hematite staining.

Area: North side of the road just east of Z-102. Pegmatites and felsic tonalites cross-cut this marble.

ID: Z-104



GPS: 10T 0657251mE 5300635mN

Description: Muscovite biotite tonalite. Weakly foliated with muscovite grains up to ~1cm.

Area: Predominantly muscovite tonalite with pegmatite and quartz veins in the area.

ID: Z-105



GPS: 10T 0658636mE 5300583mN

Description: Muscovite biotite tonalite. Mostly white mica, weakly foliated, with minor biotite.

Area: Just east of Z-100

ID: Z-106



GPS: 10T 0659329mE 5300473mN

Description: Muscovite biotite tonalite. More strongly foliated but biotite still minor.
Muscovite grains up to $\frac{1}{4}$ cm.

Area: East of Z-105. No nearby pegmatites, mostly tonalite.

ID: Z-107



GPS: 10T 0658354mE 5300837mN

Description: Muscovite biotite tonalite, moderately foliated, biotite is minor.

Area: Mostly muscovite tonalite in this area with some more biotite rich than others. Very minor tonalite pegmatites. Much of the tonalite is folded and/or slightly banded in this area.

ID: Z-108



GPS: 10T 0659911mE 5301739mN

Description: Muscovite tonalite gneiss, well foliated, maybe very minor biotite.

Area: Predominantly tonalite with large quartz vein 1-2m away.

ID: Z-109



GPS: 10T 0660196mE 5301903mN

Description: Muscovite biotite tonalite gneiss. Well foliated with equal amounts of muscovite and biotite.

Area: More heavily banded gneiss compared to past outcrops. This is above the Two Rivers quarry on a back-road.

ID: Z-110



GPS: 10T 0660128mE 5301661mN

Description: Muscovite tonalite gneiss. Heavily banded/foliated with coarse and fine grained phases. There is some minor talc-tremolite in the area.

Area: A boulder field above the Two Rivers quarry. This may have been an old quarry?

ID: Z-111



GPS: 10T 0653736mE 5304759mN

Description: Moderately well foliated muscovite tonalite.

Area: On top of Wenatchee Ridge on the west side. Samples were hard to get out of the outcrop here.

ID: Z-112



GPS: 10T 0653852mE 5304786mN

Description: Weakly foliated muscovite biotite tonalite. Minor phyllosilicates compared to past tonalites.

Area: On top of Wenatchee Ridge just east of Z-111.

ID: Z-113



GPS: 10T 0653923mE 5304731mN

Description: Biotite tonalite with minor muscovite. Moderately foliated with a small amount of coarse material cutting through on one side.

Area: Continuing along Wenatchee Ridgeline East of Z-112.

ID: Z-114



GPS: 10T 0654072mE 5304725mN

Description: Muscovite biotite tonalite gneiss. More heavily banded sample with bands of coarse and fine grained tonalite.

Area: On top of Wenatchee Ridge just east of Z-113 about half way up the “bowl.”

ID: Z-115-1



GPS: 10T 0654168mE 5304645mN

Description: Well foliated muscovite tonalite

Area: East of Z-114 about 1/3 of the way up the boulder field “bowl.” Lots of banded gneiss here with scattered talc-tremolite samples fallen from the cliffs above.

ID: Z-115-2



GPS: 10T 0654168mE 5304645mN

Description: Banded tonalite gneiss taken as example of a common 2-phase tonalite sample seen on Wenatchee Ridge.

Area: Same as Z-115-1

ID: Z-116



GPS: 10T 0654168mE 5304592mN

Description: Peridotite? Sample from a large ultramafic boulder out of situ with concentric weathering rings. The other side of the boulder is mostly talc-tremolite and the entire boulder is well rounded with round alteration rings suggesting this was a large ultramafic inclusion in the magma chamber? (Note: there are many of these large, round, ultramafic bodies in the boulder field)

Area: Near the base of the Wenatchee Ridge boulder field.

ID: Z-117



GPS: 10T 0654226mE 5304431mN

Description: Leucotonalite with minor phyllosilicates (biotite and muscovite). Weakly fractured.

Area: At the base of the Wenatchee Ridge boulder field.

ID: Z-118



GPS: 10T 0654015mE 5304242mN

Description: Weakly foliated biotite leucotonalite with minor muscovite.

Area: Lower base of the Wenatchee Ridge boulder field.

ID: Z-119



GPS: 10T 0653382mE 5303476mN

Description: Leucotonalite lacking phyllosilicates with minor tremolite on one corner.

Area: On pathway down from Wenatchee Ridge.

ID: Z-120



GPS: 10T 0653351mE 5303503mN

Description: Well foliated biotite tonalite. Sample looks very clean.

Area: On the road just west of Z-119.

ID: Z-121



GPS: 10T 0664816mE 5300594mN

Description: Biotite hornblende granodiorite with minor foliation. More mafic than past samples.

Area: Lots of quartz veins and granodiorite composition pegmatites in the area. Off the road on the North side of Lake Wenatchee. This is near the Dirty Face pluton.

ID: Z-122



GPS: 10T 0661457mE 5302607mN

Description: Muscovite tonalite with strong foliation. Mixture of fine and coarse grained material.

Area: From “No Trespassing” outcrop on north side of the road north of Wenatchee Ridge. Looks like all tonalite (Wenatchee Ridge Gneiss) in this outcrop.

ID: Z-123



GPS: 10T 0659272mE 5304530mN

Description: Muscovite tonalite with ~1cm muscovite grains.

Area: Nearby strung out UM bodies (talc tremolite?). Banded gneiss heavy in the area, this could be on the pluton boundary.

ID: Z-124



GPS: 10T 0657904mE 5306789mN

Description: Banded tonalite gneiss taken as an example of material found on this side of the pluton boundary.

Area: Outside of the pluton boundary. This looks like NRMG or some banded gneiss within the Chiwaukum Schist.

ID: Z-125



3

GPS: 10T 0658061mE 5304984mN

Description: Muscovite tonalite with minor biotite. Heavily foliated with large (1-1.5cm) muscovite lenses.

Area: Up the “dead car” road north of Wenatchee Ridge.

ID: Z-126



GPS: 10T 0659572mE 5305179mN

Description: Coarse grained muscovite tonalite with chlorite?

Area: From heavily banded gneiss area with talc-tremolite nearby. Outside the pluton boundary.

ID: Z-127



GPS: 10T 0659258mE 5302306mN

Description: Muscovite biotite leuco-tonalite (with minor chlorite?) (low amount of phyllosilicates)

Area: Wenatchee Ridge overlook near large quartz veins in a foliated tonalite outcrop.

ID: Z-128



Description: Epidote pegmatite with epidote phenocrysts up to 8cm long and ½ cm wide forming a comb texture from wall of the dike.

ID: Z-129



GPS: 10T 0658208mE 5302552mN

Description: Biotite tonalite with moderate foliation and an oxidation band on one side.

Area: ~10 meters from a large ultramafic body (UM may or may not be *in situ*)

ID: Z-130



GPS: 10T 0656698mE 5304042mN

Description: Biotite tonalite with minor chlorite.

Area: At the far end of the road in above outcrop.

ID: Z-131

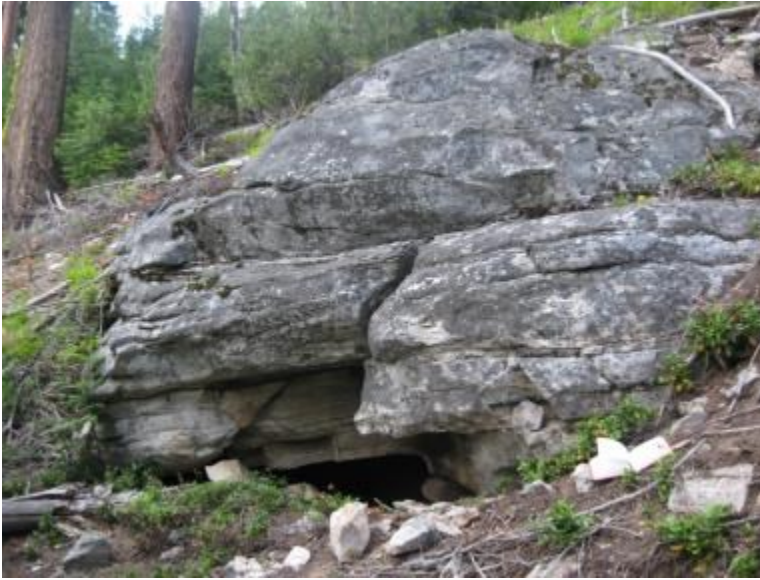


GPS: 10T 0657522mE 5303330mN

Description: Biotite tonalite gneiss with quartz lenses. Strongly banded and not weathered.

Area: Tonalite boulder on road north of Wenatchee Ridge.

ID: Z-132



GPS: 10T 0657636mE 5302186mN

Description: Biotite tonalite gneiss. Well foliated and in situ.

Area: Center of the WRO pluton down the road to the east from Z-131. Outcrop is quite weathered.

ID: Z-133-1



GPS: 10T 0657549mE 5301709mN

Description: Ultramafic inclusion with quartz veins and an amphibolite vein?

Area: Lots of ultramafic inclusions in this area just south of Z-132. Most of the outcrop is coarse tonalite with UM inclusions.

ID: Z-133-2



GPS: 10T 0657549mE 5301709mN

Description: Coarse muscovite, biotite tonalite with fine bands.

Area: Same area as Z-133-1

ID: Z-134



GPS: 10T 0664027mE 5294841mN

Description: Biotite tonalite with not much biotite. Well foliated and not too weathered.

Area: Nason ridge road boulder field by the highest antenna building. Probably from vein intruded into Chiwaukum schist.

ID: Z-135



GPS: 10T 0664018mE 5294759mN

Description: Biotite, muscovite tonalite to granodiorite. More mafic than past samples and moderately foliated.

Area: Nason Ridge road between the two top antenna towers. Lots of Chiwaukum schist in this area. The schist is garnet-rich with tonalite dikes and sills that are locally foliated and/or boudinaged (also discordant quartz veins).

ID: Z-136



GPS: 10T 0664150mE 5294859mN

Description: Muscovite, biotite tonalite. Well foliated and possibly weathered.

Area: On Nason Ridge just down the road from the antenna towers. Either outcrop or a very large boulder of WRG.

ID: Z-137-1



GPS: 10T 0664132mE 5295065mN

Description: Biotite tonalite, well foliated and not too weathered. More mafic than most samples from WRO.

Area: Well deformed outcrop within a boulder field west of the Nason Ridge road and north of Z-136. The entire outcrop is in a drainage with lots of exposed Chiwaukum schist and quartz veins.

ID: Z-137-2



GPS: 10T 0664132mE 5295065mN

Description: 2 samples taken. Both are a biotite tonalite which is well foliated.

Area: From the same outcrop as Z-137-2 about 10 meters higher up the slope with quartz veins nearby.

ID: Z-138



GPS: 10T 0654565mE 5302364mN

Description: Biotite tonalite which is moderately foliated, and not badly weathered.

Area: On the south side of WR near Jerry's WR-326 location. Many samples in this area are heavily weathered.

ID: Z-139-1



GPS: 10T 0654615mE 5302399mN

Description: Biotite, muscovite tonalite gneiss. Well foliated, clean sample.

Area: Heavily banded tonalite in the area which follows the regional foliation.

ID: Z-139-2



GPS: 10T 0654615mE 5302399mN

Description: Banded gneiss and ultramafic bodies. Sampled the ultramafic material; likely an amphibolite (or melanosome?).

Area: The ultramafics are common in this outcrop.

ID: Z-140



GPS: 10T 0654572mE 5300747mN

Description: Well banded tonalite to granodiorite with amphibole and garnet. 2 samples were taken but they may not be clean enough for geochemistry.

Area: Near the west side of the pluton boundary just south of the Little Wenatchee River. There is a large outcrop of banded gneiss with ~1cm garnets.

ID: Z-141-1



GPS: 10T 0661336mE 5300754mN

Description: Biotite tonalite. Well foliated/banded and not weathered.

Area: From quarry out of situ from above cliff. Lots of talc-tremolite in the area.

ID: Z-141-2



GPS: 10T 0661336mE 5300754mN

Description: Muscovite tonalite in situ.

Area: Also from the quarry.

ID: Z-142-1



GPS: 10T 0659052mE 5294388mN

Description: 2 samples. This tonalite is a mix of 2 other tonalites, one more felsic and one more mafic but both with biotite.

Area: Just north of Nason Creek on the south end of the WRO pluton boundary mapped by Jerry.

ID: Z-142-2



GPS: 10T 0659052mE 5294388mN

Description: 3 samples. Biotite muscovite tonalite.

Area: There are lots of tonalites at this outcrop. Most of the outcrop is heavily banded gneiss with many tonalite phases and quartz dikes. Minor talc-tremolite in the area.

ID: Z-142-3



GPS: 10T 0659052mE 5294388mN

Description: 3 samples. Biotite tonalite with quartz veins nearby.

Area: Same as Z-142-1,2.

ID: Z-143



GPS: 10T 0653525mE 5301240mN

Description: 2 samples. Biotite tonalite, moderately foliated with obvious thin weathering rind.

Area: The entire outcrop is well obscured by moss. Samples were near quartz veins.

ID: Z-144-1



GPS: 10T 0653513mE 5301451mN

Description: Highly altered/weathered tonalite.

Area: After the Little Wenatchee River crossing, headed south. Above a gravel pit/talus hill. At the top of the talus hill there is an outcrop. This was dangerous to access.

ID: Z-144-2



GPS: 10T 0653513mE 5301451mN

Description: Biotite tonalite banded gneiss with moderate foliation. Sample has tremolite(?) slickensides.

Area: Same area as Z-144-1

ID: Z-144-3



GPS: 10T 0653513mE 5301451mN

Description: Biotite metatonalite with garnet porphyroblasts/phenocrysts? May be Chiwaukum schist.

Area: Same area as Z-144-1

ID: Z-145



GPS: 10T 0665442mE 5300443mN

Description: 2 samples. Biotite granodiorite. Intermediate composition but certainly a phyllosilicate-rich intrusive phase. Possibly part of the Dirty Face pluton?

Area: Heavily banded gneiss from roadcut on the north side of the road just north of Lake Wenatchee.

ID: Z-146-1



GPS: 10T 0660778mE 5300529mN

Description: Muscovite tonalite with minor biotite.

Area: Outcrop on the north side of the road just up from the quarry. Near some pegmatite dikes with no noticeable ultramafic bodies nearby.

ID: Z-146-2



GPS: 10T 0660778mE 5300529mN

Description: 2 samples. Coarse grained muscovite tonalite.

Area: Banded gneiss is very common in this area but the samples are from a very homogenous area.

ID: Z-147 (J-100)



GPS: 10T 0663841mE 5295972mN

Description: Biotite tonalite, maybe too weathered.

Area: 10 meters east just off of the Nason Ridge trail. Coarse quartz veins were cutting the tonalite.

ID: Z-148 (J-101)



GPS: 10T 0663780mE 5295926mN

Description: Coarse grained biotite tonalite, well foliated. Also may be too weathered.

Area: Small, mostly weathered outcrop with pegmatite veins cutting through the area.

ID: Z-149 (J-103)



GPS: 10T 0661778mE 5296434mN

Description: Fine grained biotite tonalite. Lightly foliated and not too weathered.

Area: Tonalite overlying schist with quartz veins cutting through both. Outcrop is directly on the Nason Ridge trail.

ID: Z-150 (J-104)



GPS: 10T 0661779mE 5296434mN

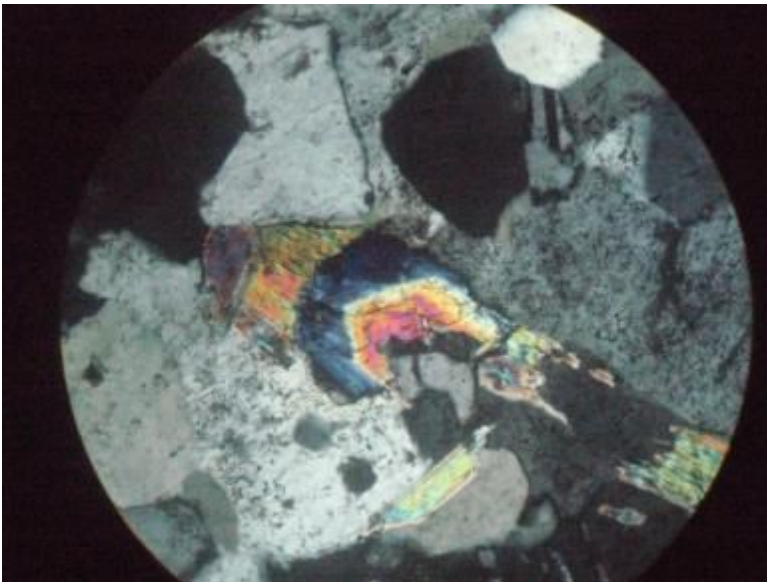
Description: Looks like a mafic biotite schist, but more coarse grained. Could be a weathered granitoid of some sort.

Area: 30 meters southwest of Nason Ridge trail in an outcrop of a homogenous but heavily altered granitoid body.

APPENDIX B. Thin Section Descriptions

WRO Samples

WR-105-16: This section contains predominately oligoclase and quartz with muscovite, epidote, opaques, and clinozoisite as accessory phases. Oligoclase shows minor sericitic alteration but is generally clean. The epidote shows textural features which indicate that much of it is magmatic. Some of the epidote especially when in contact with plagioclase, looks resorbed or secondary. Epidote is most commonly associated with muscovite and very commonly shows Fe-rich epidote cores with Fe-poor clinozoisite rims. Epidote in this section meets the criteria of magmatic epidote and occurs as grains up to 150 μm across. Plagioclase shows textures indicative of syneussis and both growth and deformation twins which taper off in many grains. Anhedral clinozoisite occurs in some of the plagioclase cores. The minor opaques in this section are likely ilmenite.



Pic # 2678 show the Fe-rich epidote core with clinozoisite rims common in this section. FOV is 1 mm

Z-107-1: This section contains predominately oligoclase, quartz, and muscovite with epidote, clinozoisite, microcline, and biotite as accessory phases. Oligoclase shows very minor sericitic alteration but is generally clean. Where epidote is present, it is most commonly associated with muscovite. Epidote in this section is more commonly fractured and resorbed in appearance as compared to WR-105-16 but a few smaller grains are euhedral, contained within muscovite, and generally meet the criteria of magmatic epidote. Epidote grains are approximately 100 μm across on average. The large grains of muscovite in this section appear to be magmatic, but the smaller grains may be secondary. Microcline occurs in this section as interstitial grains between larger plagioclase and quartz grains. Microcline does not make up more than 4% of the section. Clinozoisite occurs as one larger grain (~1.5mm across), fractured, and surrounded by large muscovite grains.

Z-108-1: This section contains predominately oligoclase, quartz, and muscovite with epidote, apatite, zircon, and biotite as accessory phases. Oligoclase shows almost no sericitic alteration except for a few areas which look to have undergone minor hydrous alteration. In these areas, secondary, fibrous muscovite has grown. Epidote is most commonly associated with muscovite and/or biotite. Epidote in this section is commonly euhedral and entirely contained within muscovite grains, although some larger epidote grains are anhedral. Euhedral epidote grains are approximately 110 μm across on average while one anhedral epidote grain is almost 250 μm across. The euhedral epidote grains which are contained within muscovite meet the criteria of magmatic epidote. Apatite occurs as a few large, high relief grains which appear almost anisotropic in the section due to their orientation. Zircon is rare, but is most easily visible within the muscovite grains.

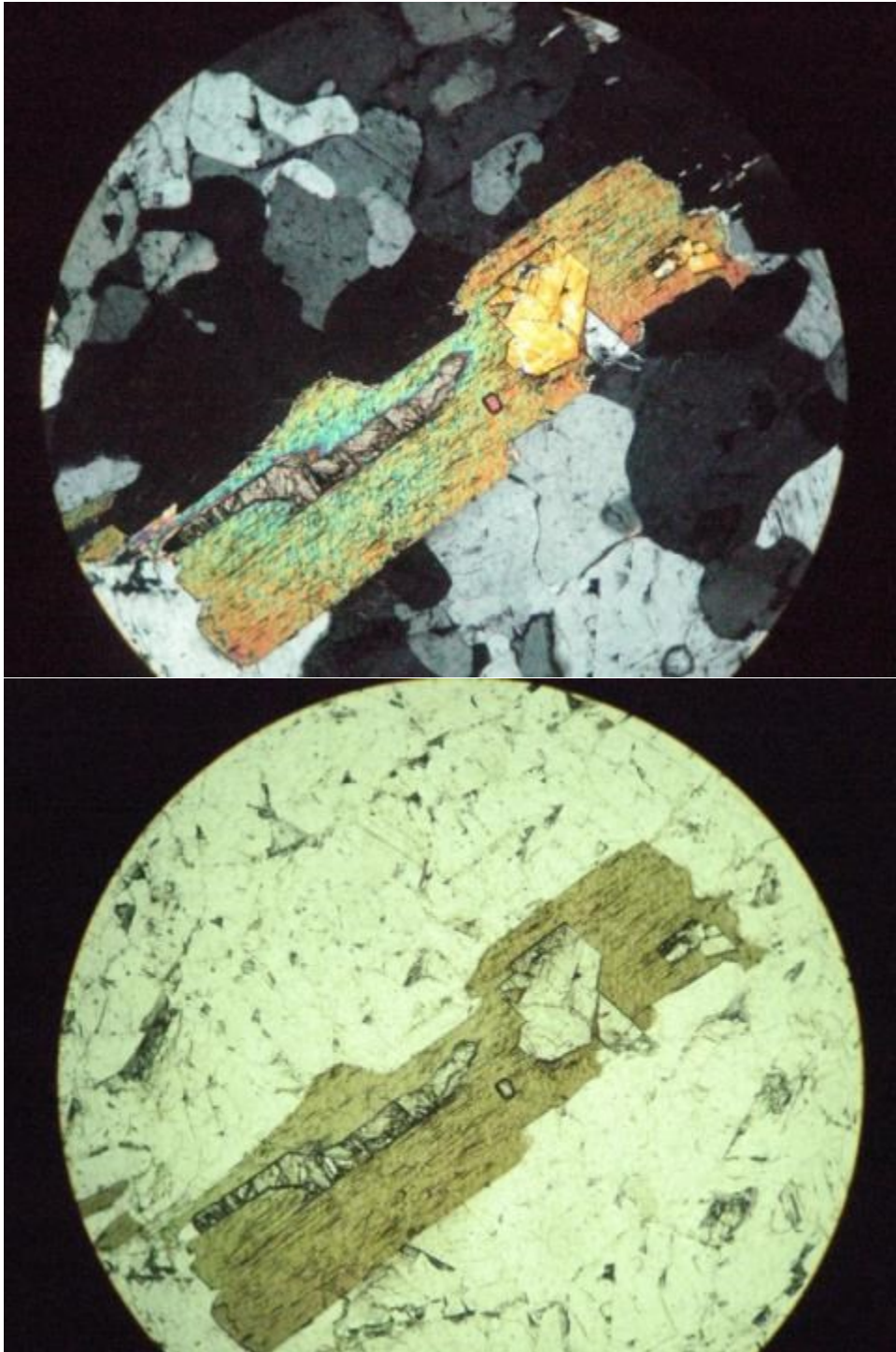
Z-120: This section contains predominately oligoclase, quartz, and muscovite with epidote, apatite, zircon, opaques, chlorite, and biotite as accessory phases. In general, this section contains much more biotite and apatite than other Z samples. Oligoclase shows minor to rather extensive sericitic alteration. Muscovite and biotite appear independently of one another, but are most commonly intergrown. Epidote and clinozoisite are most commonly associated with muscovite and/or biotite but also occur with plagioclase and quartz in this section. Epidote and clinozoisite in this section are only occasionally euhedral. Euhedral epidote grains, when they occur, are approximately 300 μm across and contained within biotite. The euhedral epidote grains which are contained within biotite meet the criteria of magmatic epidote. One such epidote appears to have a Fe-poor core and an Fe-rich rim, but this cannot be confirmed by petrography alone. Clinozoisite appears as a subhedral grain which is entirely encased by biotite in one instance in this section and may represent a rare example of magmatic clinozoisite. Despite this, the altered appearance and association with plagioclase suggests that much of the clinozoisite could be secondary. Apatite occurs as a few high relief grains with no particular textural associations. The opaque minerals are rare in this section, but are likely ilmenite. Chlorite appears as chloritization of biotite and is not extremely common this section.

WR-102-3: Pretty altered, but has great epidote textures. Epidote is not so commonly euhedral. Commonly shows clinozoisite cores with epidote rims. Fe-rich rims indicate what? Large amounts of clinozoisite, titanite, and epidote. It could be that some of this epidote is secondary, due to the altered nature of this section. However, it may also be that this rock altered preferentially from others due to its high epidote content.

Z-118: This section is predominately made up of oligoclase and quartz with muscovite, biotite, epidote and zircon as accessory phases. Muscovite and biotite are commonly intergrown

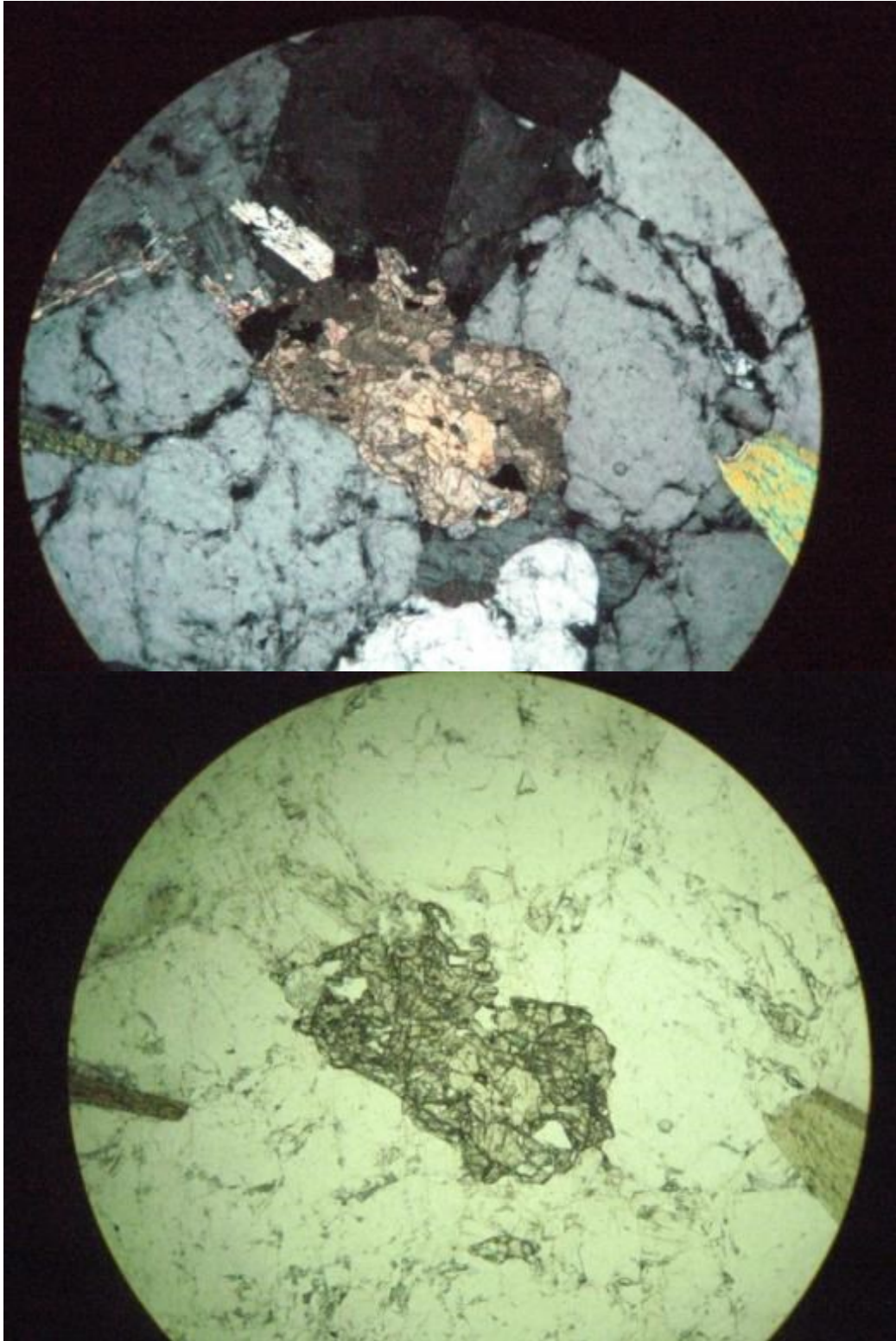
and show a consistent relationship with epidote. Oligoclase grains show sharp polysynthetic growth twins in most grains and have little to no sericitic alteration. Muscovite grains appear to be magmatic in many instances, although they occur in both large grained “clusters” as well as define the foliation in the sample along with biotite. Epidote occurs as generally anhedral masses both in the plagioclase matrix as well as encased within muscovite grains. Some of these epidote grains do meet the criteria for magmatic epidote. Epidote grains which occur within the plagioclase/quartz matrix tend to have a reaction rim.

Z-131: This section is made up of oligoclase and quartz with significant amounts of biotite, apatite, epidote, clinozoisite, titanite, and muscovite. Oligoclase shows little to moderate sericitic alteration and some evidence of anti-perthite. The epidote and clinozoisite are commonly associated with biotite and in some cases, euhedral epidote grains are entirely enclosed by biotite grains. These euhedral epidote grains meet the criteria of magmatic epidote. Titanite commonly occurs near biotite and/or epidote and in at least one case, biotite contains titanite and epidote entirely within a single grain. Muscovite is commonly intergrown with biotite where it does occur. Where epidote is not encased by biotite, it commonly appears to be resorbed, especially when in contact with plagioclase. Epidote and clinozoisite zoning relations are extremely variable in this section with some epidote appearing to have Fe-rich cores and Fe-poor rims while other grains show the opposite relationship. Epidote interference colors range from low first order to upper second order, probably reflecting variable Fe-contents. Textural evidence in this section indicates that titanite and epidote crystallized before biotite and muscovite.



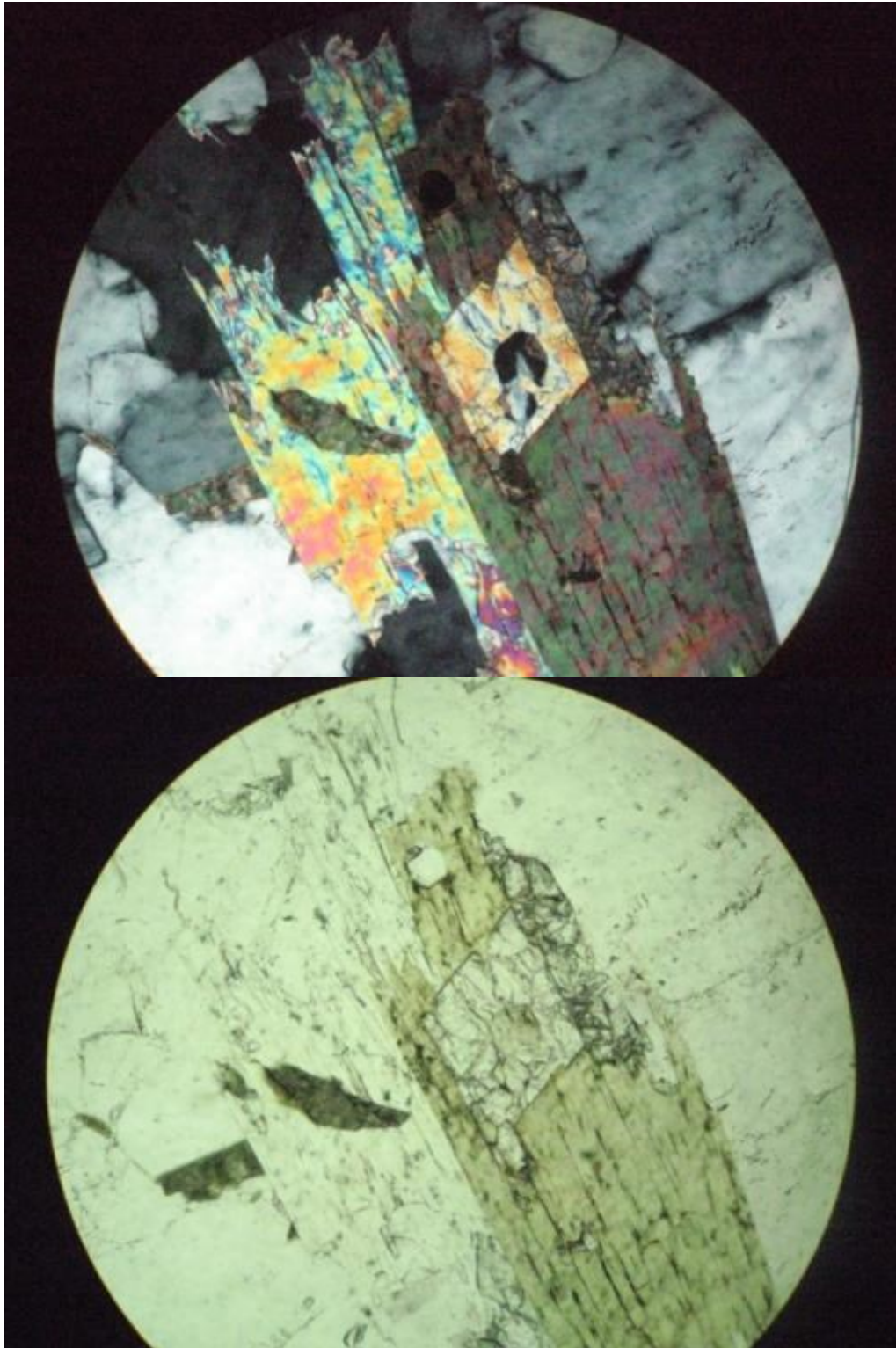
Pic # 105-2682,2683: biotite grain with epidote, titanite, and clinozoisite inclusions. FOV is 2mm. Z-131

Z-129: This section is made up of oligoclase and quartz with significant amounts of biotite, apatite, epidote, clinozoisite, titanite, and muscovite. Oligoclase shows some moderate sericitic alteration. Epidote commonly occurs with titanite and biotite as subhedral grains. When epidote is not encased by biotite or muscovite, it appears to be resorbed. Muscovite is commonly intergrown with biotite while some smaller and acicular muscovite grains appear to be the result of sericitic alteration and are likely secondary. Titanite occurs as both large aggregates of fractured grains and smaller euhedral grains. As least one large grain of clinozoisite appears in a plagioclase grain and is slightly resorbed. Epidote which is euhedral and encased by biotite meets the criteria of magmatic epidote. Muscovite is commonly intergrown with biotite and appears secondary when in smaller aggregates and likely associated with sericitic alteration. The one piece of textural evidence suggests that epidote crystallized before titanite.



Pic #- 2684,2685 – FOV is 2mm, titanite grain with subhedral epidote inclusion. Z-129

Z-138: This section contains oligoclase, quartz, and biotite with muscovite, rutile, titanite, epidote, clinozoisite, and apatite. Oligoclase shows very little sericitic alteration and quartz inclusions. Epidote shows textural relationships which indicate that biotite grew before epidote, but this epidote could be secondary. Euhedral epidote contained within biotite in some instances still meets the requirement of magmatic epidote and indicates that epidote did crystallize before biotite and muscovite. Muscovite and biotite are intergrown commonly. The textural relationship between biotite, muscovite, epidote, and titanite seen in many of the Z samples is common in this section as well. Epidote tends to have small Fe-poor cores as seen in the photo. This may indicate two periods of epidote growth. Titanite is generally anhedral and occurs most commonly with biotite. In some cases, titanite is entirely included within biotite indicating titanite crystallized before biotite. Rutile occurs rarely but is most often rimming titanite.



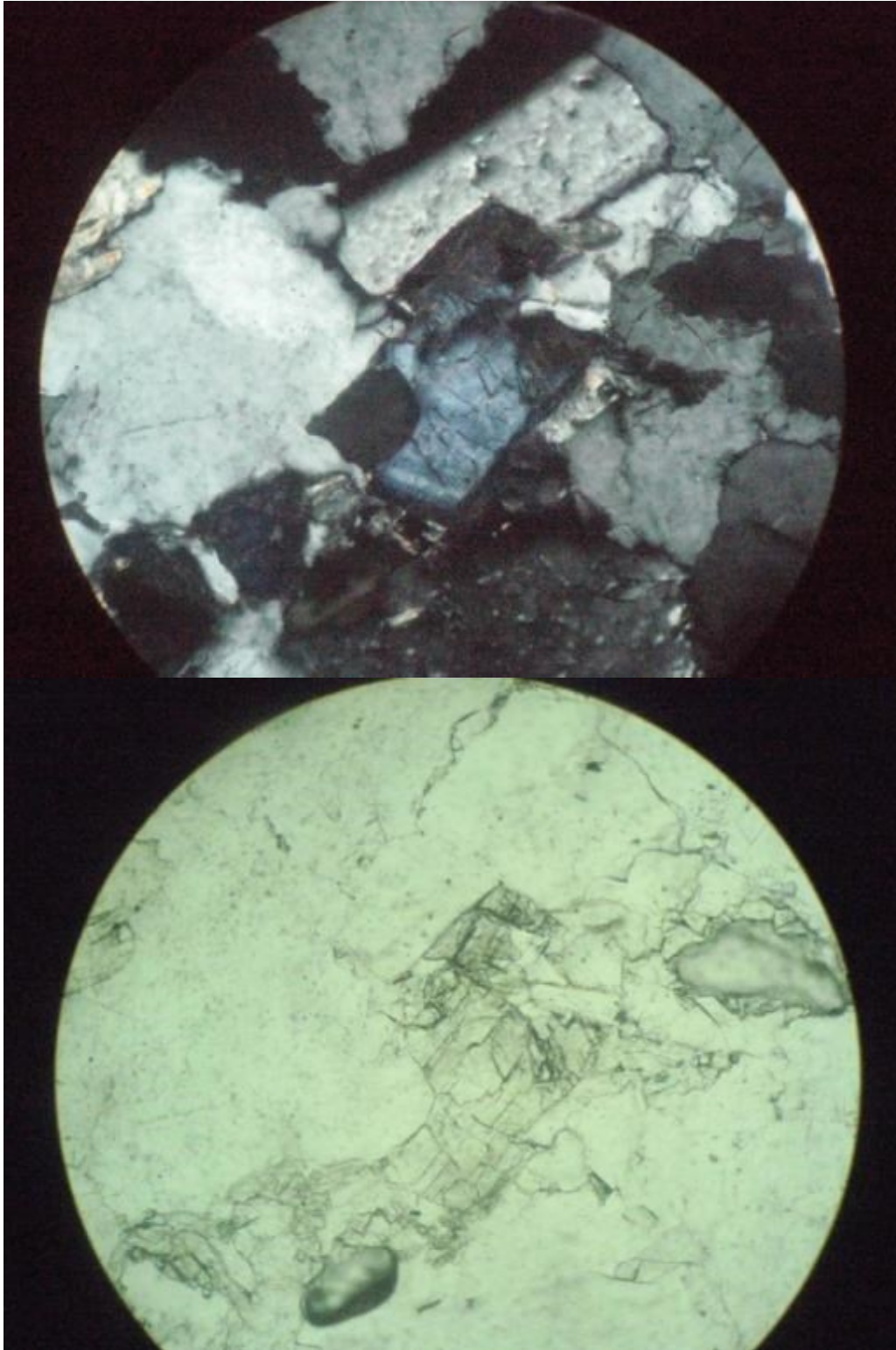
Pic #- 2686, 2687 FOV is 1mm, titanite, epidote, biotite, and muscovite. PPL bottom, XPL top.

Z-138

Z-141-1: This section contains oligoclase, quartz, biotite, and muscovite, titanite, zircon, chlorite, epidote and clinozoisite. The oligoclase commonly has biotite and quartz inclusions with minor amounts of sericitic alteration. This section contains up to 4% clinozoisite which is commonly anhedral, resorbed, light blue in XPL, and likely secondary. However, some of the clinozoisite shows more Fe-rich rims and could be primary. Chlorite appears as chloritization of biotite and is somewhat common in this section. Some of the relationships between titanite, biotite, muscovite, and epidote which are seen in the other Z samples can be seen in this section, although they are more altered in appearance. Titanite is common throughout the section and is anhedral to euhedral. This section may have evidence for clinozoisite which meets the criteria for magmatic epidote.

Z-119: This section is predominately made up of oligoclase with minor zoisite, quartz, and muscovite which occurs interstitially in larger grains between plagioclase. The oligoclase in this section shows an odd “sprinkling” of alteration which is intermixed sericite and zoisite. Zoisite has first order gray to light anomalous blue interference colors in XPL and it most easily recognized by its high relief. Zoisite is distinguished from clinozoisite, which has been common in the Z sections, by parallel extinction. The zoisite which appears as alteration is almost certainly secondary, but the larger interstitial grains could be magmatic. If magmatic, this may be a rare example of magmatic zoisite.

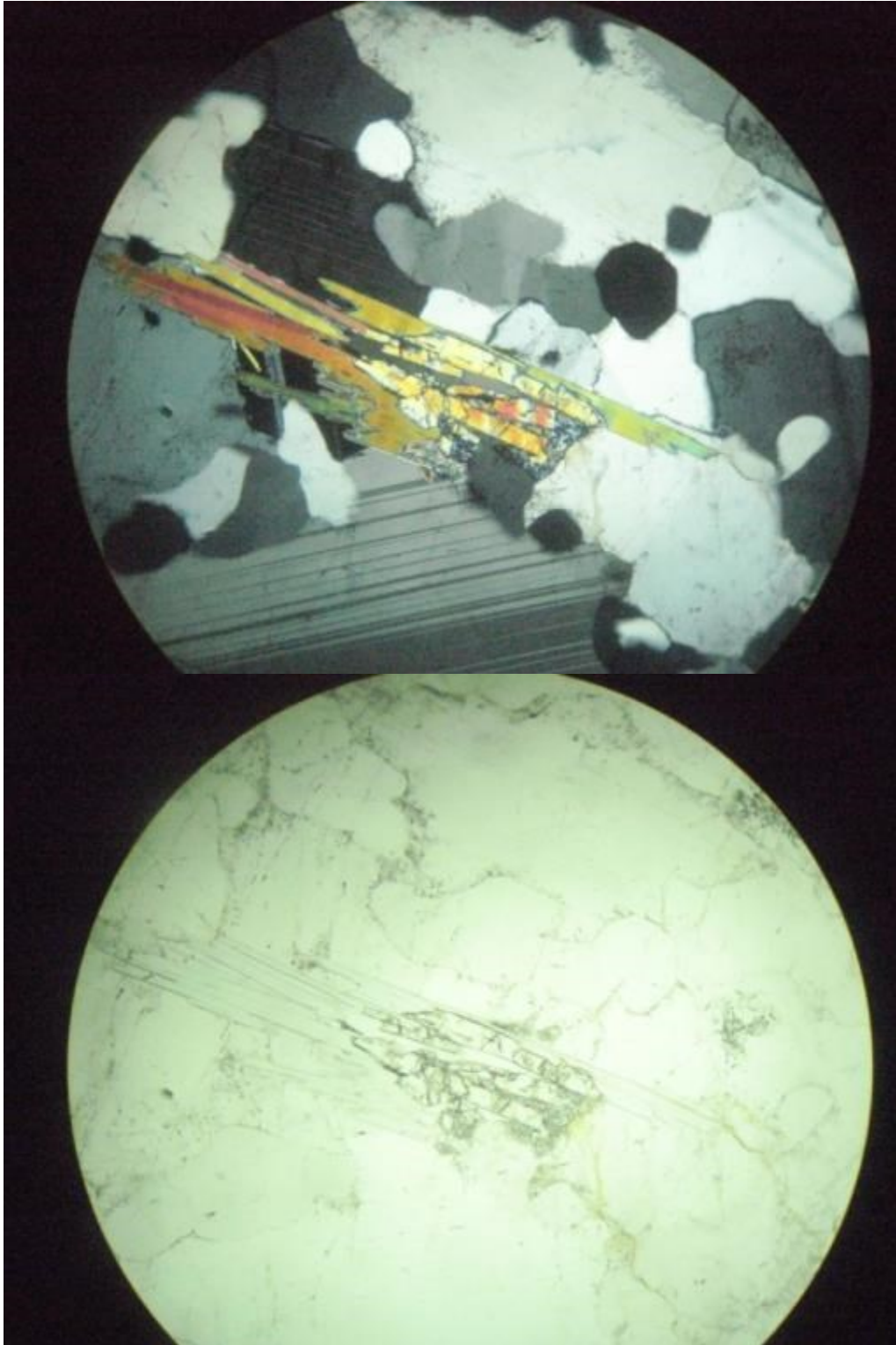
Z-123: This section is composed of oligoclase, quartz, muscovite, and minor clinozoisite. The clinozoisite occurs as subhedral grains most often associated with the muscovite grains which reach over 2 mm in size. One particular clinozoisite grain shows oscillatory zonation which could indicate a magmatic origin. Larger clinozoisite grains are typically contained within large muscovite grains such that it appears that muscovite grew after and off of the clinozoisite.



Pic #- 2688, 2689- FOV is 1mm – oscillatory zoned clinzoisite crystal surrounded by plagioclase grains. Z-123

Z-146-1: This section is composed of oligoclase and quartz with biotite, muscovite, epidote, clinozoisite, rutile, and zircon as accessory phases. Oligoclase has very light to absent sericitic alteration. One zircon grain in this section is just over 250 μm in length. Epidote is not prevalent in this section, but is almost always in occurrence with muscovite or biotite when it does appear. There are only a few euhedral epidote crystals in this section which are extremely small and do not explicitly meet the requirements of magmatic epidote. Epidote and clinozoisite show an interesting texture which indicates resorption or another type of reaction when the grains are in contact with plagioclase. Large clusters of muscovite appear to be primary whereas some of the smaller grains may be secondary. Muscovite and biotite are commonly intergrown in this section, but muscovite is more common.

Z-111-1: This section is largely made up of oligoclase and quartz with muscovite, microcline, biotite, rutile, opaques, and epidote as accessory phases. Oligoclase shows little to moderate sericitic alteration and relict normal zonation in many cases. Muscovite defines a foliation in this sample and is commonly intergrown with biotite. Opaque minerals (likely ilmenite) commonly have rutile rims and are associated with muscovite or biotite grains. Microcline is rare and can be seen associated with muscovite but not in any type of reaction. Epidote is most commonly associated with muscovite and may have been entirely encased by muscovite, but has been replaced by plagioclase in areas and has reacted with plagioclase in other areas. This epidote crystal meets the criteria of magmatic epidote and is likely magmatic in origin.



Pic # 2690 2691- FOV is 2mm – Epidote grain in muscovite with replacement by plagioclase in the middle and reaction rims with plagioclase at the bottom right. Z-111

Z-113-1: This section is largely made up of oligoclase and quartz with muscovite, microcline, clinozoisite, biotite, opaques, and epidote as accessory phases. Oligoclase shows little to moderate sericitic alteration and relict normal zonation. Biotite is much more common in this section than others which appear generally similar such as Z-111-1. Microcline is more common than in other Z samples and can be seen interstitially grown in small crystals between quartz and plagioclase. The opaque grains are not common and are likely ilmenite. Epidote and clinozoisite are most commonly associated with muscovite or biotite. Some of the epidote grains in this section are euhedral and meet the basic requirements of magmatic epidote, but there are no exquisite examples. Most of the epidote and clinozoisite are altered or resorbed in appearance.

Z-100-1: This section is made up of oligoclase intergrown with quartz and scattered muscovite, biotite, chlorite, rutile, and epidote crystals. There is an interesting texture in which many small quartz grains are included within larger plagioclase grains. The plagioclase may have therefore crystallized after quartz and trapped these quartz inclusions. Despite the pervasive quartz inclusions, the plagioclase is not significantly altered to sericite. This section also shows the common relationships between muscovite, biotite, and epidote which are seen throughout the Z samples. Chlorite only occurs as the chloritization of biotite in a few locations. Rutile occurs in at least one area as a large crystal neighbored by plagioclase and quartz. Epidote is not common in this section and only occurs in apparently altered masses with muscovite or biotite. No epidote in this section displays the explicit criteria of magmatic epidote although some of it may be. Muscovite and biotite are scattered in this section but do define a significant foliation and are commonly intergrown.

Z-104-1: This section is made up of oligoclase and quartz with epidote, rutile, opaques, biotite, muscovite, chlorite, zircon, and clinozoisite as accessory phases. Oligoclase has quartz

inclusions in some grains and typically shows sharp polysynthetic twins. Clinozoisite appears when epidote is in contact with plagioclase. Epidote is most commonly associated with biotite or muscovite. Chlorite only occurs as the chloritization of biotite and is not common in the section. Epidote is not extremely common, is typically sub to anhedral and does not show the criteria of magmatic epidote. Epidote shows variable interference colors from upper first order to upper second order. Muscovite and biotite are commonly intergrown. In one instance, epidote, ilmenite, rutile, biotite, and chlorite are found together and may indicate a reaction.

WR-102-1: This section is dominantly composed of oligoclase, quartz, and muscovite with minor biotite, microcline, epidote, titanite, clinozoisite, and apatite as accessory phases. The oligoclase has minor sericitic alteration and many grains show relict normal zonation. Microcline occurs as anti-perthite in the oligoclase and forms irregular patches. Oligoclase also commonly has quartz inclusions. Epidote and clinozoisite are most commonly associated with muscovite, sub to euhedral, and are occasionally entirely contained within muscovite grains. Titanite is not extremely common but occurs in larger muscovite grains which commonly also contain epidote or clinozoisite. Biotite is extremely rare and occurs as intergrowths with muscovite. Muscovite defines the foliation in this sample and is thought to be dominantly primary. This rock may be considered a granodiorite due to the significant amount of microcline exsolved from plagioclase. Large (1 mm long) clinozoisite grains on one edge of the section which are entirely contained within muscovite patches could be primary or secondary. Some of the epidote in this section which is euhedral and encased by muscovite certainly meets the requirements of magmatic epidote.

BG Samples

Z-137-1: This section is strongly foliated and made up of predominantly oligoclase, quartz, biotite, apatite, and muscovite, and zircon as accessory phases. The biotite and muscovite are commonly intergrown, but biotite is the dominant phyllosilicate. Zircon is most easily seen within biotite grains where it commonly forms pleochroic halos. There appear to be small garnets within biotite grains in a few places in this section. Myrmekite appears in this section but is not extremely common. For whatever reason, epidote does not appear in this section even though it has the same assemblage of the other Z samples which do contain magmatic epidote. Apatite grains are small and occur occasionally as moderate relief grains with dark gray interference colors.

N-132-7: This section contains predominantly oligoclase and quartz with biotite, muscovite, and very minor clinozoisite, and zircon as accessory phases. Oligoclase shows very minor sericitic alteration but is generally clean. Clinozoisite is extremely minor and occurs as extremely small grains (<100 μm). Zircon grains are commonly euhedral and average around 80 μm length. Biotite grains are commonly dark red, indicative of high Ti contents. Muscovite and biotite are commonly found together.

N-126-41: This section contains predominantly oligoclase, microcline, and quartz with biotite, muscovite, and very minor zircon, opaques (ilmenite) and apatite as accessory phases. The rock type is a granodiorite orthogneiss. Oligoclase in this section shows great normal zonation with calcic cores and sodic rims, indicative of an igneous origin. Oligoclase shows evidence of sericitic alteration which occurs as interesting muscovite grains inside the oligoclase which preferentially follow the cleavage planes. Biotites are commonly dark red in color. The opaque minerals are likely ilmenite and are most commonly in contact with biotite. The ilmenite

may have grown as a Ti-reducing phase in association with the Ti-rich biotites. Apatite grains appear generally elongate (60 μm long) and commonly contained within plagioclase grains. There may be very minor epidote in this section associated with muscovite and biotite but it is very uncommon and may be secondary.

N-282-1: This section is made up of oligoclase and quartz with biotite, muscovite, zircon, opaques, and apatite as accessory phases. Quartz shows strong undulose extinction in this section. Plagioclase shows some evidence for syneussis in a few places. Oligoclase shows evidence of sericitic alteration which occurs as interesting muscovite grains inside the oligoclase which preferentially follow the cleavage planes. Myrmekite occurs in plagioclase grains nearest a large biotite and muscovite “vein” which cuts across the thin section. The rock type is a tonalite orthogneiss. Apatite grains are euhedral and up to 150 μm long. Zircon grains are most commonly seen within biotite grains and produce pleochroic halos. There are a few small grains of anhedral clinozoisite within biotite grains which may be secondary. Many of the minerals in this section appear to be fractured, but not with much alteration along the fractures.

N-100-43: This section is made up of oligoclase, microcline, and quartz with biotite, muscovite, zircon, opaques, and apatite as accessory phases. This rock is likely on the verge of being a granodiorite orthogneiss. Plagioclase grains commonly show normal igneous zonation. Myrmekite occurs in plagioclase fairly commonly throughout the thin section. Microcline shows tartan twinning and occurs interstitially between plagioclase and quartz grains most commonly. Quartz does show undulose extinction, but not strongly. There is not strong alteration of the plagioclase grains, but where it does occur, muscovite (sericite) tends to grow in the cores of plagioclase along cleavage planes. Zircon grains are most commonly seen within biotite grains and produce pleochroic halos. Apatite grains are most commonly seen within microcline.

N-100-40a: This section is made up of oligoclase and quartz with biotite, muscovite, zircon, opaques, titanite, and apatite as accessory phases. Relict normal zonation can be seen in the plagioclase grains although it is fuzzy in most places. Oligoclase shows evidence of minor sericitic alteration which occurs as interesting muscovite grains inside the oligoclase which preferentially follow the cleavage planes. Titanite (up to 0.5 mm) is very common and crystals are almost always euhedral. This rock is rather well foliated with muscovite and biotite defining the dominant foliation. This section has much more zircon than many of the other samples and the zircon grains are most commonly present within biotite surrounded by pleochroic halos, although some of these halos appear to be caused by titanite inclusions as well. This is one of many samples that show anhedral quartz blebs included within plagioclase grains. Myrmekite occurs in plagioclase fairly commonly throughout the thin section.

N-100-58: This section is made up of oligoclase and quartz with biotite, garnet, zircon, opaques, clinozoisite, and apatite as accessory phases. Plagioclase shows relict, fuzzy, normal zonation which suggests an igneous origin. This rock is a garnet tonalite gneiss due to its gneissosity. Garnet occurs as subhedral grains with common biotite inclusions. Chlorite occurs with biotite as chloritization. The opaques are commonly, but not always, associated with biotite. They could be ilmenite which acted as a Ti-rich phase in this rock. Clinozoisite is not common, but occurs most commonly in contact with biotite. Clinozoisite also occurs locally alongside garnet or plagioclase. Some clinozoisite grains appear to be zoned which would indicate that they are primary (magmatic). However, the chloritization of biotite in this sample suggests that clinozoisite may also be secondary.

N-100-50: This rock is made up of oligoclase and quartz with hornblende, garnet, biotite, zircon, opaques, apatite, and titanite as accessory phases. This section is unique in that it contains

a large amount of hornblende. Additionally, the titanite grains are especially large (up to 1.5 mm). Plagioclase grains commonly show normal igneous zonation and the more calcic cores of plagioclase grains are preferentially altered to sericite or sausserite. Garnet occurs in small (0.7 mm) anhedral to subhedral grains most commonly associated with biotite. Pleochroic halos in biotite are common and are the result of zircon (grains are length slow with roughly parallel extinction). Opaques are most commonly associated with or contained within biotite or hornblende and are likely ilmenite.

APPENDIX D. Archean Comparison Data

Table 11.3. Table of major element data used for the discriminant analysis. Additional WR-XXX and N-XXX sample data used in the analysis are from Magloughlin (1986) and Magloughlin (1993), respectively.

Major Elements			SiO ₂	Al ₂ O ₃	TiO ₂	FeO	MnO	CaO	MgO	K ₂ O	Na ₂ O	P ₂ O ₅	BaO	SrO	Fe ₂ O ₃	ZrO ₂	LOI	Total	
WRO Samples	Tonalite	Z-107-1	75.38	16.25	0.04		0.00	1.19	0.15	0.83	7.24	0.02	0.04	0.07	0.29	<0.00002	0.34	101.83	
	Tonalite	Z-108	73.98	15.91	0.08		0.00	1.46	0.31	1.15	6.16	0.04	0.06	0.06	0.50	<0.000023	0.59	100.31	
	Tonalite	Z-118	73.43	16.45	0.04		0.00	1.09	0.14	0.67	7.97	0.02	0.03	0.07	0.23	<0.000023	0.20	100.35	
	Tonalite	Z-120	74.95	14.76	0.21		0.01	2.94	0.39	0.74	4.93	0.09	0.04	0.10	0.98	<0.000023	0.32	100.46	
	Tonalite	Z-129	76.83	14.33	0.15		0.00	2.42	0.42	0.58	5.43	0.06	0.04	0.08	0.69	<0.000023	0.28	101.31	
	Tonalite	Z-138	70.61	16.20	0.38		0.02	3.12	0.82	1.14	5.28	0.13	0.08	0.09	1.91	<0.000023	0.33	100.10	
	Tonalite	Z-146-1	76.24	15.25	0.04		0.00	1.38	0.17	0.95	6.24	0.10	0.07	0.06	0.27	<0.000023	0.40	101.18	
	Tonalite	Z - 100	74.36	17.07	0.07		0.00	1.60	0.21	0.99	6.39	0.03	0.07	0.07	0.27			0.37	101.49
	Tonalite	Z - 104	74.29	16.75	0.03		0.00	1.35	0.11	0.47	7.48	0.02	0.02	0.06	0.21			0.40	101.19
	Tonalite	Z - 111	71.48	17.84	0.02		0.00	1.76	0.06	0.74	7.36	0.02	0.05	0.06	0.15			0.23	99.77
	Tonalite	Z - 113	75.30	13.91	0.11		0.01	2.04	0.46	0.83	4.76	0.07	0.05	0.05	0.60			0.36	98.55
	Tonalite	Z - 119	65.17	21.77	0.00		0.00	1.79	0.06	0.46	9.79	0.01	0.07	0.17	0.04			0.34	99.67
	Tonalite	Z - 123	76.54	15.57	0.06		0.00	1.28	0.29	1.15	5.69	0.05	0.06	0.08	0.21			0.66	101.64
	Tonalite	Z - 131	71.48	15.39	0.33		0.01	3.13	0.65	1.02	4.66	0.11	0.08	0.08	1.37			0.26	98.57
	Tonalite	Z - 141 - 1	70.62	16.00	0.30		0.01	3.28	0.45	0.98	4.90	0.10	0.06	0.09	1.27			0.46	98.53
	BG Samples	Tonalite	Z-137-1	72.60	15.33	0.26		0.02	2.61	0.71	1.25	5.06	0.12	0.06	0.07	1.40	<0.000023	0.35	99.84
	From Martin et al., 2004	TTG	TTG>3.5 Ga	69.59	15.29	0.39		0.04	3.03	1.00	2.04	4.60	0.13			3.26			99.37
From Martin et al., 2004	TTG	3<TTG<3.5 Ga	69.65	15.35	0.36		0.06	2.96	1.07	1.74	4.64	0.14			3.07			99.04	
From Martin et al., 2004	TTG	TTG<3Ga	68.36	15.52	0.38		0.05	3.23	1.36	2.00	4.70	0.15			3.27			99.02	
From Drummond and Defant 1990	High-Al TTG	Cenozoic	65.88	17.49	0.30		0.08	4.79	1.26	1.44	4.25	0.13			3.20		1.21	100.03	
From Drummond and Defant 1990	High-Al TTG	Archean_DD	69.74	15.08	0.30		0.03	3.04	1.23	1.41	5.44	0.08			2.55		0.97	99.87	
Condie	TTG	Early Archean	70.40	15.20	0.31		0.06	2.74	0.96	2.22	4.71	0.10			2.79			99.49	
Condie	TTG	Late Archean	68.30	15.50	0.42		0.07	3.26	1.39	2.20	4.51	0.14			3.42			99.21	
Condie	TTG	Proterozoic 2	67.30	15.80	0.47		0.08	3.42	1.48	2.30	4.33	0.14			4.04			99.36	
Condie	TTG	Phanerozoic	65.90	16.50	0.47		0.09	4.36	1.67	2.14	4.00	0.12			4.11			99.36	
Nehring, et al., 2009	TTG gneiss (3.2 Ga)	TTG gneiss (3.2 Ga)	68.40	16.37	0.41	2.34	0.03	3.61	1.12	1.43	4.82								
Nehring, et al., 2009	TTG gneiss (3.2 Ga)	TTG gneiss (3.2 Ga)	60.27	16.47	0.96	6.33	0.10	5.33	2.90	2.01	3.91								
Nehring, et al., 2009	TTG gneiss (3.2 Ga)	TTG gneiss (3.2 Ga)	68.95	15.85	0.33	2.92	0.05	3.71	1.26	1.09	4.90								
Nehring, et al., 2009	TTG gneiss (3.2 Ga)	TTG gneiss (3.2 Ga)	71.15	15.09	0.33	2.56	0.04	3.36	0.89	1.09	4.55								
Nehring, et al., 2009	TTG gneiss (3.2 Ga)	TTG gneiss (3.2 Ga)	54.99	18.27	0.73	6.03	0.11	7.42	4.04	1.61	4.61								
Nehring, et al., 2009	TTG gneiss (3.2 Ga)	TTG gneiss (3.2 Ga)	59.25	17.16	1.12	6.57	0.09	6.04	2.17	0.33	5.23								
Winter, 2010	M-type Granitoid	M-type	67.20	15.20	0.40	4.10	0.10	4.30	1.70	1.30	4.00	0.10						98.40	
Winter, 2010	I-type Granitoid	I-type	69.50	14.20	0.40	3.10	0.10	3.10	1.40	3.50	3.20	0.10						98.50	
Winter, 2010	S-type Granitoid	S-type	70.90	14.00	0.30	3.00	0.10	1.90	1.20	4.10	2.50	0.20						98.30	
Winter, 2010	A-type Granitoid	A-type	73.80	12.40	0.30	2.70	0.10	0.80	0.20	4.70	4.10	0.00						98.90	
Winter, 2010	Archean Granitoid	Archean_Winter	69.80	15.60	0.30	2.80	0.10	3.20	1.20	1.80	4.90	0.10						99.70	

Table 11.4. Table of minor and trace element data used for the discriminant analysis. Additional WR-XXX and N-XXX sample data used in the analysis are from Magloughlin (1986) and Magloughlin (1993), respectively.

Minor / Trace Elements			Ni	Cr	Li	Sc	V	Ba	Rb	Sr	Zr	Y	Nb	Ga	As	Cu	Mo	Cd	Sn
	Rock Type	Sample																	
WRO Samples	Tonalite	Z-107-1	<0.82	0.15		0.21	1.35	328.67	8.95	538.17	0.76	0.59	0.30	17.65	<0.07	5.54	0.25		
	Tonalite	Z-108	<0.50	0.58		0.93	4.87	543.80	19.04	541.90	2.83	1.27	0.21	18.17	<0.16	1.28	0.18		
	Tonalite	Z-118	<0.49	0.85		0.10	0.42	285.73	5.59	558.23	<0.433	0.09	0.13	19.48	<0.32	1.98	0.14		
	Tonalite	Z-120	0.58	2.12		1.27	7.71	412.63	10.57	803.73	3.72	2.43	1.51	20.89	0.10	3.30	0.36		
	Tonalite	Z-129	6.98	8.10		1.04	5.57	337.77	5.98	653.90	3.68	2.52	0.81	16.68	<0.001	3.53	0.50		
	Tonalite	Z-138	1.88	4.36		1.47	14.24	709.27	24.46	732.37	3.39	2.58	2.55	25.44	0.08	4.44	0.25		
	Tonalite	Z-146-1	0.22	0.04		0.30	0.60	651.17	17.77	496.07	3.41	2.56	0.60	14.84	<0.29	2.29	0.14		
	Tonalite	Z-100	0.27	0.18	9.20	0.91	0.89	642.73	17.43	645.17	2.18	1.37	0.71	18.51	0.10	1.52	0.35	0.00	0.97
	Tonalite	Z-104	0.59	0.28	5.56	0.64	0.52	179.67	5.30	556.40	1.20	1.51	0.44	16.21	<0.002	0.76	0.39	0.02	0.47
	Tonalite	Z-111	4.57	26.93	3.49	0.11	0.64	434.00	6.54	606.57	1.00	0.15	0.95	24.41	0.05	4.13	0.79	0.02	0.17
	Tonalite	Z-113	3.06	2.75	7.16	1.64	13.22	454.50	16.32	478.80	1.97	2.95	1.32	16.62	0.10	0.53	0.70	0.03	0.84
	Tonalite	Z-119	1.97	4.13	1.48	0.19	0.30	622.43	4.02	1472.00	6.63	0.25	0.29	17.37	0.68	0.10	0.68	0.05	-0.06
	Tonalite	Z-123	7.15	58.45	6.13	0.60	7.09	581.60	20.80	702.70	4.17	0.77	0.98	14.57	0.20	2.39	0.57	0.02	0.61
	Tonalite	Z-131	3.14	5.28	16.15	1.26	10.45	714.57	21.29	756.70	2.96	1.73	2.47	21.92	0.53	1.96	0.30	0.07	1.23
	Tonalite	Z-141-1	2.87	5.92	10.07	1.31	9.15	528.17	18.71	837.00	2.35	2.46	2.71	19.59	0.81	2.79	0.78	0.37	0.80
	BG Samples	Tonalite	Z-137-1	<0.27	4.24		2.44	25.54	551.60	27.75	538.57	34.45	1.95	1.03	18.21	<0.12	1.75	0.19	
From Martin et al., 2004	TTG	TTG>3.5 Ga	12.00	34.00			39.00	449.00	79.00	360.00	166.00	12.00	8.00						
From Martin et al., 2004	TTG	3<TTG<3.5 Ga	15.00	21.00			43.00	523.00	59.00	429.00	155.00	14.00	6.00						
From Martin et al., 2004	TTG	TTG<3Ga	21.00	50.00			52.00	847.00	67.00	541.00	154.00	11.00	7.00						
From Drummond and Defant 1990	High-Al TTG	Cenozoic	7.00	6.00				670.00	23.00	760.00	65.00	3.00	6.00						
From Drummond and Defant 1990	High-Al TTG	Archean_DD	15.00	19.00				301.00	43.00	559.00	77.00	3.00	4.00						
Condie	TTG	Early Archean	17.00	45.00				500.00	76.00	362.00	152.00	8.50	6.10						
Condie	TTG	Late Archean	22.00	35.00				769.00	67.00	515.00	154.00	9.10	6.20						
Condie	TTG	Proterozoic 2	23.00	55.00				717.00	63.00	473.00	152.00	17.30	7.10						
Condie	TTG	Phanerozoic	12.00	32.00				716.00	63.00	493.00	122.00	14.50	6.70						
Nehring, et al., 2009	TTG gneiss (3.2 Ga)	TTG gneiss (3.2 Ga)	12.00	13.00		2.00	33.00	491.00	34.00	404.00	163.00	4.88	3.71						
Nehring, et al., 2009	TTG gneiss (3.2 Ga)	TTG gneiss (3.2 Ga)	16.00	19.00				12.00	114.00	942.00	48.00	813.00	130.00	11.10	4.53				
Nehring, et al., 2009	TTG gneiss (3.2 Ga)	TTG gneiss (3.2 Ga)	9.00	16.00		4.00	42.00	573.00	30.00	503.00	116.00	11.90	3.43						
Nehring, et al., 2009	TTG gneiss (3.2 Ga)	TTG gneiss (3.2 Ga)	3.00	4.00		4.00	22.00	192.00	39.00	342.00	205.00	32.00	9.31						
Nehring, et al., 2009	TTG gneiss (3.2 Ga)	TTG gneiss (3.2 Ga)	54.00	96.00		18.00	114.00	303.00	43.00	579.00	92.00	12.70	6.78						
Nehring, et al., 2009	TTG gneiss (3.2 Ga)	TTG gneiss (3.2 Ga)	24.00	8.00		16.00	81.00	145.00	5.00	514.00	375.00	16.50	7.58						
Winter, 2010	M-type Granitoid	M-type	3.00	7.00			71.00	232.00	30.00	154.00	131.00	34.00	3.00			8.00			
Winter, 2010	I-type Granitoid	I-type	8.00	20.00			57.00	519.00	164.00	235.00	150.00	31.00	11.00			9.00			
Winter, 2010	S-type Granitoid	S-type	11.00	30.00			49.00	440.00	245.00	112.00	157.00	32.00	13.00			9.00			
Winter, 2010	A-type Granitoid	A-type	1.00	2.00			6.00	352.00	169.00	48.00	528.00	75.00	37.00			2.00			
Winter, 2010	Archean Granitoid	Archean_Winter	14.00	29.00			35.00	690.00	55.00	454.00	152.00	8.00	6.00						

Table 11.4. Continued

Sb	Zn	Pb	Th	Be	Cs	Hf	U	Co	W	La	Ce	Pr	Nd	Sm	Eu	Gd	Tb	Dy	Ho	Er	Tm	Yb	Lu	Sr/Y	(La/Yb) _n	Eu/Eu*	
<0.41	17.42	4.35	0.02		0.10	<0.02	0.38	25.19	246.83	0.91	0.20	0.09	0.46	0.18	0.08	0.20	0.03	0.14	0.02	0.04	<0.012	0.02	0.00	907.02		1.23	
<0.42	19.50	5.92	0.78		0.19	0.02	0.73	24.17	245.47	1.68	5.85	0.82	3.59	0.96	0.35	0.78	0.08	0.32	0.04	0.08	<0.009	0.04	0.00	426.80	28.77	1.20	
<0.50	19.05	4.89	0.44		0.07	<0.08	0.14	19.83	201.33	0.00	2.63	0.37	1.64	0.47	0.20	0.34	0.03	0.06	0.00	0.00	<0.021	0.01	<0.0006	6416.48		1.43	
<0.41	24.50	6.35	4.11		0.19	0.04	1.82	34.61	303.70	15.84	34.43	4.19	16.90	3.43	0.96	2.33	0.22	0.78	0.09	0.16	<0.004	0.07	0.01	331.07	153.72	0.98	
<0.45	24.90	3.61	2.41		0.06	0.03	1.95	34.14	326.90	11.60	26.47	3.47	14.81	3.23	0.98	2.25	0.21	0.74	0.09	0.17	<0.003	0.07	0.01	259.76	106.01	1.05	
<0.41	79.13	7.49	3.61		0.26	0.04	1.99	23.93	235.53	15.58	33.34	4.24	17.62	3.71	1.11	2.65	0.26	0.90	0.10	0.17	<0.004	0.06	0.01	283.97	167.08	1.03	
<0.43	6.98	7.70	0.01		0.18	0.10	0.60	19.88	205.83	0.79	0.09	0.05	0.29	0.16	0.17	0.29	0.06	0.43	0.08	0.22	<0.007	0.14	0.02	193.52		2.26	
-0.51	13.01	4.69	0.57		0.18	0.08	0.67			2.03	4.36	0.59	2.60	0.77	0.36	0.75	0.09	0.36	0.05	0.10	0.01	0.06	0.01	471.96	23.42	1.42	
-0.77	9.18	3.39	0.17		0.07	0.03	0.74			0.62	1.42	0.20	0.99	0.39	0.17	0.50	0.07	0.33	0.05	0.09	0.01	0.06	0.01	369.70	7.55	1.14	
-0.78	11.48	5.01	0.04		0.02	0.05	0.11			0.13	0.32	0.04	0.16	0.04	0.04	0.04	0.01	0.02	0.01	0.01	0.00	0.01	0.00	4135.68	8.83	3.20	
-0.99	41.36	2.82	1.88		0.15	0.07	0.22			3.19	14.55	0.94	4.08	1.05	0.53	0.95	0.12	0.61	0.10	0.23	0.03	0.15	0.02	162.42	14.55	1.58	
-1.13	0.85	14.78	4.64		0.03	0.16	0.51			23.68	44.65	4.99	18.30	2.31	0.68	0.98	0.06	0.12	0.01	0.02	0.00	0.02	0.00	5810.53	652.06	1.18	
-1.28	8.34	9.52	1.69		0.20	0.12	0.41			6.09	12.52	1.57	6.48	1.35	0.39	0.86	0.07	0.25	0.03	0.05	0.01	0.03	0.00	910.63	153.28	1.02	
-1.18	75.00	7.04	4.38		0.25	0.09	1.57			19.30	38.43	4.57	18.66	3.46	1.06	2.25	0.20	0.61	0.06	0.10	0.01	0.05	0.01	437.82	242.75	1.09	
-1.03	44.39	5.95	3.63		0.32	0.10	1.48			16.97	35.01	4.31	17.85	3.62	1.06	2.48	0.24	0.82	0.09	0.15	0.02	0.08	0.01	339.88	147.17	1.02	
<0.35	56.17	6.62	2.74		1.04	0.85	0.79	22.46	218.47	1.75	22.00	1.00	4.12	0.98	0.63	0.70	0.08	0.43	0.07	0.20	<0.006	0.16	0.02	275.95	7.65	2.20	
										35.30	61.70		25.80	4.20	1.00	3.20		1.80		0.77		0.78	0.20	30.45	29.85	0.80	
										31.40	55.10		19.60	3.30	0.80	2.40		1.90		0.77		0.63	0.13	31.44	32.86	0.83	
										30.80	58.50		23.20	3.50	0.90	2.30		1.60		0.75		0.63	0.12	51.10	32.52	0.91	
										9.30	17.10		9.30	1.30	0.60							0.55	0.05		16.91	2.43	
										16.00	23.00		6.40	1.80	0.60	1.02	0.20	0.68	0.14	0.34		0.45	0.12		35.56	1.23	
			4.10			3.80	1.20			22.00	40.00		16.00	2.90	0.82	2.20	0.31					0.82	0.14	72.00	25.00	0.95	
			8.10			4.70	1.50			36.00	65.00		25.00	4.20	1.07	2.90	0.38					0.71	0.11	89.00	36.00	0.88	
			6.10			4.30	2.10			26.00	45.00		18.00	3.50	0.95	3.00	0.49					1.33	0.23	37.00	14.20	0.87	
			7.60			3.40	1.90			17.00	34.00		16.00	3.10	0.84	2.80	0.40					1.16	0.18	56.00	11.30	0.85	
			14.18			4.77				52.90	89.10	10.00	32.50	4.66	0.85	3.35		1.28		0.40		0.26	0.02			0.62	
			2.24			0.40	0.14			27.80	61.20	7.87	33.10	5.60	1.39	3.81		2.48		1.08		0.97	0.14			0.87	
			2.65			3.74				17.30	36.00	4.41	16.70	3.26	0.80	2.42		2.19		1.14		1.02	0.13			0.83	
			11.53			7.50				29.20	52.50	6.08	22.10	4.99	0.79	4.56		5.39		3.35		3.06	0.49			0.50	
						0.72	0.59			15.30	37.40	5.21	23.50	4.72	1.29	3.72		2.86		1.36		1.27	0.19			0.91	
						8.74				11.90	28.10	3.63	14.90	3.41	0.98	3.20		2.92		1.64		1.57	0.25			0.89	
							0.00	16.00		9.00	22.00		13.00	3.00	1.00	4.00	1.00	5.00				3.00	1.00			0.88	
		31.00	5.00	1.00																							0.88
		48.00	19.00	20.00			5.00	10.00		31.00	66.00		30.00	6.00	1.00												0.88
		59.00	27.00	19.00			5.00	10.00		27.00	61.00		28.00	6.00	1.00												0.88
		120.00	24.00	23.00			8.00	5.00	3.00		55.00	137.00		67.00	16.00	2.00	14.00	2.00									0.40
				7.00			5.00	2.00			32.00	56.00		21.00	3.00	1.00	2.00	0.00	1.00								1.17

APPENDIX E. WRO and BG Geochemical Data

Table 11.5. Raw geochemical data for samples taken from the field as part of this project. Note that data from Magloughlin (1986), Magloughlin (1993), and Magloughlin (pers. comm.) have been used in other graphs and models in this chapter.

WRO Samples	SiO ₂	Al ₂ O ₃	TiO ₂	FeO	MnO	CaO	MgO	K ₂ O	Na ₂ O	P ₂ O ₅	BaO	SrO	Cr ₂ O ₃	Fe ₂ O ₃	ZrO ₂	LOI	Total
Z-107-1	75.38	16.25	0.04		0.00	1.19	0.15	0.83	7.24	0.02	0.04	0.07		0.29	<0.00002	0.34	101.83
Z-108	73.98	15.91	0.08		0.00	1.46	0.31	1.15	6.16	0.04	0.06	0.06		0.50	0.00	0.59	100.31
Z-118	73.43	16.45	0.04		0.00	1.09	0.14	0.67	7.97	0.02	0.03	0.07		0.23	0.00	0.20	100.35
Z-120	74.95	14.76	0.21		0.01	2.94	0.39	0.74	4.93	0.09	0.04	0.10		0.98	0.00	0.32	100.46
Z-129	76.83	14.33	0.15		0.00	2.42	0.42	0.58	5.43	0.06	0.04	0.08		0.69	0.00	0.28	101.31
Z-138	70.61	16.20	0.38		0.02	3.12	0.82	1.14	5.28	0.13	0.08	0.09		1.91	0.00	0.33	100.10
Z-146-1	76.24	15.25	0.04		0.00	1.38	0.17	0.95	6.24	0.10	0.07	0.06		0.27	0.00	0.40	101.18
Z-100	74.36	17.07	0.07		0.00	1.60	0.21	0.99	6.39	0.03	0.07	0.07		0.27		0.37	101.49
Z-104	74.29	16.75	0.03		0.00	1.35	0.11	0.47	7.48	0.02	0.02	0.06		0.21		0.40	101.19
Z-111	71.48	17.84	0.02		0.00	1.76	0.06	0.74	7.36	0.02	0.05	0.06		0.15		0.23	99.77
Z-113	75.30	13.91	0.11		0.01	2.04	0.46	0.83	4.76	0.07	0.05	0.05		0.60		0.36	98.55
Z-119	65.17	21.77	0.00		0.00	1.79	0.06	0.46	9.79	0.01	0.07	0.17		0.04		0.34	99.67
Z-123	76.54	15.57	0.06		0.00	1.28	0.29	1.15	5.69	0.05	0.06	0.08		0.21		0.66	101.64
Z-131	71.48	15.39	0.33		0.01	3.13	0.65	1.02	4.66	0.11	0.08	0.08		1.37		0.26	98.57
Z-141-1	70.62	16.00	0.30		0.01	3.28	0.45	0.98	4.90	0.10	0.06	0.09		1.27		0.46	98.53
BG Samples																	
Z-137-1	72.60	15.33	0.26		0.02	2.61	0.71	1.25	5.06	0.12	0.06	0.07		1.40	0.00	0.35	99.84
WRO Samples	Ni	Cr	Li	Sc	V	Ba	Rb	Sr	Zr	Y	Nb	Ga	Ge	As	Cu	Mo	Cd
Z-107-1	<0.825	0.15		0.21	1.35	328.67	8.95	538.17	0.76	0.59	0.30	17.65	<0.630	<0.075	5.54	0.25	
Z-108	<0.507	0.58		0.93	4.87	543.80	19.64	541.90	2.83	1.27	0.21	18.17	<0.530	<0.167	1.28	0.18	
Z-118	<0.493	0.85		0.10	0.42	285.73	5.59	558.23	<0.433	0.09	0.13	19.48	<0.75	<0.322	1.98	0.14	
Z-120	0.58	2.12		1.27	7.71	412.63	10.57	803.73	3.72	2.43	1.51	20.89	<0.092	0.10	3.30	0.36	
Z-129	6.98	8.10		1.04	5.57	337.77	5.98	653.90	3.68	2.52	0.81	16.68	<0.266	<0.001	3.53	0.50	
Z-138	1.88	4.36		1.47	14.24	709.27	24.46	732.37	3.39	2.58	2.55	25.44	0.05	0.08	4.44	0.25	
Z-146-1	0.22	0.04		0.30	0.60	651.17	17.77	496.07	3.41	2.56	0.60	14.84	<0.651	<0.29	2.29	0.14	
Z-100	0.27	0.18	9.20	0.91	0.89	642.73	17.43	645.17	2.18	1.37	0.71	18.51		0.11	1.52	0.35	0.00
Z-104	0.59	0.28	5.56	0.64	0.52	179.67	5.30	556.40	1.20	1.51	0.44	16.21		0.00	0.76	0.39	0.02
Z-111	4.57	26.93	3.49	0.11	0.64	434.00	6.54	606.57	1.00	0.15	0.95	24.41		0.05	4.13	0.79	0.02
Z-113	3.06	2.75	7.16	1.64	13.22	454.50	16.32	478.80	1.97	2.95	1.32	16.62		0.10	0.53	0.70	0.03
Z-119	1.97	4.13	1.48	0.19	0.30	622.43	4.02	1472.00	6.63	0.25	0.29	17.37		0.68	0.10	0.68	0.05
Z-123	7.15	58.45	6.13	0.60	7.09	581.60	20.80	702.70	4.17	0.77	0.98	14.57		0.20	2.39	0.57	0.02
Z-131	3.14	5.28	16.15	1.26	10.45	714.57	21.29	756.70	2.96	1.73	2.47	21.92		0.53	1.96	0.30	0.07
Z-141-1	2.87	5.92	10.07	1.31	9.15	528.17	18.71	837.00	2.35	2.46	2.71	19.59		0.81	2.79	0.78	0.37
BG Samples																	
Z-137-1	<0.275	4.24		2.44	25.54	551.60	27.75	538.57	34.45	1.95	1.03	18.21	<0.46	<0.125	1.75	0.19	

Table 11.5. Continued

Sn	Sb	Zn	Pb	Th	Cs	Hf	U	Co	W	La	Ce	Pr	Nd	Sm	Eu	Gd	Tb	Dy	Ho	Er	Tm	Yb	Lu	Eu/Eu*
	<0.412	17.42	4.35	0.02	0.10	<0.027	0.38	25.19	246.83	<0.91	0.20	0.09	0.46	0.18	0.08	0.20	0.03	0.14	0.02	0.04	<0.012	0.02	0.00	1.23
	<0.42	19.50	5.92	0.78	0.19	0.02	0.73	24.17	245.47	1.68	5.85	0.82	3.59	0.96	0.35	0.78	0.08	0.32	0.04	0.08	<0.009	0.04	0.00	1.20
	<0.504	19.05	4.89	0.44	0.07	<0.085	0.14	19.83	201.33	<0.002	2.63	0.37	1.64	0.47	0.20	0.34	0.03	0.06	0.00	0.00	<0.021	<0.01	<0.0006	1.43
	<0.415	24.50	6.35	4.11	0.19	0.04	1.82	34.61	303.70	15.85	34.43	4.19	16.90	3.43	0.96	2.33	0.22	0.78	0.09	0.16	<0.004	0.08	0.01	0.98
	<0.458	24.90	3.61	2.41	0.06	0.03	1.95	34.14	326.90	11.60	26.47	3.47	14.81	3.23	0.98	2.25	0.21	0.74	0.09	0.17	<0.003	0.07	0.01	1.05
	<0.416	79.13	7.49	3.61	0.26	0.04	1.99	23.93	235.53	15.58	33.34	4.24	17.62	3.71	1.11	2.65	0.26	0.90	0.10	0.17	<0.004	0.06	0.01	1.03
	<0.433	6.98	7.70	0.01	0.18	0.10	0.60	19.88	205.83	<0.797	0.09	0.05	0.29	0.16	0.17	0.29	0.06	0.43	0.08	0.22	<0.007	0.14	0.02	2.36
0.97	-0.52	13.01	4.69	0.57	0.18	0.08	0.67			2.03	4.36	0.59	2.60	0.77	0.36	0.75	0.09	0.36	0.05	0.10	0.01	0.06	0.01	1.42
0.47	-0.77	9.18	3.39	0.17	0.07	0.03	0.74			0.62	1.42	0.20	0.99	0.39	0.17	0.50	0.07	0.33	0.05	0.09	0.01	0.06	0.01	1.14
0.17	-0.78	11.48	5.01	0.04	0.02	0.05	0.11			0.13	0.32	0.04	0.16	0.04	0.04	0.04	0.01	0.02	0.01	0.01	0.00	0.01	0.00	3.20
0.84	-0.99	41.36	2.82	1.88	0.15	0.07	0.22			3.19	14.55	0.94	4.08	1.05	0.53	0.95	0.12	0.61	0.10	0.23	0.03	0.15	0.02	1.58
-0.06	-1.13	0.85	14.78	4.64	0.03	0.16	0.51			23.68	44.65	4.99	18.30	2.31	0.68	0.98	0.06	0.12	0.01	0.02	0.00	0.02	0.00	1.18
0.61	-1.28	8.34	9.52	1.69	0.20	0.12	0.41			6.09	12.52	1.57	6.48	1.35	0.39	0.86	0.07	0.25	0.03	0.05	0.01	0.03	0.00	1.02
1.23	-1.18	75.00	7.04	4.38	0.25	0.09	1.57			19.30	38.43	4.57	18.66	3.46	1.06	2.25	0.20	0.61	0.06	0.10	0.01	0.05	0.01	1.09
0.80	-1.03	44.39	5.95	3.63	0.32	0.10	1.48			16.97	35.01	4.31	17.85	3.62	1.06	2.48	0.24	0.82	0.09	0.15	0.02	0.08	0.01	1.02
	<0.350	56.17	6.62	2.74	1.04	0.85	0.79	22.46	218.47	1.75	22.00	1.00	4.12	0.98	0.63	0.70	0.08	0.43	0.07	0.20	<0.006	0.16	0.02	2.20